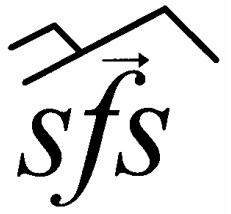

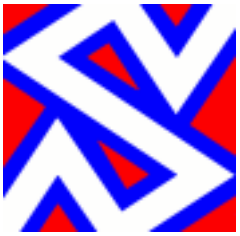

THERMOPHYSICS 2007

PROCEEDINGS

Editor: Jozef Leja

October 11 – 12, 2007
Kočovce chateau, Slovakia

THERMOPHYSICS 2007
PROCEEDINGS

Editor: Jozef Leja
Vydavateľstvo STU, Bratislava 2007
ISBN 978-80-227-2746-4

Contents

Preface

It is pleasure for research group at the Department of Physics of Faculty of Civil Engineering at Slovak University of Technology in Bratislava to host the eleventh meeting of the Thermophysical Society – Working Group of the Slovak Physical Society. The meeting was held on October 11 and 12, 2007 in the Kočovce chateau, Western Slovakia.

The seminar Thermophysics is meeting of scientists working in the field of investigation of heat transfer and measurement of thermophysical and other transport properties of materials. Over 20 participants of the seminar delivered 17 lectures in which their authors presented current research progress. The aim of the seminar was to attract not only prominent scientists but also young physicists.

The proceedings are also available at the homepage of the Thermophysics http://www.tpl.ukf.sk/thermophysics or upon a request at the e-mail address jozefa.lukovicova@stuba.sk.

Organize committee would like to express thanks to all participants for their interesting contribution.

Jozefa Lukovičová

Accuracy of transient methods

P. Dieška

Department of Physics, STU FEI

Ilkovičova 3, 812 19 Bratislava, Slovakia

October 11, 2007

Concept

- Experiment $\{t_n, T_n\}_{n=1}^{N}$

  $\mathbf{b} = \{b_j\}_{j=1}^{N_b}$

- Model $T_{model} = f(t, \mathbf{a}, \mathbf{b})$

  $\mathbf{a} = \{a_i\}_{i=1}^{N_a}$

- Fitting model parameters to experimental data: determined, overdetermined problem

Accuracy estimation - overdetermined problem

Least squares optimization $\mathbf{min}\{\sum_{n=1}^{N}[T_n - f_n(\mathbf{a},\mathbf{b})]^2\}$

where $f_n(\mathbf{a},\mathbf{b}) = f(t_n,\mathbf{a},\mathbf{b})$

t_n ... deterministic parameter

$\mathbf{b}$, $\{T_n\}_{n=1}^{N}$ ... independent random variables

$\mathbf{a}$ ... dependent random variables

$$\sum_{n=1}^{N}(T_n - f_n)\frac{\partial f_n}{\partial a_i} = 0, \qquad i = 1, 2, \ldots N_a \tag{1}$$

There are estimated the moments:

$$< a_i > \text{ as a solution of equation (1)}$$
$$< b_j > \text{ from other measurements}$$

$$< (b_j - < b_j >)(b_k - < b_k >) > \sim \delta_{jk} u(b_j)^2 \quad (2)$$
$$< T_n > \sim f_n(< \mathbf{a} >, < \mathbf{b} >) \quad (3)$$
$$< (T_n - < T_n >)(T_m - < T_m >) > \sim \delta_{nm} u(T)^2 \quad (4)$$
$$< (T_n - < T_n >)(b_k - < b_k) > \sim 0 \quad (5)$$

Now we estimate the uncertainty

$$u(a_i)^2 \sim < (a_i - < a_i >)^2 > = < (\Delta a_i)^2 > \sim < (da_i)^2 > \quad (6)$$

Differentiating the equation (1) we obtain

$$\sum_{i=1}^{N_a} A_{ki} da_i = \sum_{n=1}^{N} dT_n \frac{\partial f_n}{\partial a_k} + \sum_{j=1}^{N_b} B_{kj} db_j, \quad k = 1, 2, ..N_a \tag{7}$$

where

$$A_{ki} = \sum_{n=1}^{N} \left[(f_n - T_n) \frac{\partial^2 f_n}{\partial a_k \partial a_i} + \frac{\partial f_n}{\partial a_k} \frac{\partial f_n}{\partial a_i} \right] \simeq \sum_{n=1}^{N} \frac{\partial f_n}{\partial a_k} \frac{\partial f_n}{\partial a_i} \tag{8}$$

$$B_{kj} = -\sum_{n=1}^{N} \left[(f_n - T_n) \frac{\partial^2 f_n}{\partial a_k \partial b_j} + \frac{\partial f_n}{\partial a_k} \frac{\partial f_n}{\partial b_j} \right] \simeq -\sum_{n=1}^{N} \frac{\partial f_n}{\partial a_k} \frac{\partial f_n}{\partial b_j} \tag{9}$$

Solution of equation (7) has the form

$$da_k = \sum_{i=1}^{N_a} A_{ki}^{-1} \Big(\sum_{n=1}^{N} dT_n \frac{\partial f_n}{\partial a_i} + \sum_{j=1}^{N_b} B_{ij} db_j \Big), \quad k = 1, 2, ..N_a \tag{10}$$

and the uncertainty of a_k is with respect to equation (2) - (6) and (10)

$$u(a_k)^2 = \sum_{i=1}^{N_a} \sum_{i'=1}^{N_a} A_{ki}^{-1} A_{ki'}^{-1} \left[A_{i'i} u(T)^2 + \sum_{j=1}^{N_b} \sum_{j=1}^{N_b} B_{ij} B_{i'j} u(b_j)^2 \right] \tag{11}$$

$$\boxed{u(a_k)^2 = C_{kT}^2 u(T)^2 + \sum_{j=1}^{N_b} C_{kj}^2 u(b_j)^2}$$

where the sensitivities are

$$C_{kT} = \sqrt{A_{kk}^{-1}} \tag{12}$$

and

$$C_{kj} = \sum_{i=1}^{N_a} A_{ki}^{-1} B_{ij} \tag{13}$$

The elements of matrix $\mathbf{A}$ and $\mathbf{B}$ are defined with equations (8) and (9). It is seen that

$$\mathbf{A} \sim N \qquad \mathbf{B} \sim N$$

therefore $C_{kT} \sim \frac{1}{\sqrt{N}}$ and C_{kj} is N-independent. For power-like dependence it is useful to define indices

$$\nu_{kj} = \frac{\partial \log(a_k)}{\partial \log(b_j)} = \frac{b_j}{a_k} C_{kj} \tag{14}$$

Then for relative uncertainties we can write the equation

$$u_r(a_k)^2 = C_{kT}^2 \frac{u(T)^2}{a_k^2} + \sum_{j=1}^{N_b} \nu_{kj}^2 u_r(b_j)^2 \tag{15}$$

Application to simple model

1D model: The temperature response on the stepwise heat flow from planar heat source:

$$T(t,x) = T_0 \left[\frac{e^{-v^2}}{\sqrt{\pi} v} - \Phi^*(v) \right] \tag{16}$$

where $T_0 = qx/\lambda$

q ... heat flow density at source

x ... axial space coordinate of thermometer

λ ... thermal conductivity

$v = \frac{x}{2\sqrt{kt}}$

k ... thermal diffusivity

t ... time

We apply the formula (13) on the relation (16). The obtained indices are constant ones:

$\nu_{k,x} = 2$	$\nu_{k,q} = 0$
$\nu_{\lambda,x} = 1$	$\nu_{\lambda,q} = 1$

Application to more complicated model

2D model: The temperature response on the stepwise heat flow from planar heat source - cylindric sample with radial Newtonian heat transfer from sample surface:

$$T(t,x) = T_0 \frac{R}{x} \sum_{\xi} \frac{\beta}{\xi(\xi^2+\beta^2)J_0(\xi)} \left[e^{-2uv}\Phi^*(v-u) - \ e^{2uv}\Phi^*(v+u) \right] \quad (17)$$

where Φ^* is the complementary error function,
$u = \xi \frac{\sqrt{kt}}{R}$
R ... sample radius
$\beta = \frac{R\alpha}{\lambda}$
α ... heat transfer coefficient
ξ is the root of the equation

$$\beta J_0(\xi) - \xi J_1(\xi) = 0$$

J_0, J_1 ... Bessel functions of the first kind

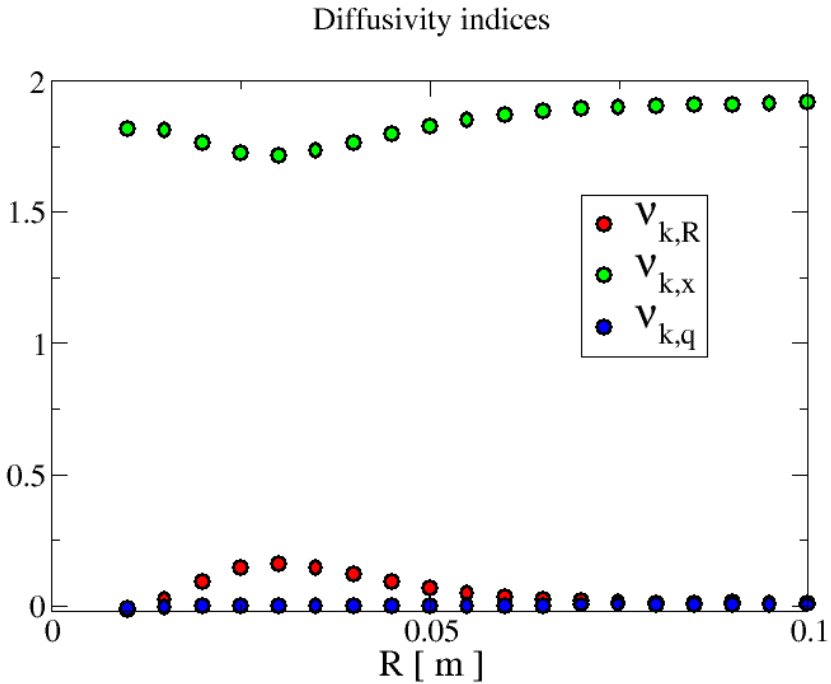

Figure 1:

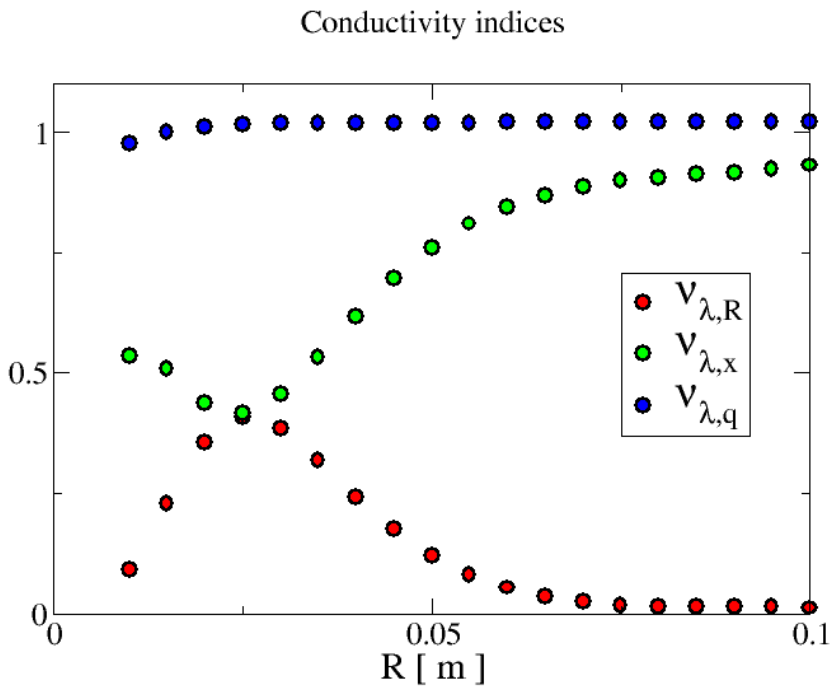
Conductivity indices
1
0.5
0
0
0.05
0.1
R [m]
$\nu_{\lambda,R}$
$\nu_{\lambda,x}$
$\nu_{\lambda,q}$

Figure 2:

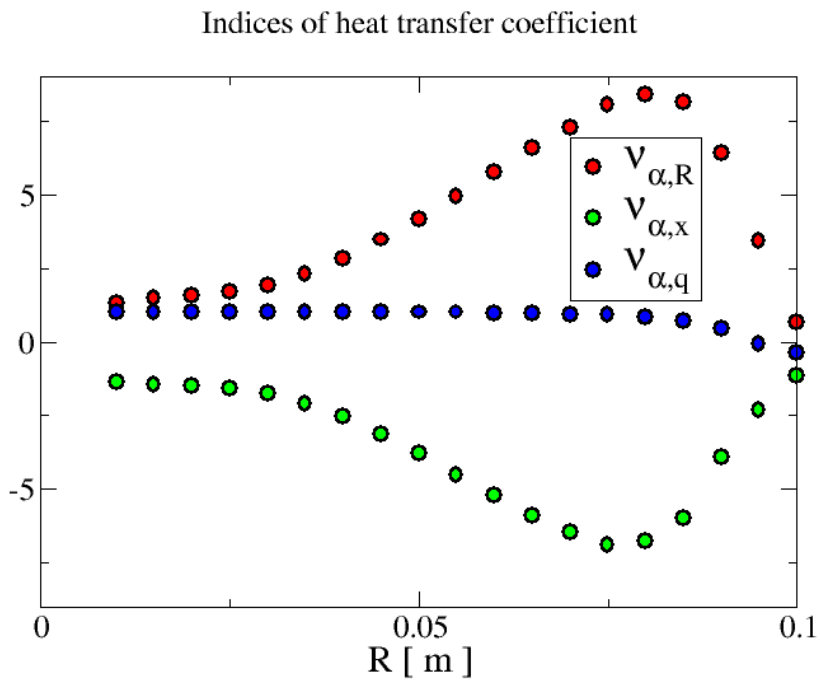
Indices of heat transfer coefficient
5
0
-5
0
0.05
0.1
R [m]
ν α,R
ν α,x
ν α,q

Figure 3:

INVERSE ALGORITHMS FOR TIME DEPENDENT BOUNDARY RECONSTRUCTION OF MULTIDIMENSIONAL HEAT CONDUCTION MODEL

M. Pohanka, J. Horský*

Summary: *Comprehensive quantitative information on the heat transfer phenomena is not available for quenching of hot moving surfaces. Attention is focused on the search for boundary conditions describing the heat transfer in engineering applications of spray cooling of metal surfaces. Direct measurements of boundary conditions in many industrial applications or in experiments that simulates these processes are impossible. Thus temperature histories are recorded inside the investigated body and the boundary conditions are computed using inverse heat conduction algorithms using experimental data. Sequential Beck's inverse algorithm and identification methods are discussed. Combining measurement with an inverse analysis often results in an ill-posed problem. Such problems are extremely sensitive to measurement errors. The distance of the measurement point from the investigated surface strongly influences the shortest impulse that can be reconstructed by an inverse method. Based on magnitude of stabilization factor the degradations of reconstructed boundary conditions are presented..*

1. Introduction

For computational methods knowledge of boundary conditions is necessary. Those conditions can be computed for simple cases, however, they must be obtained from measurements in most cases. Boundary conditions can be measured directly on the surface or if not possible we can do the measurement inside the investigated body and then we have to use an inverse task to compute boundary conditions from measured values. In our case we concentrate on boundary conditions during water cooling of hot steel products or of hot working rolls (Horský 2005). In these cases it is not possible to measure cooling intensity directly on the surface and we have to measure temperature history inside the body and to compute boundary conditions using an ill-posed inverse task. The accuracy of the computed results is strongly dependent on two factors: distance of the thermocouple from the investigated surface and on the additional noise in the measured data.

* Ing. Michal Pohanka, Ph.D.; Doc. Ing. Jaroslav Horský, CSc.: Heat Transfer and Fluid Flow Laboratory; Brno University of Technology; Faculty of Mechanical Engineering; Technická 2896/2; 616 69 Brno; Czech Republic; Phone +420 54114 3283; Fax +420 54114 2224; E-mail: pohanka@fme.vutbr.cz

2. Measurement

Experimental conditions are prepared in such way, which resembles as close as possible to the real mill conditions (Raudenský 2003). There are two basic parameters, which should be kept. The first is the initial temperature of tested sample and the second is the speed of sample motion. To measure boundary conditions a special experimental stand was developed for these tests.

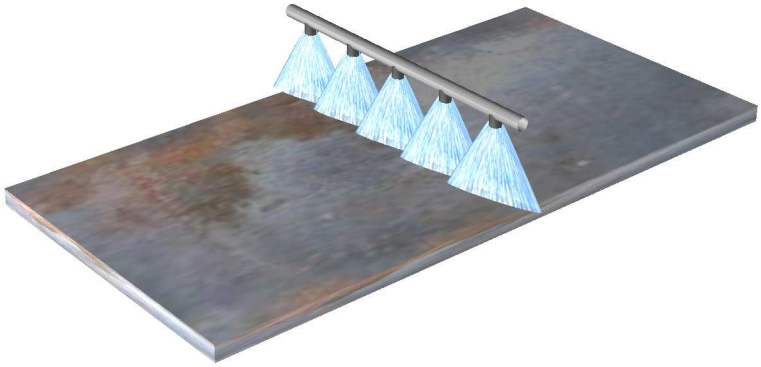

Figure 1 – High-pressure water nozzles with flat water stream removing oxide layers from a hot surface steel.

Experimental stand

The experimental stand was built to study the cooling of linearly moving objects. A six meter long girder carrying a movable trolley and a driving mechanism (see Figure 2) forms the basic part of the experimental device. An electronic device measuring the instant position of the trolley is embedded in the trolley. The driving mechanism consists of an electric motor controlled by a programmable unit, a gearbox, two rollers and a hauling rope. The girder is divided into three sections. The marginal sections are used for the trolley's acceleration or deceleration. The velocity of the trolley is constant in the mid-section and it is here where the spray nozzles quench the measured sample.

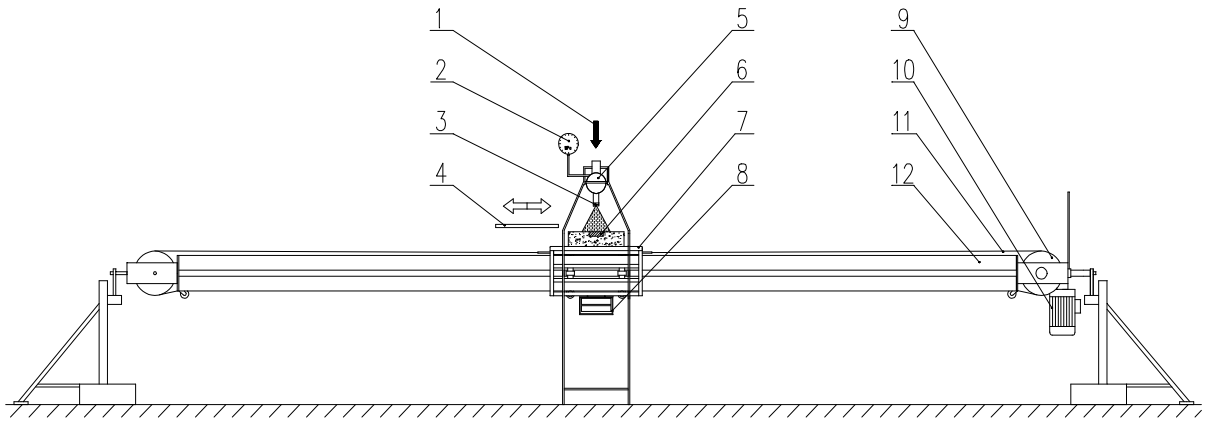

Figure 2 – Principal scheme of the linear test bench (1-cooling medium supply, 2-pressure gauge, 3-nozzle, 4-moving deflector, 5-manifold, 6-tested sample, 7-moving trolley, 8-datalogger, 9-roller, 10-electric motor, 11-hauling steel wire rope, 12-girder).

The procedure of the experiment is as follows:

- An electric heater heats the test plate to an initial temperature of the experiment.
- The plunger water pump is switched on and the pressure is adjusted.
- A driving mechanism moves the test plate under the spraying nozzles. After recovering the temperature field in the plate, the movement of the plate under the spraying nozzles is repeated.
- The temperature is measured using special temperature sensor inside the investigated steel plate and the temperature is recorded into data logger memory.
- The positions of the test plate and the thermocouples (in the direction of movement) are recorded together with the temperature values. The record of instant positions is used for computation of instant velocities and positions while moving under the spray.

3. Sensor description

To measure temperature inside the body, special sensors with built-in K-thermocouples are used as shown in Figure 3. The main body of the sensor is made of stainless austenitic steel. A hole of 1.1 mm in diameter for a thermocouple is made from the side of the sensor. The axis of the hole is 1 mm under the investigated surface and is perpendicular to the expected heat flux, so that the most important part of the inserted thermocouple lies in one isotherm. Inside the sensor, a shielded ungrounded K thermocouple is placed. The gap between the sensor and the thermocouple is filled with copper or ceramic material that can be exposed to a higher temperature than copper.

Sensors of this type are used mainly for descaling experiments but very similar sensors are used for measuring temperature during the rolling process. During measurements that serve for computing heat transfer coefficient (HTC), the sensors are placed in the steel object on which the HTC is investigated (see Figure 1).

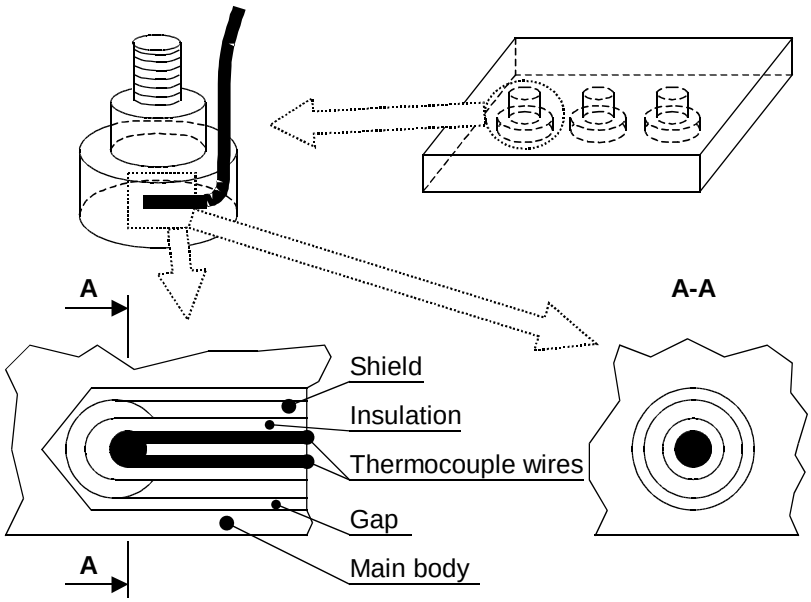

Figure 3 – Application of sensor, and its structure in detail.

None sensors are exactly the same. The positions of the junction point inside the shielded thermocouple differ. Also the hole inside the sensor is a bit bigger than the thermocouple so that its position can differ. As the thickness of the material in the gap differs, the heat resistance does too. These are the main reasons why the calibration experiment are done for each sensor (Pohanka 2002). An optimization method is used for finding the appropriate thermal conductivity of the material that fills the gap in the upper and lower parts and depth of installed thermocouple.

4. Computational Model

A 2D axis symmetric model was used as shown in Figure 4. The model includes the shielded thermocouple with all its parts. The thermocouple must be taken into account because the homogeneity of material is disturbed by the inserted thermocouple, and thus the temperature profile is also disturbed.

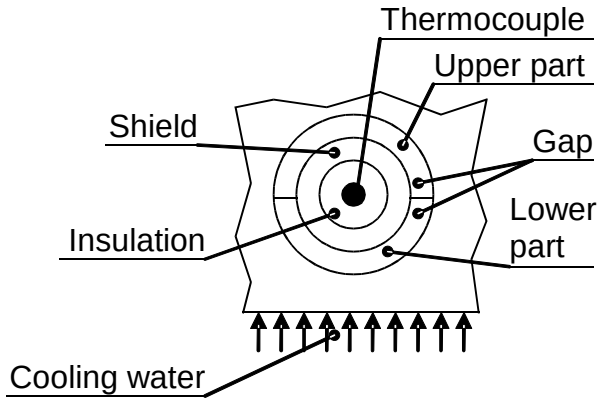

Figure 4 – Computational 2D model.

An example of the temperature field around the thermocouple is shown in Figure 5. A quite flat circular part represents the cross-section of the thermocouple. The surface temperature (at Y=0 mm) is also disturbed by the installed thermocouple.

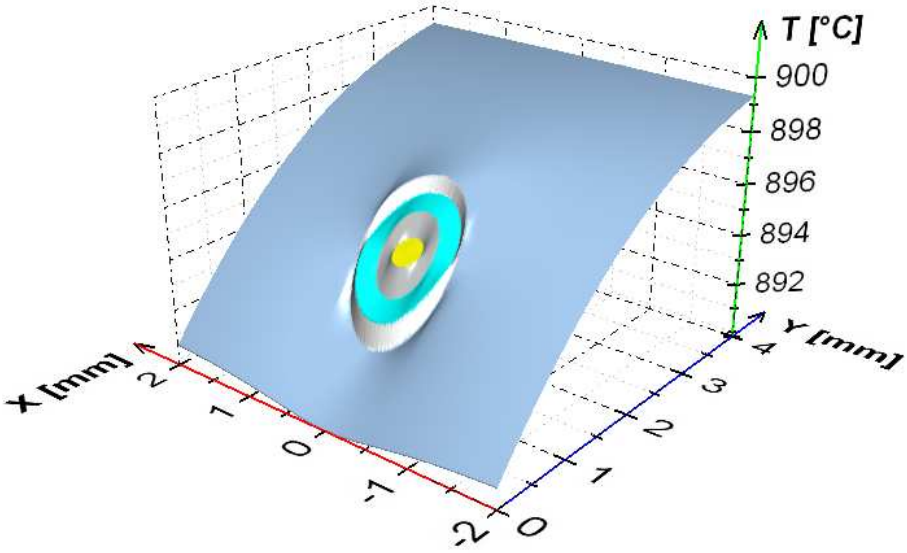

Figure 5 – Temperature profile of the optimized 2D model.

This 2D model and the general unsteady heat conduction equation

$$\frac{\partial}{\partial x}(k\frac{\partial T}{\partial x})+\frac{\partial}{\partial y}(k\frac{\partial T}{\partial y})=\rho\cdot c_p\frac{\partial T}{\partial t} \tag{1}$$

are used for computing the temperature profile and temperature history Incropera (1996). The Control Volume method is used for solving Eq. (1) as described in Patankar (1980). This 2D model is fully insulated on the surface except the investigated surface with water cooling.

5. Evaluation using inverse task

The pass under the nozzle causes temperature drop in the material sample. This information together with material properties and calibration characteristics of temperature sensor is used as an input for the inverse heat conduction task. The results of computation are surface temperature, heat flux and heat transfer coefficient (HTC). Two approaches will be discussed here: sequential Beck's approach (1985) and Identification method Raudenský (2002).

Sequential Beck's approach

The main feature of Beck's approach is sequential estimation of the time varying boundary conditions. Beck demonstrated that function specification and regularization methods could be implemented in a sequential manner and that they gave in some cases nearly the same results as the whole domain estimation. Moreover the sequential approach is computationally more efficient. Beck's approach has been widely used to solve inverse heat conduction problems to determine unknown boundary or material property information.

The method uses sequential estimation of the time varying boundary conditions and uses future time steps data to stabilize the ill-posed problem. The HTC is found after determining the heat flux at the surface. To determine the unknown surface heat flux at the current time t^m, the measured temperature responses $T_i^{*,m}$, are compared with the computed T_j^m from the forward solver (e.g. FDM, FVM, FEM, etc.) (Patankar 1980), using n_f future time steps

$$SSE=\sum_{f=m+1}^{m+n_f}\sum_{j\equiv i;i=1}^{n_T}(T_i^{*,f}-T_j^f)^2\ . \tag{2}$$

Using the linear minimization theory, the value of the surface heat flux that minimizes Eq. (2) is

$$\hat{q}^m=\frac{\sum_{f=m+1}^{m+n_f}\sum_{j\equiv i;i=1}^{n_T}(T_i^{*,f}-T_j^f|_{q^m=0})\zeta_i^f}{\sum_{f=m+1}^{m+n_f}\sum_{i=1}^{n_T}(\zeta_i^f)^2} \tag{3}$$

where $T_j^f|_{q^m=0}$ are the temperatures at the temperature sensor locations computed from the forward solver using all the previously computed heat fluxes, but without the current one q^m. The ζ_i^f is the sensitivity of the i^{th} temperature sensor at time t^f to the heat flux pulse at time t^m. These sensitivity coefficients are mathematically the partial derivatives of the computed temperature field to the heat flux pulse, but in this case they physically represent the rise in temperature at the temperature sensor location for a unit heat flux at the surface. The sensitivity coefficient of our interest is defined as

$$\zeta_j^m = \frac{\partial T_j^m}{\partial q^m} \tag{4}$$

Once the heat flux is found for the time t^m, the corresponding surface temperature T_0^m may be computed using the forward solver. When the surface heat flux q^m and surface temperature T_0^m are known, the heat transfer coefficient is computed from

$$h^m = \frac{\hat{q}^m}{T_\infty^m - (T_0^m + T_0^{m-1})/2} \,. \tag{5}$$

This approach is limited to linear problems. However, it can be extended to nonlinear cases. The modification of this procedure involves an outer iteration loop which continues until the computed temperature field is unchanging. The nonlinearity requires iteration only to determine the present value of the heat flux, while the computations to determine the surface temperature and heat transfer coefficient need only be performed once for each time t^m. The sensitivity coefficients are also nonlinear, due to the dependence of the thermal properties on the temperature field, and they must be computed for each iteration.

Once the heat transfer coefficient at the "present" time is computed, the time index *m* is incremented by one, and the procedure is repeated for the next time step. For *n* measured time steps only *n – f* can be computed owing to the use of future data as a regularizing approach.

Sequential Beck's approach in multi-dimensions

The sequential approach can also be used for multidimensional IHCP. The temperatures in one-, two-, or three-dimensional objects with temperature independent thermal properties can be obtained using

$$\boldsymbol{T} = \boldsymbol{T}|_{\boldsymbol{q}=\boldsymbol{0}} + \boldsymbol{\varsigma}\,\boldsymbol{q} \tag{6}$$

where

$$\boldsymbol{T} = \begin{bmatrix} \boldsymbol{T}(m) \\ \boldsymbol{T}(m+1) \\ \vdots \\ \boldsymbol{T}(m+f-1) \end{bmatrix}, \quad \boldsymbol{T}(i) = \begin{bmatrix} T_1^i \\ T_2^i \\ \vdots \\ T_{n_{T^*}}^i \end{bmatrix}, \quad \boldsymbol{q} = \begin{bmatrix} \boldsymbol{q}^{(m)} \\ \boldsymbol{q}^{(m+1)} \\ \vdots \\ \boldsymbol{q}(m+f-1) \end{bmatrix}, \quad \boldsymbol{q}(i) = \begin{bmatrix} q_1^i \\ q_2^i \\ \vdots \\ q_{n_{q^*}}^i \end{bmatrix},$$

$$\boldsymbol{\varsigma} = \begin{bmatrix} \boldsymbol{\zeta}(1) & & & \\ \boldsymbol{\zeta}(2) & \boldsymbol{\zeta}(1) & & \\ \vdots & & \ddots & \\ \boldsymbol{\zeta}(f) & \boldsymbol{\zeta}(f-1) & \cdots & \boldsymbol{\zeta}(1) \end{bmatrix}, \quad \boldsymbol{\zeta}(i) = \begin{bmatrix} \zeta_{1,1}(i) & \cdots & \zeta_{1,n_{q^*}}(i) \\ \vdots & \ddots & \\ \zeta_{n_{T^*},1}(i) & & \zeta_{n_{T^*},n_{q^*}}(i) \end{bmatrix} \tag{7}$$

The sequential approach then temporary assumes that q is independent on time. Then using

$$\boldsymbol{Z} = \boldsymbol{\varsigma}\,\boldsymbol{I}^* \quad \text{where} \quad \boldsymbol{I}^* = \begin{bmatrix} 1_1 & & 0 \\ & \ddots & \\ 0 & & 1_n \end{bmatrix} \quad \text{where} \quad n = n_{q^*} \tag{8}$$

the function to minimize is

$$SSE = (\boldsymbol{T}^{*,m} - \boldsymbol{T}^{m}|_{q=0} - \boldsymbol{Z}^{m}\boldsymbol{q}^{m})^{T}(\boldsymbol{T}^{*,m} - \boldsymbol{T}^{m}|_{q=0} - \boldsymbol{Z}^{m}\boldsymbol{q}^{m}) \tag{9}$$

The matrix derivative of Eq. (9) with respect to $\boldsymbol{q}$ gives the estimated heat fluxes

$$\hat{\boldsymbol{q}}^{m} = [(\boldsymbol{Z}^{m})^{T}\boldsymbol{Z}^{m}]^{-1}(\boldsymbol{Z}^{m})^{T}(\boldsymbol{T}^{*,m} - \boldsymbol{T}^{m}|_{q=0}) \,. \tag{10}$$

After it is obtained, m is increased by one and the procedure is repeated for the next time step.

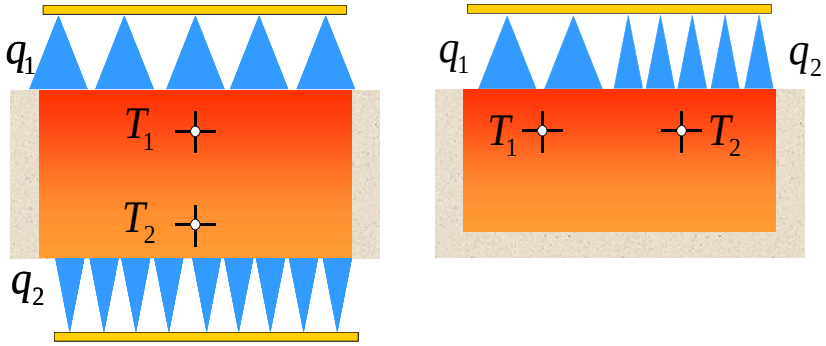

Figure 6 – Multidimensional models and multiple heat fluxes.

Identification method

Probably the main disadvantage of the Beck algorithm is that it assumes constant heat flux (in space domain) on the surface close to the installed thermocouple. As we saw in Figure 5, the surface temperature is disturbed by the installed thermocouple. Knowing that HTC is constant for wide temperature ranges we find out using Eq. (5) that the surface heat flux is not constant. It is even more obvious for surface temperatures approaching temperature of the coolant medium. The disturbances in our cases were over 30%.

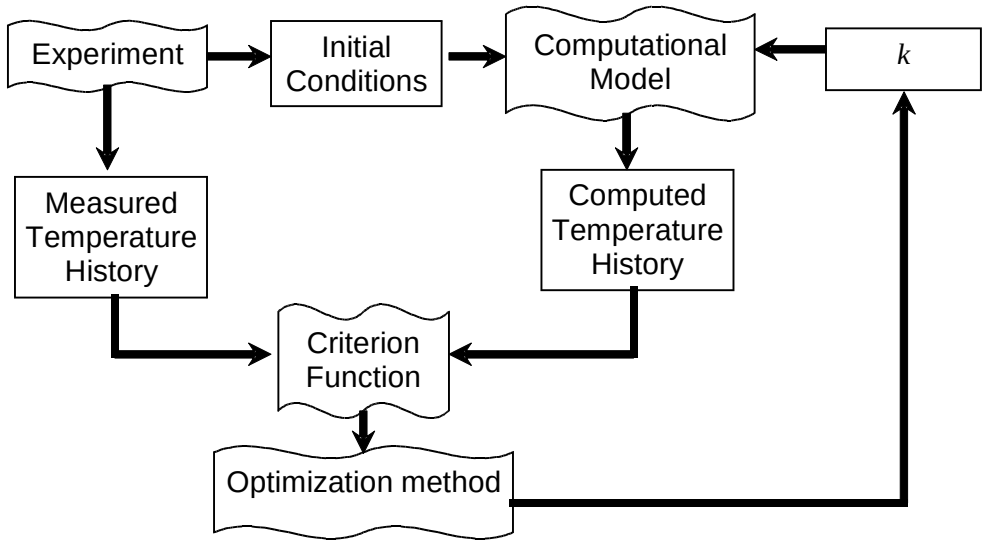

Figure 7 – Data flow during the identification process.

The identification method minimizes the error function in Eq. (2). First, an experiment is performed to obtain initial conditions and the measured temperature history inside the sensor. Using the initial conditions and the computational model, the temperature history is computed using HTC for a few time steps. This number of time steps is called number of forward time

steps. Bigger distance of the installed thermocouple from the investigated surface requires bigger stabilization and thus larger number of forward time steps. The time dependent HTC on boundary can be described using a linear function during these several forward time steps. The computed and measured temperature histories are used in the criterion function Eq. (2). The minimum of this function is found using Brent's method (see Figure 8) or Downhill Simplex optimization method for multidimensional problems (see Figure 9). These optimization methods minimizes the Eq. (2) by changing the boundary conditions e.g. the *k* parameter that is direction of HTC (see Figure 7). The minimum of the criterion function represents the best HTC. For each step HTC and a new temperature history is computed.

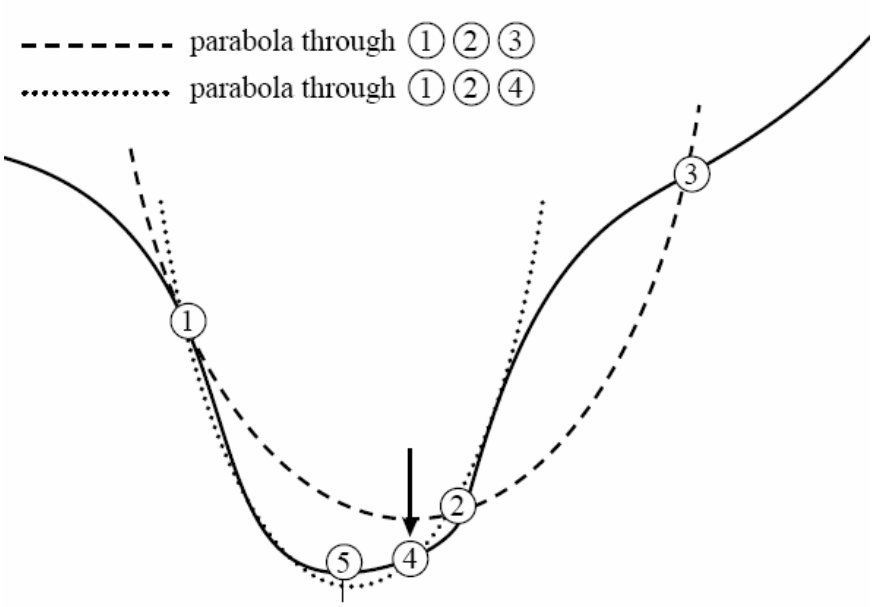

Figure 8 – Brent's method

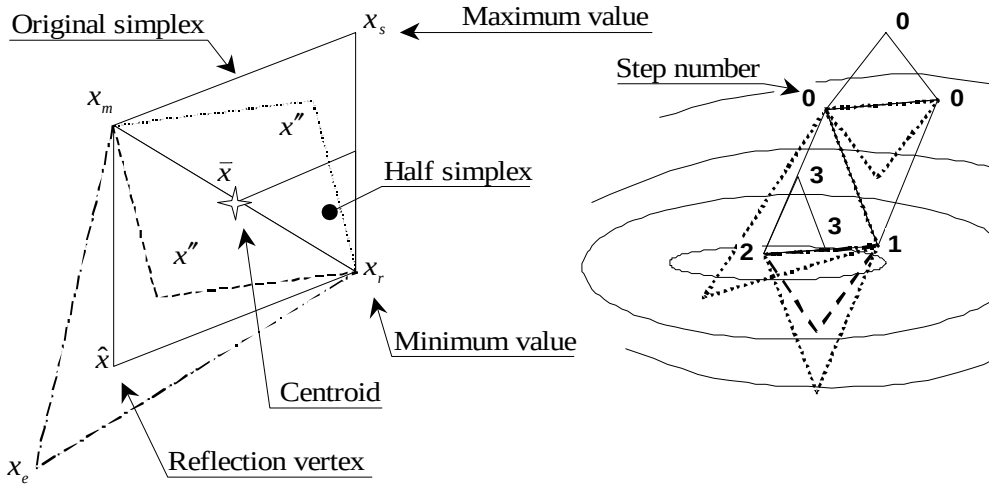

Figure 9 – Downhill simplex method

6. Results

Real measured data were taken to compare sequential Beck's approach with identification method. Tree different computations were made (see Figure 10). The first and the second computations used sequential Beck's approach with 5 and 15 forward steps, respectively. The third one used multidimensional optimization method. For the time when the HTC peak occurred the following equations were used as interpolating functions

$$HTC(x)=(\delta-\gamma)\cdot e^{\frac{-(x-\mu)^2}{2\sigma^2}}+\gamma$$
$$\sigma=\begin{Bmatrix}\sigma_L & for\ x<\mu\\ \sigma_R & for\ x\geq\mu\end{Bmatrix} \qquad (11)$$

where the parameters δ and γ represent the maximum and minimum value of the HTC, respectively. The parameter σ describes the shape in the x direction. The shape for $x<\mu$, where μ represents the nozzle position, is different from $x\geq\mu$. Hence the parameter σ is divided into the two parameters σ_L and σ_R for the left and right sides, respectively.

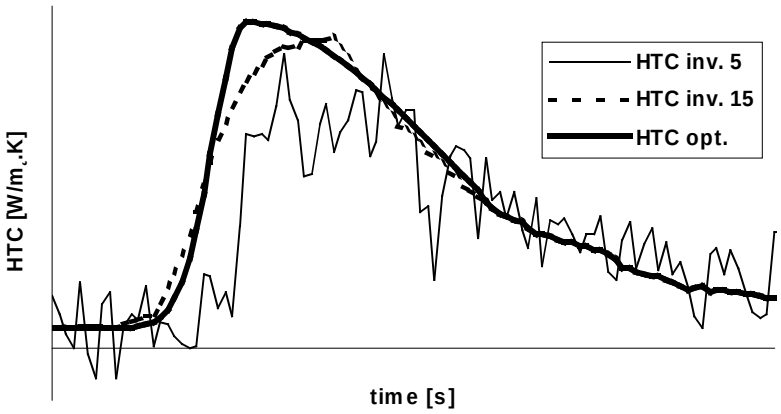

Figure 10 – Comparison of HTC history around HTC maximum.

Classical approach with 5 forward steps matched the measured temperature history almost perfectly. The RMS error was only 0.093 K and the maximum error was 0.25 K. But the computed HTC is very noisy because the HTC tries to follow all noise in the measured temperature history.

The computation with 15 forward steps shows that the noise can be quite well suppressed. But the computed temperature history does not follow the measured very well, the RMS error increased to 0.273 K and the maximum error was 0.96 K. High numbers of forward steps limit the maximum steep and also maximum value of the computed HTC. The shape of the HTC is also deformed and the maximum is moved to the right on time axis.

Identification method with interpolated curve removed noise in the computed HTC and matched very well the measured temperature history. The RMS error was 0.203 K, which is very close to the noise in measured data. The maximum error was only 0.38 K, which is much lower than in case of classical approach with 15 forward steps.

7. Conclusion

Mathematical procedures and precise inverse computations are used for evaluation of experimental results. Final output format of data are boundary conditions which can be used in numerical models of these processes. This technology makes it possible for engineers and scientists to construct more realistic mathematical models of physical processes.

The combination of two described methods allows increasing precision of inverse calculation. The methods allow evaluating long temperature records. The new investigative approach does not have the negative impact on stability of inverse task.

8. Acknowledgment

The theoretical part of this research work was supported by the Czech Grant Agency within the project No.106/06/0709.

9. Literature

Beck, J. V.; Blackwell, B.; Charles, R. C. (1985) *Inverse Heat Conduction: Ill-posed Problems*. New York: Wiley. ISBN 0-471-08319-4.

Horský, J.; Raudenský, M.; Pohanka, M. (2005) Experimental study of heat transfer in hot rolling and continuous casting. In *Material Science Forum*. Switzerland: Trans Tech Publication, Vols. 473–474, pp. 347–354. ISBN 0-87849-957-1.

Incropera, F. P.; DeWitt, D. P. (1996) *Fundamentals of Heat and Mass Transfer.* 4th ed. New York: Wiley. ISBN 0-471-30460-3.

Patankar, S. V. (1980) *Numerical Heat Transfer and Fluid Flow.* Hemisphere Publishing Corporation. ISBN 0-891-16522-3.

Pohanka, M.; Raudenský, M. (2002) Determination of heat resistances between installed thermocouple and body used for computing heat transfer coefficients. In *Engineering mechanics 2002*, Svratka (Czech Republic), pp. 227–228. ISBN 80-214-2109-6.

Raudenský, M.; Pohanka, M.; Horský, J. (2002) Combined inverse heat conduction method for highly transient processes. In *Advanced computational methods in heat transfer VII*, Halkidiki: WIT Press, pp. 35–42. ISBN 1-85312-9062.

Raudenský, M.; Horský, J.; Pohanka, M.; et al. (2003) Experimental Study of Parameters Influencing Efficiency of Hydraulic Descaling. In *4th Int. Conf. Hydraulic Descaling*. London, pp. 29–39.

THE PROGRESS IN DEVELOPMENT OF NEW MODELS FOR PULSE TRANSIENT METHOD

V. Boháč[1], P. Dieška[2] and Ľ. Kubičár[1]

[1] *Institute of Physics SAS, Dúbravská cesta 9, 845 11 Bratislava, Slovakia, vlastimil.bohac@savba.sk*
[2] *Department of Physics, STU, Ilkovičova 3, Bratislava, Slovakia, peter.dieska@stuba.sk*

Abstract:
The ideal models that are describing measurement methods for the thermophysical properties of solids are usually simple. Their advantage is that they involve just one or two free parameters that could be estimated by simple mathematical procedures. Unfortunately in real experiment the situation is limited by specimen geometry and thus the principally simple model derived for usually infinitive media could not be valid. This gives rise to the additional effects that influence the accuracy of the measurements. The most important of them are the heat loss effect form the sample surface caused by final geometry of the specimen as well as the stabilized temperature of the specimen holder that fixes the temperature at the specimen surfaces. The result is that the heat flux that forms planar isotherm penetrates into the specimen is deformed in time and thus the ideal model is valid just in limited time window. Then the evaluation procedure is based on manual selection of the time window for evaluation. This is complicated and depends on the subjective selection of the user. Newly derived multi-parametric models are accounting mentioned parameters. This is on the cost of mathematical complexity of evaluation procedures but it is not dependent on user as the evaluation procedure uses not limited time window for parameters estimation.
This paper review the methodology used in several steps. It is shown how to develop procedures for testing and how to find criteria for particular cases. The improvements of the existing and new physical models that are taking into account the real experimental conditions are discussed.

Keywords:
pulse transient method, thermophysical properties, heat loss effect, real physical models

INTRODUCTION

A modern technology requires rapid development of materials and their testing methods. Thermal properties of materials are one of basic criteria how to recognize between good and bad in a new offer on a market. Thus the new testing procedures are required in this area also. The class of transient techniques has been developed that should satisfy all the testing requirements of new technology [1, 2, 3, 4, [5]].

The use of any technique is conditioned by good knowledge of physical model and the effects influencing the resulted data. Consequently the working methodology of measurements, the evaluation procedures and testing of physical models are prerequisite condition for perfect experiment. The basic question is the reliability of the method that depends on experimental conditions and adequate physical models that should account all experimental circumstances.

In the case of basic idel model for a pulse transient technique a specimen of infinitively large specimen was accounted. It was assumed a planar form of isotherms that penetrates into the specimen from the heat source that generates a heat in aform of dirac pulse. No additional effects were taken into account. The problem comes with real specimen size when disturibing effects are causing the decrease of measurement reliability. Thus research for a new physical approach to solve deficiency in the size (large amount) of testing material was started.

At the pulse transient method the problem was concentrated on a real problem with finite geometry of the specimen that invokes additional effects that harm the efficiency of standard way of the measurement evaluation. One of dominant effects found by data analysis is the heat loss effect from free specimen surface. This effect could be avoided by various ways using different physical models working with infinite and finite geometry and heat losses effect. The new physical aproach could solve a problem with the deficiency in a large amount of testing material.

Three different models used for data evaluation and four evaluation methods are discussed in this paper. As a model material a PMMA specimens of different thickness were used. When the ideal model and standard one point evaluation procedure was used the data were strongly influenced by heat loss effect at different thickness of the specimen. There are discussed two approaches how to avoid this problem in real experiment. The first approach uses limited time of recorded data (time window) and ideal model with infinite geometry for parameters evaluation. Here it was prooved that the temperatures recorded at short times are not influenced by heat loss effect. The next approach at new models introduce next parameters - a heat transfer coefficient that represents heat loss effect from the free sample surface and real geometry, e.g. the real radius and length of the specimen. Results obtained within developed methodology agree with recommended data within 5% for all discussed models.

Methodology found show the way of parameters estimation when possible effects does not influence the reliability of the results.

THEORY

In previous works we observed various disturbance effects that were eliminated by searching the ideal geometry of the specimen. The modified model used in older works considered real pulse width instead of Dirac's pulse. Experimental arrangement is draw in Figure 1.

Ideal model with infinite specimen geometry is used to keep low number of unknown parameters but sometimes do not satisfy the real experiment. A detailed study has to be performed to find experimental circumstances when disturbing effects influence ideal model. Then, the modified model has to be used that take into account additional disturbing effects characterized by corresponding, and usually unknown parameters [6, 7, 8, 9]. In the following we introduce a

difference in models based on ideal case when assuming infinite specimen geometry and the real pulse duration and a new model with real sample radius and heat loss effect from the free sample surface. The principle of the method is to record the temperature transient response to the heat pulse generated by plane heat source and to calculate the thermophysical parameters from the characteristic features of measured curve (Fig. 1). Transient temperature response measured at the distance *h* from the heat source is calculated according temperature function *T(h,t)* providing that ideal model (Eq. 1.) is valid [1]. In an ideal model we assume that a planar temperature wave is not deformed as it penetrates into the deep of the specimen bulk (white-dotted area in the Fig. 1). The problem is that the temperature isotherms are not planar over the cross section of the specimen and are deformed at the edges by the heat losses from the sample surface for large distances.

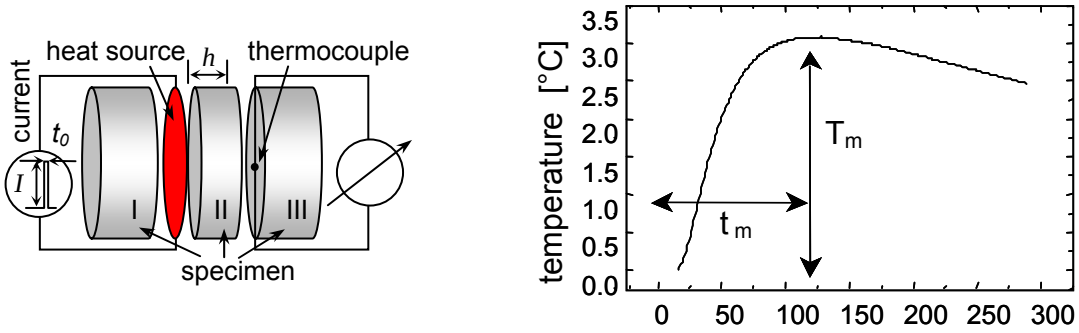

Figure 1. The principle of the pulse transient method (left). The example of the temperature response for PMMA is on the right.

Ideal model

In previous experiments a correction of model considering the real pulse width t_0 was applied to ideal model. Pulse of lower power, but of longer duration replaces the Dirac's pulse as the big instant power can damage specimen. Then, the modified ideal model is characterized by equation [1]

$$T(h,t) = \frac{2 \cdot q_0}{c\rho\sqrt{k}} \left[\sqrt{t} \cdot i\Phi^* \left(\frac{h}{2\sqrt{kt}} \right) - \sqrt{t - t_0} \cdot i\Phi^* \left(\frac{h}{2\sqrt{k(t - t_0)}} \right) \right] \quad (1)$$

where

$$i\Phi^* = \frac{e^{-x^2}}{\sqrt{\pi}} - x \cdot erfc(x) \quad (2)$$

Here q_0 means heat flux from the source, *c* is specific heat, *k* is thermal diffusivity and *t* is time. Equation 1 should be used for data evaluation by fitting procedure.

One point evaluation model

At the standard experiment due to fast calculations we use simple relations for the evaluation of the thermal diffusivity, specific heat and thermal conductivity. These relations were derived for the maximum of temperature response (one-point evaluation procedure). The thermal diffusivity is calculated according equation

$$k = h^2 / (2t_m \cdot f_a) \tag{3}$$

and specific heat

$$c = q_0 t_0 / (\sqrt{2\pi e}\,\rho h T_m) \cdot f_c \tag{4}$$

where f_a and f_c are correction factors and ρ is the density of material. T_m is maximum of transient temperature response at time t_m (Fig. 1.)

$$f_a = (t_m/t_0 - 1) \cdot \ln\left(\frac{t_m/t_0}{t_m/t_0 - 1}\right) \tag{5}$$

$$f_c = 2 \cdot \exp(1/2)\sqrt{\pi f_a} \cdot t_m/t_0 \left\{1/\sqrt{\pi}\left[\exp(-f_a/2) - \sqrt{1 - t_0/t_m}\,\exp\left(f_a (t_m/t_0)/2(t_m/t_0 - 1)\right)\right] - \right.$$
$$\left. - \sqrt{f_a/2}\left[erfc\left(\sqrt{f_a/2}\right) - erfc\left(\sqrt{f_a (t_m/t_0)/2(t_m/t_0 - 1)}\right)\right]\right\} \tag{6}$$

Thermal conductivity is given by

$$\lambda = h q_0 t_0 / (2t_m \sqrt{2\pi e} T_m) \frac{f_c}{f_a} \tag{7}$$

Real model

In the next steps several models were derived that takes into account the real radius of the specimen and it‘s real lenght as well as the next parameter that represents the heat flow from the specimen surface into the surrounding. The case of real specimen with heat loss effect is drawn in figure 3. and the infrared picture from experiment in figure 4.

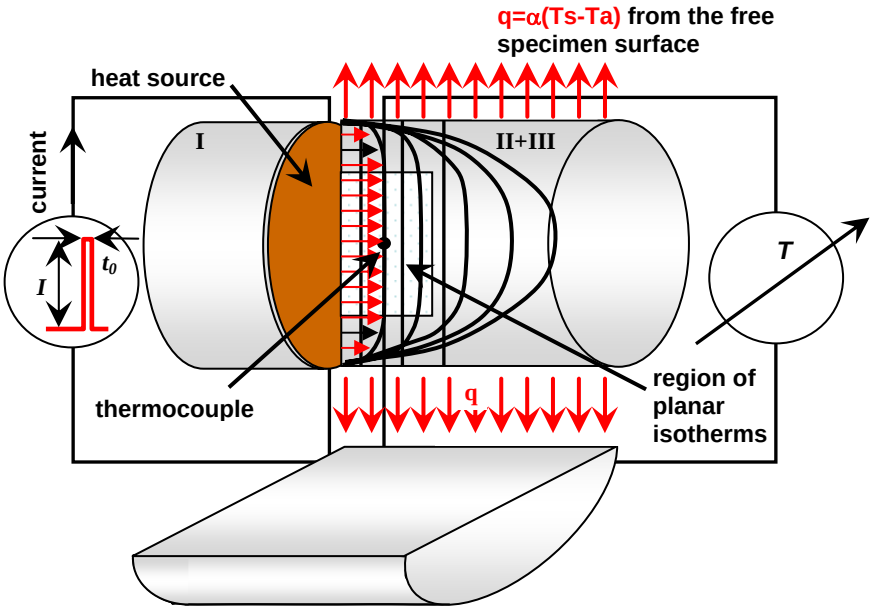

Figure 2. Drawing that represents development of the heat flow outside the specimen. Planar isotherms inside the specimen near the surface are deformed. q is the heat flow outside the specimen, Ts and Ta – surface and ambient temperatures, α - Heat transfer coefficient.

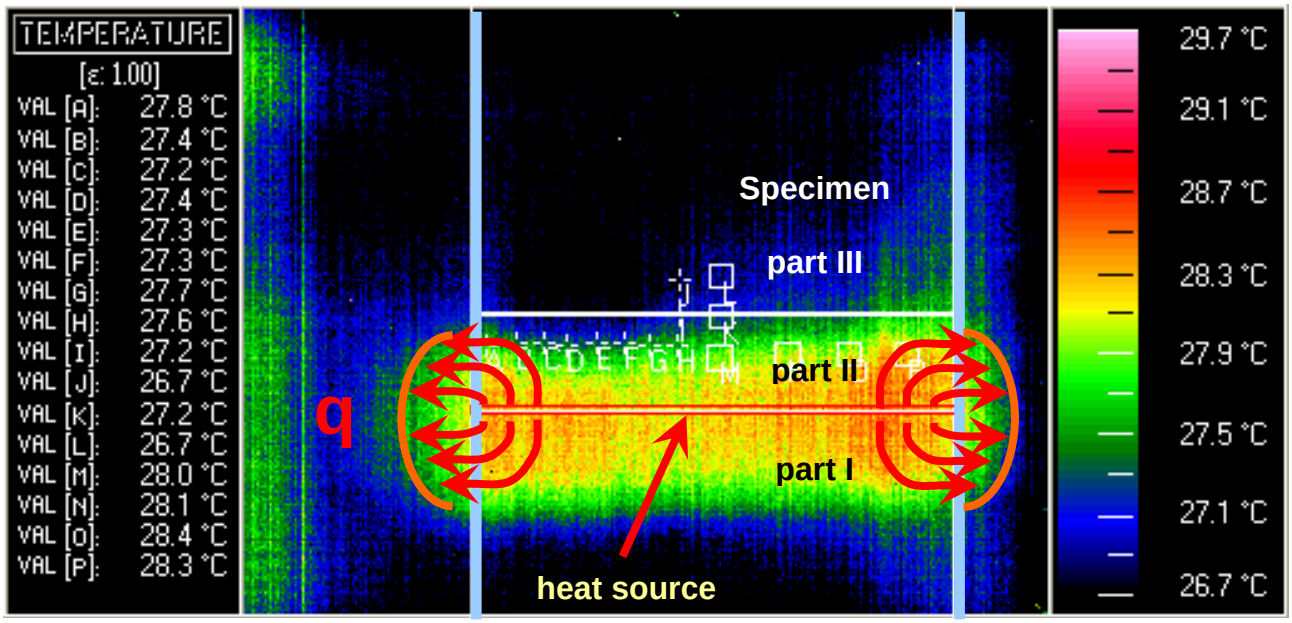

Figure 3. Infrared picture of specimen representing the spreaded heat pulse taken in time when maximum of the temperature response was ritched. The heat flow from the sample surface is denoted by red arrows.

The previous problem with heat loss effect shown in drawing and in picture of a heat loss effect was solved in a two steps. The new models were derived at defined initial and boundary conditions for basic heat transport equation. The heat losses were taken into account at real radius of the specimen and heat source R for the first model and also infinite length L for the second new model.

Real model for finit radius and infinite length (model 3). This model considering heat losses from the specimen surface, the specimen radius, and infinite length (figure 4). In this case the heat loss from the specimen surface is considered by heat transfer coefficient α. The temperature function of the heat equation according to [10] has a form

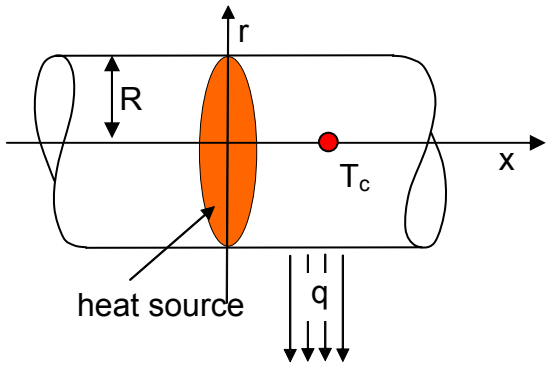

Figure 4. Model of specimen having finite radius R, infinite length and heat losses form the sample surface. The model parameters are of the same meaning like in a case of ideal model.

$$T_c(t,x,r)=\beta\frac{Q}{\lambda}R\sum_{i=1}^{\infty}\frac{J_0\left(\xi_i\frac{r}{R}\right)}{\xi_i\left(\xi_i^2+\beta^2\right)J_0(\xi_i)}\left[e^{-\xi_i\frac{x}{R}}\Phi^*\left(\frac{x}{2\sqrt{kt}}-\xi_i\frac{\sqrt{kt}}{R}\right)-e^{\xi_i\frac{x}{R}}\Phi^*\left(\frac{x}{2\sqrt{kt}}+\xi_i\frac{\sqrt{kt}}{R}\right)\right] \quad (8)$$

where $\beta = \frac{\alpha R}{\lambda}$; $\{\xi_i\}$ are the roots of the equation $\beta J_o(\xi) - \xi J_1(\xi) = 0$, Q – is the heat output power per unit area of the heat source and $\Phi^*(x) = 1 - \Phi(x)$ is complementary error function,. $\Phi(x) = \frac{2}{\sqrt{\pi}} \int_0^x e^{-t^2} dt$.

The equation (8) characterizes the step-wise measuring regime. For the duration of the heat pulse t_0, the temperature for $t > t_0$ is expressed by the equation

$$T^*(t,x,r) = T(t,x,r) - T(t - t_o, x, r) \tag{9}$$

where $T(t,x,r)$ and $T(t-t_0,x,r)$ are given by the equation (8). The equation (9) characterizes the pulse transient regime.

$$c = \frac{\lambda}{k \cdot \rho}$$

Real model for finit radius, finite length and stabilized temperature of the specimen holder at the specimen end (model 9). This model considering the heat loss from specimen surface (finit specimen radius), finite length of the specimen and T_0 – the heat sink temperature is on ther Figure 5.

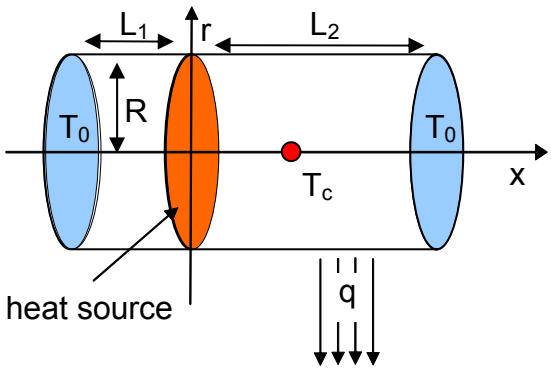

Figure 5. Model using the specimen of finite radius R, finite length L and L_1 and heat losses form the sample surface represented by.

The temperature function of the heat equation in this case has the form

$$T_c(t,x,r) = T_0 \frac{8R^2}{(L_1 + L_2)x} \sum_{\zeta} \frac{\beta}{\zeta^2 + \beta^2} \frac{J_0\left(\zeta \frac{r}{R}\right)}{J_0(\zeta)} \times g(t,x,\zeta) \tag{10}$$

where $\beta = \frac{R\alpha}{\lambda}$, $T_0 = \frac{qx}{\lambda}$ and

$$g(t,x,\zeta) = \sum_{n=1}^{\infty} (-1)^{n-1} \frac{1 - \exp\left\{\frac{-kt}{R^2}\left[\zeta^2 + \left(n\pi \frac{R}{L_1 + L_2}\right)^2\right]\right\}}{\zeta^2 + \left(n\pi \frac{R}{L_1 + L_2}\right)^2} \sin\left(n\pi \frac{L_1}{L_1 + L_2}\right) \sin\left(n\pi \frac{L_2 - x}{L_1 + L_2}\right)$$

Meaning of another parameters are denoted in figure 6 as well as in previous model. Again, for the duration of the heat pulse t_0, the temperature for $t > t_0$ is expressed by the equation 9.

MEASUREMENTS

All experimental measurements were performed in RTB1.02 chamber (IP SAS) at the temperature 25°C with the temperature stability 0.01÷0.02 K. As a model material a PMMA specimens of different thickness were used. For higher data reliability the statistics at least 5 subsequent measurements were done for each sample thickness.

For the data evaluation there were used various methods (procedures) that uses one point procedure evaluation (ideal model) as well as fitting procedures. Subsequently there were calculated a theoretical responses using corresponding models and were compared with experimentally measured one. The models used assumed experimental conditions with model that uses real pulse width and infinite geometry of the specimen (uses one point evaluation procedure and time window fit procedure), real pulse width, heat loss, finite radius and infinite length of the specimen (fit procedure), real pulse width, heat loss, finite radius and finite length of the specimen (fit procedure).

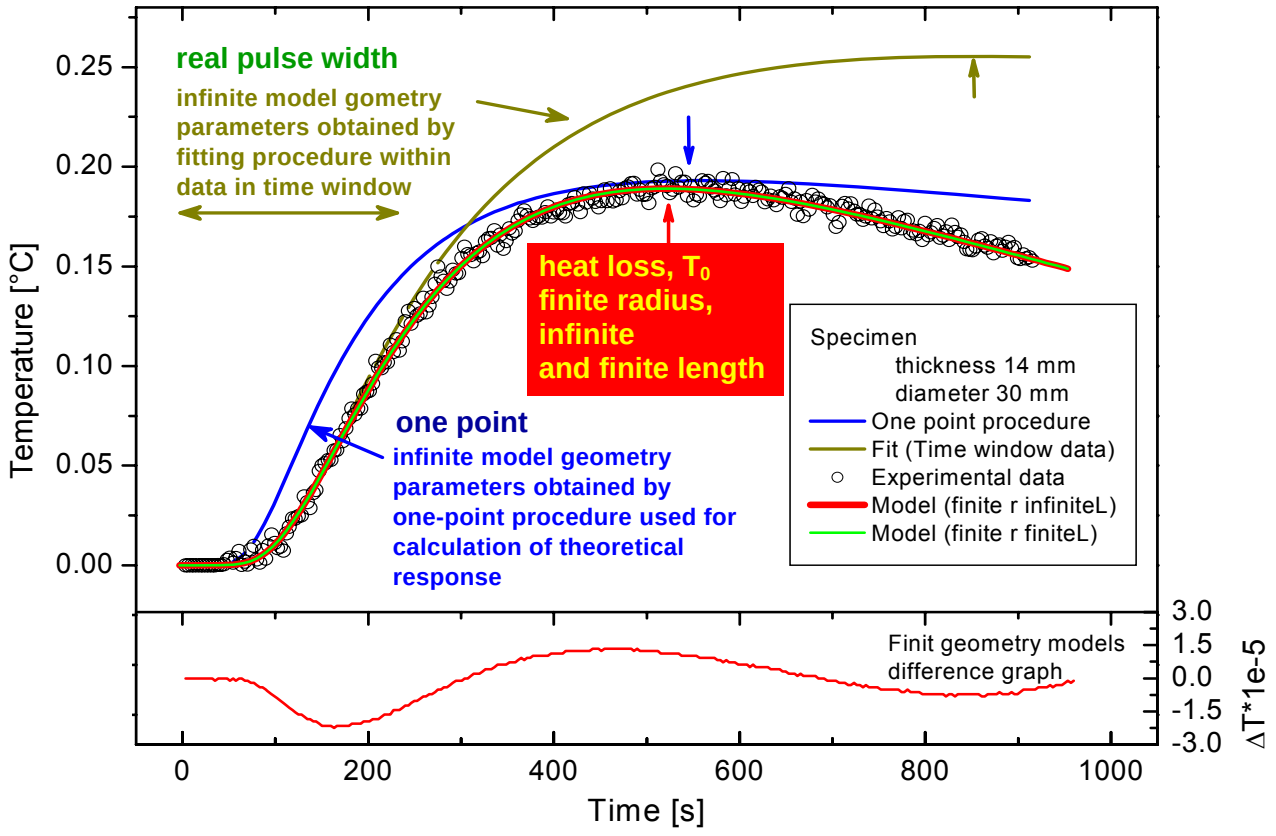

Figure 6. Comparison of experimentaly measured data of temperature response (circles) with the theoretically calculated temperature responses using 4 different evaluation procedures based on 3 models. The difference graph is at the bottom of drawing to illustrate small difference in fit quality between the new models.

The comparison betweeen the real data and theoretically calculated temperature responses based on three models we illustrate in Figure 6 on the data measured on specimen with diameter of

50 mm and the specimen thickness of 20 mm. For the calculation of theoretical responses the parameters obtained by 4 evaluation procedures were used for the calculation of theoretical responses. All the theoretical temperature responses in figure 6 were calculated using thermophysical parameters evaluated by four different procedures – one point evaluation (Eq. 2 and 3.), fit of the data for small times up to 200 s. using Eq. 1 and the fit of all data using combinations of Eq. 9 with equation 8 for first model and equation 10 for second model with real geometry.

Procedure one. In the previous works it was used ideal model (Eq. 1), and one point evaluation procedure for parameters estimation (Equations 3, 4 and 7). Parameters calculated by this procedure were influenced by heat loss effect and data were shifted towards higher values as it is cler from Figure 7 – the plot of thermophysical data vs. specimen thickness. Due to problem with the heat loss effect just data measured at the specinen thickness that ranges from 6 to 8 mm are supposed for reliable. This thickness range was declared as optimized geometry. Within this model, when using standard one point evaluation procedure (Equations 3, 4 and 7) it was found that the heat losses from the sample surface aparently increases the measured values of all thermophysical parameters (Figure 7). The data shift dependens on specimen geometry, (e.g. the thickness and radius) and depends on time during which the experiment was influenced by this factor. Next it was found that the influence of heat source effects for low thicknesses causes lowering of values of thermophysical parameters. This is caused by heat capacifty of the heat source as well as by contact resistance.

Procedure two. The next evaluation procedure uses data in limited time region for data evaluation by fitting procedure based on Equation 1 [9]. In practice this limited time region was named as a "time window for data evaluation" and was already taken from a region of temperatures recorded at lower times, e.g. the times when temperatures did not reach the maximum of the temperature response. With an increasing time the increase of temperature difference between the theoretically calculated temperature response and really measured one is clear (Figure 6). These differences satisfy to effect of the heat loss from the sample surface when the temperature inside the specinmen is lowered (Figure 2 and 6). Figure 6 shows an illustration of this effect measured on PMMA specimen. All the experimental details for this procedure were described in [9]. Figure 6 shows that the shape of experimental response is different as the theoreticaly calculated one for this model due to known effect.

Compared results obtained with the previous procedure are in Figure 7. Situation is improved and all data were pushed down towards the values on the line with recommended data.

Procedure three. Experimental data of temperature response was fitted by equation 9 assuming equation 8 for given geometry of this model. The fit on Figure 6 match the experimental data. The resulted parameters are in figure 7 and are again dissipated around recommended values of thermophysical parameters.

Procedure four. Experimental data of temperature response was fitted by equation 9 assuming equation 10 for this last geometry arrangement. The fit Figure 6 match the experimental data in whole time range also. The resulted parametwers are in figure 7 and are closer to recommended values of thermophysical parameters than previous model mainly for higher specimen thicknesses.

The difference in shape of a theoretically calculated temperature response using parameters calculated by one point procedure from equations 1 and 2 is evident. The better situation is in the case of fitting procedure of data from initial time window (in the range from 1 up to 200 s depicted by line with arrows) by the equation 1. Here we can see clear effect of the decrease of the temperature response in comparison with ideal case when no heat loss is assumed. In the case of two models assuming real sample radius, finit length and heat loosses from the sample surface the values of the temperature response theoretically calculated fits the experimentaly measured one. There is just small difference between the fit of the new models. A difference graph in figure 7 at the bottom is given for illustration.

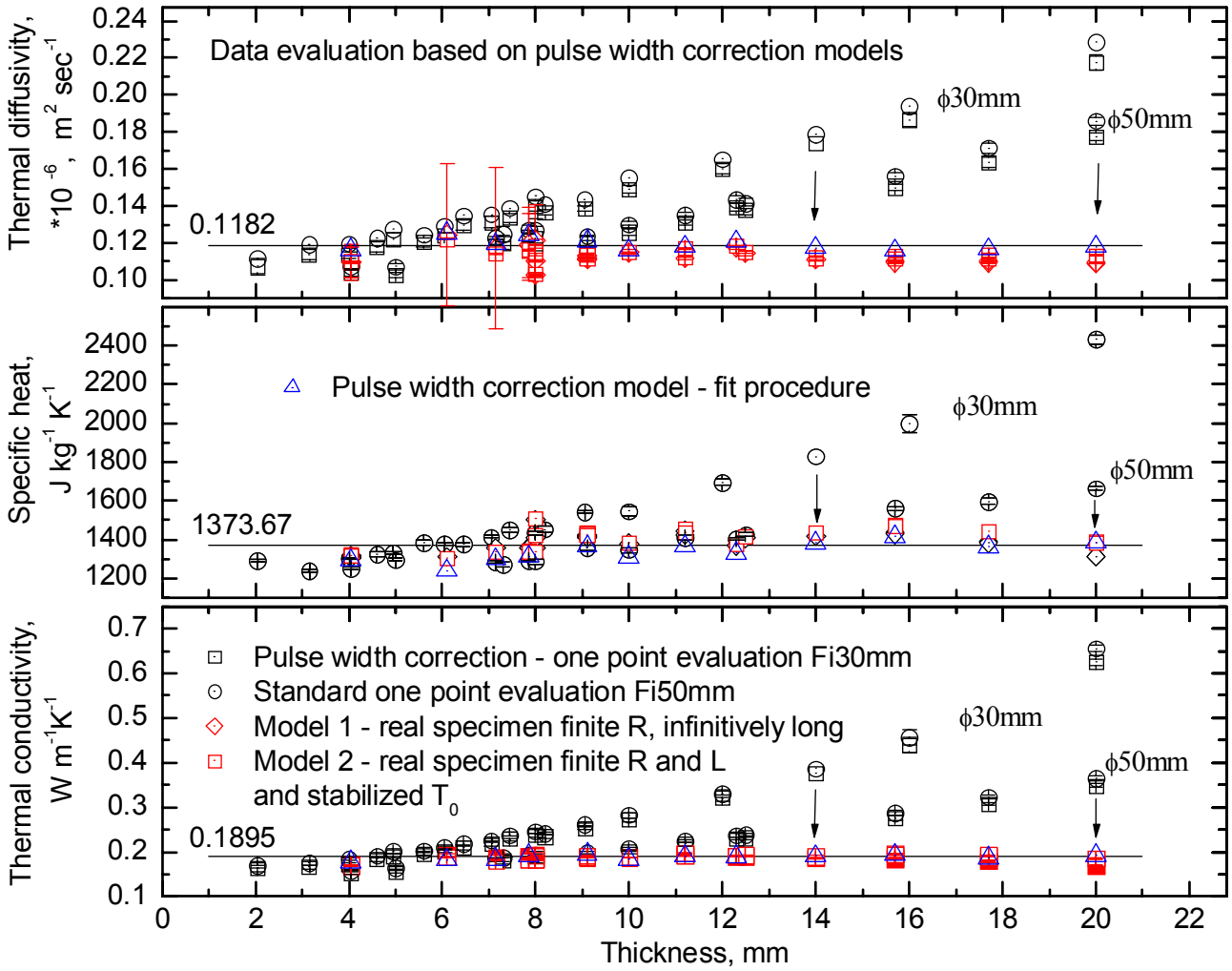

Figure 7. thermophysical data measured on PMMA obtained for different specimen thicknesses.

CONCLUSIONS

The PMMA was used for the measurement of thermophysical properties as model material for the testing of new and existing thermophysical models for pulse transient technique. It was shown methodology how to optimize the experiment geometry and shown methodology how to test and improve the model reliability.

It was discussed heat loss effect and it's influence on the reliability of measured parameters. It was given a methodology reviewed in several steps using different ways of parameters estimation, e.g. the model assuming real pulse width using one point procedure that is available only for the specimens having optimal geometry, the same model using fitting procedure of onset of temperature response (subjective for the choice of the fitting time interval), and models assuming heat loss from the sample surface as well as finite geometry of the specimen.

The optimal geometry as well as proper time window criteria was found when no influences of mentioned effects take place during experiment. Here the one point evaluation model was used for the case of data measured at optimal geometry and the fitting procedure evaluation for the data taken from the onset of a temperature response (time window) for larger specimen thicknesses.

It was shown that the fitting procedure based on model assuming infinite sample geometry should be used just in a time window of the initial onset of the temperature response. This

procedure requires to sets manually the time window for evaluation by fitting procedure and thus it seems to be not very objective as it depends on user. The advantage of one point evaluation procedure that uses ideal model is, that is simple and independend on user, but it is available only under the condition when optimized specimen geometry is used [9].

The presented new models are assuming real sample radius and heat loss effect from the sample surface. The fit of the real experiment is excellent and operates automatically.

In a given methodology the error of the measurements were suppressed. Resulted estimated parameters are within 5 percents of the recommended values.

ACKNOWLEDGEMENTS

Authors are thankful to Dr. Hammerschmidt, PTB for providing specimens of PMMA. The work was supported by Slovak grant agency under a project numbers No. 2/5100/25 - Study and modeling of the thermophysical properties of composites.

REFERENCES

[1] Kubičár, Ľ. (1990): Pulse method of measuring basic thermophysical parameters.Comprehensive Analytical Chemistry, ed. G. Svehla, Elsevier, Amsterdam, Tokyo, Oxford, New York

[2] Kubičár, Ľ. Boháč, V. (1999): Review of several dynamic methods of measuring thermophysical parameters. in "Proc. of 24th Int. Conf. on Thermal Conductivity / 12th Int. Thermal Expansion Symposium", ed. P.S. Gaal, D.E. Apostolescu, Lancaster: Technomic Publishing Company, pp. 135–149.

[3] Gustafsson S.E. 1991. Rev. Sci. Instrum. 62:797-804

[4] Sabuga W., Hammerschmidt U. International Journal of Thermophysics, 1995, 16 (2): 557-565

[5] Krempaský J.: Meranie termofyzikálnych veličín. Vyd. SAV, Bratislava, 1969, 1-288.

[6] Xin - Gang Liang, 1995 Meas. Sci. Technol. 6 467 – 471

[7] Stosch R, Hammerschmidt, 26th Int. Thermal Conductivity Conference, Cambridge, 4-6, August, 2001,USA

[8] V. Boháč, Ľ. Kubičár, V. Vretenár, HIGH TEMP-HIGH PRESS. 2003/2004, Vol. 35/36, pp. 67-74

[9] V. Boháč et all. Methodology of parameter estimation of pulse transient method and the use of PMMA as standard reference material. Proc. TEMPMEKO 2004, 22 - 25 June 2004 Dubrovník, Croatia

[10] Dešková M., Dieška P., Boháč V., Kubičár Ľ.: Determination of temperature field and an analysis of influence of certain factors on a temperature fields. In collection of manuscripts of the 17th ECTP, 2005, Bratislava, Slovakia. Vozár L., Medveď I. and Kubičár Ľ. editors. (CD-ROM).

APPLICATION OF MAXWELL MIXING RULE IN THE MEASUREMENT OF THERMAL CONDUCTIVITY OF POROUS BUILDING MATERIALS

Zbyšek Pavlík, Lukáš Fiala, Robert Černý

Czech Technical University in Prague, Faculty of Civil Engineering, Department of Materials Engineering and Chemistry, Thákurova 7, 166 29 Prague, Czech Republic, email: pavlikz@fsv.cvut.cz, fialal@fsv.cvut.cz, cernyr@fsv.cvut.cz

Abstract:
Thermal conductivity of a cement-based composite material in dependence on moisture content ranging from the dry state to the water fully saturated state is studied both experimentally and theoretically in the paper. The measurement is performed in laboratory conditions under constant temperature by impulse technique. The experimental data are analysed using the Maxwell-Garnett's mixing rule and the validity of the results is verified by Wiener's bounds. On the basis of performed calculations, the suitability of applied homogenization technique for evaluation of thermal conductivity vs. moisture content function is discussed and its limitations are given.

Keywords:
Thermal conductivity, homogenization techniques, cement-based composites

INTRODUCTION

Cement-based composite materials contain always a significant amount of pores. As the thermal conductivity of the air, filling the porous space of the materials, is approximately 0.026 W/mK [1] and the thermal conductivity of cement stone is (depending on the amount and the type of aggregates) in the range of 1-3 W/mK [2], the total pore volume, distribution of pores, their shapes and cross connections can affect the thermal conductivity of cement-based materials in a very significant way. In usual service conditions of buildings, the cement-based composites always contain certain amount of water that can originate from several sources. The thermal conductivity of water is 0.60 W/mK [1], which is more than 20 times higher than of the air. Therefore, if water is present in the pore space, its effect competes with the effect of air, and the thermal conductivity of a porous composite material can be considered as a result of this competition together with the effect of the cement matrix.

Thermal conductivity as the main parameter describing the heat transport is often subject of measurements for various types of building materials because it plays decisive role in the process of building structures design regarding to thermal resistance and fire protection. In the literature, many examples of thermal conductivity measurements of cement-based materials can be found. However, mostly just one single value is determined (see, e.g., the reviews in [2] – [4]). The dependence of thermal conductivity on moisture content was studied for instance in [5] where empirical relations were obtained but such experiments can be considered as relatively rare.

Homogenization theories working with the concept of an effective medium have proven very useful in a variety of applications in mechanics and in the theory of electricity and magnetism where they already belong to well established treatments (see, e.g., [6]). Their utilization in heat transfer was much less frequent until now. Within the last couple of years, some references

appeared on using the effective media theories for estimation of thermal conductivity of refractory materials, foams, polymer-based composites but for cement-based composites their use is still exceptional.

In this paper, experimental determination of moisture dependent thermal conductivity is done for a composite material on cement basis. The experimental data are analysed on the principle of homogenization using the Maxwell-Garnett‘s mixing rule.

EXPERIMENTAL METHOD AND STUDIED MATERIAL

The thermal conductivity was determined using the commercial device ISOMET 2104 (Applied Precision, Ltd.). ISOMET 2104 is a multifunctional instrument for measuring thermal conductivity, thermal diffusivity, and volumetric heat capacity. It is equipped with various types of optional probes, needle probes are for porous, fibrous or soft materials, and surface probes are suitable for hard materials. The measurement is based on the analysis of the temperature response of the analyzed material to heat flow impulses. The heat flow is induced by electrical heating using a resistor heater having a direct thermal contact with the surface of the sample. The measurements were done in dependence on moisture content form the dry state to fully water saturated state. The moisture content in the samples was measured by gravimetric method.

The measurements were done for carbon fiber reinforced cement composite (CFRC) produced in the laboratories of VUSH Brno (CZ). The composition of CFRC material (calculated among the dry substances only) is presented in Table 1. Portland cement used was CEM I 52.5 produced in cement factory Mokrá (CZ), carbon fiber was PAN-type. The water/cement ratio corresponding to the amount of water added into the mixture was 0.9.

Table 1 Composition of the carbon fiber reinforced cement composite in mass-% of dry substances

Cement	Microdorsilite	Plasticizer	Carbon fiber	Wollastonite	Methyl-cellulose	Defoamer	Microsilica
39.71	16.50	0.98	0.98	39.60	0.11	0.16	1.96

The samples were produced using a successive homogenization procedure. First, wollastonite, microdorsilite and microsilica were homogenized in a mixing device, then cement and methylcellulose were added and the dry mixture was homogenized again. The dry well homogenized mixture was thoroughly mixed with water, defoamer and plasticizer. Then, the carbon fibers were added and the mixture shortly mixed again. Finally, the prepared mixture was vacuum-treated in special moulds with perforated bottom. The material was autoclaved at 180 °C and then dried at 105 °C. After the time period of 28 days after mixing, the samples were prepared for testing.

The measured samples were cut from the plates of 10 mm thickness. For any particular moisture content, five specimens of 60 x 60 x 10 mm were used in the measurements of thermal conductivity. The measurements were performed in the laboratory conditions at 24±1 °C and 30-35 % relative humidity.

HOMOGENIZATION THEORY

In terms of a homogenization theory, a porous material can be considered basically as a mixture of three phases, namely solid, liquid and gaseous phase. In the cement based material

studied in this work, the solid phase is represented by cement, microdorsilite, carbon fibers and wollastonite, the liquid phase by water and the gaseous phase by air. Therefore, the homogenization was performed in three steps. The first task was the determination of thermal conductivity of the cement matrix. This was done on the basis of the known thermal conductivities and amounts of its constituents. In this work, the thermal conductivity of cement matrix was calculated using the Rayleigh [7] mixing rule

$$\frac{\lambda_M - 1}{\lambda_M + 2} = f_c\left(\frac{\lambda_c - 1}{\lambda_c + 2}\right) + f_m\left(\frac{\lambda_m - 1}{\lambda_m + 2}\right) + f_{cf}\left(\frac{\lambda_{cf} - 1}{\lambda_{cf} + 2}\right) + f_w\left(\frac{\lambda_w - 1}{\lambda_w + 2}\right), \tag{1}$$

where λ_M is the thermal conductivity of cement matrix, λ_c thermal conductivity of cement (2 W/mK), λ_m thermal conductivity of microdorsilite (0.33 W/mK), λ_{cf} thermal conductivity of carbon fibers (9.8 W/mK) and λ_w thermal conductivity of wollastonite (2 W/mK), f_c volumetric fraction of cement, f_m volumetric fraction of microdorsilite, f_{cf} volumetric fraction of carbon fibers and f_w volumetric fraction of wollastonite. The values of thermal conductivities of particular components of cement-based composite were taken from CRC Handbook of Chemistry and Physics [1]. Remaining components forming the solid matrix were not taken into account since their amount in the material is of secondary importance regarding the total thermal conductivity of the studied material.

The second step was the determination of thermal conductivity of the dry material where only the solid and gaseous phases are to be considered. This was realized using the volumetric fraction of the air obtained in porosity measurements and the known thermal conductivities of the matrix and the air. The total open porosity of the studied material was measured by mercury porosimetry and calculated from the total intrusion volume and known bulk density. The results of these measurements are given in Table 2.

Table 2 Basic parameters of the porous space of the studied cement-based composite material

Bulk density [kg/m^3]	Total intrusion volume [cm^3/g]	Total pore area [m^2/g]	Median pore diameter [μm]	Total open porosity [-]
1468	0.216	42.97	0.0236	0.32

For the evaluation of thermal conductivity of the whole material, which is the third and last step of the homogenization procedure, the mixing is performed for cement matrix, air and water. The mixing was done using Maxwell-Garnett's formula [8] based on the assumption that the basic thermal conductivity of the composite material is that of the solid matrix. The Maxwell-Garnett's formula extended to the three-phase system (originally it was derived for a two phase system only) is expressed in equation

$$\frac{\lambda_{eff} - \lambda_M}{\lambda_{eff} + 2\lambda_M} = f_a\left(\frac{\varepsilon_a - \lambda_M}{\varepsilon_a + 2\lambda_M}\right) + f_{fw}\left(\frac{\varepsilon_{fw} - \lambda_M}{\varepsilon_{fw} + 2\lambda_M}\right), \tag{2}$$

where λ_{eff} is the effective thermal conductivity of the whole porous material, λ_M the thermal conductivity of cement matrix, λ_a thermal conductivity of air, λ_{fw} thermal conductivity of free water, f_a volumetric fraction of air and f_{fw} volumetric fraction of free water.

For the verification of obtained results, Wiener's bounds [9] for parallel and serial model were used. These bounds in fact represent upper and lower limits of the effective thermal conductivity vs. water content function. The Wiener's bounds are given in the following relations

$$\lambda_{eff} = \frac{1}{\frac{\lambda_M}{\lambda_M} + \frac{f_a}{\lambda_a} + \frac{f_{fw}}{\lambda_{fw}}}, \tag{3}$$

$$\lambda_{eff} = f_1\lambda_1 + f_2\lambda_2 + f_3\lambda_3 . \tag{4}$$

RESULTS AND DISCCUSION

The measured results of the dependence of thermal conductivity on moisture content are given in Fig. 1, together with the thermal conductivity vs. moisture content functions calculated using the Maxwell-Garnett's formula and Wiener's parallel and serial bounds.

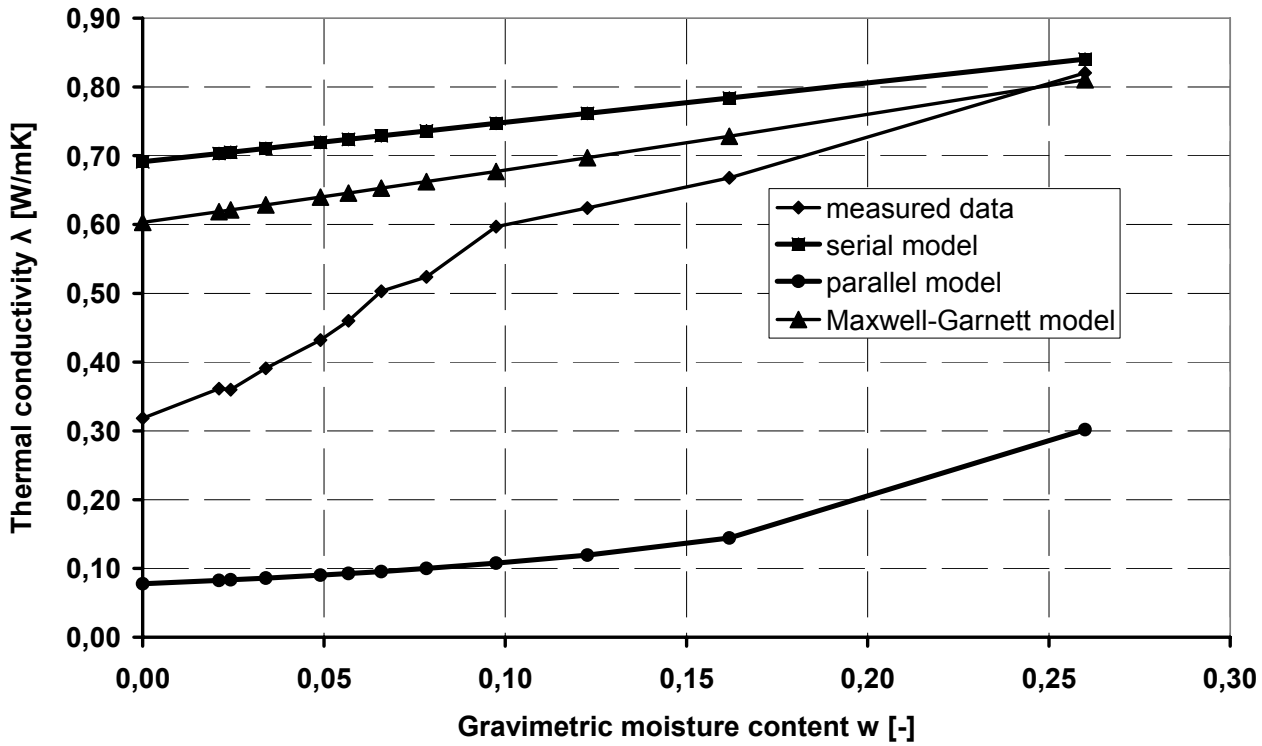

Figure 1 Thermal conductivity of cement based composite material

The experimental results give information on a very substantial moisture effect on thermal conductivity of the studied material which is in basic agreement with its relatively high total open porosity. From the point of view of Wiener's bounds, we can see that the calculated results as well as the experimentally measured data lie between the serial and the parallel model, which basically justifies the reasonable accuracy of both experiment and calculations. Looking at the data from the point of view of accuracy of the analyzed Maxwell-Garnett's formula we can see very high

differences (up to 50 %) between measured and calculated data especially for lower moisture contents. For higher moisture contents the measured and calculated values are in slightly better agreement but also here the differences are typically about 10 %. The differences in the range of lower moisture contents are probably caused by the inaccuracies in the thermal conductivity values of the particular components forming the matrix of the material taken from CRC Handbook of Chemistry and Physics [1]. The better agreement in the range of higher moistures can be attributed to the higher effect of water thermal conductivity (measured with sufficient accuracy in many references) on the thermal conductivity of the composite.

CONCLUSIONS

The measured data presented in this paper can find utilization in practical applications of the studied cement based composite material containing carbon fibers. However, the application of Maxwell-Garnett's mixing formula for the calculation of thermal conductivity in dependence on moisture content was not found to provide useful estimates of measured data. Some other, more detailed analysis will be necessary, with a particular attention to the thermal conductivity values of the components of the cement matrix.

ACKNOWLEDGMENT

This research has been supported by Ministry of Education, Youth and Sports of Czech Republic, under project No MSM: 6840770031.

REFERENCES

[1] Lide D. R. (ed.), CRC Handbook of Chemistry and Physics, 79th Edition, CRC Press, Boca Raton, 1998.

[2] Černý R., Rovnaníková P., Transport Processes in Concrete, Spon Press, London, 2002.

[3] Neville A. M., Properties of Concrete, Pitman, London, 1973.

[4] Bažant Z. P., Kaplan M. F., Concrete at High Temperatures: Material Properties and Mathematical Models, Longman, Harlow, 1996.

[5] IEA-Annex XIV, Condensation and Energy, Volume 3, Material Properties, International Energy Agency, Leuven, 1991.

[6] Sihvola A., Electromagnetic Mixing Formulas and Applications, The Institution of Electrical Engineers, London, 1999.

[7] Lord Rayleigh, On the influence of obstacles arranged in rectangular order upon the properties of the medium. Philos. Mag. 34(1892), pp. 481–502.

[8] Maxwell Garnett, J.C., Colours in metal glasses and metal films. Trans. Of the Royal Society (London) 203 (1904), pp. 385-420.

[9] Wiener, O., Die Theorie des Mischkoerpers fuer das Feld der stationaeren Stroemung. Abhandlungen der Mathematischen-Physischen Klasse der Königlichen Sächsischen Gesellschaft der Wissenschaften 32(1912), pp. 509-604.

Critical behavior of selected composites – experimental investigation

Ing. Jozef Bielek, CSc.,
Department of Physics, FEI STU, Bratislava,
812 19 Ilkovičova 3

jozef.bielek@stuba.sk

Abstract:

Contribution deals with the application of set of selected physical parameter in the study of a critical composite systems behaviour. The paper concentrates on thermophysical parameters.

Predložená práca bude sa zaoberať vybranými zloženými materiálovými systémami na báze polyolefínov (homopolymér **PE**, resp. **PP**), ktoré boli modifikované v období ropnej krízy **$CaCO_3$**, resp. **kaolínom** so zameraním na vybrané termofyzikálne parametre, predovšetkým **λ** – súčiniteľ tepelnej vodivosti, ku skúmaniu ktorého bola použitá stacionárna porovnávacia metóda [1], ktorá umožnila pre tieto systémy dosiahnuť najlepšie výsledky. Práce [2-7] preukazujú isté pokusy zvládnutia tejto problematiky vo svete, na báze prevažne **elektrónovej perkolácie** [7] pomocou ktorej bolo možné modifikačnými prímesami pretvoriť **dielektrikum na elektrický vodič**. Práca [5] tab. 7 pekne vymedzila prechod od jednoduchých materiálov k zloženým materiálovým systémom.

Experimentálne preukázanie narušenia pravidla látkovej bilancie umožnilo p. Prof. Š. Bartovi jednoznačne poukázať na **fonónový príspevok** cez jasné a jednoducho zavedené **kritické indexy,** o ktorých pre naše pomery monografia [16] neposkytla **žiadne informácie,** okrem poukazu na **kooperatívne** pôsobenie. Veľmi cenné príspevky boli získane v spolupráci s Bratislavskými elektrotechnickými závodmi, n. p., pri skúmaní **epoxidovej živice** modifikovanej kryštalickým **SiO_2** [11-13]. Tento systém bol preskúmaný pomocou impulznej metódy s plošným zdrojom [1]. Aj na tieto výsledky sme získali AO a boli primerane zverejnené.

Patentové spisy [18-19] podchycujú skúmanie **gumárenskej zmesi** výrobku n. p., Gumárne, Púchov, pomocou impulznej metódy s plošným zdrojom [1], pri jej modifikovaní **hydroxidom hlinitým**, spolu s preukázaním jeho vlastnosti pôsobiť, ako **retardér horenia**.

Posledný patentový spis [20] sa týka zmesí **Cu-C**, **Ag-C** a **Au-C** cez hodnotenie elektrickej rezistivity dvoch homogénne zmiešaných práškových zmesí zhutnených metódou izostatického lisovania na zabezpečenie výslednej pórovitosti blížiacej sa nule. Tento postup umožnil náhradu cenovo náročnejšieho **Ag** a **Au**. Práca [21] poukazuje na jej ocenenie v rámci špičkových aktivít medzinárodnej spolupráce.

Literatúra:

[1] J. Krempaský: Meranie termofyzikálnych veličín; V SAV, Bratislava, 1969.
[2] T. H. Blakeley, A. E. S. White: Plansee Proc. 2nd Seminar, Reute/Tyrol. , 1955, F. Benesovsky, ed., pp. 335-345, Pergamon Press, London, 1956.
[3] S. R. Broadbent, J. M. Hammersley: Proc. Camb. Philos. Soc. 53(1957) 629.
[4] W. D. Kingery: J. Am. Ceram. Soc., 42(1959) 617.
[5] R. J. Weiss: Solid State Physics for Metallurgies, Pergamon Press, Oxford, 1963.
[6] J. Gurland: Transactions of the Metallurgical Society of AIME, Vol. 236(1966/May) 642-646
[7] S. Kirkpatrick: Percolation and Conduction. Rev. of Mod. Phys. 45(1973/4) 574-588.
[8] Š. Barta, J. Bielek: Súčiniteľ tepelnej vodivosti polyolefínov plnených minerálnymi plnivami; Realizačná správa št. výsk. úlohy č. P14-123-204-03/E03; EF SVŠT, Bratislava, 1980.
[9] J. Bielek, Š. Barta, K. Veselý: Jav perkolácie fonónov; Prihláška objavu č. PO 49/80.
[10] J. Bielek, Š. Barta, K. Veselý: acta phys. slov. 32(1982)151-152.
[11] Š. Barta a kol.: Efektívny súčiniteľ tepelnej vodivosti systému epoxid-SiO_2. 8. konferencia čs. fyzikov, Bratislava, 27. – 30. 8. 1985.
[12] Š. Barta a kol.: Efektívny súčiniteľ teplotnej vodivosti systému epoxid-SiO_2. 8. konferencia čs. fyzikov, Bratislava, 27. – 30. 8. 1985.
[13] Š. Barta a kol.: Efektívny objemové merné teplo systému epoxid-SiO_2. 8. konferencia čs. fyzikov, Bratislava, 27. – 30. 8. 1985.
[14] K. Veselý, F. Kratochvíl, Š. Barta, J. Bielek: Autorské osvedčenie č. 230 057. Zmes na báze polyolefínov so zvýšeným súčiniteľom tepelnej vodivosti. Úřad pro vynálezy a objevy, ČSSR, Praha, 10. 7. 1986.
[15] J. Bielek, Š. Barta, K. Veselý: Perkolácia fonónov; Úřad pro vynálezy a objevy, ČSSR, Praha, 19. 3. 1987.
[16] R. A. Bareš: Kompozitní materiály; SNTL, Praha, 1988.
[17] Š. Emmer, J. Bielek, A. Havalda: Copper-graphite composite material for application to sliding electrical contacts. Journal de Physique IV, 3 (1993) 1799-1804.
[18] Š. Barta, M. Košík, J. Bielek, R. Karas, J. Kvasnica, P. Suran, I. Zamboj: Patentový spis č. 279 430. Gumárenská zmes so zvýšeným súčiniteľom tepelnej a teplotnej vodivosti. ÚPV SR, B. Bystrica, 04. 11. 1998.
[19] J. Bielek, Š. Barta, M. Košík, K. Balog: Patentový spis č. 279 769. Spôsob plnenia horľavých polymérnych kompozitov retardérom horenia. ÚPV SR, B. Bystrica, 12. 03. 1999.
[20] J. Bielek, Š. Emmer, J. Kováčik: Patentový spis č. 284 768. Zmesi **Cu-C**, **Ag-C** a **Au-C** na aplikáciu na klzné elektrické kontakty s najvyššou prúdovou hustotou. ÚPV SR, B. Bystrica, 12. 10. 2005.
[21] Š. Barta, J. Bielek: Determination of Thermal, Electro-Magnetic and Mechanical-Elastic Properties of Heterogeneous Materials. Proc. of the Japan- Central Europe Joint Workshop on Advanced Computing in Engineering. Editors: M. Akiyama, M. Kleiber, Warsaw, 1994, pp. 173-178.

Derivation of the Boundary Condition for a Heat Source

F. Čulík , J. Lukovičová[1]

Abstract

A special method of derivation the boundary condition is shown in this paper on the base of the inhomogeneous heat conduction equation. The term on the right side of the equation considers the influence of a heat source in creation the corresponding temperature field in solids. The 1-D case for a planar heat source is studied in details.

1. Determination and a physical meaning of the heat source term

1.1 An Introduction

Inhomogeneous differential heat conduction equation can be derived on the base of internal energy balance equation

$$\frac{\partial u(\boldsymbol{r},t)}{\partial t} + \nabla \cdot \boldsymbol{q}(\boldsymbol{r},t) = \sigma_u(\boldsymbol{r},t) \tag{1}$$

where the density of internal energy is $u(\boldsymbol{r},t)$, the heat flux is $\boldsymbol{q}(\boldsymbol{r},t)$ (the density of the heat flow) and $\sigma_u(\boldsymbol{r},t)$ - is a source term. It is assumed that the mass transport does not exist. In a case, when no work is done by the system (or on the system) it is a heat source term according to the first law of thermodynamics.
The equation (1) defines the heat flux $\boldsymbol{q}(\boldsymbol{r},t)$ [1] together with the eqs. (2), (3), (4)

$$\frac{\partial u}{\partial t} = \rho c \frac{\partial T}{\partial t} \tag{2}$$

(ρ, c – density and specific heat)

$$\sigma_u = \frac{d\dot{Q}}{dV} = \frac{dP}{dV} \tag{3}$$

where $\dot{Q} = P$ is the heat power of a heat source (V – volume).

[1] František Čulík, Jozefa Lukovičová, Dpt. of Physics, Civil Engineering Faculty, Slovak University of Technology, Bratislava, SR.

$$\boldsymbol{q} = -\lambda \text{ grad } T \tag{4}$$

The eq. (4) is known as the first Fourier's law (λ – thermal conductivity, T – temperature).

2. A planar heat source

Further on, we restrict our study to a planar heat source located at $x = 0$. This is the border of two media in thermal contact: (1) $x < 0$ and (2) $x > 0$ with different thermal properties ρ_1, c_1, λ_1; ρ_2, c_2, λ_2 (density, specific heat, thermal conductivity). We assume that the heat flux

$$\boldsymbol{q} = \left(q\left(x,t\right),0,0\right) \tag{5}$$

and isothermal surfaces are planes orthogonal to *x*-axis.

Then, the problem is reduced to one-dimensional problem 1-D. In this case the eq. (1) takes the form

$$\rho c \frac{\partial T\left(x,t\right)}{\partial t} + \frac{\partial q\left(x,t\right)}{\partial x} = \frac{1}{S}\frac{\partial P\left(x,t\right)}{\partial x} \tag{6}$$

S is the area of a heat source. Integration of this equation (fig. 1) in limits

$$-\varepsilon \le x \le \varepsilon, \quad \varepsilon \ge 0\,, \quad y,z \in S \tag{7}$$

Fig. 1

---

gives

$$S\int_{-\varepsilon}^{\varepsilon}\left(\rho c \frac{\partial T\left(x,t\right)}{\partial t} + \frac{\partial q\left(x,t\right)}{\partial x}\right)dx = \int_{-\varepsilon}^{\varepsilon}\frac{\partial P\left(x,t\right)}{\partial x}\,dx \tag{8}$$

From this eq. we obtain after a limiting process

$$q_2\left(+0,t\right) - q_1\left(-0,t\right) = q_s\left(t\right) \tag{9}$$

because

$$\lim_{\varepsilon\to 0}\left\{\rho_2 c_2\int_0^{\varepsilon}\frac{\partial T_2\left(x,t\right)}{\partial t}dx - \rho_1 c_1\int_0^{-\varepsilon}\frac{\partial T_1\left(x,t\right)}{\partial t}dx\right\} =$$

$$\lim_{\varepsilon\to 0}\left\{\rho_2 c_2\frac{\partial}{\partial t}\int_0^{\varepsilon}T_2\left(x,t\right)dx - \rho_1 c_1\frac{\partial}{\partial t}\int_0^{-\varepsilon}T_1\left(x,t\right)dx\right\} = 0 \tag{10}$$

$$\lim_{\varepsilon\to 0}\int_{-\varepsilon}^{\varepsilon}\frac{\partial q(x,t)}{\partial x}dx=\lim_{\varepsilon\to 0}\left[q_2(\varepsilon,t)-q_1(-\varepsilon,t)\right]=q_2(+0,t)-q_1(-0,t) \tag{11}$$

$$\lim_{\varepsilon\to 0}\int_{-\varepsilon}^{\varepsilon}\frac{\partial P(x,t)/S}{\partial x}\,dx=\lim_{\varepsilon\to 0}\int_{-\varepsilon}^{\varepsilon}q_s(t)\delta(x)\,dx=q_s(t) \tag{12}$$

where

$$q_s(t)=P(t)/S \tag{13}$$

This is in accord with our assumption that a heat source is placed in the plane at $x=0$
This implies

$$P(x,t)/S=\frac{P(t)}{S}\theta(x)=q_s(t)\theta(x) \tag{14}$$

$\theta(x)$ is the Heaviside's step-wise function

$$\theta(x)=\begin{cases}0 & x<0\\ 1 & x>0\end{cases} \tag{15}$$

and following relations were used for the Dirac function $\delta(x)$

$$\delta(x)=\frac{d\theta(x)}{dx},\qquad \int_{-\varepsilon}^{\varepsilon}\delta(x)\,dx=1 \tag{16}$$

Accounting the Fourier's law the boundary condition (9) can be rewritten as follows

$$\lambda_1\frac{\partial T_1(-0,t)}{\partial x}-\lambda_2\frac{\partial T_2(+0,t)}{\partial x}=q_s(t) \tag{17}$$

Integral form of the boundary condition (17) is

$$\lambda_1\int_0^t\frac{\partial T_1(-0,t')}{\partial x}dt'\;-\lambda_2\int_0^t\frac{\partial T_2(+0,t')}{\partial x}dt'=\frac{1}{S}\int_0^t P(t')\,dt' \tag{18}$$

The heat produced by unit area of the planar heat source in the time interval *t*

$$Q=\int_0^t q_s(t')\,dt'=\frac{1}{S}\int_0^t P(t')\,dt' \tag{19}$$

is splitting into two parts: The heat transferred through unit area into medium (1) (to the left) with thermal conductivity λ_1 is equal

$$Q_1 = -\int_0^t q_1(-0,t')\,dt' = \lambda_1 \int_0^t \frac{\partial T_1(-0,t')}{\partial x}\,dt' \tag{20}$$

and that one transferred through unit area into medium (2) (to the right) with thermal conductivity λ_2 equals

$$Q_2 = \int_0^t q_2(-0,t')\,dt' = -\lambda_2 \int_0^t \frac{\partial T_2(-0,t')}{\partial x}\,dt' \tag{21}$$

Now, eq. (18) can be written as

$$Q_1 + Q_2 = Q \tag{22}$$

3. Discussion

The boundary condition (9) says: A planar heat source creates discontinuity of the normal component of the heat flux in the plane of its location. The difference of these components by crossing this plane equals the heat power of a heat source unit area. The heat flow is directed from the planar heat source away (to the media where temperature is lower that one of the source.) This is a heating process of the media.

In a case of cooling when a planar heat source is replaced e.g. by a cold thin plate the direction of the heat flow will be opposite (to the cold plate from media assuming their temperature is higher that one of the cold plate).

Finally, if there is no heat source the normal component remains continuous. Then, it holds at the both sides of the plane $x = 0$: $q_1(+0,t) = q_2(-0,t)$

In theoretical determination of the temperature field there is a need to solve differential heat conduction equation under the initial and boundary conditions. Knowledge of temperature development at a given place in a material is necessary for experimental investigation of its thermal parameters. We mention here the Pulse transient method. Mathematical formulae describing a temperature field in a specimen contain thermal parameters. Fig. 2 shows the scheme of experimental setup (in approximation when 3-D case is reduced to 1-D) [2].

Fig. 2

The heat pulse creates a planar heat source at $x = 0$. It is the border plane of two specimen parts $1 \Leftrightarrow 2$. A thermocouple serves for temperature measurement at $x = h$ between $2 \Leftrightarrow 3$. Initial temperature is constant (the same in each of tree parts being in mutual thermal contact). A small heat pulse is applied to the specimen. Unknown thermal parameters of the middle part namely, thermal diffusivity, thermal conductivity and specific heat are then calculated upon temperature response according to a simplified model.

Acknowledgement
Financial support of the project VEGA 1/4204/07 is gratefully acknowledged.

References

[1] H. J. Kreuzer, Nonequilibrium Thermodynamics and its Statistical Foundations, Clarendon Press-Oxford 1981
[2] Vretenár V.: Extended version of Pulse transient method, Proceedings of Thermophysics, 2005, Contents, pp. 92-103, October 2005, Meeting of the Thermophysical Society, SAS Bratislava 2005. http://www.tpl.ukf.sk/engl_vers/thermophys/

APPENDIX

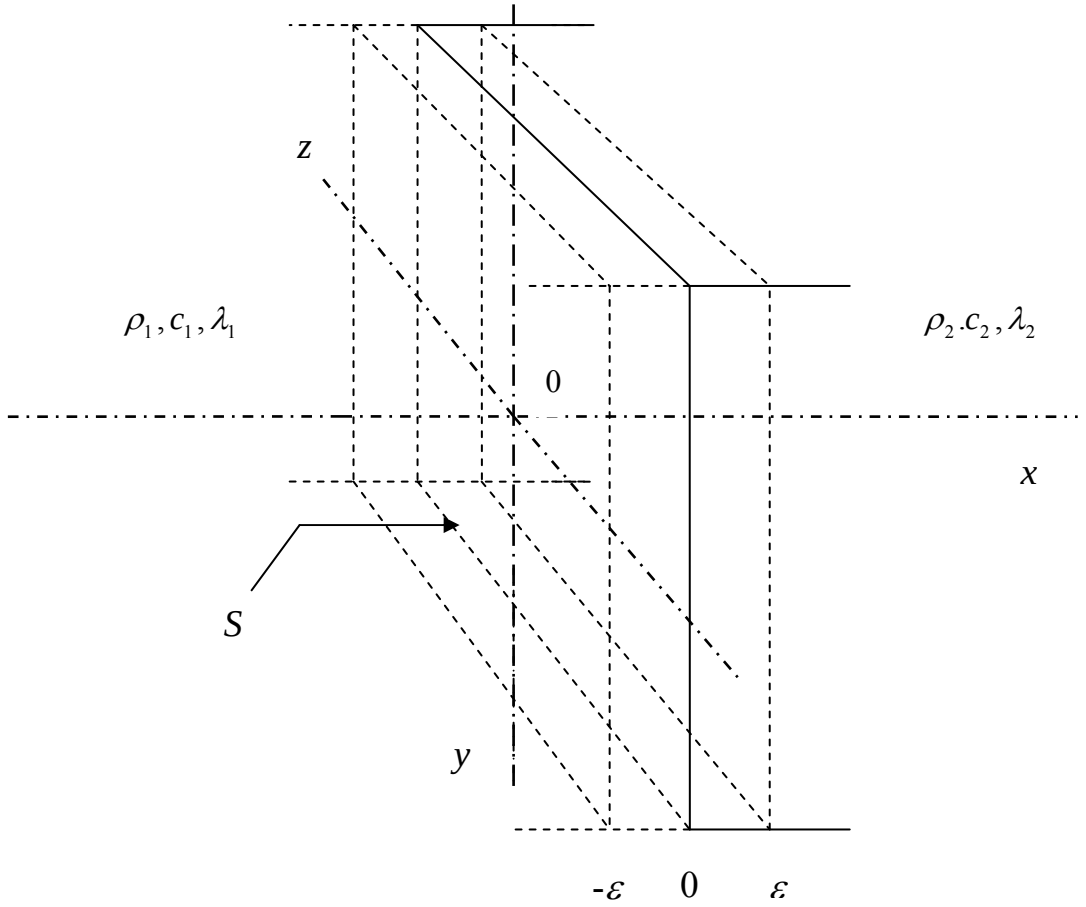

Fig.1. Two layers with different thermal properties each of the thickness ε. A planar heat source acts in the plane at $x = 0$. This is the plane of a mutual thermal contact of both media.

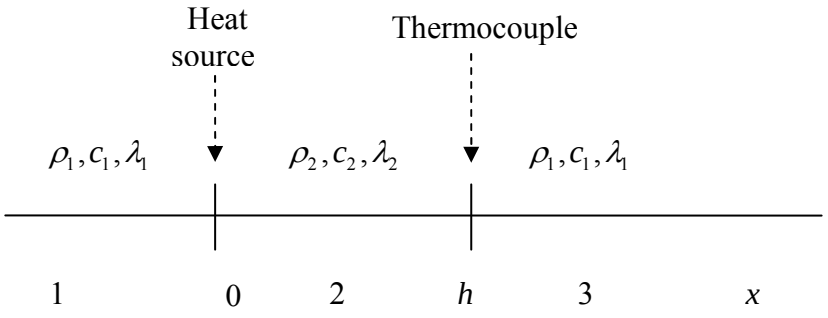

Fig. 2 A specimen setup is consisting of two outer parts (1, 3) hawing known identical thermal properties and one middle part (2) of unknown thermal properties.

DETERMINATION OF BOUNDARY RADIANT HEAT FLUXES BETWEEN THE SURFACE OF A BUILDING CONSTRUCTION AND THE NIGHT SKY

Stanislav Šťastník, Jiří Vala, Radek Steuer

Brno University of Technology, Faculty of Civil Engineering, Veveří 331/95, 602 00 Brno, Czech Republic, e-mail addresses: Stastnik.S@fce.vutbr.cz , Vala.J@fce.vutbr.cz , Steuer.R@fce.vutbr.cz

Abstract:
All radiant heat fluxes between the exterior surfaces of building constructions and the night sky were neglected in the past. However, the application of modern materials and the increasing thermal insulation ability of advanced structures elevate the significance of such heat fluxes. The more precise evaluation of the reciprocal radiant heat transfer between the night atmosphere and the building surface requires knowledge of the spectral emissivity as a function of wavelength. The paper discusses both the quantitative determination of radiant heat fluxes and the measurement of the spectral emissivity of surfaces.

Keywords:
radiative heat transfer, emissivity, thermal emissive power, building physics

INTRODUCTION

Permanent increasing of thermal insulating requirements for external building structures has brought along the series of structural and material changes in their composition. Insulation of objects with help of external contact thermal insulating systems (ETICS) has become ordinary solution. Thus, not everyone realizes that surface layers of insulating system became its strongly loaded part. Great temperature and moisture load of external layers take place due to combination of both climatic effects and building physics' properties of structural layers of ETICS which directly influences the service life of the whole system.

Interaction of climatic effects with modern composition of insulating systems also cause predisposition of insulated facades to appearance of unsightly green incrustation on a façade's surface. Algae growth on a building surface with ETICS is enabled mostly by virtue of night under-cooling of surface layers under the temperature of the ambient air and consequent water vapour condensation on a façade's surface. The source of such periodic phenomena is radiation of thermal energy by the façade's surface. The detailed description of a given topic is comprised in the issues [6] and [7].

It is necessary to know boundary radiant heat fluxes between surface of a building structure and a night sky for more accurate calculation of thermal-moisture processes proceeding in surface layers of ETICS. Unfortunately, this issue has been considerably omitted within building industry so that this paper was created to fill the gap – it deals with measurements of radiative properties of surfaces leading to determination of radiant heat fluxes between surface of a building structure and a night atmosphere.

DASH OF THEORY – DEFINITION AF BASIC QUANTITIES OF RADIATION

As the physics of radiation does not belong to common disciplines of building engineering, the basic used quantities necessary for good orientation in the rest of the paper will be explained and defined in the following chapter. This chapter deals with radiation of real and so-called ideal black bodies and the quantities such as emissivity and spectral emissivity defining thermal radiation of surfaces of real materials. Let us assume that following equations and definitions are valid for bodies and their surfaces which do not transmit the given radiation and entire such radiation impacting on their surface is either reflected or absorbed.

Surfaces of all bodies with non-zero thermodynamic temperature including building surfaces radiate electromagnetic radiation. It has been described by famous Stephan-Boltzman Law; surface emissive power H [W.m-2] can be then expressed

$$H = \varepsilon \cdot \sigma \cdot T^4 \tag{1}$$

where σ is Stephan-Boltzman constant ($\sigma \approx 5{,}67.10^{-8}\ W.m^{-2}.K^{-4}$), T is temperature of radiating surface in Kelvins and ε *[-]* is its emissivity. Emissivity expresses ratio between emissive power H of the given real surface and radiation H_0 of a surface of perfect black body (with emissivity equal to one). It possesses value from 0 to 1 and it is in this form dependent of temperature of radiating surface. Emissivity of surface of a black body equals one.

Surface with such defined "half-space" emissivity, let us say 0.9, does not necessarily have in a perpendicular view intensity of radiation accurate 0.9 of intensity of radiation of black body with the same temperature. It may radiate slightly strongly in this direction. And, vice versa, if we observe it sideways, its radiance may be weaker [1]. In other words, intensity of radiation[1] $I\ [W.sr^{-1}.m^{-2}]$ of radiating surface alters with the angle α *[rad]* measured from normal to the given surface. And what is important: it may alter differently for surfaces made of various materials.

$$I = \frac{dH}{d\omega} = \frac{\varepsilon_\alpha \cdot H_0}{\pi} \tag{2}$$

Where ω *[sr]* is a spatial angle, α *[rad]* is an angle measured from a normal to the surface. Index α expresses emissivity only in a given direction. Then ε_α *[-]* is called directional emissivity. Intensity of radiation of the given surface I is dependent only on the angle α measured from normal. Directional emissivity is usually decreasing function of an angle α. Intensity of radiation of an ideal diffusive so-called "Lambert" surface may be expressed as following:

$$\varepsilon_\alpha \cong \varepsilon_n \cdot \cos\alpha \tag{3}$$

ε_n is directional emissivity in a normal direction to surface. For determination of dependency of directional emissivity of a specific material in a direction, it is possible to measure it approximately by means of infrared spectrometers with special adapter. In our case, however, we will assume that the above mentioned assumption is valid. Thus, we will not further deal with this dependency of emissivity in direction.

Bodies radiate electromagnetic radiation mostly in range of wavelength (4 to 50) micrometers – belonging to infrared range of spectrum[2] – under ordinary temperature conditions. Spectral radiation of perfect black surface with emissivity equal to one $H_{\lambda 0}\ [W.m^{-2}.m^{-1}]$ depending on

[1] Note. This paper unconventionally relates intensity of radiation onto surface element! (thus quantities $[W.sr^{-1}.m^{-2}]$) Therefore it is a somewhat local intensity of radiation which can be represented in case of homogeneous surface as intensity of radiation of 1 m^2 of area surface.

[2] Such a body radiation with ordinary temperature is used to be denoted as long-wave radiation and Sun radiation as short-wave radiation in technical literature.

wavelength has been described by Planck's relation for spectral distribution of radiation of a black surface:

$$H_{\lambda 0} = \frac{dI_0}{d\lambda} = \frac{8\pi hc^2}{\lambda^5 \exp\left(\frac{hc}{k\lambda T} - 1\right)}, \tag{4}$$

where: λ is wavelength of electromagnetic radiation *[m]*,
h Planck's constant $6{,}62618.10^{-34}$ *J.s*,
c light velocity in vacuum $299\ 792\ 458$ *m.s*$^{-1}$,
k Boltzman constant $1{,}38066.10^{-23}$ *J.K*$^{-1}$.

Index *0* at H_0 and $H_{\lambda 0}$ expresses that it means radiation of perfect black surface with emissivity equal to one.

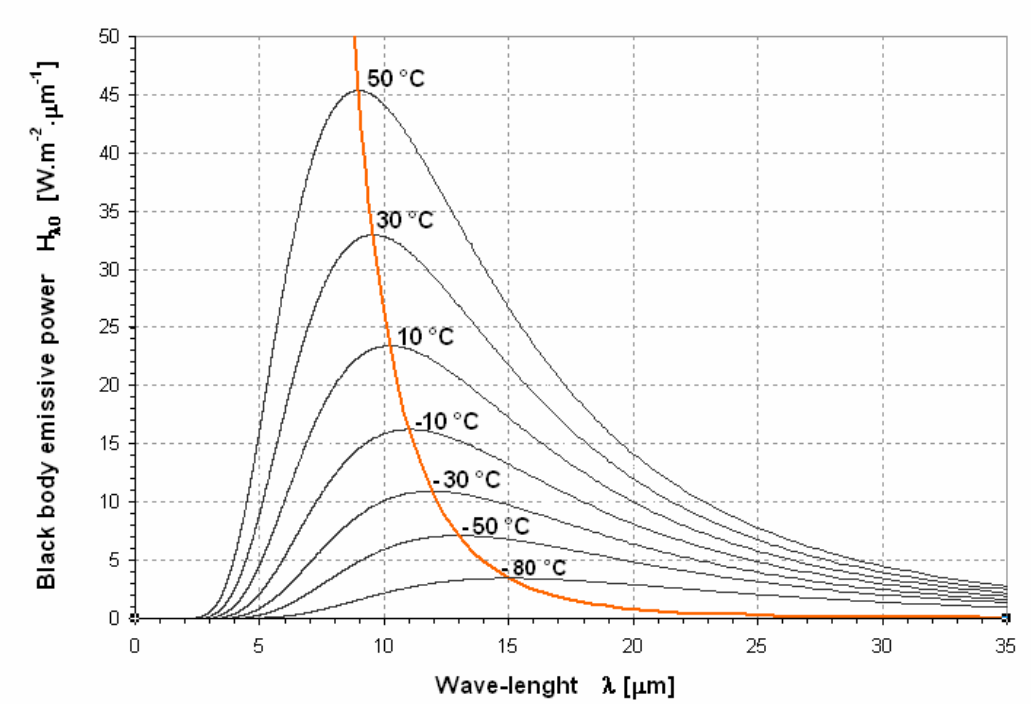

Figure 1: Curves of spectral radiation $H_{\lambda 0}$ of black surface depending on wavelength λ captured for various temperatures. Red line connects maxima of these curves.

To make things even more complicated, let us state that ratio between spectral radiation of real and black body with the same temperature in dependency on wavelength is not constant. We may consider this for accurate calculations of radiation among various surfaces using spectral emissivity ε_λ *[-]* which is the ratio between spectral radiation of the given specific surface and surface of a black body. Then, it holds true that spectral radiation of real body H_λ *[W.m*$^{-2}$*.m*$^{-1}$*]* is

$$H_\lambda = \frac{dH}{d\lambda} = \varepsilon_\lambda \cdot H_{\lambda 0} \tag{5}$$

In case, we would like to be more precise in the description of a surface of real body, we may use so-called directional spectral emissivity H_λ *[W.m*$^{-2}$*.m*$^{-1}$*]* for determination of spectral intensity of radiation I_λ *[W.m*$^{-2}$*.sr*$^{-1}$*.m*$^{-1}$*]*

$$I_\lambda = \frac{dI}{d\omega\, d\lambda} = \frac{\varepsilon_{\lambda\alpha} \cdot H_{\lambda 0}}{\pi} \tag{6}$$

For our purposes, we will use simplified assumption from equation (3) that spectral intensity of radiation corresponds to cosine law of radiation. Thus, we will assert that we only need to know for our purposes only spectral emissivity ε_λ.

Spectral emissivity ε_λ has in addition convenient property – it is not on principle dependent on temperature within small temperature range where microstructure of substance does not change. That is why, it is possible to use spectral emissivity measured e.g. at 20 °C for calculation of surface radiation of plasters in range of real temperatures approx. –10 °C up to +50 °C because we do not expect substantial changes in material microstructure of a plaster in this temperature range which would normally have significant effect to value of spectral emissivity.

Further important property of spectral emissivity is the fact that its value (and unit) is according to Kirchhoff's Laws equal to spectral absorption a_λ. Spectral absorption a_λ expresses relation between surface of absorbed compound of spectral radiation and overall spectral radiation impacting onto surface. This equivalence is often used for experimental determination of values of emissivity and spectral emissivity.

$$\varepsilon_\lambda = a_\lambda \tag{7}$$

If we wanted to determine emissivity ε for certain temperature[3] from realized dependency of spectral emissivity $\varepsilon_\lambda(\lambda)$ on wavelength as accurate as possible, we can use the fact that emissivity ε may be expressed also as a ratio of intensity of radiation of a given surface H to intensity of radiation of black body surface H_0:

$$\varepsilon = \frac{H}{H_0} = \frac{\int_0^\infty H_\lambda \, d\lambda}{\int_0^\infty H_{\lambda 0} \, d\lambda} = \frac{\int_0^\infty \varepsilon_\lambda(\lambda) \dfrac{8\pi hc^2}{\lambda^5 \exp\left(\dfrac{hc}{k\lambda T} - 1\right)} d\lambda}{\int_0^\infty \dfrac{8\pi hc^2}{\lambda^5 \exp\left(\dfrac{hc}{k\lambda T} - 1\right)} d\lambda} \tag{8}$$

SPECTRAL EMISSIVITY AND HEAT FLUXES

Energy leaks from bodies by radiation which may manifest as temperature drop of a body in practise. However, bodies usually do not radiate into an empty space but they radiate against surrounding surfaces mutually. They also can partially absorb electromagnetic radiation coming from other surfaces. When the body is completely surrounded with objects with similar emissivity and the same or only slightly different temperature (e.g. as bodies in some room), resulting heat flux among them in negligibly small. When bodies with significantly different temperatures radiate towards each other (e.g. external surfaces against night sky), the influence of difference of their mutual radiant heat fluxes causes implication of heat flux between the bodies.

For easier approach, let us study simply defined case of radiation of horizontal surface against night sky. This model case shows that such loss spectral heat flux from a building surface $q_{r\lambda}$ [$W.m^-$

[3] Note: General dependency ε_λ on temperature has been in the following equation neglected. Therefore, temperature for which ε_T is being determined, must fulfil conditions stated two paragraphs higher with respect to measured dependency $\varepsilon_\lambda(\lambda)$.

$^{2}.m^{-1}]$ is equal to spectral heat flux $q_{r\lambda em}$ radiated by a surface with deduction of absorbed compound of spectral heat flux by a surface coming onto a surface from night sky (atmosphere).

$$q_{r\lambda} = q_{r\lambda em} - q_{r\lambda abs} = \varepsilon_{\lambda} H_0 - \varepsilon_{\lambda} q_{r\lambda atm} \tag{9}$$

where: $q_{r\lambda}$ resulting loss spectral radiant heat flux leaving the surface of horizontal surface radiating against night sky $[W.m^{-2}.m^{-1}]$,
$q_{r\lambda em}$ spectral radiant heat flux emitted from a surface $[W.m^{-2}.m^{-1}]$,
$q_{r\lambda abs}$ spectral radiant heat flux from night sky absorbed by a surface $[W.m^{-2}.m^{-1}]$,
$q_{r\lambda atm}$ spectral radiant heat flux impacting on a given surface from night sky $[W.m^{-2}.m^{-1}]$.

If we want to express radiant heat flux q_r $[W.m^{-2}]$ from spectral radiant heat flux $q_{r\lambda}$ $[W.m^{-2}.m^{-1}]$, it is possible to simply integrate equation (8) along the wavelength

$$q_r = \int_0^{\infty} \varepsilon_{\lambda}(\lambda) \cdot \left(\mathrm{H}_{\lambda 0}(\lambda) - \mathrm{q}_{r\lambda atm}(\lambda) \right) d\lambda \tag{10}$$

As it is obvious from the above mentioned, it is convenient to carry out experimentally dependency of surface spectral emissivity ε_{λ} on wavelength for accurate determination of mutual radiant fluxes between night atmosphere and a building surface.

EXPERIMENTAL ASSESSMENT OF SPECTRAL EMISSIVITY

Infrared spectrometer can be used for experimental assessment of spectral emissivity ε_{λ}. Instead of former spectrometers based on a principle of disperse spectrophotometry, more accurate and faster FT-IR spectrometers based on a principle of Michaelson's wave interferometer and use of Fourier's transformation (which gives the explanation for letters FT in its name) are more often used at present. One such a modern device (Nicolet 380 from a producer Thermo Electron Corporation) is in the possession of Institute of Technology of Building Materials and Elements at Faculty of Civil Engineering, Brno University of Technology. The mentioned device works within the range of wavelengths 1.28 – 28.5 μm – which is relatively suitable range for assessment of spectral emissivity for purposes of above outlined calculations of radiation of building surfaces against night sky.

Necessary equipment for the measurement besides infrared spectrometer is also convenient measuring adapter. Adapters using reflex techniques for measurement resulting from the equation (7) – Kirchhoff's Law – may be used for measuring spectral emissivity. Adapters are adapted for measuring reflectivity of examined surface for a given radiation whereas we come out from our known relation that supplement to one to spectral reflectivity r_{λ} is equal to spectral absorption a_{λ} which is equal to spectral emissivity ε_{λ} from equation (7).

$$\varepsilon_{\lambda} = a_{\lambda} = 1 - r_{\lambda} \tag{11}$$

For the measurement of spectral reflection r_{λ}, two types of adapters can be used– either the adapter with integration sphere, types of which are suitable for accurate assessment of overall "half-space" spectral emissivity, or much cheaper adapter for diffusive reflection can be used; its integration mirror does not embrace all directions of the entire half-space around a testing sample but is seems sufficient due to its smooth surfaces. Description of function of individual adapters and discussion about their suitability for various measurements would apparently produce a separate

issue. That is why we only briefly mention that we used adapter for diffusive reflection called PIKE EasiDiff^{TM} lent free of charge by company NICOLET CZ.

RESULTS OF THE MEASUREMENT AND AN EXAMPLE OF THEIR PROCESSING

The following graph no. 2 shows an example of measured result of spectral reflectivity r_λ of a testing sample (silicate plaster modified by addition of additive slightly decreasing its emissivity). Displayed curves also document variance of measured values of one sample.

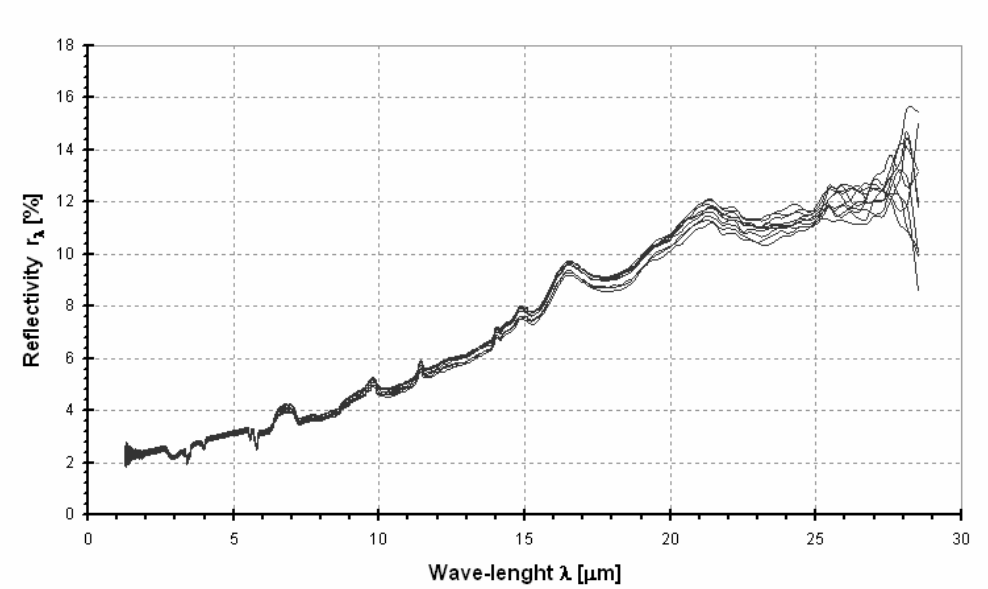

Figure 2: Spectral reflectivity r_λ *measured 10 times at 10 various spots of one testing sample*

The following graph no. 3 shows spectral emissivity ε_λ of the same testing sample obtained from graph no. 2 by means of the equation (11).

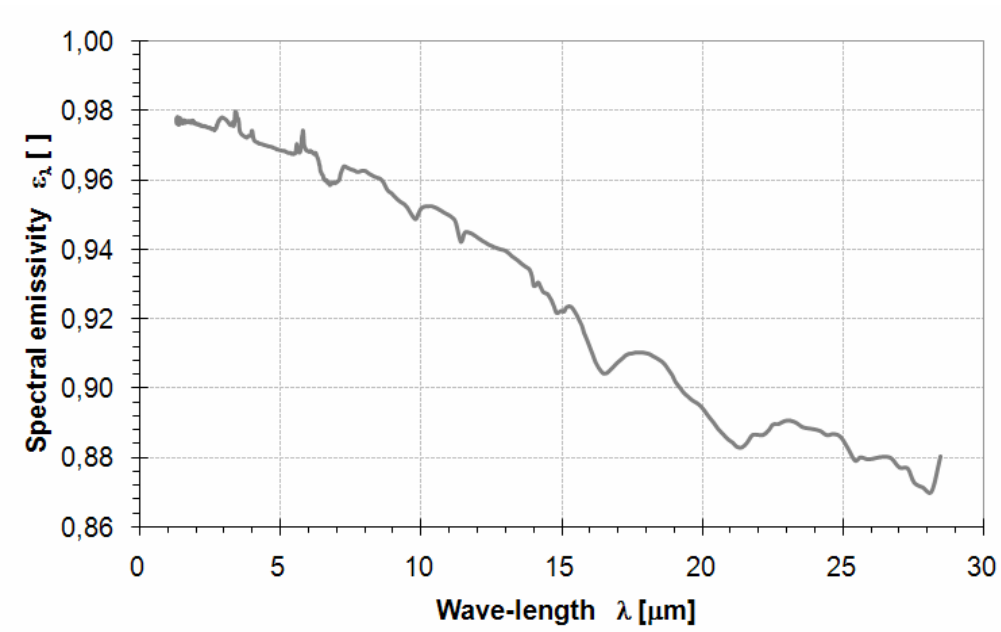

Figure 3: Spectral emissivity ε_λ *obtained as an average from measurement in graph no. 2 and evaluated from the equation (11).*

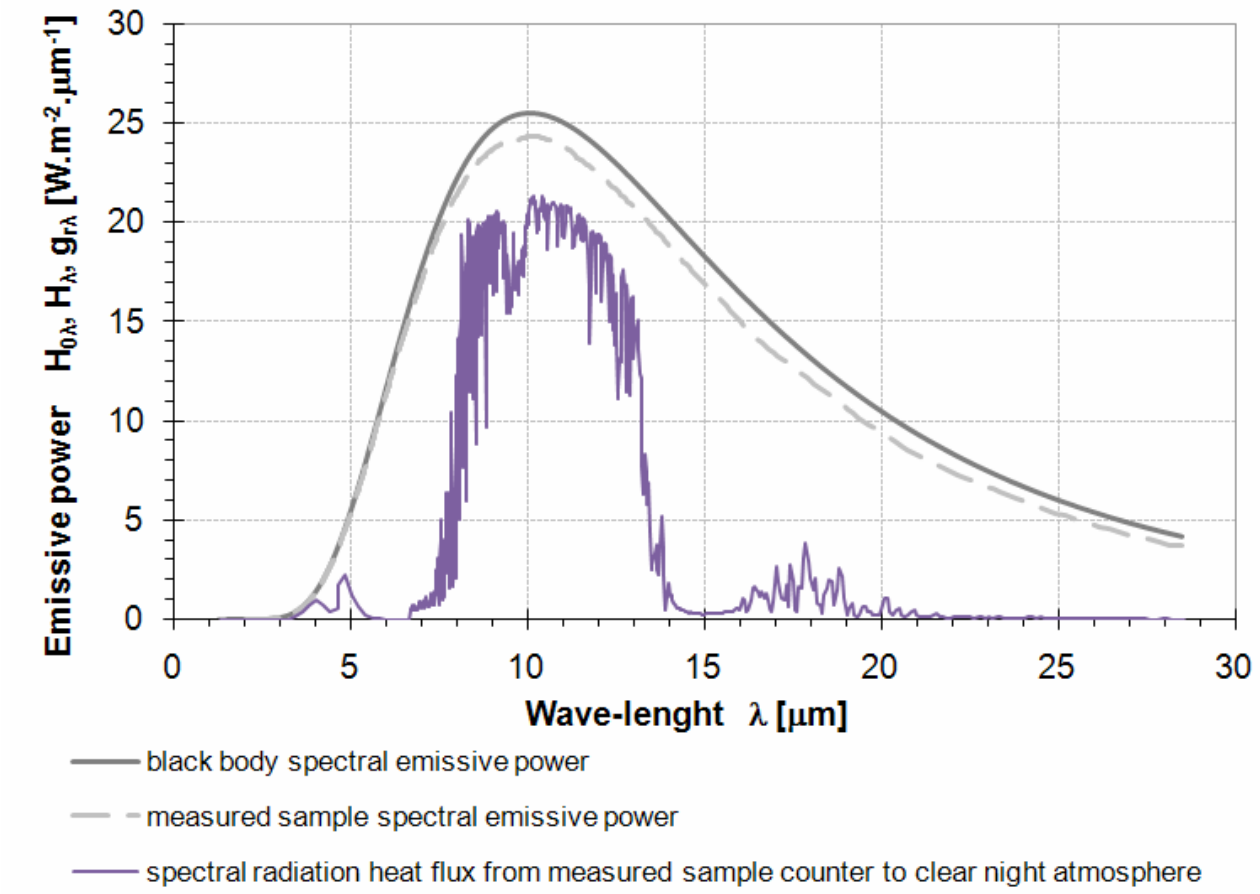

Figure 4: Calculated spectral radiation of black surface $H_{\lambda 0}$*, in comparison with spectral radiation of surface* H_λ *of measured sample and spectral radiant heat flux* $q_{r\lambda}$ *of sample surface oriented horizontally against clear night sky. All three curves of values of spectral surface radiation are calculated for temperature of radiating surface 15 °C.*

Graph no. 4 shows a black curve of spectral radiation $H_{\lambda 0}$ of perfect black body calculated from the equation (4). We can compare it with a red curve of spectral radiation H_λ of a measured sample obtained from the equation (5). The green curve represents resulting spectral radiant heat flux $q_{r\lambda}$ defined by means of the equation (9) for specific state of cloudless summer atmosphere. All three curves of values of spectral surface radiation displayed in the graph are calculated for temperature of a radiating surface 15 °C.

After integration of dependencies of spectral radiation (graph no. 4) over entire range of wavelengths 0 up to $+\infty$ we obtain intensity of radiation of black surface at 15 °C $H_0 = 391\ W.m^{-2}$, intensity of radiation of measured sample surface $H = 364\ W.m^{-2}$ and radiant heat flux of horizontally oriented sample against clear sky $q_r = 105\ W.m^{-2}$.

Overall emissivity for a certain temperature can be determined in accordance with the equation (8) from measured dependency of spectral emissivity on wavelength $\varepsilon_\lambda(\lambda)$. If we wanted to calculate dependency of overall emissivity ε on temperature by means of the equation (8) for temperature interval fulfilling the conditions listed by the equation (8), we can do so – the result is displayed by curve in the graph no. 5. We will see that for small temperature ranges valid for most of building engineering calculations, it has no sense to complicate the calculation with assumption of emissivity being dependent on temperature $\varepsilon(T)$; the assumption for it being a constant value calculated for some average temperature will be also sufficient.

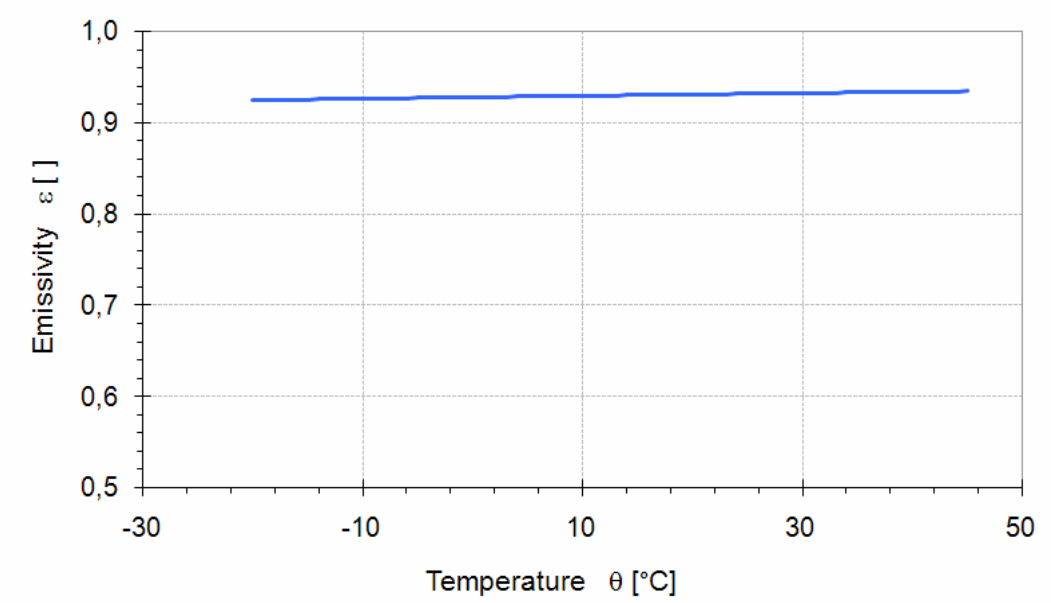

Figure 5: Overall emissivity ε of measured sample (the blue curve) depending on temperature. Calculated due to the equation (8), integrated numerically over the range of wavelengths for which spectral emissivity has been measured.

CONCLUSION

The paper indicates some possibilities of determining spectral emissivity of various surfaces. It can be important for more accurate determination of boundary radiant heat fluxes for some thermal-technical calculations, particularly for determination of radiant heat fluxes between surfaces of building structures and night sky.

This paper has been elaborated with support of grant GA ČR 103/05/H044 and research project No. 1M6840770001 within activities of the CIDEAS research centre. Measurements on the infrared spectrometer was realized by virtue of cooperation and free-of-charge lending of measuring adapter by company NICOLET CZ.

REFERENCES

[1] HOLLAN, J. Zářivé toky a emisivity v praxi. In *Proceedings of Juniorstav 2004*. Brno, VUT v Brně. 2004. ISBN 80-214-2560-1. available online as toky_emi.* in directory: http://astro.sci.muni.cz/pub/hollan/e_papers/prednasky

[2] ŠŤASTNÍK, S.; HOLLAN, J.; STEUER, R. Možnosti určení emisivity materiálů pomocí infračervené termografie. In *Proceedings of Non-Destructive Testing In Engineering Practice 2006*. Brno, VUT v Brně. 2006. p. 181 - 186. ISBN 80-7204-487-7. available online as omitky06.* in directory: http://amper.ped.muni.cz/jenik/LW-infrared

[3] website: Kirtland Air Force Base: http://www.kirtland.af.mil/afrl_vs/

[4] MODEST, M., F. *Radiative Heat Transfer*. 1sted. McGraw-Hill, Inc., 1993. ISBN 0-07-042675-9.

[5] Witt, M. H.: *Heat and Moisture in Building Envelopes*, TU Eindhoven, 2006.

[6] STEUER, R.; ŠŤASTNÍK, S. Růst řas na fasádách s vnějším kontaktním zateplením. In *Proceedings of Tepelná ochrana budov 2007*. Štrbské pleso, Slovakia, VKC Intenzíva s.r.o. 2007. p. 154 - 157. ISBN 978-80-969243-5-6.
[7] ŠŤASTNÍK, S.; BRADÁČ, O.; KMÍNOVÁ, H.; STEUER, R. Projev emisivity na povrchovou degradaci stavebních materiálů. In *Tepelná ochrana budov*. 2005. 2005(2). p. 15 - 16. ISSN 1213-0907.

EFFECT OF DRYING TEMPERATURE ON PROPERTIES OF HARDENED GYPSUM

Pavel Tesárek, Robert Černý

Czech Technical University in Prague, Faculty of Civil Engineering, Department of Materials Engineering and Chemistry, Thákurova 7, 166 29 Praha 6, Czech Republic, tesarek@fsv.cvut.cz, cernyr@fsv.cvut.cz

Abstract:
Experimental research dealing with the effect of drying temperature on the properties of hardened flue gas desulphurization (FGD) gypsum is presented in the paper. The measurements of basic thermal and hygric parameters of FGD gypsum modified by the addition of hydrophobization substances and plasticizers are carried out, using the specimens subjected to two different thermal drying regimes, with the maximum temperatures of 40 °C and 80 °C, before the measurements. Bulk density, open porosity, thermal conductivity, volumetric heat capacity, water absorption coefficient and apparent moisture diffusivity are determined and compared to the properties of hardened gypsum without any admixtures.

Keywords:
hardened gypsum, thermal stability

INTRODUCTION

Thermal stability of hardened gypsum belongs to the tasks which are not yet resolved with clear outputs. This is one of the reasons why gypsum is not used in exterior applications. The problem of water removal from gypsum is relatively complex mainly because samples of hardened gypsum contain both physically and chemically bound water.

Calcined gypsum – hemihydrate $CaSO_4 \cdot ½\ H_2O$ – can be produced by various technologies. Nowadays, still relatively new but already very promising seems to be its production using the dehydration of waste flue gas desulfurization (FGD) gypsum – dihydrate $CaSO_4 \cdot 2H_2O$ – at the temperatures of 110 to 150 °C. Then, β-form of hemihydrate (calcined gypsum) is formed according to the equation, which describes the process of calcination:

$$CaSO_4 \cdot 2H_2O \rightarrow CaSO_4 \cdot ½\ H_2O + 1\ ½\ H_2O. \quad (1)$$

The solid structure of calcined gypsum is created by reverse hydration from hemihydrate to dihydrate according to equation

$$CaSO_4 \cdot ½\ H_2O + 1\ ½\ H_2O \rightarrow CaSO_4 \cdot 2H_2O \quad (2)$$

Factors which affect the removal of chemically and physically bound water are temperature, relative humidity and pressure (air pressure or vacuum). If the critical temperature when starts the

dehydration of calcium sulfate dihydrate to hemihydrate is exceeded gypsum is somewhere between the two stages: dihydrate and hemihydrate.

The opinions of various researchers on the critical temperature are very different. Schulze et al. [1] and Řičánek [2] state that this temperature is 40 °C or 42 °C, respectively. Šatava [3] dried gypsum samples at the temperature of 40 °C. These values of critical temperature are similar to the drying temperature of gypsum samples recommended by the Czech standards [4] and [5]. However, in another studies Kupilík [6] and Wirsching [7] determined the critical temperature to be higher than 70 °C. Turk and Bounini [8] compared world standards for gypsum and gypsum plasters. They found that the recommended drying temperatures for gypsum were between 35 °C and 50 °C. The same authors, however, presented their own DTA results which showed that gypsum samples after drying over 80 °C always exhibited two peaks but separation of these peaks was complicated.

In this paper, the effect of two thermal drying regimes of hardened FGD gypsum specimens, with the maximum temperatures of 40 °C and 80 °C and at atmospheric pressure, on the measured hygric and thermal properties is investigated.

EXPERIMENTAL METHODS

Basic physical properties, namely bulk density, matrix density and open porosity, were measured by water vacuum saturation method [9]. Each sample was dried in a drier to remove majority of the physically bound water. After that the samples were placed into desiccator with distilled water. During three hours air was evacuated with vacuum pump from the desiccator. The specimen was then kept under water not less than 24 hours.

The water absorption coefficient and apparent moisture diffusivity representing the moisture transport parameters were determined from a one dimensional water sorption experiment [10]. The specimen was water and vapor-proof insulated on four lateral sides and the face side was immersed 2 mm in the water. A constant water level in the tank was achieved using a bottle placed upside down. The known water flux into the specimen during the suction process was then employed to the determination of the water absorption coefficient. The apparent moisture diffusivity was calculated using the water absorption coefficient and saturated water content [10].

Thermal conductivity and volumetric heat capacity were determined using the commercial device ISOMET 2104 (Applied Precision, Ltd.). ISOMET 2104 is a multifunctional instrument equipped with various types of optional probes. Needle probes are for porous, fibrous or soft materials, surface probes are suitable for hard materials. The measurement is based on the analysis of the temperature response of the analyzed material to heat flow impulses. The heat flow is induced by electrical heating using a resistor heater having a direct thermal contact with the surface of the sample.

MATERIALS AND SAMPLES

β-form of calcined gypsum with purity higher than 98 % of flue gas desulfurization (FGD) gypsum was used in the investigations. It was produced in the electric power station Počerady, CZ. The reference material without any admixtures was denoted as S0.

Two plasticizers and three hydrophobization admixtures were used for modifications of the basic calcined gypsum. For the first modification (denoted as S1) we used the plasticizer PERAMIN SMF 20 with a concentration of 0.5% of the mass of the solid phase. The second modification S2 was done using the plasticizer MELMENT F 4000 with a concentration of 0.2% of mass of the solid phase. The amount of plasticizers was chosen in such a way that the consistence of the gypsum paste was approximately the same as that of the reference material. The third modification contained the hydrophobization admixture IMESTA IBS 47, an alloy

hydrophobization powder for gypsum compounds produced by Imesta Inc., Dubá u České Lípy, CZ. Concentration of this admixture for material which was demoted as S3 was 0.5% by mass. The modified gypsum material denoted as S4 contained the admixture ZONYL 9027 (a fluorochemical solution that provides a durable, subsurface, transparent, protective barrier against oil and water on porous surfaces) produced by Du Pont, USA. This admixture was used as 5% water solution. The last modification denoted as S5 contained 5% water solution of the hydrophobization admixture ZONYL 301 produced by Du Pont again.

Two different temperatures were used for drying of gypsum samples, namely 40 and 80 °C. Therefore, the particular samples are denoted as either 40 or 80 to distinguish between the chosen drying regimes. Table 1 shows the detailed composition of gypsum mixtures including the water/gypsum ratio.

Table 1 Composition of measured materials

Material	Type of the admixture	Name of the admixture	Concentration	Water/gypsum ratio
S0	-	-	-	0.627
S1	plasticizer	Peramin SMF 20	0.5 % by mass	0.500
S2	plasticizer	Melment F 4000	0.2 % by mass	0.500
S3	hydrofobization admixture	Imesta IBS 47	0.5 % by mass	0.627
S4	hydrofobization admixture	Zonyl 9027	5% solution	0.627
S5	hydrofobization admixture	Zonyl 301	5% solution	0.627

The samples were mixed according to the Czech standard ČSN 72 2301 [11]. For the measurements of particular physical, thermal and hygric parameters, we used the following specimens: basic properties and apparent moisture diffusivity – 6 specimens 50 x 50 x 23-25 mm, thermal conductivity and volumetric heat capacity – 6 specimens 70 x 70 x 70 mm.

EXPERIMENTAL RESULTS AND DISCUSSION

The basic properties of both reference and modified gypsum for the drying temperatures of 40 and 80 °C are shown in Table 2. The values of bulk density and porosity were similar for the materials S0, S3, S4 and S5, the differences being up to 10% no matter the drying temperature. This can be explained by the same water/gypsum ratio used in the preparation of reference and hydrophobized materials. The application of plasticizers (S1 and S2) led to decrease in porosity by about 10% and increase in bulk density up to 10% compared to the reference specimens. This is an expected consequence of the application of plasticizers and the decrease of the water/gypsum ratio. The comparison of results achieved for samples dried at the temperatures of 80 °C and 40 °C shows that higher bulk density and lower porosity had the materials which were dried at 40 °C. This means that some originally chemically bound water was removed after drying to 80 °C.

Table 2 Basic physical properties of measured materials

Material	Bulk density [kgm^{-3}]	Matrix density [kgm^{-3}]	Open porosity [% by volume]
S0-80	1019	2530	60
S1-80	1124	2495	55
S2-80	1089	2577	58
S3-80	998	2530	61
S4-80	962	2530	62
S5-80	930	2530	63
S0-40	1170	1900	38
S1-40	1270	1950	35
S2-40	1250	1935	35
S3-40	1100	1900	42
S4-40	1060	1900	44
S5-40	1120	1900	41

Table 3 shows thermal and hygric properties of studied materials. The samples used for measurements were dried at first and then stored at laboratory conditions: relative humidity 50% and temperature about 20 °C. The materials dried at 80 °C had all almost the same values of thermal conductivity and volumetric heat capacity. For the drying temperature of 40 °C the differences were higher. The lowest thermal conductivity exhibited the material S4, the highest had the materials S1 and S2 produced using plasticizers. This corresponds with the open porosity measurements in Table 2. The values of thermal conductivity of samples dried at 80 °C were about two times lower then for materials dried at 40 °C. This is also in good agreement with the measured basic properties (see Table 2). The volumetric heat capacity was not affected by the drying temperature in a significant way. The differences were only up to 5%.

From the point of view of water transport properties the application of hydrophobization admixtures was successful for S4 (ZONYL 9027) and S5 (ZONYL 301). The water absorption coefficient decreased about 5 times and apparent moisture diffusivity more by one order of magnitude compared to the reference specimens. In the material S3 (IMESTA IBS 47) the hydrophobization had a lower effect which was quite comparable with the use of plasticizers (S1 and S2). The drying temperature affected only water transport properties of the materials S1, S2 and S3 in a significant way. Water absorption coefficient of the specimens dried at 40 °C was about two times lower than for those dried at 80 °C. This is in basic accordance with the open porosity data in Table 2. The hydrophobization used for the materials S4 and S5 was the same successful for both drying temperatures. On one hand, this confirms the proper function of both hydrophobization admixtures, no matter the drying temperature. On the other, this effect may also be partially due to the secondary hydration after the specimens dried at 80 °C came in contact with water because the

water absorption coefficient of the reference material was found to be basically unaffected by drying temperature as well.

Table 3 Thermal and hygric properties of measured materials

Material	Thermal conductivity [$Wm^{-1}K^{-1}$]	Volumetric heat capacity [$Jm^{-3}K^{-1}$]	Water absorption coefficient [$kgm^{-2}s^{-1/2}$]	Apparent moisture diffusivity [m^2s^{-1}]
S0-80	0.22	1.49 E+6	0.31	2.6 E-7
S1-80	0.22	1.50 E+6	0.25	2.1 E-7
S2-80	0.23	1.50 E+6	0.31	2.5 E-7
S3-80	0.22	1.48 E+6	0.25	1.5 E-7
S4-80	0.21	1.46 E+6	0.06	7.3 E-9
S5-80	0.21	1.46 E+6	0.11	2.6 E-8
S0-40	0.43	1.58 E+6	0.30	6.1 E-7
S1-40	0.53	1.63 E+6	0.14	1.6 E-7
S2-40	0.54	1.64 E+6	0.13	1.4 E-7
S3-40	0.40	1.56 E+6	0.14	1.2 E-7
S4-40	0.36	1.55 E+6	0.06	1.9 E-8
S5-40	0.43	1.53 E+6	0.06	2.0 E-8

CONCLUSIONS

The measurements of basic physical, hygric and thermal properties in this paper have shown that the drying temperature was an important factor affecting the properties of gypsum in a significant way. Drying at 80 °C was apparently not a suitable treatment because already the basic properties of both reference and modified gypsum materials were changed very remarkably in a comparison to drying at 40 °C. Apparently, some originally chemically bound water was removed after heating to 80 °C which meant that the material was not thermally stable at this temperature any longer. Therefore, it can be concluded that the critical temperature for the dehydration of calcium sulfate dihydrate to hemihydrate lies somewhere between 40 and 80 °C. The relatively close results obtained for water transport properties of specimens dried at 40 and 80 °C for some studied materials which was in a clear contradiction to the measured data of bulk density and open porosity were probably achieved due to the secondary hydration taking place after the contact of the specimens with water.

ACKNOWLEDGEMENT

This research has been supported by the Ministry of Industry and Trade of Czech Republic, under grant No. FT-TA3/005.

REFERENCES

[1] Schulze W., Tischer, W. Lach V.: Necementové malty a betony. Praha: SNTL 1990. pp. 20-31.

[2] Řičánek. M.: Sádra a její vlastnosti. In Sádra v památkové péči. Seminář společnosti STOP. Praha: STOP 2002. pp. 4-13.

[3] Šatava. V.: Studie procesu tvrdnutí suspenzí sádry. Doktorská disertační práce. Praha: AVČR. 1968. 180 p.

[4] ČSN EN ISO 12 570. Tepelně vlhkostní chování stavebních materiálů a výrobků – Stanovení vlhkosti sušením při zvýšené teplotě. ČNI 2001. 12 p.

[5] ČSN EN 12 859 (ČSN 72 3610). Sádrové tvárnice – Definice. požadavky a zkušební metody. ČNI 2002. 22 p.

[6] Kupilík. V.: Chování sádry v různých provozních podmínkách. In Sádra v památkové péči. Seminář společnosti STOP. Praha: STOP 2002. pp. 14-22.

[7] Wirsching. F.: Drying and Agglomeration of Flue Gas Gypsum. In The Chemistry and Technology of Gypsum. Philadelphia: American Society for Testing and Materials 1984. pp. 161-174.

[8] Turk D.H. – Bounini L.: The Effect of Sorbet Water on the Determination of Phase Composition of $CaSO_4.H_2O$ Systems by Various Methods. In The Chemistry and Technology of Gypsum. Philadelphia: American Society for Testing and Materials 1984. pp. 49-56.

[9] Roels S., Carmeliet J., Hens H., Adan O., Brocken H., Černý R., Pavlík Z., Hall C., Kumaran K., Pel L., Plagge R., Interlaboratory Comparison of Hygric Properties of Porous Building Materials, Journal of Thermal Envelope and Building Science, 27 (2004), 307-325.

[10] Kumaran M.K., Report on Measurements to Determine Moisture Diffusivity of Eastern White Pine, IEA Annex XXIV Report T3-CA-92/04, 1994.

[11] ČSN 72 2301 Sádrová pojiva. Klasifikace. Všeobecné technické požadavky. Zkušební metody Vydavatelství, Úřad pro normalizaci a měření 1979. 12 p.

FACTORS INFLUENCING MEASUREMENTS OF THE THERMAL CONDUCTIVITY BY HOT BALL METHOD

Ľudovít Kubičár[1], Vladimír Štofanik[1], Vlastimil Boháč[1], Ulf Hammerschmidt[2]

[1]Institute of Physics SAV, Dúbravská cesta 9, SK-845 11 Bratislava, Slovakia
[2]Physikalishe-Technishe Bundesanstalt, Braunschweig,
Email: kubicar@savba.sk

Abstract

The paper discusses the principle and the construction of the hot ball sensor for measurement of the thermal conductivity. The sensor in a form of a small ball generates heat and simultaneously measures the temperature response. Real properties of the hot ball, contact thermal resistance between the hot ball and the surrounding material and the influence of the connecting wires are analyzed. Reliability of the hot ball sensor has been studied considering reassembling and the use of 6 individual hot ball sensors. Reproducibility below 1% was found in the whole range of thermal conductivities using fixed setup. Reassembling using the same material made uncertainty within 2% percent and variation in thermal conductivity data within 7% when different hot ball sensors were used.

Key words: transient methods, hot ball method, disturbing effects, contact thermal resistance, heat capacity of the hot ball

1 Introduction

Recently a new class of dynamic methods – transient methods for measuring thermophysical properties has started to spread in research laboratories as well as in technology. The principal difference between classical and transient methods consists in variability of specimen size, measuring time and number of measured parameters. Transient methods need significantly shorter time for a measurement and possess high variability in specimen size. Some transient methods can determine the specific heat, thermal diffusivity and thermal conductivity within a single measurement [1- 4]. A set of new innovative instruments started to spread on the marked that are based on transient methods. Recently portable instruments and monitoring systems have been introduced onto market. Construction of such devices has evoked a search for suitable sensors that would provide information on the thermophysical properties of tested objects. By now a principle of the hot wire in the needle probe [5] and in the hot bridge [6] has been the most often used in portable instruments. Recently, a principle of a hot ball sensor in two components configuration, i.e. a heat source and a thermometer fixed apart from each other has been published [7].

The present paper deals with the hot ball sensor in a single component configuration i.e. when a heat source and a thermometer are unified in a single unit. The working equation is derived. Disturbing factors, the real properties of the ball, the thermal contact between the ball and the surrounding medium and the connecting wires

to the hot ball sensor are analyzed. Construction of the hot ball, the corresponding instrument and the measurement methodology is discussed. The calibration based on the materials that have been tested within the intercomparison measurements is performed.

2 Hot Ball Sensor

Model of the hot ball sensor is shown in Fig. 1. A heat source in a form of a small ball starts to deliver constant heat for t > 0 and simultaneously it measures the temperature response (Fig. 2. The temperature response is of a transient form stabilizing to a constant value T_m after some time.

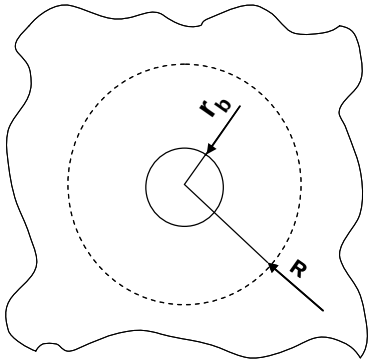

Fig. 1. Model of the hot ball method.

This moment is used to determine the thermal conductivity of the surrounding medium. It should be stressed that the steady state regime of the hot ball has nothing to do with the one used in the Guarded Hot Plate technique. The latter is based on the existence of the heat and the cold plates (heater and sink) while the former utilizes physics of the heat spread from the spherical heat source. The heat penetrates to sphere with radius R during the temperature stabilization to T_m. Thus the determined thermal conductivity corresponds to material within this sphere. Then an averaged value is to be determined for inhomogenous materials.

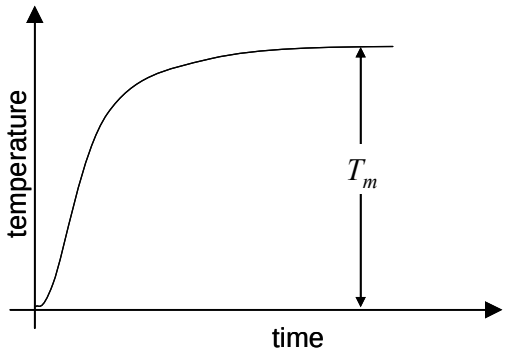

Fig. 2.: The temperature response corresponding to ball heat output q = const. for t > 0.

3 Theory of Hot Ball Sensor

The working equation of the hot ball sensor is based on an ideal model. The ideal model assumes a constant heat flux F per surface unit from the empty sphere of radius r_b into the infinitive medium starting to be delivered for times t > 0. Then the temperature distribution within the medium is characterized by the function [8]

$$T(r,t) = \frac{r_b^2 F}{r\lambda}\left\{\operatorname{erfc}\left(\frac{r-r_b}{2\sqrt{at}}\right) - \exp\left(\frac{r-r_b}{r_b} + \frac{at}{r_b^2}\right)\operatorname{erfc}\left(\frac{r-r_b}{2\sqrt{at}} + \frac{\sqrt{at}}{r_b}\right)\right\} \tag{1}$$

where erfc(x) is error function defined by $\operatorname{erfc}(x) = 1 - \frac{2}{\pi}\int_0^x \exp\left(-\zeta^2\right)d\zeta$ and λ and a are thermal conductivity and thermal diffusivity of the surrounding medium, respectively. The equation (1) is a solution of partial differential equation for heat conduction for $r \geq r_b$ considering boundary and initial conditions

$$T(r,t) = 0, \quad t = 0,$$

$$\lambda\frac{\partial T(r,t)}{\partial r} = -F\,, \; F = const, \; r = r_b, \; t > 0.$$

Function (1) gives a working equation (2) of the measuring method in long time approximation $t \to \infty$ assuming that temperature is measured at the surface of the empty sphere $r = r_b$

$$\lambda = \frac{q}{4\pi r_b T_m(t \to \infty)} \tag{2}$$

where the heat flux of the empty sphere F is recalculated to the overall heat ball production q according $F = q/4\pi r_b^2$, and T_m is stabilized value of the temperature response. The empty sphere represents an ideal hot ball of radius r_b characterized by a negligible heat capacity and high thermal conductivity $\lambda_b \to \infty$. Similar methodology has been applied for deriving the working equation of the hot wire method [1].

The measuring method based on function (1) belongs, in fact, among the class of transient ones. Nevertheless, the heat source of the spherical symmetry possesses a special feature i.e. it yields the steady state in long times and this moment is utilized to measure the thermal conductivity.

4 Analysis of disturbing effects

A hot ball must be constructed of parts generating constant heat on one hand and measuring the temperature response on the other hand. Then real properties of the ball and its thermal contact to the surrounding medium – the tested material influence the measuring process. In addition the electrical wires connecting the ball might influence the measuring process. Theoretical analysis of such hot ball structure requires a sophisticated mathematical approach that might not always provide the expected information. Therefore, we accept simplified models of the ball represented by a

homogenous material ascribed to the heater as well as to the thermometer. Two models will be analyzed, namely a heat capacity model and a steady state model. Both models concern the properties of a real heat source. Influence of the connecting wires will be analysed experimentally, only as this effect requires too complicated theoretical model.

Heat capacity model. Assuming that the ball is a perfect conductor, the measured temperature can be ascribed to the surface temperature of the ball as the Eq. (2) requires. Such ball has its own heat capacity causing a deviation from the ideal model. In addition some contact thermal resistance 1/H (H - contact thermal conductance) between the ball and the medium might exist. A model including the heat capacity of the ball Mc^* (M and c* are mass and specific heat of the ball, respectively) and the contact thermal resistance $1/H$ is characterized by the function valid for large values of time[9]

$$T_b(t) = \frac{q}{4\pi\lambda r_b}\left[\frac{1+r_b h}{r_b h} - \left(\frac{r_b}{\sqrt{\pi a t}}\right) - \frac{{r_b}^2\left[2+r_b h(2-f)\right]}{2hf\pi^2\sqrt{at}}\right] + \ldots\ldots \tag{3}$$

where $f = 4\pi {r_b}^3 \rho \frac{c}{Mc^*}$, q is heat supplied over the surface at $r = r_b$, M is mass and c^* the specific heat of the ball, respectively and c, ρ are specific heat and density of the medium, respectively and $h = H/\lambda$, H is contact thermal conductance. The Eq. (3) is a solution of partial differential equation for heat conduction considering the boundary and initial conditions

$$\lambda \frac{\partial T_{med}(r,t)}{\partial t} + H(T_b - T_{med}) = 0, \quad r = r_b, \quad t > 0,$$

$$H(T_b - T_m) + c^* M \frac{\partial T_b}{\partial t} = F, \quad r = r_b, \quad t > 0.$$

The heat capacity of the ball Mc^* and the contact thermal resistance $1/H$ disturbs the transient and thus it influences the measuring process. Assuming that the parameters of the ball are the following: heat output q = 6 mW, radius r_b = 1 mm, and of the tested material: density ρ = 1000 kg m^{-3}, thermal conductivity λ = 0.5 W m^{-1} K^{-1} and the thermal diffusivity a = 0.5 mm^2·sec^{-1} one obtains transients using function (3) shown in Fig. 3 and 4 for a set of the ball heat capacities Mc^* and contact thermal conductances. The used input data represent the most often used experimental conditions. The calculations have been performed considering medium made of polymer.

A negligible influence of the heat capacity of the ball Mc^* has been found in the broad range of the parameter $Mc^* = 10^{-5} \div 1$ J m^{-3} K^{-1} (Fig. 3). The calculations have been performed considering rather non-ideal contact thermal conductance, i.e. H = 1000 W m^{-2} K^{-1}. Rather strong influence of the contact resistance on transient has been found (see Fig. 4). Calculations have shown that the contact thermal conductivity H should reach $H >$ 6 000 W m^{-2} K^{-1} to keep conditions of the ideal model.

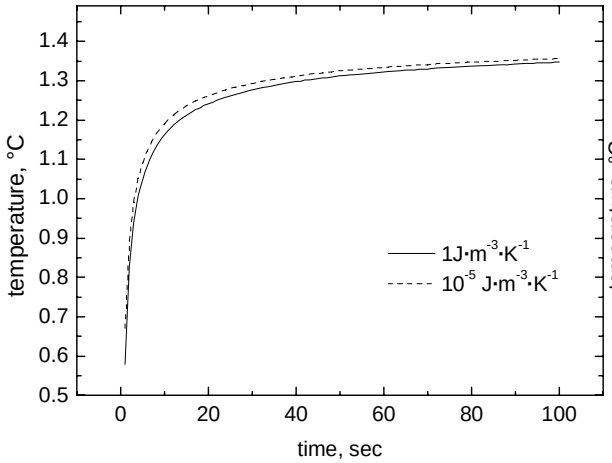

Fig. 3. Transients calculated using (3). Parameter heat capacity of the ball *Mc**.

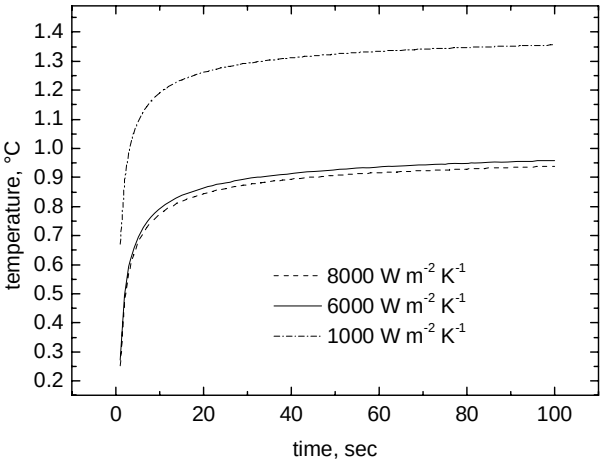

Fig. 4. Transients calculated using (3). Parameter contact thermal conductance *H*.

A criterion of the steady state regime has been searched due to the calculation of transient (3) considering real ball parameters (contact thermal conductance H = 10 000 W m^{-2} K^{-1} and heat capacity Mc^* = 4·10^{-5} J m^{-3} K^{-1}) and parameters of the medium (density ρ = 1000 kg m^{-3}, thermal conductivity λ = 0.5 W m^{-1} K^{-1} and the thermal diffusivity a = 0.5 mm^2 s^{-1}). The working equation (2) has been used for thermal conductivity evaluation using point by point (value T_m in eqation (2)) of the scanned temperature response. A 5% deviation (0.5 – λ_{com})/0.5 from the thermal conductivity input λ_{in} = 0.5 W m^{-1} K^{-1} has been found after 65 s (see Fig. 5).

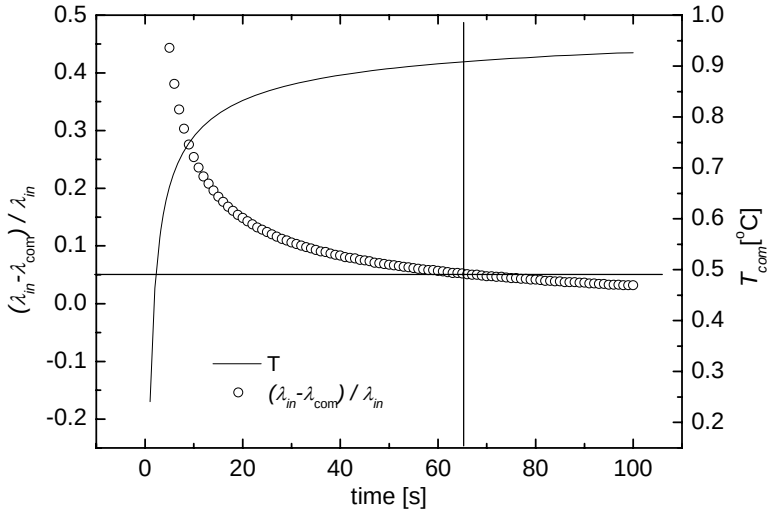

Fig. 5.: Estimation of the measuring time

This test has shown that the steady state regime can be accepted after 65 s for materials of thermal conductivity λ = 0.5 W m^{-1} K^{-1}. A deviation can be reduced in case of longer measuring time.

Steady state model. The previous analysis was based on the assumption that the ball is a perfect heat conductor. This corresponds to the experimental setup of high difference in thermal conductivity between the ball body and the surrounding medium – tested material. However, the ball properties are given by producer. Therefore, we look for

criterion of a thermal conductivity range of the tested materials to obtain reliable results. As the transient properties were discussed in the previous case the steady state regime is to be analyzed, only. In case the ball and the surrounding medium represent different materials a solution of the partial differential equation is to be sought. The function has the form [10]

$$T_b(r) = q\frac{\left[r_b^2 - r^2 + \frac{2}{H}r_b\lambda_b + 2r_b^2\left(\frac{\lambda_b}{\lambda}\right)\right]}{8\pi\lambda_b r_b^3} \quad \text{for } r < r_b \tag{4}$$

and

$$T(r) = \frac{q}{4\pi r\lambda} \quad \text{for } r > r_b \tag{5}$$

where $T_b(r)$ and $T(r)$ characterize temperature distribution within the ball and the medium, respectively, $1/H$ is the thermal contact resistance, r_b and λ_b is the ball radius and its thermal conductivity, respectively and q is the overall heat production of the ball during time unit.

The functions (4) and (5) have been found by solution of partial differential equation for heat conduction considering the boundary and initial conditions

$$T_b(r) = T(r) = 0, \quad t = 0,$$

$$\lambda_b \frac{\partial T_b(r,t)}{\partial r} = \lambda \frac{\partial T_{med}(r,t)}{\partial r}, \quad r = r_b, \quad t > 0$$

$$\lambda \frac{\partial T_{med}(r,t)}{\partial r} + h(T_b - T_{med}) = 0, \quad r = r_b, \quad t > 0.$$

Analysis of the influence of contact thermal resistance has been performed considering different materials of the ball (thermal conductivity range λ_b from 0.2 up to 1 W m^{-1} K^{-1}) and two different values of the contact thermal conductance H =10000 and 1000 W m^{-2} K^{-1} (Fig. 6 left). The surrounding medium represents material of thermal conductivity λ = 0.5 W m^{-1} K^{-1}. A ball radius is to be 1 mm and a heat output of the ball q = 0.006 W. The shape of the temperature distribution inside the ball is the same, just it is shifted towards the higher values in the case of non-ideal contact. No influence on the temperature distribution in medium can be recognized. This follows from the Eq. (5). In practice a ball of specific thermophysical properties is used for a range of materials having different thermal conductivity. Then weight of the thermal contact conductance on measuring process depends on thermal conductivity of the testing material. Fig. 6 righ gives an overview on the role of the thermal contact between the ball and the medium. The plots have been calculated for the thermal contact conductance H = 1000 W m^{-2} K^{-1}. Clearly the temperature drop at the thermal contact is the same for all of the medium thermal conductivities assuming the identical ball heat output q = 0.006 W. Nevertheless, its weight is negligible for a medium of low thermal conductivity.

Variation of the thermal conductivity of the medium influences its temperature distribution strongly, providing the same ball heat output q = 0.006 W is used while no changes can be found within the ball and at the thermal contact. Above statement is of high importance considering the measuring regime. Looking at the temperature distribution within the ball and the medium one can find that for low thermal conductivity medium the temperature gradient within the ball can be neglected, i.e. the conditions of the ideal model are nearly reached.

The measured average temperature instead of the ball surface temperature and the temperature drop at contact cause data shift when Eq. (2) is used. However, this shift remains the same for different surrounding mediums. Thus a correction based on calibration using standard materials could be introduced. Reliable measurements can be obtained for the materials of low thermal conductivity.

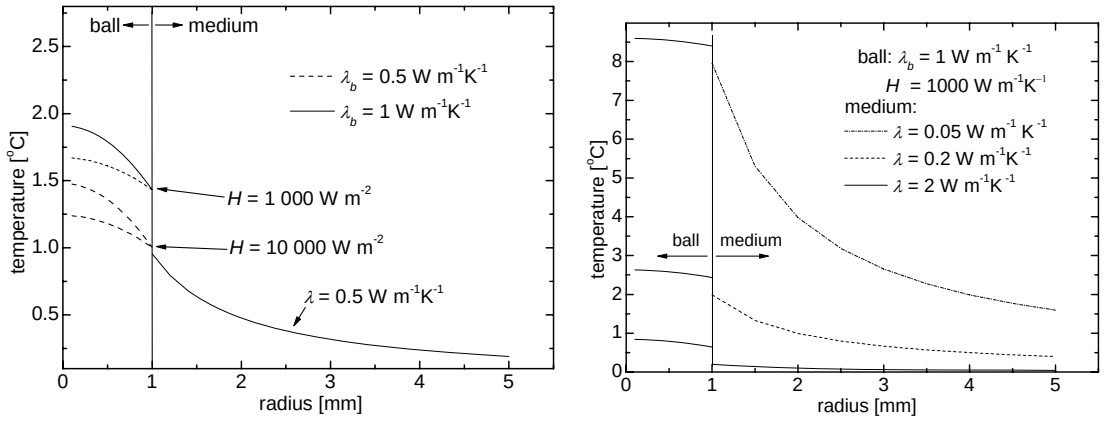

Fig. 6. Temperature distribution within the ball and the surrounding medium. Parameters: thermal conductivity of the ball λ_b and surrounding medium λ, and the contact thermal conductance between the ball and the medium H.

5 Experiment

The strategy of the theory verification is based on the calibration of the hot ball sensors by the Eq. (2) rewritten in a form

$$q / T_m = 4\pi r_b \lambda = A\lambda \tag{6}$$

where A is a constant $A = 4\pi r_b$. The ratio q/T_m is a linear function of thermal conductivity that will be tested using different materials. In principle, the hot ball sensor is an absolute method for measuring the thermal conductivity providing that the assumptions given by the theory are completed. In addition the function (6) will be plotted using ball radius r_b = 1.05 mm. A difference between the experimental data and the theoretical function should indicate the weight of the thermal contact and the temperature gradient within the ball.

Table 1 gives basic characteristics of the tested materials along with the experimental parameters used during measurements. The tested specimen consisted of two blocks and the sensor was placed in the contact of the two specimen surfaces. To improve the thermal contact a groove was made into one specimen block in which the

ball was placed. A contact paste (Middland Silicones Ltd) was used for the thermal contact improvements of the ball and the specimen. While testing a porous structure the contact surfaces were covered by epoxy varnish to prevent the paste diffusion into material. A hot ball sensor has been immersed into paste or fluid in case of not solid materials. The solidified materials have been tested in a setup configuration arranged prior to solidification by immersion of a ball into the tested medium.

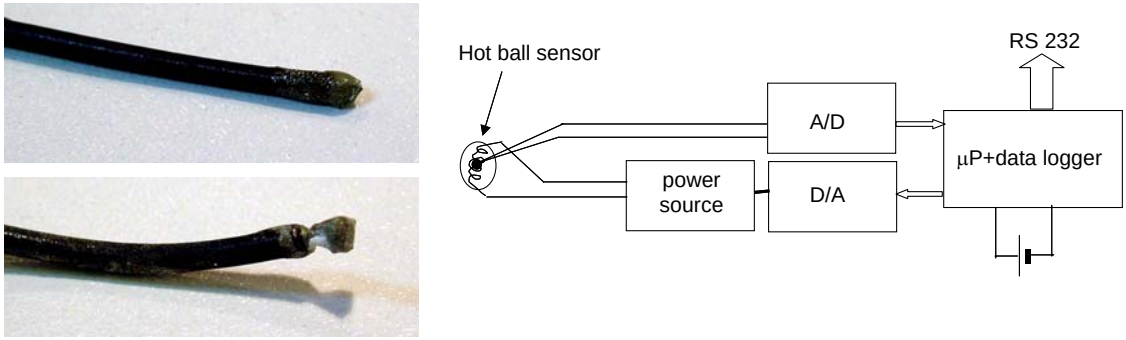

Fig. 7. Photos of two balls prepared in different design (left) and the scheme of instrument for measuring thermal conductivity by the hot ball method (right).

Table 1. Materials and experimental parameters for calibration hot ball sensor.

Material	Thermal conductivity [$W \cdot m^{-1} \cdot K^{-1}$]	Structure	q [mW]	Block size [mm]
Cement Paste	-	water-powder mixture	5.0	-
Stiffened Paste	-	opened pores	5.0	-
Hardened Paste	-	opened pores	5.0	-
Water	0.52 (25°C)	fluid	4.5	-
Ice	2.2 (-5°C)	compact	4.5	-
Basetect	-	paste	2.5	-
Sandstone	1.9	opened pores	6.5	50x50x20
PMMA	0.19	compact	2.5	ϕ50, length 25
Aerated Concrete	0.155	opened pores anisotropic	2.5	150x150x50
Calcium Silicate	0.097	opened pores	1.5	150x150x50
Phenolic Foam	0.06	opened pores	2.0	150x150x50
Styrodur	0.0435	cosed pores	3.5	150x100x30
Air	0.027	gas	1.5	
Wood Composite	0.025	ribbons	6.0	300x300x40

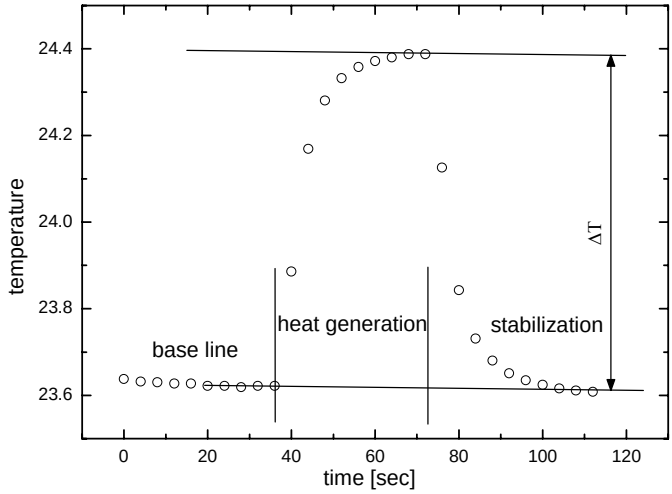

Fig. 8.: Signal of the hot ball sensor measured by monitoring system RTM 1.01.

RTM 1.01 instrument has been used for measurements. Scheme of the instrument is shown in Fig. 7. Typical measurement signal is shown in Fig. 8 along with the characteristic points used for the calculation of the thermal conductivity. The measuring procedure consists of the specimen temperature measurement representing base line, switching on the heating and simultaneously scanning the ball temperature. When the ball temperature has stabilized, the heating is interrupted and a period of temperature equilibration follows. When the temperature in the specimen is equilibrated the next measurement may be realized. The repetition rate of the measurements depends on thermal conductivity and it takes from 10 up to 60 minutes.

6 Results

A test of the measurement reliability has been performed provided that the ball heat output varies in a broad range. The ball radius r_b = 1.05 mm has been used. The results are shown in Fig. 9 left. Data on thermal conductivity are stable in the range 2.5 – 30 mW within $\delta\lambda$ = +/- 0.0007 $W \cdot m^{-1} \cdot K^{-1}$. The measured data are shifted to higher values (see Table I). The shift is constant within a broad range of ball heat output. The test has shown that the measured data are not influenced by the ball heat output.

A test of steady-state regime has been made using the PMMA and measuring parameters q = 0.0025 W, ball radius r_b = 1.05 mm and measuring period (heating time) 3000 s. The scanned temperature along with the calculated thermal conductivity is shown in Fig. 9 right. Equation (2) was used for data evaluation point by point of the scanned temperature response. A small temperature increase was found after the heating was switched off. Therefore the base line was approximated by a line that connects third and 210th point. Then the temperature T_m, included in the calculation, is established as a difference between this base line and a response point. Data on thermal conductivity started to be stabilized above 500 s.

Sensors are not of a regular ball shape therefore one may assume that data may be scattered comparing individual sensors. In addition, the groove made in the used materials is also not of the regular shape. Therefore, in order to obtain an overview on data statistics the following strategy of the experimentation has been chosen. Eight different sensors were tested. At least 5 measurements at fixed setup and 2 re-assembling have been realized for every sensor/material configuration. A reassembling

consists of cleaning the groove, a deposition of the contact paste at the groove point where the ball is fixed, fixing the ball into the groove and assembling both parts of the tested materials together into one unit.This procedure was applied for phenolic foam, calcium silicate, PMMA and sandstone, only. Data obtained on a set of materials specified in Table 1 are shown in Fig. 10.

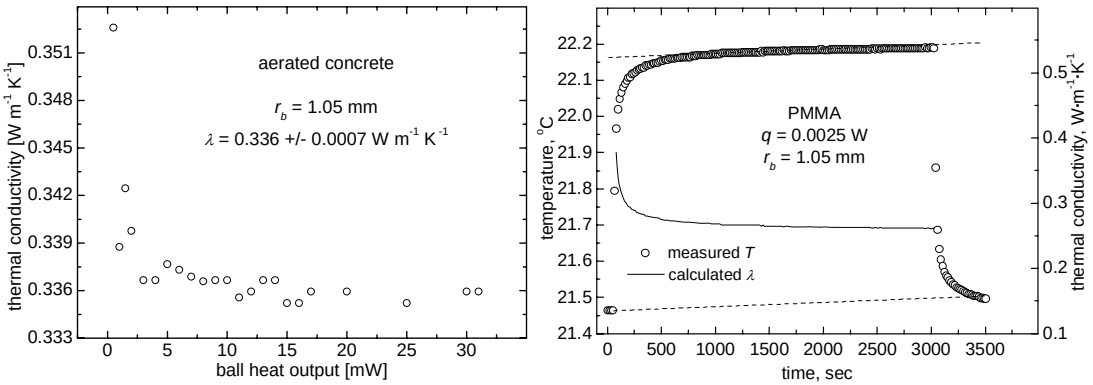

Fig. 9. Thermal conductivity of the aerated concrete as a function of the ball heat output (left), temperature response and thermal conductivity of the PMMA as a function of the time (right).

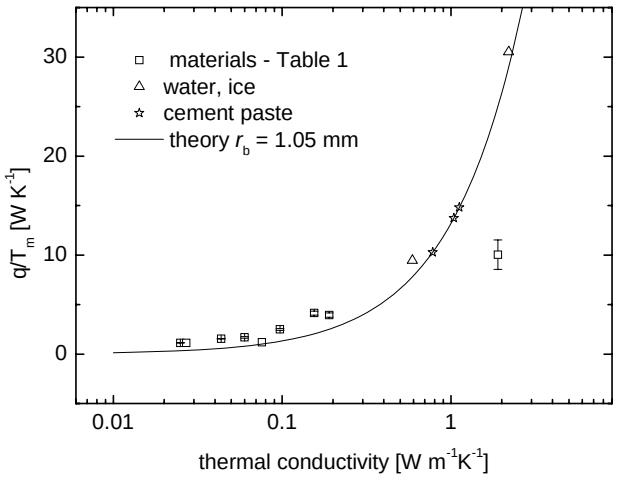

Fig. 10. Calibration function of the hot ball sensors. The full line follows ideal model (Eq. (6)) using ball radius q = 1.05 mm.

Analysis of data statistics has shown that the measurement reproducibility of the assembled specimen setup is rather high. Data scatter well below 1%. Reassembling induces data scattering within 3-5%. The highest contribution to the data scattering has been obtained in combination of the re-assembling and use of different sensors. The corresponding error bars are shown in Fig. 10. Two sets of sensors marked as HB300 (see Fig. 7 left – upper photo) and HB 400 (see Fig. 7 left – lower photo) have been included in calibration. Three kinds of materials have been tested, namely gas, fluids, paste and solids. Fluid (water) and paste (cement powder + water mixture, basetect) indicate significantly smaller deviations from the theoretical values. Similar feature can

be found for solidified materials (cement paste, ice). The thermal contact between the ball and the surrounding material has been established already in fluid state and it survived after solidification. Therefore a small deviation from the theoretical values can be found even for this kind of materials. A clear data shift can be found for all other solid materials. Data are shifted to higher values for low thermal conductivity materials and to lower values for high thermal conductivity materials.

7 Discussion

A theoretical curve is plotted in the Fig. 10. using Eq. (6) where the ball radius is assumed to be r_b = 1.05 mm. A data shift to higher values (a difference between the experimental and theoretical value) can be found for low thermal conductivity range and to lower ones for high thermal conductivity range. To analyze the possible sources of data shift the working Eq. (2) is rewritten in a form

$$\lambda_{app} = \frac{q_o + q_w}{4\pi r_b (T_m + \delta T_b + \delta T_c)} = \lambda \frac{\left(1 + \frac{q_w}{q_o}\right)}{\left(1 + \frac{\delta T_b}{T_m} + \frac{\delta T_c}{T_m}\right)} \tag{7}$$

where λ follows ideal model (Eq. (2)) considering ball heat output q_o, $q = q_w + q_o$ is overall ball heat output, δT_b - temperature drop across the radius of the ball, δT_c – temperature drop at the thermal contact and q_w the heat loss through the connecting wires. A temperature T_m and a ball heat output q_o has to be used in Eq. (2) to obtain the correct data (see Fig. 11).

Two limiting cases can be found at the measurement considering Eq. (7). When high thermal conductivity materials are measured the lower value λ_{app} in comparison to the real one λ is calculated due to the significant contribution of both drops of temperature, a drop within the ball and a drop at the contact (see Fig. 11). The heat loss q_w is negligible as heat transport from the ball to the surrounding medium is highly effective. In addition, a changeable thermal contact may be achieved due to reassembling. This is a case of sandstone where data on thermal conductivity are shifted down (see Fig. 10) and, in addition high data scattering is found due to reassembling and use of different sensors. Generally, the higher thermal conductivity of the medium the stronger influence of the thermal contact on measuring process can be found.

An opposite situation can be found when low thermal materials are measured. Then both of the temperature drops, a drop within the ball and a drop at the contact are negligible but the heat loss through the wires q_w starts to play a role in the measuring process. This disturbing factor shifts the calculated thermal conductivity to the higher values.

The ball and thermal contact properties as well as heat loss through the connecting wires have been estimated using the Egs. (2), (4), (5) and (6) and scans of the temperature response from experiments on some materials given in Table 1. While measuring process of the high thermal conductivity materials is influenced by the hot ball and the contact properties the heat loss through the contact wires affects the experiment for low thermal conductivity materials.

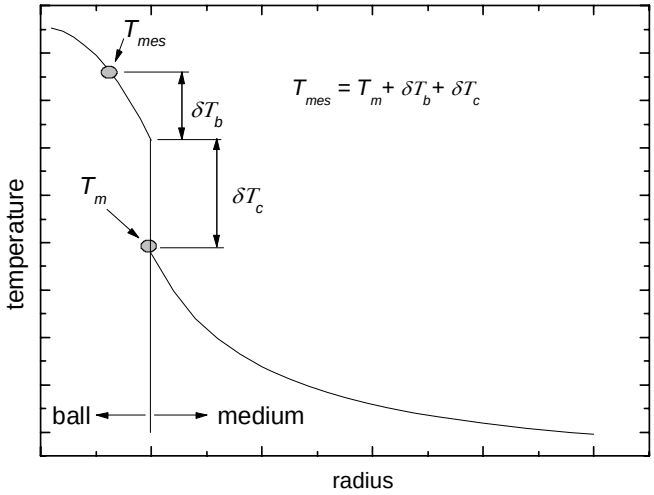

Fig. 11.Temperature distribution within the ball, thermal contact and the medium during the experiment.

Considering experimental data measured by the hot ball sensor (radius r_b = 1.05 mm) on sandstone and using ball heat output q = 0.006 W and measuring time 11 s one obtains experimental temperature response T_m = 0.676 ^oC. Using Eg. (2) one obtains q/T_{meas} = 8.875 J K^{-1} and apparent thermal conductivity λ_{app} = 0.6424 W m^{-1} K^{-1}. Using real thermal conductivity of sandstone λ = 1.9 W m^{-1} K^{-1} (Table 1) one obtains theoretical value q_o/T_m = 26.26 J K^{-1} (see Fig. 10). We assume that heat loss through the connecting wires is negligible $q_w \rightarrow 0$ due to high thermal conductivity of sandstone. Using (7) one obtains $\delta T_b + \delta T_b = 1.96 T_m$ that yields $\delta T_b + \delta T_b$ = 0.449^{o}C while theoretical temperature response corresponding to point T_m shown in Fig. 11 has value T_m = 0.229^{o}C, only. Thus the ball and the thermal contact properties strongly influence the resulting value of the thermal conductivity. Using Eqs. (4) and (5) one can estimate the contact thermal conductivity H. Assuming that the hot ball works in a regime of nearly perfect conductor the contact thermal conductivity is around H = 160 W m^{-1} K^{-1}. The estimated value is too low. However, data scattering of the thermal conductivity indicates that the thermal contact plays a serious role. In addition thermal conductivity of the ball is around $\lambda_b \sim 1$ W m^{-1} K^{-1} that is comparable to the sandstone thus one needs to include thermal properties of the ball into analysis, too. Then the resulted thermal contact conductivity would be higher.

The assumption has been accepted for experiments with low thermal conductivity materials that the ball and the thermal contact properties do not influence the measuring process, i.e. $\delta T_b/T_m + \delta T_b/T_m \rightarrow 0$ and the heat loss through the connecting wires affects the measuring process. Then we obtain estimations for heat loss through the connecting wires q_w/q_0 (Eq. 7) given in Table 2. Estimations have been performed in the following way: Using the ball heat output q one measures the temperature response T_{meas}. Using Eq. (2) one obtains q/T_{meas} and apparent thermal conductivity λ_{app}. Using real thermal conductivity λ (Table 1) one obtains the theoretical value q_o/T_m (see Fig. 10). Using (7) one obtains q_w and the theoretical ball heat output corresponding to the point T_m (T_m is a true value as $\delta T_b/T_m + \delta T_b/T_m \rightarrow 0$) shown in Fig. 11 has value q_o, only. Thus the connecting wires to represent a disturbing factor shifting data on thermal conductivity to higher values. Looking at Table 2 in detail one can find that q_w/q_0 grows with lowering the thermal conductivity of the measured materials, i.e. heat loss through the connecting

wires increases with lowering the thermal conductivity of the surrounding material. Data corresponding to wood composite is an exception from the above mentioned rule due to its structure.

Table 2.: Estimations of heat loss through the connecting wires.

Material	q [mW]	T_{meas} [°C]	q/T_{mes} [J K^{-1}]	λ_{app} [W m^{-1} K^{-1}]	q_0/T_m [J K^{-1}]	q_w [mW]	q_0 [mW]	q_w/q_0
PMMA	2.5	0.731	3.42	0.248	2.622	0.576	1.9	0.303
Calcium silicate	1.5	0.651	2.35	0.178	1.28	0.666	0.833	0.800
Phenolic foam	2	1.453	1.44	0.110	0.792	0.860	1.14	0.750
Styrodur	3.5	3.04	1.166	0.088	0.573	1.75	1.74	1.00
Wood composite	6	4.305	1.44	0.109	0.329	4.58	1.42	3.22

Measurement accuracy by a hot ball method requires a more detailed experimental as well as a theoretical analysis. While experimentation with different diameters of the connecting wires may help to optimise the hot ball method for testing low thermal conductivity materials a new approach has to be worked out for measurement of high thermal conductivity materials where contact thermal resistance plays a predominant role.

8 Conclusion

A new version of the transient method – the hot ball method for measuring thermal conductivity has been presented. The method is based on delivering constant heat by a heat source in the form of a ball into the non-limited surrounding medium for times $t > 0$. A working equation of the hot ball based on a model of the empty sphere in a non-limited surrounding medium has been found. Theoretical analysis of the measuring process based on a model of a ball made of the perfect conductor working in transient regime and a model of a ball made of the real material working in the steady state regime have been presented. The analysis gives a criterion for the thermal conductivity of the ball material λ_0 and surrounding medium λ. Good measurements can be obtained for $\lambda_0 > \lambda$. A hot ball sensor has been constructed consisting of two elements a heater and a thermometer. Both elements are fixed in a ball by epoxy resin. Diameter of the ball ranges within 2÷2.3 mm. A verification of the theory has been performed using a set of materials having the thermal conductivity in the range from 0.027 up to 2.2 W m^{-1} K^{-1}. Additional study needs to be performed in order to clear measurement uncertainty in detail.

Acknowledgements

Authors would like to thank to Mohamad Abid for measurements on water and ice and Marian Markovic for technical support. This work has been supported by the EU project G6RD-CT2000-00266 and by VEGA project 2/5100/25.

References

[1] Kubičár Ľ, Boháč V. Kubičár Ľ., Boháč V., *Review of several dynamic methods of measuring thermophysical parameters*. in "Proc. of 24th Int. Conf. on Thermal Conductivity / 12th Int. Thermal Expansion Symposium", ed. P.S. Gaal, D.E. Apostolescu, Lancaster: Technomic Publishing Company (1999), pp. 135–149

[2] Kubičár Ľ. Kubičár L., 1990, *Pulse Method of Measuring Basic Thermophysical Parameters*, in Comprehensive Analytical Chemistry, Vol XII, Thermal Analysis, Part E, Ed Svehla G, (Amsterdam, Oxford, New York, Tokyo: Elsevier)

[3] Hammerschmidt U and Sabuga W, 1995 Int. J on Thermophysics 21 1255 - 1278

[4] Gustafsson S E, 1991 Rev. Sci. Instrum. 62 767 - 804

[5] Lockmuller N, Redgrove J, Kubičár Ľ, 2003/2004 High Temp High Press, 35/36, 127

[6] Model, R., Stosch, R., Hammerschmidt, U., Virtual Experiment Design for the Transient Hot-Bridge Sensor, Int. J on Thermophysics, (2007) in print

[7] Haifeng Zhang, Liqun He, Shuxia Cheng, Zaiteng Zhai and Dayong Gao, 2003 Meas Sci, 14, 1369

[8] Carslaw H., S., Jaeger J., C., Conduction of Heat in Solids, (Clarendon Press, Oxford), pp.248 (1956)

[9] Carslaw H., S., Jaeger J., C., Conduction of Heat in Solids, (Clarendon Press, Oxford), pp.350 (1956)

[10] Carslaw H., S., Jaeger J., C., Conduction of Heat in Solids, (Clarendon Press, Oxford), pp.232 (1956)

HOMOGENIZATION TECHNIQUES FOR DETERMINATION OF THERMAL CONDUCTIVITY OF POROUS MATERIALS

Robert Černý, Zbyšek Pavlík

Czech Technical University in Prague, Faculty of Civil Engineering, Department of Materials Engineering and Chemistry, Thákurova 7, 166 29 Prague, Czech Republic, email: cernyr@fsv.cvut.cz, pavlikz@fsv.cvut.cz

Abstract:
Homogenization principles are frequently used for estimation of various parameters of composite materials. Their application is most common in the stress-strain analysis and electromagnetic theory. In this paper, the utilization of mixing rules based on homogenization principles for determination of moisture dependent thermal conductivity is discussed. In terms of homogenization, a porous material is considered as a mixture of three or four phases, namely the solid, liquid and gaseous phase in three-phase systems, and the extra bound-water phase is added in four-phase systems.

Keywords:
Thermal conductivity, moisture content, homogenization

INTRODUCTION

The envelope of any building continuously responds to the changes in indoor and outdoor temperature, air pressure and humidity conditions. This results in an exchange of energy and mass (air as well as moisture) between the indoor and outdoor environments through the envelope. Building physicists refer to these phenomena as “heat, air and moisture transport” through building materials and structures [1]. Designers and builders are always interested, especially for economical reasons and durability and service live problems, in knowing the long-term performance of building envelope, as subjected to the transport processes. That is why the thermal properties of building materials appear to be of particular importance for their practical applications whereas the majority of them contain significant amount of pores that can be in specific cases filled by water. Every catalogue list of any material producer of building materials contains thermal conductivity, sometimes also specific heat capacity but they give only single characteristic values mostly that represent mainly properties of dry materials. In the dry building material heat transfer is a combination of conduction, radiation from the surfaces of the pores and convection within the pores. Thus, in a practical use of thermal conductivity all three modes of heat transfer are to be counted with. However, absolutely dry materials occur in the conditions of building sites very rarely. Also the materials already inbuilt in the structures and exposed to the climatic loading exhibit the dependence of their properties on moisture changes. If the material is wet, heat transferred by moisture in the capillaries and the enthalpy changes that accompany phase transitions also add to the density of heat flow rate. From this appears the necessity to determine thermal conductivity of porous materials as a function of moisture content. Since the experimental measurement of thermal properties in dependence on moisture is very time consuming, new approaches are explored and tested in materials research. In this paper, the applicability of

homogenization techniques for determination of moisture dependent thermal conductivity of porous building materials is studied.

HOMOGENIZATION THEORY AND MIXING FORMULAS

In terms of homogenization theory, the porous material is considered as a mixture of three or four phases, namely the solid, liquid and gaseous phase (in four phase systems, the effect of bound water can be included) that forms the solid matrix and porous space of the material. The solid phase is formed by the materials of the solid matrix. The liquid phase is represented by water and gaseous phase by air. In the case of dry material, only the solid and gaseous phases are considered. The volumetric fraction of air in porous body is given by the measured total open porosity. In case of penetration of water, a part of the porous space is filled by water. For the evaluation of thermal conductivity of the whole material (i.e., the effective thermal conductivity), the thermal conductivities of the particular constituents forming the porous body have to be known.

The effective thermal conductivity of a multi-phase composite cannot exceed the bounds given by the thermal conductivities and volumetric fractions of its constituents. The upper bound is reached in a system consisting of plane-parallel layers disposed along the heat flux vector. The lower bound is reached in a similar system but with the layers perpendicular to the heat flux. These bounds are usually called Wiener's bounds, according to the Wiener's original work [2] and can be expressed by the following relations

$$\lambda_{eff} = \frac{1}{\frac{f_1}{\lambda_1} + \frac{f_2}{\lambda_2} + \frac{f_3}{\lambda_3} + \frac{f_4}{\lambda_4}}, \tag{1}$$

$$\lambda_{eff} = f_1\lambda_1 + f_2\lambda_2 + f_3\lambda_3 + f_4\lambda_4, \tag{2}$$

where Eq. (1) represents the lower limit and Eq. (2) the upper limit of effective thermal conductivity (f_j is the volumetric fraction of the particular phase, λ_j its thermal conductivity).

The mixing of phases resulting in effective thermal conductivity functions falling between the Wiener's bounds can be done using many different techniques. We will give couple of characteristic examples of mixing formulas in what follows which were successfully applied by various scientists especially for dielectric mixing in the past and we will introduce them modified for thermal conductivity expressions. Only self-consistent formulas will be accounted for which allow to model the material behaviour in sufficiently wide moisture range.

The Lichtenecker's equation [3]

$$\lambda_{eff}{}^{k} = \sum_{j=1}^{4} f_j \lambda_j{}^{k} \tag{3}$$

is a straightforward generalization of Wiener's formulas. The parameter k in Eq. (1) varies within the [-1, 1] range. Thus, the extreme values of k correspond to the Wiener's boundary values. The parameter k may be considered as describing a transition from the anisotropy at k = -1.0 to another anisotropy at k = 1.0.

Another mixing treatment was introduced by Rayleigh [4] and a little bit later, with a somewhat different theoretical justification, by Maxwell Garnett [5]. It consists in perception of a continuous phase 1 (in the particular case of a wet porous medium it is the solid matrix) containing randomly distributed spherical scattering particles of discontinuous phases 2, 3 and 4 (in the above

mentioned case it is air, free water and bound water, respectively). The formula by Rayleigh can be expressed (in a simple extension from the original 2 to 4 phases) as

$$\frac{\lambda_{eff}-1}{\lambda_{eff}+2}=\sum_{j=1}^{4} f_j\left(\frac{\lambda_j-1}{\lambda_j+2}\right). \tag{4}$$

The formula by Maxwell Garnett (extended to the four-phase system again) can be written as

$$\frac{\lambda_{eff}-\lambda_1}{\lambda_{eff}+\lambda_1}=\sum_{j=2}^{4} f_j\left(\frac{\lambda_j-\lambda_1}{\lambda_j+\lambda_1}\right). \tag{5}$$

The derivation of Maxwell-Garnett's formula is based on the assumption that the basic thermal conductivity of the composite is that of the solid matrix. Bruggeman [6] made a further step towards generalization of this treatment and assumed that the basic thermal conductivity is the thermal conductivity of the mixture. The resulting formula reads

$$\frac{\lambda_{eff}-\lambda_1}{\lambda_{eff}+2\lambda_{eff}}=\sum_{j=2}^{4} f_j\left(\frac{\lambda_j-\lambda_1}{\lambda_j+2\lambda_{eff}}\right). \tag{6}$$

Later, a variety of mixing formulas appeared which reflected the various shapes and topologies of liquid and gaseous phase inclusions within the porous medium. In one of the most popular models of this type Polder and van Santen [7] extended the Bruggeman formula to elliptical inclusions and formulated its three useful simplifications (given in somewhat different algebraic form). The first of them, the original one, is valid for spherical inclusions, the second for needle-shape inclusions and the third for their disc shape. The resulting mixing formulas can be written as

$$\lambda_{eff}=\lambda_1+\sum_{j=2}^{4} f_j(\lambda_j-\lambda_1)\cdot\frac{3\lambda_{eff}}{2\lambda_{eff}+\lambda_j}, \tag{7}$$

$$\lambda_{eff}=\lambda_1+\sum_{j=2}^{4} f_j(\lambda_j-\lambda_1)\cdot\frac{5\lambda_{eff}+\lambda_j}{3\lambda_{eff}+3\lambda_j}, \tag{8}$$

$$\lambda_{eff}=\lambda_1+\sum_{j=2}^{4} f_j(\lambda_j-\lambda_1)\cdot\frac{2\lambda_j+\lambda_{eff}}{3\lambda_j}. \tag{9}$$

Because of the large difference between the thermal conductivity of free and bound water in porous medium, Dobson et al. [8] extended the Lichtenecker's [3] power-law formula and arrived at the relation

$$\theta=\frac{\lambda_{eff}{}^{\alpha}-\theta_{bw}(\lambda_{bw}{}^{\alpha}-\lambda_{fw}{}^{\alpha})-(1-\psi)\lambda_s{}^{\alpha}-\psi\lambda_a{}^{\alpha}}{\lambda_{fw}{}^{\alpha}-\lambda_a{}^{\alpha}}, \tag{10}$$

where θ_{bw} is the amount of water bonded on pore walls [m^3/m^3], λ_{bw} the thermal conductivity of bound water (according to [9], the bound water can be assumed to have the same thermal conductivity as ice, so near -20°C it is equal to 2.4 W/mK), λ_{fw} the thermal conductivity of free

water (0.6 W/mK), λ_a the thermal conductivity of air (0.026 W/mK), ψ the total open porosity, and α is an empirical parameter.

De Loor [10] used the Polder-van Santen model [7] for disc inclusions and formulated its extension in the form

$$\theta = \frac{3(\lambda_s - \lambda_{eff}) + 2\theta_{bw}(\lambda_{bw} - \lambda_{fw}) + 2\psi(\lambda_a - \lambda_s)}{\lambda_{eff}(\frac{\lambda_s}{\lambda_{fw}} - \frac{\lambda_s}{\lambda_a}) + 2(\lambda_a - \lambda_{fw})} + \frac{\lambda_{eff}\theta_{bw}(\frac{\lambda_s}{\lambda_{fw}} - \frac{\lambda_s}{\lambda_{bw}}) - \lambda_{eff}\psi(\frac{\lambda_s}{\lambda_a} - 1)}{\lambda_{eff}(\frac{\lambda_s}{\lambda_{fw}} - \frac{\lambda_s}{\lambda_a}) + 2(\lambda_a - \lambda_{fw})}, \qquad (11)$$

where λ_s is thermal conductivity of solid matrix.

The introduced mixing models were tested in many practical cases, especially in dielectric mixing applications (see e.g. [11], [12]), and their perspectives for determination of moisture dependent thermal conductivity seem to be very promising.

CONCLUDING REMARKS

The main objective of the paper was to show the potential for using dielectric mixing models based on homogenization theory for calculation of thermal conductivity of partially water saturated porous building materials. On the basis of previous applications of Bruggeman's type mixing models and Lichtenecker's formula for estimation of thermal conductivity of mineral wool boards [13] and cement based composite materials [14] it can be concluded that application of homogenization techniques can provide useful estimates of measured data even for these highly inhomogeneous materials. However, a unified formula could not be found in the whole range of moisture content until now and detailed experimental and theoretical analysis is still needed.

ACKNOWLEDGMENT

This research has been financially supported by Czech Ministry of Education, Youth and Sports, under project No MSM 6840770031.

REFERENCES

[1] Kumaran M. K., IEA ANNEX 24, Heat, Air and Moisture Transfer in Insulated Envelope Parts, Final Rpeort, Volume 3, Task 3: Material Properties, 1996.

[2] Wiener, O., Die Theorie des Mischkoerpers fuer das Feld der stationaeren Stroemung. Abhandlungen der Mathematischen-Physischen Klasse der Königlichen Sächsischen Gesellschaft der Wissenschaften 32(1912), 509-604.

[3] Lichtenecker, K., Die Dielektrizitaetskonstante natuerlicher und kuenstlicher Mischkoerper. Physikalische Zeitschrift, 27(1926), 115–158.

[4] Lord Rayleigh, On the influence of obstacles arranged in rectangular order upon the properties of the medium. Philos. Mag. 34(1892), 481–502.

[5] Maxwell Garnett, J.C., Colours in metal glasses and metal films. Trans. Of the Royal Society (London) 203 (1904), 385-420.

[6] Bruggeman D.A.G., Berechnung verschiedener physikalischen Konstanten von heterogenen Substanzen, I. Dielektrizitaetskonstanten und Leitfaehigkeiten der Mischkoerper aus isotropen Substanzen. Annalen der Physik, 24(1935), Ser. 5, 636-664.

[7] Polder D., van Santen J. H., The effective permeability of mixtures of solids. Physica 12(1946), 257–271.

[8] Dobson M. C., Ulaby F. T., Hallikainen, M.T., El-Rayes, M.A., Microwave dielectric behavior of wet soil. Part II: Dielectric mixing models. IEEE Trans. Geosci. Remote Sensing GE-23(1985), 35-46.

[9] Moy J. H., Chan King-Cham, Dollar A. M., Bound water in fruit products by the freezing method, Journal of Food Science 36 (3), 1971, 498–499.

[10] De Loor G.P., Dielectric properties of heterogeneous mixtures containing water. J. Microwave Power 3, 1968, 67-70.

[11] Goncharenko A. V., Generalizations of the Bruggeman equation and a concept of shaped-distributed particle composites, Physical review E68, 041108, 2003.

[12] Fiala L., Pavlík Z., Jiřičková M., Černý R., Sobczuk H., et al., Measuring Moisture Content in Cellular Concrete Using The Time Domain Reflectometry Method, 5th International Symposium on Humidity and Moisture [CD-ROM], Rio de Janeiro: Inmetro, 2006.

[13] Jiřičková M., Pavlík Z., Fiala L., Černý R., Thermal Properties of Mineral Wool Materials Partially Saturated by Water, International Journal of Thermophysics 27(2006), 1214-1227.

[14] Mňahončáková E., Jiřičková M., Pavlík Z., Fiala L., Rovnaníková P., et al., Effect of Moisture on Thermal Conductivity of a Cementitious Composite, International Journal of Thermophysics 27(2006), 1228-1240.

LASER INFRARED PHOTOTHERMAL RADIOMETRY OF ISOTROPIC MAGNETITE COMPOSITE

Alena Palackova

Department of Physics, Faculty of Civil Engineering, Slovak University of Technology, Bratislava, Radlinskeho 11, 813 68 Bratislava, Slovakia
alena.palackova@stuba.sk

Abstract

Photothermal techniques are widely used to monitor photoexcited carrier kinetics and transport in materials in a noncontacting and nondestructive manner. The main thermal and electronic transport parameters are derived from the photothermal amplitude and phase (frequency domain) or time evolution (time domain) dependencies. In this work, the laser infrared photothermal radiometry is used to study the thermal properties of natural rubber magnetite composite.

Key words: laser, infrared photothermal radiometry, composite materials

1 Introduction

Commonly used plastics have a low thermal conductivity. However new applications require new materials with an enhanced or high thermal conductivity. By the addition of suitable fillers to plastics, the thermal behavior of polymers can be changed up to significant higher thermal conductivity (diffusivity). The higher thermal conductivity can be achieved by the use of suitable filler. Published values of thermal conductivities of the same filler materials in different polymer matrices vary drastically and a comparison of different materials is impossible.
Photothermal studies are based on the well known fact that the absorption of an intensity modulated or pulsed irradiation by semiconductors results in temperature and plasma density profiles whose temporal behavior is affected by the thermal and electrical transport characteristics of the material, thus allowing the main thermal and electronic transport parameters to be derived from the photothermal amplitude and phase frequency domain dependencies.

2 Experiment

2.1. Experimental method

The experimental method and the mathematical model were described in [1].
The measurement is not bound to the excitation geometry (radius of the source or line width). The laser beam is line focused and then passed through the square-wave filter. The only condition is that the excitation frequency has to be low enough so that the thermal waves from the opposite sides of an unheated zone due to the grating have effective wavelengths of the order of $\lambda/4$ so as to interfere with one another (fig.1).

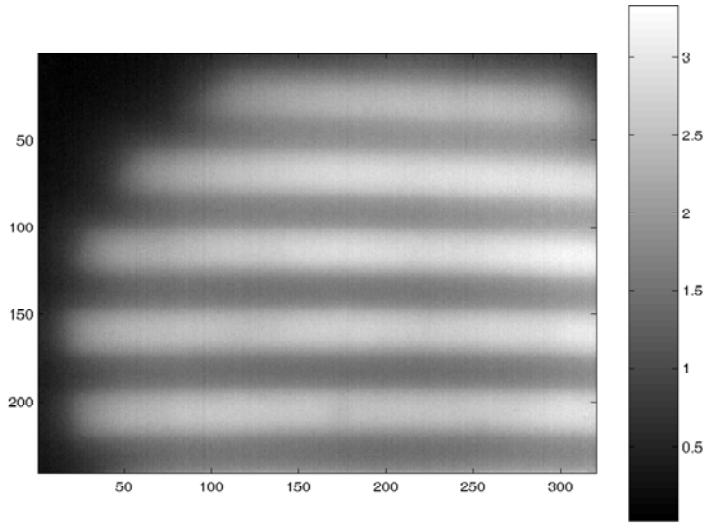

Fig. 1: The interference picture of the sample

Used mathematical model gives the resulting temperature oscillations in space. The modulation depth of the temperature amplitude and phase can be easily determined from the absolute difference of the extremes of the modulation (fig.2 and fig. 3).

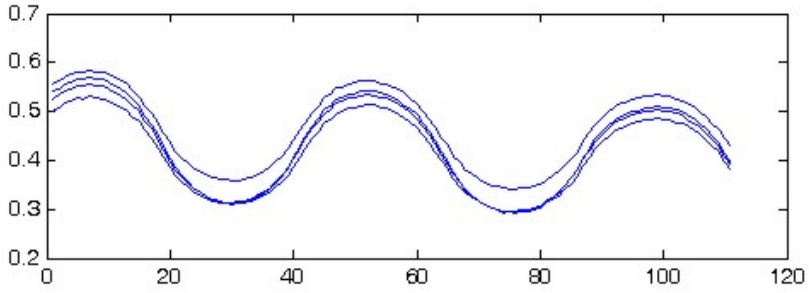

Fig 2: Amplitude modulation of temperature perpendicularly to the grating bands, $\lambda = 4$ mm.

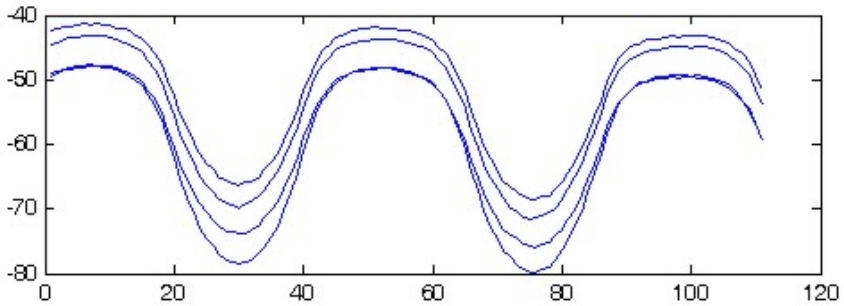

Fig 3: Phase modulation of temperature perpendicularly to the grating bands $\lambda = 4$ mm.

2.2. Materials

We used composite material consists of natural rubber matrice and the strontium ferrite filler ($SrFe_{12}O_{19}$).

The filler content of the measured samples is in the table 1.

Sample (No.)	Filler volume fraction (%)	Weight fraction (%)
5	11.9	29.7
3	12.9	31.7
1	13.8	33.5
8	16.9	38.9
9	17.7	40.3
7	18.6	41.7
4	20.9	45.3
6	23.8	49.6

Table 1: Identification of samples

3 Results

To illustrate the influence of the filler fraction on thermal properties one can compare too extreme filler volume contents: 11.9% (sample 5) and 20.9% (sample 4).

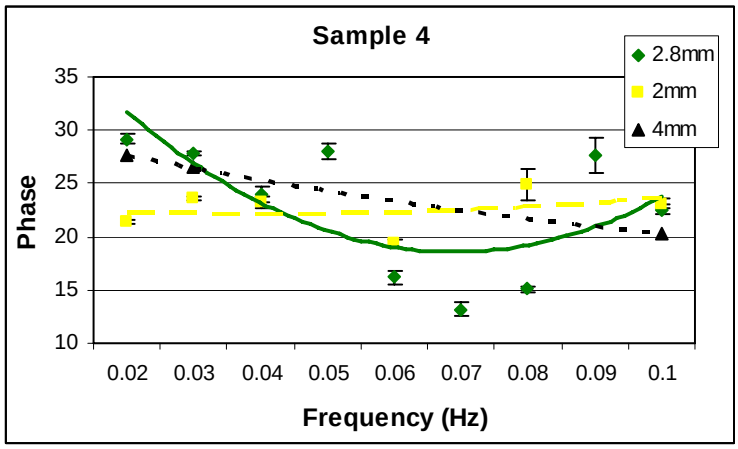

Fig. 4: Modulation phase of temperature for the sample 4 as a function of frequency for different gratings.

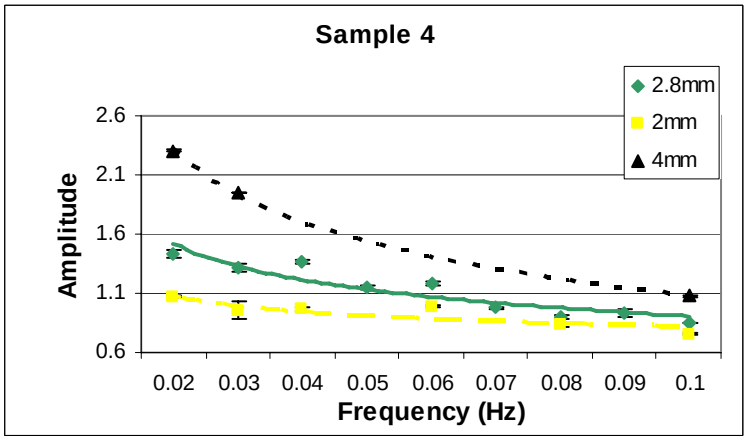

Fig. 5: Modulation amplitude of temperature for the sample 4 as a function of frequency for different gratings.

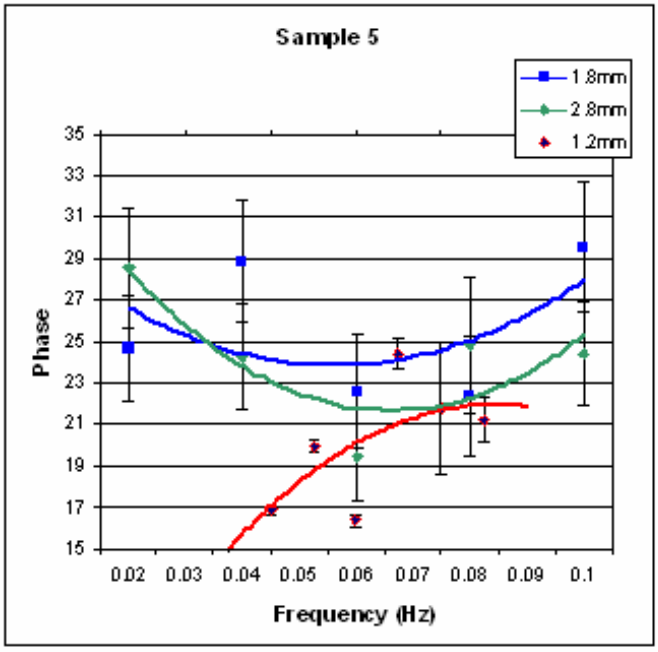

Fig. 6: Modulation phaseof temperature for the sample 5 as a function of frequency for different gratings.

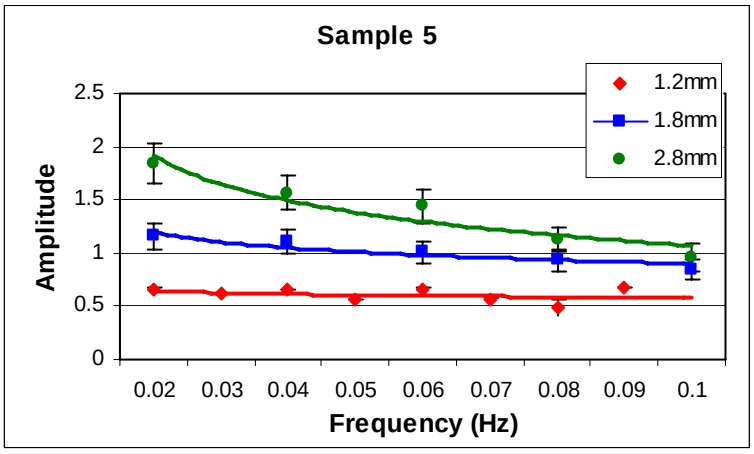

Fig. 7: Modulation amplitude of temperature for the sample 5 as a function of frequency for different gratings.

There are fitting two values, the amplitude of the field's normalized amplitude and phase modulation. There is conducted a parametric study in order to analyze the influence of each property to the temperature field. The specific heat $C = 800 J/kg.K$ and the density was calculated for each sample. The final thermal conductivities are: $(2.74 \pm 0.34) W/mK$ for the sample 4 and $(1.19 \pm 0.29) W/mK$ for the sample .5

The thermal properties were found by fitting the thermal wave field for all excitation frequencies.

Conclusions and discussion

The theory is neglecting the possible presence of internal optical reflections, optical diffusion and assumes constant thermal properties. These conditions are not perfectly fulfilled and not even well known. As can be seen in figures 1 and 6 the phase was also clearly much more affected with the offset at the center of excitation.

Acknowledgements

The author wish to acknowledge valuable discussions with, Prof. Glorieux and Dr. Kalogiannakis.
The work has been supported by research project APVT 51-30704.

References

[1] G. Kalogiannakis, D. Van Hemelrijck: Thermal characterization of anisotropic media in photothermal point, line, and grating configuration. JOURNAL OF APPLIED PHYSICS 100, 063521 (2006)

MESUREMENT OF LOCAL CONVECTIVE SURFACE HEAT TRANSFER COEFFICIENT BY PHOTOELECTRIC METHOD

Peter Mihalka, Milan Drzik, Peter Matiasovsky

Institute of Construction and Architecture, Slovak Academy of Sciences,
Dubravska cesta 9, 845 03 Bratislava 45, Slovakia, usarmipe@savba.sk

Abstract:
The surface transport coefficients modelling in complex models of the heat, air and moisture transport in a building supposes the local modelling of internal surface heat transfer in a hygrothermal zone. For this purpose the algorithm has been created for iterative computational determination of local convective surface heat transfer coefficients by CFD simulation tool. The convective surface heat transport coefficients determined by the algorithm were tested by experimental measurements for chosen surfaces configurations with use of the photoelectric measurements of the air refractive index gradient in a boundary layer.

Keywords:
boundary layer, convective heat transfer coefficient, photoelectric method

1. INTRODUCTION

In order to evaluate the heat transfer coefficient a method of photoelectric probing of the refractive index gradients has been developed. The boundary layer was mapped in detail, the temperature gradients and temperatures were determined and approximated with an analytical solution for the laminar convection regime and then compared with a results simulated by a CFD tool.

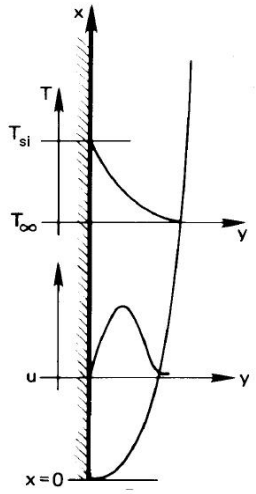

Fig. 1 Heat transfer and fluid flow near heated vertical plate

2. THEORY

The wall surface convective heat flux can be defined by the empirical Newton law [4]:

$$q = h.(\theta_{si} - \theta_{\infty}) \tag{1}$$

where h is the surface heat transfer coefficient.
The density of steady-state heat flow is determined by the Fourier law of heat conduction [4]:

$$q = -\lambda.\frac{d\theta}{dy} \tag{2}$$

where: dT/dy is the temperature gradient along the y-axis, λ is the thermal conductivity of air.

Using the equations (1) and (2) the value of convective heat transfer coefficient can be evaluated [4]:

$$h = \frac{-\lambda \cdot \left.\frac{d\theta}{dy}\right|_{y=0}}{\theta_{si} - \theta_{\infty}} \tag{3}$$

The experimental determination of the temperature gradient is based on the relationship between the air density dependent on the air temperature and refractive index. This relation is described by the Lorenz-Lorentz law [1]:

$$\frac{n^2 - 1}{n^2 + 2} \cdot \frac{1}{\rho} = \frac{N}{M} = const. \tag{4}$$

where: n is the air refractive index [-], ρ is the air density [kg/m^3], N is the air molar refraction [m^3/mol], M is the air molar mass [g/mol]
The refractive index for a current light wavelength is a function of the air density [1]:

$$n = n(\rho) \tag{5}$$

In the range of 300 – 400 K and under the atmospheric pressure the air can be regarded as an ideal gas. The dependence between air density and temperature is given by the state equation [1]

$$\frac{p.V}{T} = R \quad \text{i.e.} \quad \rho = \frac{p.M}{R.T} \tag{6}$$

where: p is the air pressure [Pa], T is the absolute temperature [K], V is the air molar volume [m^3/mol], R is the universal gas constant [J/mol.K].
Under the assumption of isobaric condition, the air density change is proportional inversely to the temperature change, then the refractive index variation is proportional to the air temperature change [1]:

$$\frac{n_0 - 1}{n - 1} = \frac{\rho_0}{\rho} = \frac{T}{T_0} \tag{7}$$

In a literature the basic constant can be found for the relationship between air temperature change and refractive index change for the wavelength of 650 nm at the temperature of 300 K [1]:

$$\frac{dn}{dT} = 0.961.10^{-6} \tag{8}$$

Then, the mutual relationship between the refractive index gradients and temperature gradients is as follows:

$$\frac{dT}{dy} = \frac{1}{0.961 \cdot 10^{-6}} \cdot \frac{dn}{dy} \tag{9}$$

Considering the constant distribution of refractive index along the path of optical detection by laser beam and appropriate geometrical relations, a final equation for beam deviation in the detector place is [2, 3]:

$$\frac{\partial n}{\partial y} = \frac{2 \cdot n_0 \cdot \Delta y}{L^2} \tag{10}$$

where: L is the laser beam path length [m], n_0 is the refractive index $\cong 1.0$ for air, Δy is the laser beam deviation.
With use of the equations (10) and (9) the wall temperature gradient near a wall surface and then the near wall temperature profile has been evaluated. Finally, applying the equations (10), (9) and (3) the convective heat transfer coefficients can be computed.

3. EXPERIMENT

For the purpose of experiment the vertical flat plates consisting of two symmetrically heated parts has been fabricated. Two materials with different thermal conductivity were used. In the first case the plate consisted of two gypsum boards (G) with the embedded heating foil the dimensions of which were 0.52 x 0.50 x 0.02 m. In the second case the gypsum boards were replaced by the polished aluminium plates (A) with dimensions of 0.5 x 0.5 x 0.09 m. The foil heating input was 197 W/m^2 at 220 V.
In a case of the gypsum plate with relatively low thermal conductivity (0.15 W/m.K) some heterogeneity of the surface temperature field was expected. The perimeter of the plate was therefore thermally insulated with the 0.003m thick expanded polystyrene belt and aluminium foil. The gypsum plate was used at the experiments with higher surface-ambient temperature differences.
The aluminium plate has a significantly higher thermal conductivity (204 W/m.K) providing a higher homogeneity of surface temperature field. This plate was applied at experiments with low surface-ambient temperature differences.

The configuration of measurement equipment is shown in figure 2. The laser source in the figure is in the position y = 0 mm, thus the laser beam is visible on the plate surface (at bottom).

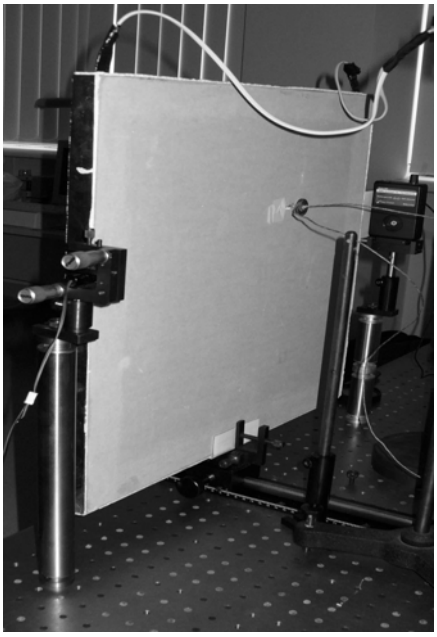

a

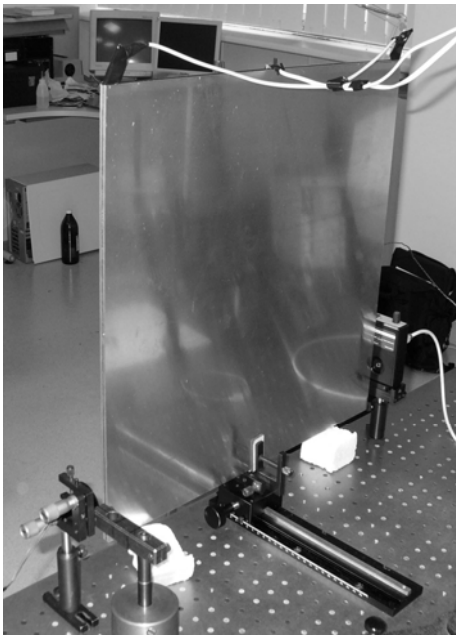

b

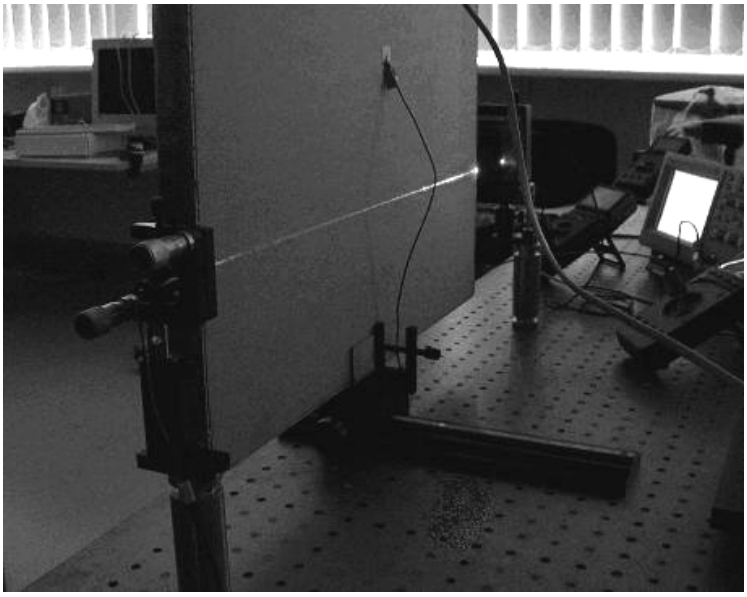

c

Fig. 2 Image of measurement set up: a – surface G (gypsum boards), b – surface A (aluminium plates), c - laser beam illuminating heated wall

The measurement set consists of the laser diode 10 mW/650 nm (Fig. 3 a) with the wavelength of light 650 nm and the double photodiode detector (Fig. 3 b). The air and surface temperatures were measured by thermocouples and in a case of gypsum plate also with the infrared camera NEC TH7102MX. The thermocouples sensitivity was 0.1^{o}C.

Under the calm air conditions with the absence of temperature gradient and dominant air speed, the laser beam impacts both halves of the photodiode detector equally. If the air temperature gradient occurs, the air density decreases, the laser beam deviates from a straight line and the photodiode

captures the difference between the two laser detecting halves (Fig. 4 b). This difference is observed by the voltmeter and is proportional to the deviation of beam from a straight line.

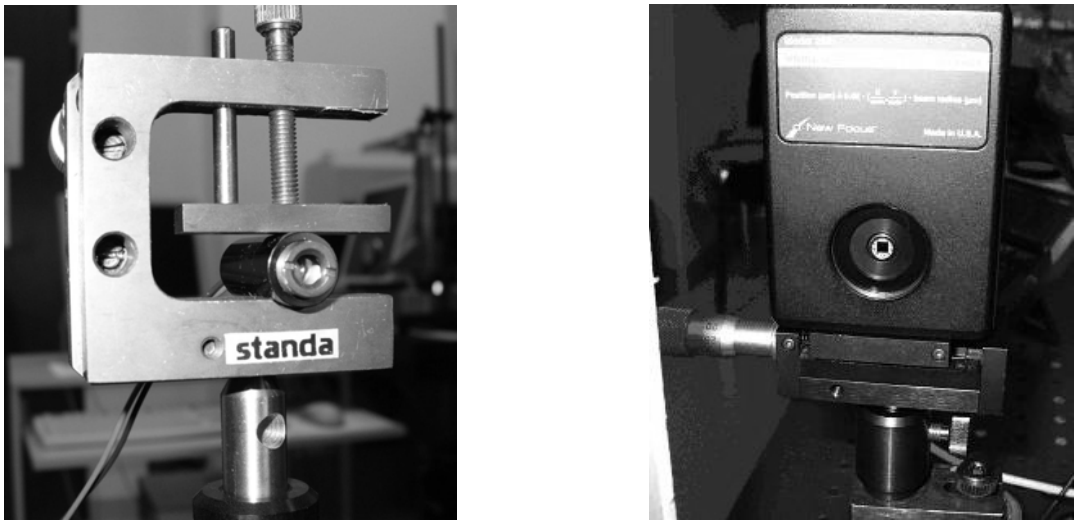

a b

Fig. 3 Measurement apparatus
a – laser diode, b – double photodiode detector with screw micrometer

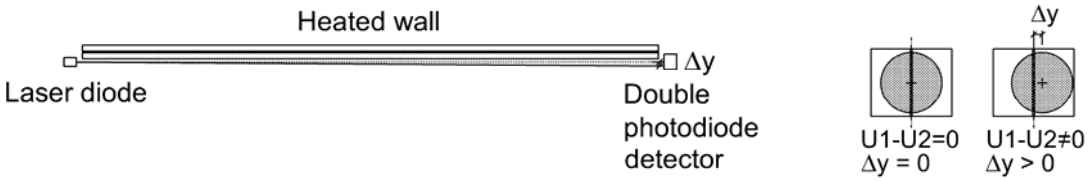

a b

Fig.4 Principle of laser beam deviation measurement
a – laser beam deviation along the heated vertical plate, b – laser beam impact onto the double photodiode, left image - with no temperature gradient, right image - with temperature gradient

During the measurements the laser diode and photodiode detectors had a fixed position and the heated plate was moved in defined steps using a screw micrometer. The values of the gradients signal were read after the air consolidation.

The adjustment of the state $dn/dy = 0$ was made by the moving of the heated plate outside the boundary layer and by using the screw micrometer at the double photodiode detector. The calibration of the relation between mV and μm then can be reached.

The measurements were made within the distances from $y = 0.002$ up to 0.026 m. The measurements at smaller distances were not possible as the smallest distance is limited due to a finite laser beam diameter (about 0.0015 m) and also by the fact that the heated plate surfaces were not ideally flat.

The evaluation process assumes the constant temperature gradient along the heated plate. In fact, there was not possible to keep the constant distribution of surface temperature along the whole gypsum plate area (Fig. 5 a). A correction of the path length along the heated plate was necessary (Fig. 5 b)

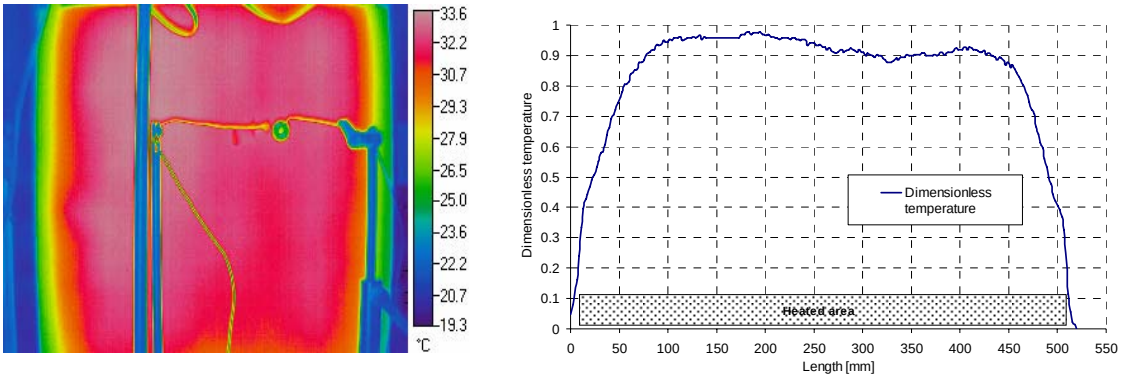

a b

Fig. 5 Surface temperature variation along laser beam path (plate G): a – thermography, b-temperature profile along laser beam

The correction was made by integrating the temperature profile along laser beam path what represents area of temperature profile function. Dividing the integrated temperature profile by average temperature, the corrected laser beam path length can be evaluated.

$$L` = \frac{\int_a^b t(x)}{t_{average}} \tag{11}$$

where *a* and *b* are coordinates of the beginning and the end of the plate. Applying equation (11) the corrected laser beam path length 0.49 m was obtained.

4. RESULTS

The measured results were compared with known analytical solutionsof the natural convection along the vertical plate [2], [3]. The measured temperature gradients courses were approximated by Gauss regression the shape (15):

$$\frac{d\theta}{dy} = a + b \cdot e^{-\left(\frac{y-c}{d}\right)^2} \tag{12}$$

where the parameters *a, b, c, d* determined by the regression.
Subsequently the function of temperatures near the plate could be obtained by the integration of function $d\theta/dy$:

$$\theta(y) = \int \frac{d\theta}{dy} dy = a \cdot y + \frac{1}{2}\pi^{\frac{1}{2}} \cdot d \cdot erf\left(\frac{y}{d} - \frac{c}{d}\right) \cdot b + C \tag{13}$$

where *C* is the integration constant, which has for $y = 0$ has the value θ_{si}:

$$C = \theta_{si} + \frac{1}{2} \cdot \pi^{\frac{1}{2}} \cdot d \cdot erf\left(-\frac{c}{d}\right) \cdot b \tag{14}$$

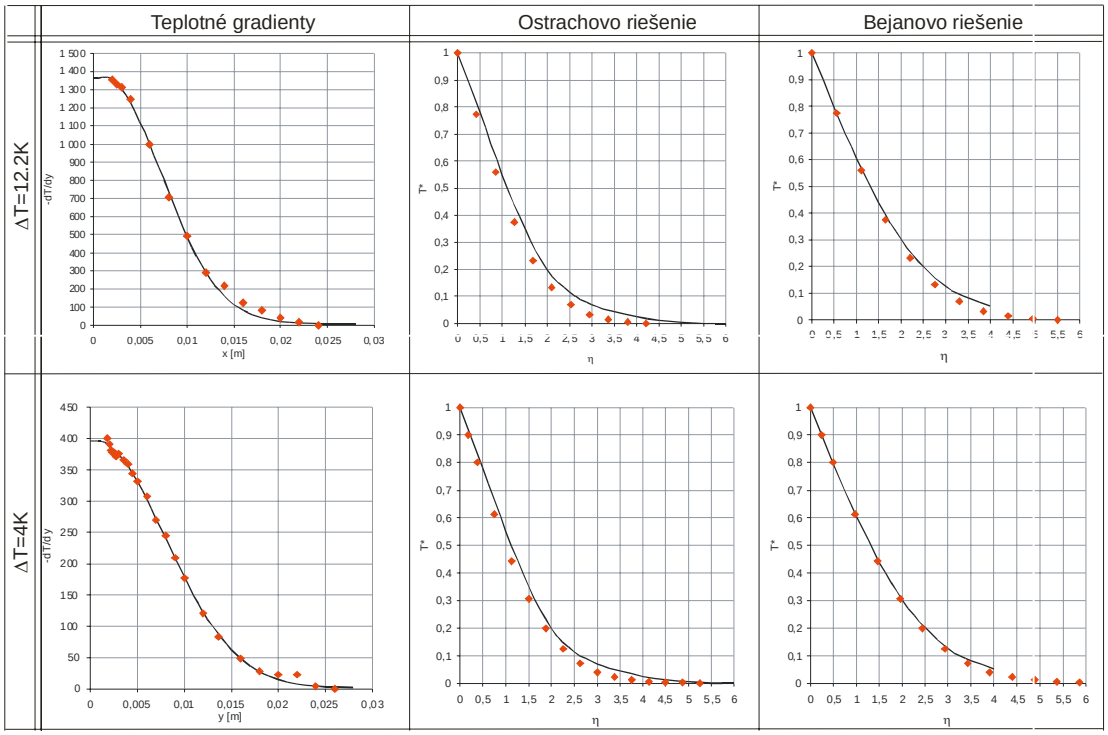

Fig. 6 Results of measurements compared with analytical solutions

The comparison of measured and calculated temperature profiles is in figure 6. From the comparison of measured and calculated results a good agreement is evident. The straight comparison of the obtained values with known empirical retaionships is not possible, as the obtained values are local character, determined by not only the temperature difference but also the spatial coordinates.

5. CONCLUSIONS

The photoelectric method enables to mesure the temperature gradients in a boundary layer, using the temperature dependence of light refractive index in air. In comparison with other methods the errors at the measured temperature profile derivations are limited. Potential innacuracies are caused by the forced convection of ambient air. The method is applicable for measurements at low temperature differences.

Acknowledgement
Financial support of the project APVT-51-030704 is gratefully acknowledged.

REFERENCES

[2] FOMIN, N.A. (1989): Speckle interferometrija gazovych potokov, Nauka I technika, Minsk (in Russian)
[3] VASILJEV, L.A. (1968): Tenevije metody, Nauka, Moscow (in Russian)
[4] CHAPMAN, A.J. (1960): Heat transfer, The Macmillan Company, New York
[5] SCHLICHTING, H. (1979): Boundary-Layer theory, McGraw-Hill7

METHODS FOR DETERMINATION OF HIGH-TEMPERATURE PROPERTIES OF ALUMINOSILICATES

Jan Toman, Lucie Zuda, Robert Černý

Czech Technical University, Faculty of Civil Engineering, Department of Materials Engineering and Chemistry, Thákurova 7, 166 29 Prague 6, Czech Republic, email: toman@fsv.cvut.cz, lucie.zuda@fsv.cvut.cz, cernyr@fsv.cvut.cz

Abstract:
Methods suitable for determination of high temperature values of specific heat capacity and thermal conductivity of alkali activated aluminosilicate materials are presented in the paper and their practical application is tested for a selected aluminosilicate composite in the temperature range up to 1200 °C.

Keywords:
Aluminosilicates, high temperatures, thermal conductivity, specific heat capacity

INTRODUCTION

Alkali-activated aluminosilicate materials are known to exhibit remarkable high-temperature resistance and very favorable mechanical properties. Therefore, this type of materials is capable of replacing classical Portland or blended cement as traditional binder in concrete in the situation where high temperature resistance of the material is required. The knowledge of their high-temperature properties is, however, indispensable for their proper application in fire resistance measures. In this paper, methods suitable for determination of high temperature values of specific heat capacity and thermal conductivity of alkali activated aluminosilicate materials are presented and their practical application is tested for a selected aluminosilicate in the temperature range up to 1200 °C.

METHODS FOR DETERMINATION OF HIGH-TEMPERATURE PROPERTIES

As the adiabatic methods are not very suitable for measuring high-temperature specific heat capacity of building materials, mainly because of the necessity to use relatively large samples, a nonadiabatic method by Toman and Černý [1] was chosen for the determination of temperature-dependent specific heat capacity. We will present the main idea of the method in what follows.

The nonadiabatic calorimeter has a mixing vessel with a volume of 2.5 L. The volume of the measuring fluid (water in this case) is about 1 L. The maximum volume of the measured samples is 1 L. The amount of heat loss of the nonadiabatic system is determined using a calibration. The calorimeter is filled with water, whose temperature is different from the ambient air. Then, the relation of water temperature to time, $T_c(t)$, is measured. Six thermocouples are used to measure the water temperature. The air temperature measured by the same thermometers at two points must be kept constant (the maximum deviation of about 1 K during the measurement is permitted). Therefore, the experiments are performed in an isolated room where sudden changes of temperature can be eliminated. The mixing vessel is located on a laboratory stand ensuring direct contact of its bottom with the ambient air. A low-speed ventilator fan near the calorimeter bucket is used to reach steady-convection conditions.

The measuring method itself is based on well-known principles. The sample is heated to a predetermined temperature T_s in a furnace and then put into the calorimeter with water. Then, the relation of water temperature to time $T_w(t)$ is measured, water being slowly stirred all the time, until the temperatures of the measured sample and the calorimeter are equal. The corrected (adiabatic) temperature $T_r(t)$ taking the heat loss into account is calculated using the corrections $\Delta T(t_i)$ obtained from the calibration curve $T_c(t)$,

$$T_r(t_i) = T_w(t_i) + \Delta T(t_i), \tag{1}$$

where

$$\Delta T(t_i) = \sum_{j=1}^{i} \Delta T(\Delta t_j) \tag{2}$$

$$t_i = \sum_{j=1}^{i} \Delta t_j . \tag{3}$$

Practically it means that the correction of the temperature T_w at the time t_i from the beginning of the experiment due to heat loss to the surroundings during the time interval of Δt_i, $\Delta T(\Delta t_i)$, is determined using the calibration curve $T_c(t)$ at the point T_w. The total temperature correction for the time t_i is obtained by adding up the particular corrections $\Delta T(\Delta t_j)$ from the time equal to zero to the time t_i.

The theoretical equilibrated temperature of the sample-calorimeter system at the end of the test T_e is then calculated as

$$T_e = \lim_{t \to \infty} T_r(t) . \tag{4}$$

The heat balance of the sample-calorimeter system can be written in the form:

$$mc(T_s - T_e) = (K + m_w c_w)(T_e - T_{wo}) + \Delta m \cdot L - Q_r \tag{5}$$

where m is the mass of the sample, c is the specific heat capacity of the sample in the temperature interval $[T_e, T_s]$, K is the heat capacity of the calorimeter, m_w is the mass of the water, c_w is the specific heat capacity of water, T_{wo} is the initial water temperature, L is the latent heat of evaporation of water, Q_r is the reaction heat, Δm is the mass of evaporated water,

$$\Delta m = m + m_{cw} - m_s - \Delta m_N - \Delta m_{sc} \tag{6}$$

m_{cw} is the mass of the calorimeter with water before the measurement, m_s is the mass of the system calorimeter-water-sample after measurement, Δm_N is the mass of water, naturally evaporated during the measurement (this heat loss is already included in the heat loss calibration curve), Δm_{sc} is the change of mass due to the chemical reaction of the sample with water (e.g., hydrolysis). This value can be obtained as $\Delta m_{sc} = m - m_D$, where m_D is the mass of the dried sample after the measurement. The remaining symbols in Eq. (5) are the same as before.

Determining the specific heat capacity c directly from Eq. (5) we would obtain a mean value of the specific heat capacity, c_0, in the interval $[T_e,T_s]$ by

$$c_0 = \frac{(K + m_w c_w)(T_e - T_{wo}) + \Delta m \cdot L - Q_r}{m(T_S - T_e)} \tag{7}$$

However, from the physical point of view, it is more correct to determine the value of the specific heat capacity "point-wise", in accordance with the definition of specific heat capacity,

$$c(T_i) = \frac{\partial h}{\partial T}(T_i) \tag{8}$$

where h is the specific enthalpy.

Using relation (8) to determine the specific heat capacity, we have to specify the zero-point of the enthalpy scale, i.e., we have to ensure that all the enthalpy calculations are related to a certain constant temperature. This reference temperature can be, for example, T_k = 0 °C. Upon adding

$$Q = m \cdot c_e \cdot (T_e - T_k) \tag{9}$$

where c_e is the mean specific heat capacity of the sample in the temperature interval $[0,T_e]$, to both sides of equation (5), and dividing by m, we obtain the following

$$h(T_s) = \frac{(K + m_w c_w)(T_e - T_{wo}) + \Delta m \cdot L - Q_r}{m} + c_e(T_e - T_k)\,. \tag{10}$$

The value of c_e is considered to be constant, taking into account the condition

$$T_s - T_e >> T_e - T_k \tag{11}$$

and it can be measured, for example, using the classical adiabatic method.

Performing a set of measurements for various sample temperatures T_i, we obtain a set of points $[T_i, h(T_i)]$. A regression analysis of this point-wise given function results in a functional relationship for $h = h(T)$ and, using relation (8), also in the function $c = c(T)$ as the first derivative of h with respect to T.

For the determination of high-temperature thermal conductivity we used the double integration method, a dynamic method based on an inverse analysis of the temperature field which was used previously for determination of moisture diffusivity in dependence on moisture content [2]. As the heat conduction equation is of the same type as the moisture conduction equation, the method of inverse analysis presented in [2] can be applied also for thermal conductivity determination with only slight modifications.

The basic principle of the method consists in measuring the temperature field $T(x,t)$ in the sample at one-sided heating and the subsequent solution of the inverse heat conduction problem. We suppose $T(t)$ and $T(x)$ to be monotonic functions and choose a constant value of temperature, $\tau=T(x,t)$. Then must exist one-to-one parametrizations $x=x_o(\tau,t)$, $t=t_o(\tau,x)$ where both x_o and t_o are monotonic functions. Considering this fact, an integration of heat conduction equation by x and t leads to

$$\int_{t_1}^{t_n}\int_{0}^{x_0(\tau,t)} \rho c \frac{\partial T}{\partial t}\,\mathrm{d}x\mathrm{d}t = \lambda(\tau)\int_{t_1}^{t_n} \frac{\partial T}{\partial x}(x_0(\tau,t),t)\mathrm{d}t - \int_{t_1}^{t_n} \lambda[T(0,t)]\frac{\partial T}{\partial x}(0,t)\mathrm{d}t \tag{12}$$

where

$$-\lambda[T(0,t)]\frac{\partial T}{\partial x}(0,t) = j_Q(0,t) \tag{13}$$

is the heat flux at x=0.

The left-hand side (LS) of Eq. (12) can be modified by accounting for the shape of the integration area:

$$LS = \int_{t_1}^{t_n}\int_{0}^{x_0(\tau,t)} \rho c \frac{\partial T}{\partial t}\,\mathrm{d}x\mathrm{d}t = \int_{0}^{x_0(\tau,t)}\mathrm{d}x\int_{t_1}^{t_n} \rho c \frac{\partial T}{\partial t}\mathrm{d}t + \int_{x_0(\tau,t_1)}^{x_0(\tau,t_n)}\mathrm{d}x\int_{t_0(\tau,x)}^{t_n} \rho c \frac{\partial T}{\partial t}\mathrm{d}t \tag{14}$$

Denoting

$$\int \rho c \frac{\partial T}{\partial t}\,\mathrm{d}t = \int \rho(T)c(T)\mathrm{d}T = I_T(T) \tag{15}$$

we obtain

$$\begin{aligned} LS &= \int_{0}^{x_0(\tau,t_1)}\left[I_T(T(x,t_n)) - I_T(T(x,t_1))\right]\mathrm{d}x + \int_{x_0(\tau,t_1)}^{x_0(\tau,t_n)}\left[I_T(T(x,t_n)) - I_T(\tau)\right]\mathrm{d}x = \\ &= \int_{0}^{x_0(\tau,t_n)} I_T(T(x,t_n))\,\mathrm{d}x - \int_{0}^{x_0(\tau,t_1)} I_T(T(x,t_1))\,\mathrm{d}x - I_T(\tau)[x_0(\tau,t_n) - x_0(\tau,t_1)] \end{aligned} \tag{16}$$

Substituting (16) into (12) we arrive at

$$\lambda(\tau) = \frac{\int_{0}^{x_0(\tau,t_n)} I_T(T(x,t_n))\,\mathrm{d}x - \int_{0}^{x_0(\tau,t_1)} I_T(T(x,t_1))\,\mathrm{d}x - I_T(\tau)[x_0(\tau,t_n) - x_0(\tau,t_1)] - \int_{t_1}^{t_n} j_Q(0,\mathrm{t})\,\mathrm{d}t}{\int_{t_1}^{t_n} \frac{\partial T}{\partial x}(x_0(\tau,t),t)\,\mathrm{d}t} \tag{17}$$

where for $t_j > t_i$ the heat flux at x=0 can be calculated as

$$j_Q\left(0, \frac{t_j + t_i}{2}\right) = \frac{1}{t_j - t_i}\int_{0}^{D}\left[\rho(T)c(T)T(x,t_j) - \rho(T)c(T)T(x,t_i)\right]\mathrm{d}x \tag{18}$$

where D is the length of the one-dimensional domain under consideration.

The measuring procedure consists then in the following. One-side heating of a specimen (for cement based materials and similar composites typically 71x71x71 mm) with thermally insulated

lateral faces is realized using a furnace where a constant temperature is maintained. Along the longitudinal axis of the sample, a set of temperature sensors is positioned, which makes it possible to record the temperature field through a measuring unit by a PC. From the measured $T(x,t_i)$ curves, a set of 8-10 curves is chosen, and these curves are used in the computational treatment. First, the measured $T(x,t_i)$ curves are subject of a regression analysis. Then, we choose a temperature value τ, determine the integration area for this value and calculate the corresponding value of thermal conductivity $\lambda(\tau)$ by Eq. (17). This procedure is repeated for a sufficient number of τ values so that we finally obtain a point-wise given function $[\tau_i, \lambda(\tau_i)]$.

MATERIALS AND SAMPLES

Fine-ground slag of Czech origin (Kotouč Štramberk, Ltd.) was used for sample preparation. As alkali activator, water glass solution was used. It was prepared using Portil-A dried sodium silicate preparative (Cognis Iberia, s.l. Spain). The sand aggregates were normalized according to EN 196-1 with the granulometry PG1, PG2, PG3. The composition of the mixture for sample preparation is presented in Table 1.

The technology of sample preparation was as follows. First, the silicate preparative was mixed with water. The solution was then mixed into the homogenized slag-sand mixture. The final mixture was put into 71x71x71 mm molds and vibrated. The specimens were demolded after 24 hours and then stored for further 27 days in water bath at laboratory temperature. Three specimens were studied for every measurement.

Table 1 Composition of mixture for sample preparation

Sand [g]			Slag [g]	Alkali-activation silicate admixture [g]	Water [ml]
PG1	PG2	PG3			
450	450	450	450	90	190

EXPERIMENTAL RESULTS AND DISCUSSION

Bulk density and open porosity of the studied aluminosilicate material in dependence on temperature are presented in Table 2. The data were obtained using the common water vacuum saturation method. We can see that the porosity begins to increase significantly after heating to 600 °C, achieves its maximum at 800 °C, and at 1000 °C and 1200 °C it is not changed significantly.

Table 2 Porosity and bulk density of the studied aluminosilicate material as functions of temperature

Temperature [°C]	Porosity [m^3/m^3]	Bulk density [kg/m^3]
25	0.18	2170
200	0.22	2100
400	0.17	2170
600	0.22	2070
800	0.24	2030
1000	0.24	2050
1200	0.23	2050

Fig. 1 shows the dependence of specific heat capacity of the studied aluminosilicate material on temperature. The *c(T)* function has a maximum between 400 °C and 500 °C and after decreasing a little at 700 °C it begins to increase very sharply, with a maximum at about 1100 °C. This last maximum is too high for any pure specific heat capacity considerations (it exceeds two times the value of specific heat capacity of water). However, it should be noted that the result of the applied method is in fact a value of "effective specific heat capacity" which may also reflect some other changes in enthalpy as for instance the enthalpy of chemical reactions taking place in a particular temperature range or enthalpy of phase change. In our case it means that a highly exothermal reaction could take place in the temperature range of approximately 800-1100 °C.

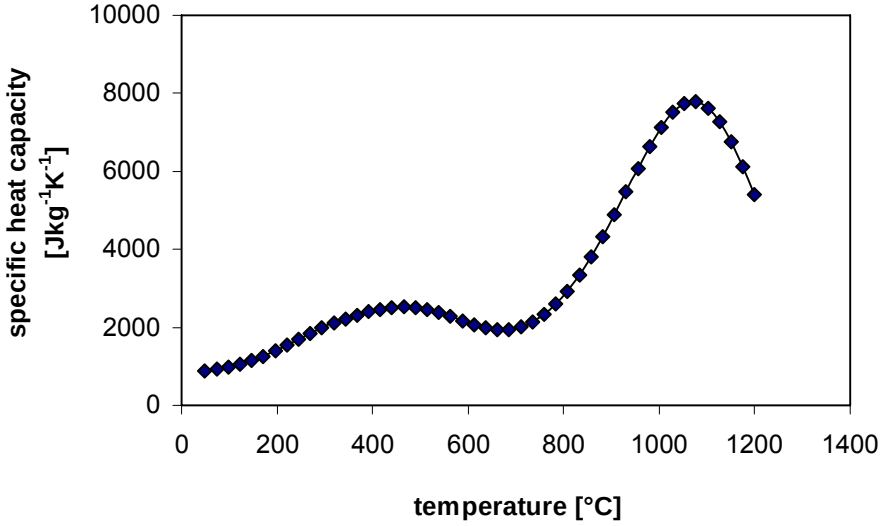

Figure 1 Specific heat capacity of the studied aluminosilicate material as function of temperature

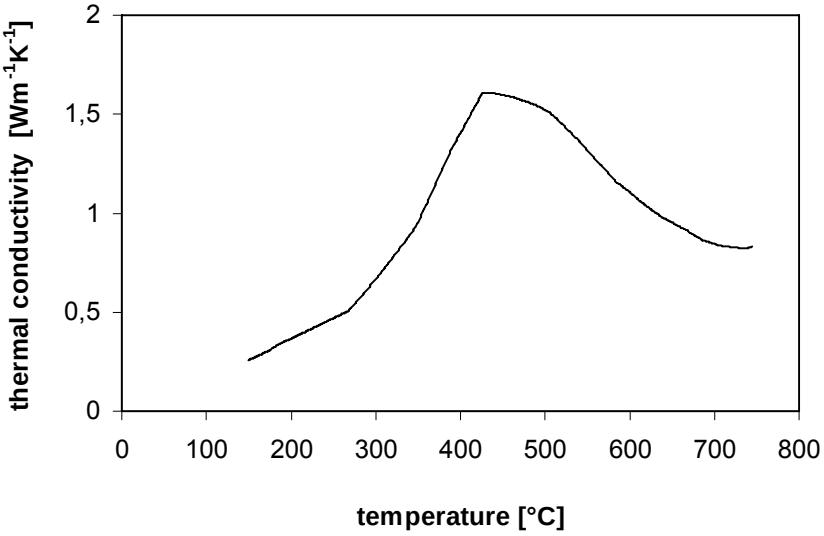

Figure 2 Thermal conductivity of the studied aluminosilicate material as function of temperature

The thermal conductivity vs. temperature function determined by the double integration method in Fig. 2 increased about three times between 150 °C and 400 °C and then it began to decrease. The observed increase in thermal conductivity may be related to the increase in porosity in the temperature range of 25-600 °C (see Table 2). The later decrease may be caused by the structural changes in the material resulting in variations of the porous structure.

CONCLUSIONS

The methods for measurement of specific heat capacity and thermal conductivity in high temperature range up to 1200 °C in this paper were shown to be well applicable for the studied alkali activated aluminosilicate. The material itself was found to be very stable up to 1200 °C and its thermal conductivity decreased with the increasing temperature for the temperatures higher than 400 °C which is a very positive feature for a material potentially applicable as fire protecting layer in building structures.

ACKNOWLEDGEMENT

This research has been supported by the Ministry of Education, Youth and Sports of Czech Republic, under grant No MSM: 6840770031.

REFERENCES

[1] Toman J, Černý R: High-Temperature Measurement of the Specific Heat of Building Materials. High Temp.- High. Press., vol. 25, 1993, pp. 643-647.

[2] Drchalová J, Černý R: Non-Steady-State Methods for Determining the Moisture Diffusivity of Porous Materials. Int. Comm. Heat and Mass Transfer, vol. 25, 1998, pp. 109-116.

PORE STRUCTURE AND THERMAL CONDUCTIVITY OF BURNT CLAY BRICKS

Olga Koronthalyova, Peter Matiasovsky

Institute of Construction and Architecture, Slovak Academy of Sciences, Dubravska 9, 845 43 Bratislava, Slovakia. e-mail: usarkoro@savba.sk, usarmat@savba.sk

Abstract:
Commonly manufactured burnt clay bricks were analysed from the aspect of the relationships between their microstructure and dry thermal conductivity. On the base of the analysis a simple microstructural model of thermal conductivity was proposed. The proposed model was compared with the microstructural model developed for the calcium silicate hydrates based composite materials.

Keywords:
Thermal conductivity, clay brick, porosity, fractal dimension

INTRODUCTION

Most of the building materials are composites and their thermal parameters represent the effect resulting from the properties of their particular phases and components. Usually the composite consists of the bonding matrix, aggregate and pore space. The thermal conductivity of the dry porous material is given by the properties of the solid phase as a whole and by the pore volume. The known relationships among the solid phase properties pore structure parameters and material thermal parameters enable to model thermal properties of the porous materials only from the knowledge of properties of the solid phase and the pore space.

In the previous work [6] the relationship between the thermal conductivity and pore structure parameters for dry CSH-based mortars, plasters and insulation boards was analysed. It was found out that in the first approximation the thermal conductivity of tested materials was proportional inversely to the second power of their total porosity. It was also shown that the thermal conductivity of the tested materials could be modeled by serial configuration of the aggregate with bulk paste and interfacial transition zone conductivities, weighted by the power function of their volume fractions. The exponents of the power function were determined using the particular components fractal dimensions.

With the aim to verify this approach on a different building material the relationship between the thermal conductivity and pore structure parameters was analysed for burnt clay bricks.

Burnt clay bricks are common building material manufactured from the clay-sand mixture (the portion of the sand can be from 30 to 50%). The burning takes place at temperatures 900 - 1000°C. Their microstructure is dependent of the particle size distribution, mineralogical and chemical composition, type of burning additives and the way of burning [2,3].

THEORY

Macroscopic thermal conductivity of composite material can be expressed using the thermal conductivities of particular components. For the continuous high conductivity components fractions with the discrete low continuity components the macroscopic thermal conductivity can be modeled by the summation of particular components:

$$\lambda = \sum_i \lambda_i \cdot (\Phi_i - \Phi_{i,crit})^{n_i} \quad (1)$$

Where λ_i is thermal conductivity of component,
Φ_i is component volume fraction,
$\Phi_{i,crit}$ is the critical volume needed for a connected network to be formed through the material,
$n_i = 1 + FD$,
FD is the fractal dimension of the component or pore volume fraction [5].
In case of parallel configuration of the components $n_i = 1$.

In case of discrete high conductivity components in the continuous low conductivity or pore volume fractions the following relation can be applied:

$$\lambda = \frac{1}{\sum_i \frac{(\Phi_i - \Phi_{i,crit})^{n_i}}{\lambda_i}} \quad (2)$$

Where $n_i = 1$ for serial configuration of the components, $n_i > 1$ in case of dispersion of the low conductivity component.

In the previous work [6] the following empirical relation between thermal conductivity and total porosity was found out for CHS based materials:

$$\lambda = \frac{1}{\frac{\Phi^2}{0.064}} \quad (3)$$

It was also shown that the thermal conductivity of the tested materials could be modeled by serial configuration of the aggregate with bulk paste and interfacial transition zone conductivities by the following relation:

$$\lambda = \frac{1}{\frac{(\Phi_{aggregate} + \Phi_{paste} - \Phi_{pasteITZ})^{n1}}{\lambda_{aggregate}} + \frac{(\Phi + \Phi_{pasteITZ})^{n2}}{\lambda_{ITZ}}} \quad (4)$$

Where λ_{ITZ} is thermal conductivity of interfacial zone + porosity.
The porosity and solid phases fractal dimensions were estimated as FD ≈ 1.0.

EXPERIMENTAL

The pore structure parameters and dry thermal conductivity were determined for four types of burnt clay bricks.

The pore size distribution, the open porosity and the specific surface area of pores were studied using the mercury intrusion porosimetry (MIP): the high-pressure porosimeter mod. 2000 and macro-porosimeter mod. 120 (both Carlo Erba, Milan). This system enables determination of micropores with the radius from 3.7 up to 7500 nm and of larger pores with a radius up to 0.06mm. The porosimetry measurement was carried out by the fraction of broken dried (up to 105°C) samples. Specific surface area of pores was determined using the cylindrical model. The open porosity was also determined from the suction test.

The thermal conductivity was measured by transient pulse method using the commercial device ISOMET 2104 with the surface probe API 210412. The used surface probe is suitable for thermal conductivities in the range from 0.3 to 2 W/m·K. The measurement is based on the analysis of the temperature response of the practically semi-infinite body to the heat flow impulse. The heat flow is generated by electrical heating using a resistor heater having a direct thermal contact with the surface of the sample.

The samples were conditioned under laboratory conditions: 28°C and 36% relative humidity and they can be practically considered as dry.

RESULTS AND DISCUSSION

The total porosity, specific surface area and pore radius median values, determined by MIP are presented in Tab. 1. The values of open porosity, determined from suction test, bulk and true density and the measured values of thermal conductivity are in Tab. 2. Because for the clay bricks the values of open porosity and total porosity are practically identical [3], the values of open porosity were used in the following analysis of the relationships between the thermal conductivity and microstructure.

In Fig. 1 the relationship between the total porosity and thermal conductivity of tested bricks is compared with the previous measurements of CHS materials and the empirical relation (3). As can be seen from the figure the dependence thermal conductivity/porosity dependence of bricks can be in the first approximation expressed by empirical relation (3) similarly like in case of CHS materials.

The clay bricks structure is characterised by configuration of discrete solid components in continuous low thermal conductivity phases. Therefore it was expected that the model of thermal conductivity could be based on relation (2). Analogously to the relation (4) for CHS based materials the thermal conductivity of dry clay bricks was expressed using the model of the serial configuration of solid and low thermal conductivity phases:

$$\lambda = \frac{1}{\frac{(\Phi_{solid} - \Phi_{ITZsolid})^{n1}}{\lambda_{solid}} + \frac{(\Phi + \Phi_{ITZsolid})^{n2}}{\lambda_{ITZ}}} \tag{5}$$

Table 1. Pore structure parameters of the bricks (MIP)[Bagel 2001]

Material	Total porosity	Specific surface area [m^2/g]	Pore radius median [nm]
Brick D	0.3	-	-
Brick L	0.28	2.39	559.1
Brick P	0.50	8.07	535.1
Brick S	0.43	1.44	542.9

Table 2. Open porosity (suction test), true density and dry thermal conductivity of the bricks

Material	Bulk density [kg/m^3]	Open porosity [-]	True density [kg/m^3]	Thermal conductivity λ [W/m·K]	λ standard deviation [W/m·K]
Brick D	1724	0.3	2460	0.656	±0.018
Brick L	1710	0.33	2550	0.625	±0.033
Brick P	1377	0.42	2370	0.397	±0.015
Brick S	1426	0.44	2590	0.456	±0.014

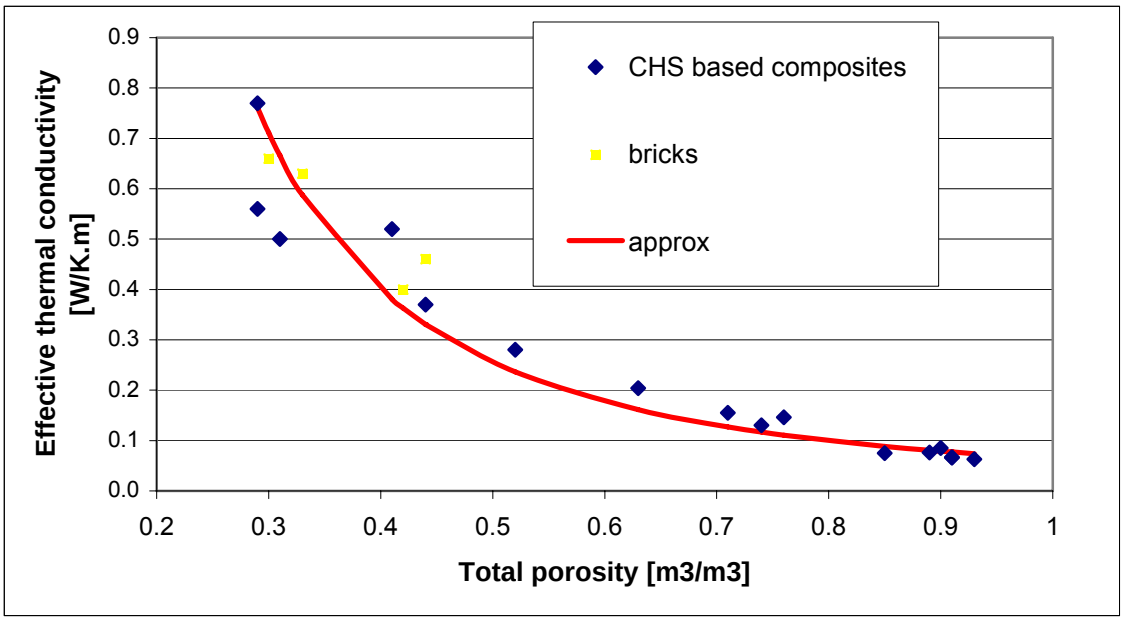

Fig. 1 Thermal conductivities of clay bricks and CHS based materials vs. total porosity. Comparison of the measured values and empirical approximation (1)

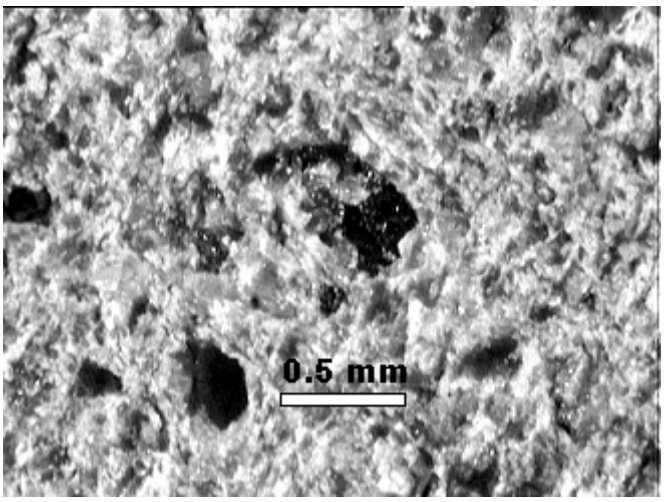

Fig. 1 Optical microscopy of brick L

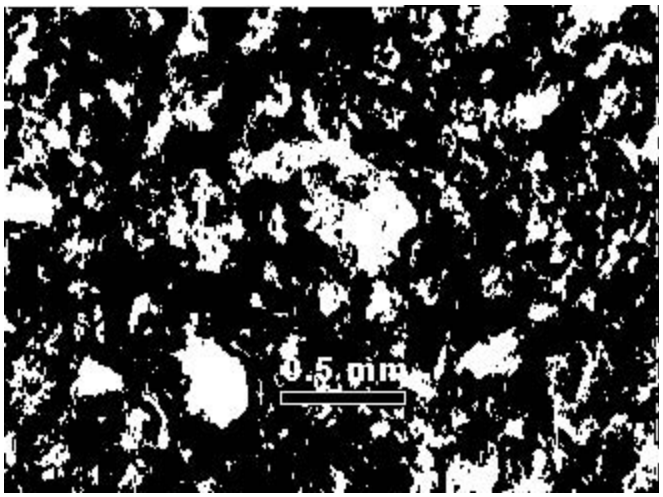

Fig. 3 Binary image of microscopy – brick L

The fractal dimensions were determined from SEM pictures (Fig. 2, 3) of the considered materials by a box counting method [8]. The fractal dimensions and corresponding exponents of the bricks components are in Tab. 3. The considered thermal conductivity of the clay brick body with density equal to ca 2500 kg/m^3 (Tab. 2) was about 1.5 W/m·K [7]. As the thermal conductivity of interfacial zone (including its porosity) the value 0.064 W/m·K, corresponding to the value measured for the pure CHS – xonotlite [4], was considered. It was also supposed that the interfacial zone volume fraction represented 10% of the total porosity in average.

The comparison of the measured thermal conductivities/total porosity relation for clay bricks and CHS based materials with the relation (5) is shown in Fig. 4. As can be seen from the Fig. 5, the measured values of clay bricks are in a satisfactore agreement with the relation (5). It was also found out that the value 0.064 W/m·K could qualify the thermal conductivity of the pore space + interfacial zone fraction also in case of burnt clay bricks.

With the aim to evaluate the sensitivity of the relation (5) to the used material parameters, the influence of the values of thermal conductivity of clay brick body and pore space + interfacial zone fraction was analysed. The changes of the thermal conductivity of clay brick body within the interval ± 30% of the original value had negligible influence on the resultant thermal conductivity/porosity relation for the considered porosities. On the other hand the changes of the thermal conductivity of pore space + interfacial zone fraction had noticable influence. In Fig. 5 the effect of the thermal conductivity of pore space + interfacial zone fraction changes within the interval of ± 9% of the original value is presented.

Table 3 Fractal dimensions and corresponding exponents of tested bricks

Component	Fractal dimension	Exponent
Solid phase	FD = 0.0	$n_1 = 1$
Porosity	FD = 1.7	$n_2 = 2.7$

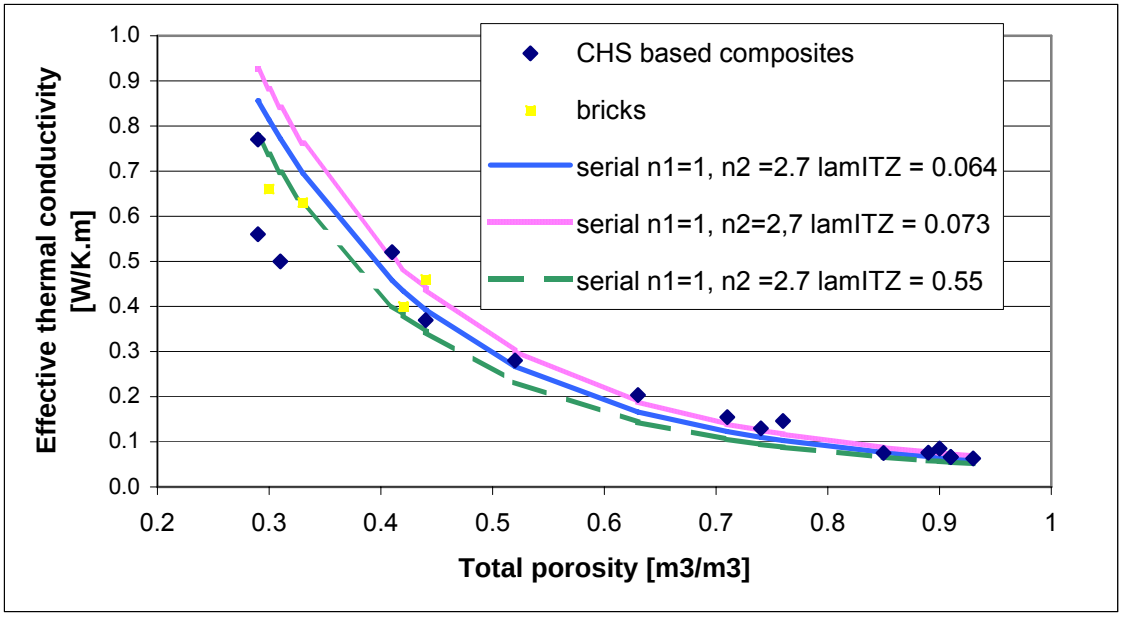

Fig. 4 Thermal conductivities of clay bricks and CHS based materials vs. total porosity. Comparison of the measured values and relation (4)

CONCLUSIONS

The relation between microstructure and effective thermal conductivity was investigated for four types of burnt clay bricks.

The effective thermal conductivity of dry clay bricks can be similarly, like thermal conductivity of CHS based mortars, plasters and insulation boards, modelled by serial configuration of solid and porous - low thermal conductivity - phases.

In the model the degree of the dispersion of low thermal conductivity phase is expressed by a power low. The exponent contains the pore space fractal dimension.

The fractal dimension can be determined with the use of image analysis.

ACKNOWLEDGEMENTS

Authors wish to thank the APVT-51-303704 and VEGA (Grant No 2/5100/27) for the financial support of this work.

REFERENCES

Bagel, L. (2001) Structural parameters of clay bricks. Internal report. Institute of Construction and Architecture, SAS, Bratislava (in Slovak).

Cultrone, G. et al. (2004) Influence of mineralogy and firing temperature on the porosity of bricks. *Journal of the European Ceramic Society.* Vol. 24, pp. 547-564.

Dondi, M. et al. (2005) Water vapour permeability of clay bricks. *Construction and Buillding Materials.* Vol. 17, pp. 253-258.
Koronthályová, O., Matiašovský, P. (2003). Thermal Conductivity of Fibre Reinforced Porous Calcium Silicate Hydrate-based Composites. *Journal of Building Physics*, Vol. 26, No. 4, pp.71- 89.
Meng, B. (1994) Calculation of moisture transport coefficients on the basis of relevant pore structure parameters. *Materials and Structures*
Matiašovský, P., Koronthályová, O. (2005) Thermal Conductivity of Mortars and Fractal Properties of their Microstructure. In *Proceedings of Thermophysics 2004*, USTARCH SAV, ISBN 80-969371-8-9. Bratislava, 2005, pp. 38 - 45.
Raznjević, K. (1984) Thermophysical Tables, ALFA Bratislava, (in Slovak).
Zmeskal, O. et al. HarFa – Harmonic and fractal image analysis. http://www.fch.vutbr.cz/lectures/imagesci/harfa.htm

Problem of elimination of undesirable thermal flows at thermophysical measurements

Ivan Baník, Jozefa Lukovičová

Abstract
The undesirable thermal flows at thermophysical measurements arise as a consequence of the non-existence of perfect thermal insulators. These flows can be minimalized through suitable thermal shielding. The use of the thermal shielding enables to increase the precision of the thermophysical measurements. In the paper some special cases of the thermal shielding are introduced and analyzed.

1. Introduction

At measurement of the thermophysical parameters of samples a task arises to eliminate or, at least to minimalise undesirable breakaway of heat into surrounding of a sample, it means to eliminate undesirable thermal flows. A perfect thermal insulator does not exist. A possible way out to achieve this goal can be a thermal shielding. Such shielding complicates situation for an experimentalist but, it enables to obtain more precise results. Further on, we describe a few special cases of the thermal shielding in measurements with selected temperature regime.
It is known a large number of measuring methods and set-ups. Many of them are described in papers [1 – 20]. J.Krempaský [4] estimated that there exist approximately 500 measuring methods.
The method sused for measuring thermophysical parameters of materials can be divided into steady state and dynamic ones. While the former use a steady state temperature field in side the sample, the latter use a dynamic temperature field. The dynamic methods can be characterized as follows. The temperature of the sample is stabilized and uniform. Then the dynamic heat flow in the form of a pulse or stepwise function is applied to the sample. The thermophysical parameters of the material can be calculated from the temperature response.
Dynamic methods represent a large group of techniques with various geometrical arrangements [21-38]. The following method belong to this group: Transient hot wire [33], Transient hot strip [34], Pulse transient, Step-wise transient, Hot plate transient, Hot disc transient, Gustafsson probe [35], Dynamic plane source [36], Extended dynamic plane source (EDPS) [37] and Laser flash method [38].
The measuring procedure consists of theory and experiment. The theoretical model of the experiment is described by the partial differential equation for the heat transport. The temperature function is a solution of this equation with boundary and initial conditions corresponding to the experimental arrangement. The experiment consists in measuring the temperature response and fitting the temperature function over the experimental points. Using the least squares procedure following thermophysical parameters can be estimated: thermal diffusivity a, thermal conductivity λ and specific heat capacity c.
Obtaining theoretical requirements (conditions) for some measuring method – it is one step on the route to the realization of a measurement.
A creation of proper conditions for its realization is the next important aspect of a measurement. Among them is also an elimination or restriction of heat losses in the measurement. Heat losses could devalue results of a measurement. Heat losses may be caused by a conduction, convection as well as radiation. Radiation is significant mainly in measurements at high temperatures.
A shielding method was used for an elimination of heat losses at first in calorimetry [39, 40]. Adiabatically shielded calorimeters were mainly used in measurements of specific heat capacities of various substances, namely metals [40, 41, 42].

Simple methods of shielding were first used in measurements of thermal conductivity, mainly in stationary and quasi-stationary methods of the measurement [17,18]. Heat losses manifest themselves mostly in long-time measurements (in stationary as well as quasi-stationary measurements). A distinctive case of non-stationary methods is the method of a constant increase in temperature [8,12,43]. The method of a constant increasing of temperature is a especially case of non stationare methods. Heat losses are less important in short-time measurements.

The reliability of every measurement confirms a quantitative statement of its uncertainty [44-46]. The sources of uncertainty in thermophysical methods can be divided in to two parts. The first part is caused by the deviations from the theoretical model. The second part is created by uncertainties of input parameters measurements.

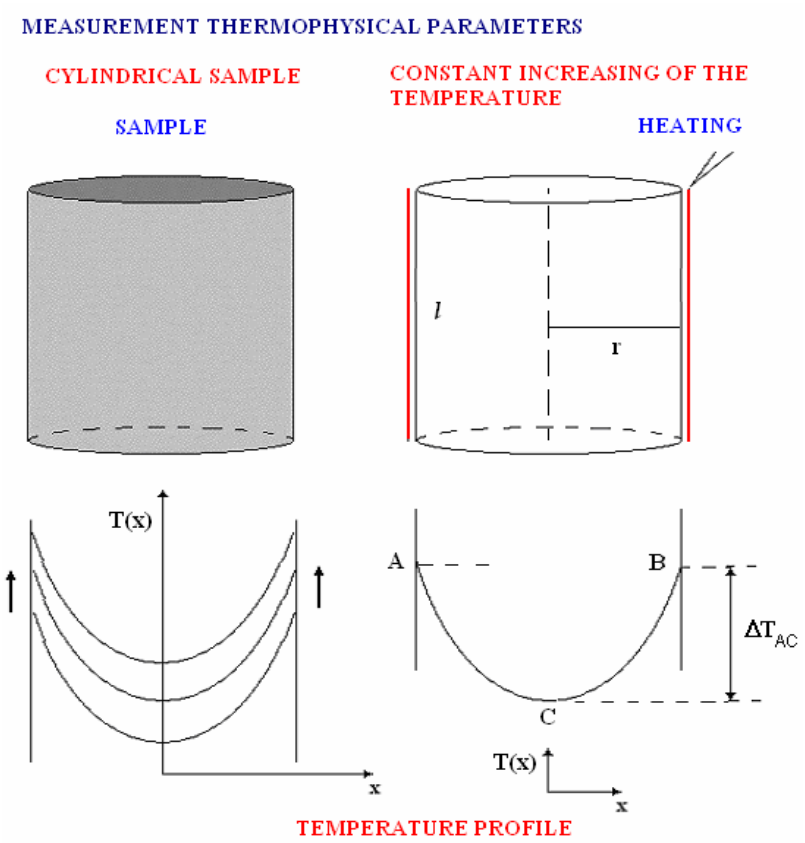

Fig. 1

2. Thermal shielding at steady increasing temperature methods

At steady increasing temperature method the rate of temperature increase is the same everywhere within a sample so that derivation of temperature relative to the time τ is constant [1-8]. Then it holds

$$\frac{dT}{d\tau} = const$$

Such temperature regime usually erases in a sample if a thermal insulated sample is heated with a thermal source of constant power (after some onset time).

2.1 Cylindrical sample heated at its border surface

The scheme of experimental setup is depicted in Fig. 1. A face of sample is cylindrical. Its surface is heated by a stove of constant heat power. At a constant rate of increasing

temperature at the cylindrical sample surface arises a parabolic temperature profile $T(x)$. Minimum of temperature is at the axis of the cylinder. If we know the difference ΔT_{AC} of the temperature T_A at the surface and that one T_C at the cylinder axis, and knowing the temperature rate $\dot{T}$ and power P then we can determine the diffusivity a_C of the sample as well as specific heat c_C. Naturally, we need to find out to this aim dimensions of the sample. Moreover, if the density of that sample ρ_C is known these data permit us to determine the thermal conductivity λ_C of sample.

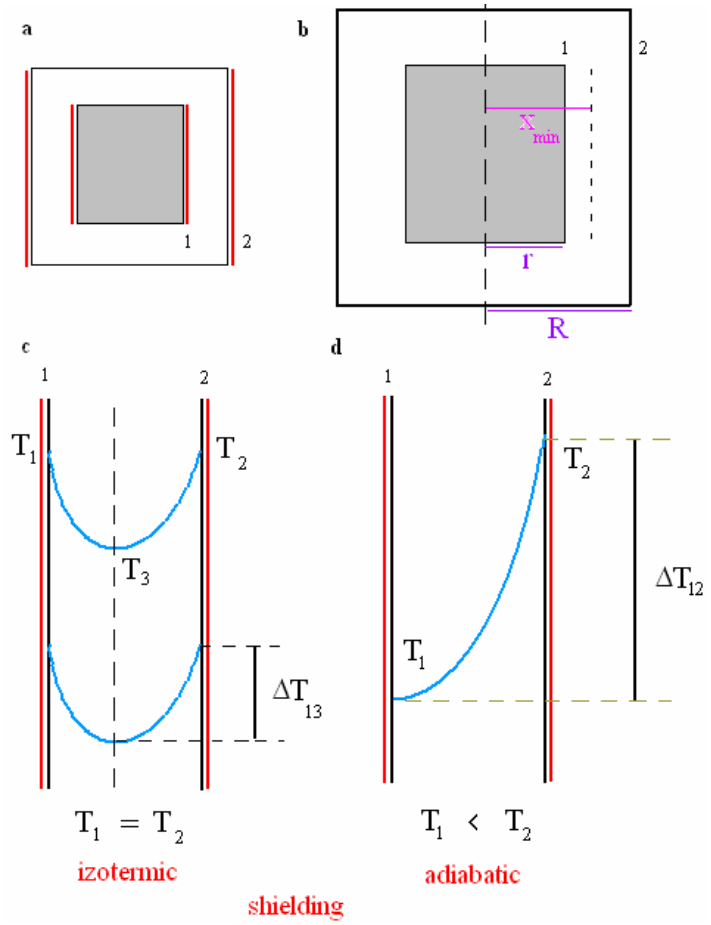

Fig. 2

Then formulae are valid for upper mentioned quantities

$$a_c = \frac{r^2}{2\Delta T_{AC}} \frac{dT}{d\tau}, \qquad \lambda_c = a_c c_c \rho_c, \qquad c_c = \frac{P}{m_c \, dT/d\tau}$$

where m_C is mass of the cylindrical sample.

Up to now a thermal loss was ignored at the upper described measurement method. Practically, the thermal loss has to be protected; it means to eliminate undesirable thermal flows.

2.1.1 Radial thermal flow shielding

Loss of heat of a cylindrical sample passing through lower and upper circular areas will be not yet considered. The thermal loss across boundary cylindrical surface of a sample in a given setup is minimalized throughout thermal shielding. It consists of a thermal insulating layer

between surface 1 and 2 and heated metallic screen in form of a cylindrical tube surrounding the thermal insulating layer.
The shielding can be isothermic or adiabatic.

Isothermic shielding

In a case of an isothermic shielding the temperature T_2 is identical with the temperature T_1 of the external cylindrical surface of the sample every time. In this way radial thermal flow is protected across insulating layer and at the first sight it seams that the thermal loss is excluded completely. Actually, the things are a little different. We want to pointed out that the heating stove placed at the boundary sample surface heated also a part of insulation, because at the regime of increasing temperature the temperature of isolation also increases. From this viewpoint it is important to determine what part of insulation is heated by the stove of the sample and what part is heated by the stove of the screen. This knowledge permits more precisely to determine the heat supplied by the stove to the sample alone.

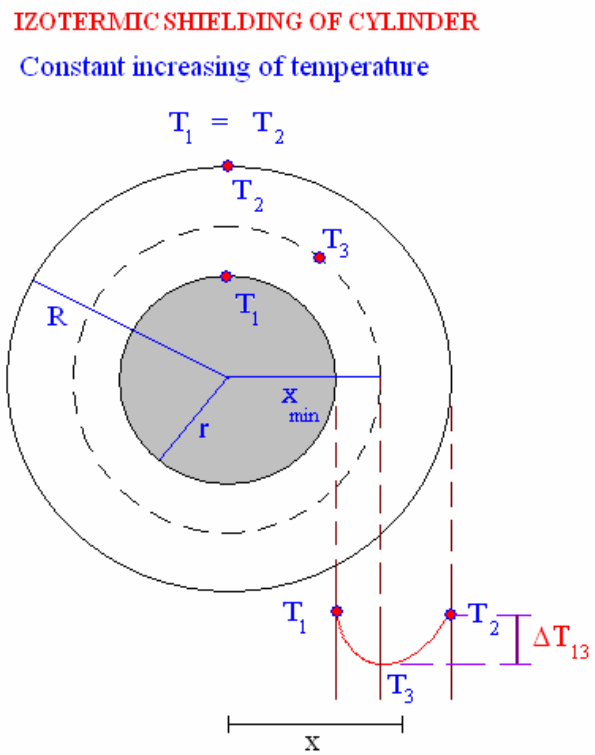

Fig. 3

At the constant temperature rate of the system by isothermic shielding the temperature T_1 of the external sample surface is equal to the temperature of the screen T_2 anytime. These temperatures uniformly increase. At the upper described regime a more complex temperature profile is created across the insulating layer because in deep of insulator the temperature is retarded in comparison with temperatures $T_1 = T_2$ at the surfaces. In this way created temperature profile is shifted uniformly to the higher temperature. It looks like as a process in measured sample alone. The shape of the temperature function in insulator is more complex (and not exactly parabolic) that one in the sample. See Fig. 2c and Fig. 3.
Analysis of this problems leads to the conclusion that the temperature minimum in isolating layer surrounding cylindrical sample lies at the distance $x_{\min}$ from the cylinder axis, where

$$x_{\min} = \sqrt{\frac{R^2 - r^2}{2\ln\frac{R}{r}}} \qquad (1)$$

This result one can obtain as follows: one determines thermal flow passing through cylindrical surface with radius x in interval $r < x < x_{\min}$. This heat is used to the heating of an insulating cylindrical layer with radius from x up to $x_{\min}$. By analogy, one determines thermal flow passing through cylindrical surface with radius x from interval $x_{\min} < x < R$, considering that corresponding heat crossing this surface is used for heating of the insulating cylindrical layer with radius lying in interval of $(x_{\min}, x)$. Integration of two formulae obtaining this way leads to two expressions for temperature difference between points 1 and 2; 2 and 3 respectively. At an isothermic shielding values of those differences have to be equal (identical) because the temperature at the points 1 and 2 are equal ($T_1 = T_2$)

Analyzing this problem one can achieves following analytical expression for temperature profile $T(x,\tau)$ in insulating layer ($x \in (r, R)$)

$$T(x,\tau) = \frac{1}{4a}\frac{dT}{d\tau}\left(x^2 - x_{\min}{}^2 - 2\,x_{\min}{}^2 \ln\frac{x}{x_{\min}}\right) + T(x_{\min},\tau) \qquad (2)$$

where for x_m relation (1) is still valid. Term $T(x_{\min},\tau)$ represents the minimal temperature of isolation at the time τ. It holds $T(x,\tau) = T(x) + k\tau$. The term $T(x)$ expresses an intrinsic temperature profile of isolation which is uniformly shifted to the higher temperatures due to the condition

$$\frac{dT}{d\tau} = const$$

As temperature minimum is at the cylindrical surface with radius x_m temperature gradient is zero at this surface. Through this cylindrical surface doesn't pass anymore thermal flow at a measurement. It implies that the cylindrical part of insulation of radius between r and $x_{\min}$ is heated by the stove located on the specimen. The other outer part of the insulation (its radius is in interval $(x_{\min}, R)$ is heated by outer shielding stove.

A thermal power P_C submitted to the specimen is smaller than the stove power P on the specimen. We can write

$$P_C = P - c\,m_{13}\frac{dT}{d\tau}$$

where c is a specific heat of isolation and m_{13} - mass of the corresponding inner part of isolation. Mass m_{iv} can be determined from known density ρ_{i} of isolation and volume of the insulator's cylindrical layer (inner radius *r,* outer - $x_{\min}$).

With respect to (2) we can write for the temperature differences

$$\Delta T_{13} = \Delta T_{23} = \frac{1}{4a}\frac{dT}{d\tau}\left(r^2 - x_{\min}{}^2 - 2\,x_{\min}{}^2 \ln\frac{r}{x_{\min}}\right)$$

where $\Delta T_{13} = T_1 - T_3 = T_2 - T_3 = \Delta T_{23}$, considering the temperature T_1 at the surface of the sample is equal as the temperature at the screen T_2. T_3 is the temperature at $x_{\min}$ in isolation where the temperature possesses its minimum.

This difference at the constant temperature increase becomes unchanged (while diffusivity stays unchanged).
This account enables correction of the stove power connected with heating of inner insulating part. In this way the measurement of sample thermal parameters is more precise.
For the temperature difference $\Delta T_{13} = \Delta T_{23}$ it holds also

$$\Delta T_{13} = \frac{1}{4a}\frac{dT}{d\tau}\left(R^2 - x_{\min}{}^2 - 2\, x_{\min}{}^2 \ln\frac{R}{x_{\min}} \right)$$

Adiabatic shielding
Shielding is called adiabatic if thermal flow throughout entire outer surface of a sample (including a stove at its surface) is zero. Such a state can be achieved when within the isolation a temperature profile will be created with a minimum of the corresponding temperature function $T(x)$ resting just at the cylindrical surface of the sample. This state shows Fig. 2d.
Thermal flow analysis of a similar type as in the case of an isotermic shielding showed that this case occurs when the temperature of the screen T_2 is of some amount ΔT_{21} higher than the temperature T_1 at the sample surface

$$\Delta T_{21} = \frac{1}{4a}\frac{dT}{d\tau}\left(R^2 - r^2 - 2r^2 \ln\frac{R}{r} \right)$$

A way out is to express thermal flow across a cylindrical surface with the radius x inside interval $r < x < R$ and a fact that corresponding heat isolation of the thickness $r - x$
Inside isolation one can express the temperature profile in isolation as

$$T(x,\tau) = \frac{1}{4a}\frac{dT}{d\tau}\left(x^2 - r^2 - 2r^2 \ln\frac{x}{r} \right) + T(r,\tau)$$

In the case of an adiabatic shielding a heating stove at a sample transmits to the sample whole thermal power. There is not need for correction.

2.1.2 Shielding of cylindrical bases

In method of steady increase with heating at the surface of a cylinder the temperature profile $T(x)$ inside a homogeneous sample is parabolic as mentioned earlier. While, the thermal loss is neglected across both basic areas of a cylinder there will be a similar parabolic distribution of the temperature at the basic circular areas. A shielding of the basic areas will be harder than the shielding of the enveloping cylindrical surface. We are going to describe two suitable methods of the thermal shielding.

Method No 1
This method employs two or more sliced screen (disc 1) constructed in such way that its effective diffusivity a_{eff} is nearly the same as the diffusivity of the sample. Practically, after first measurement of the sample parameters with application of a shielding the screen will be adapted to the new measured value of the quantity *a.*
For two-layer screen can be proved following formula

$$a_{ef} = \frac{\lambda_1 h_1 + \lambda_2 h_2}{c_1\rho_1 h_1 + c_2\rho_2 h_{21}}$$

where h_1 and h_2 denote the thickness of screening layers. The meaning of all other symbols is apparent. This relation one can easily spread onto multilayer screens.
Multilayer screen is less adaptable and as fare as we don't know parameters of each layer it can be prepared only by experience. If it is correctly done, at the analogical increase of the temperature on the sample periphery the temperature profile inside will satisfy the temperature profile on the cylindrical sample base.
Of course, the temperature regime inside the screen disturbs particularly venting of heat into surrounding. This state one can improve by a double shielding. It means by using of two analogical screens with an isolation layer in between. In this way in the screen which is attached to the sample base a thermal profile approaches better to the perfect one.
This fact can be reasoned via theoretical model and corresponding calculation methods of numerical mathematics.

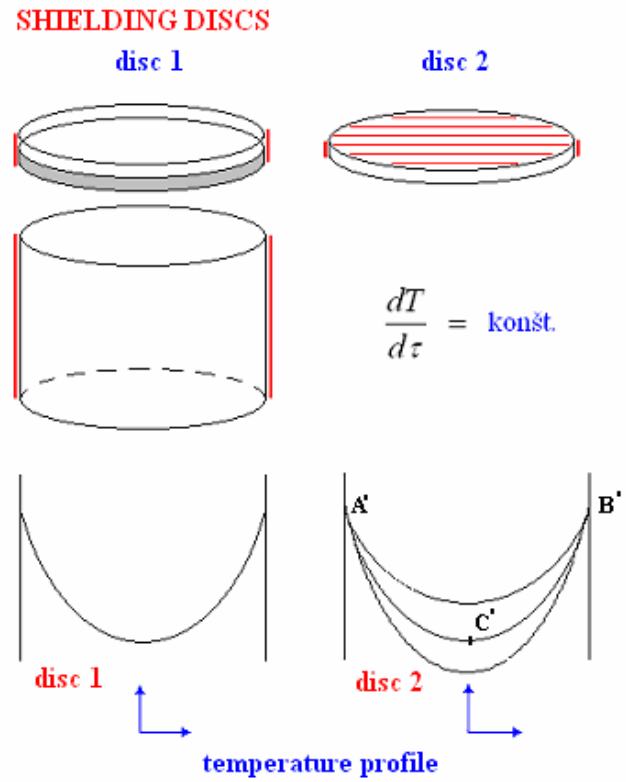

Fig. 4

Method No 2
A better possibility for shielding basic surfaces of a cylinder offers a screen (disc 2) with planar heat source at its circular surfaces. Diffusivity for such a screen has to be less than is the diffusivity of a sample. Without applying of heating the temperature profile of a screen at an increase of temperature would not correspond to the profile in sample. Instantaneous temperature at the middle of the screen by increasing of temperature would be lower than the temperature at the middle of cylindrical sample. A planar heating of the screen permits to fit a temperature profile of screen so that it would correspond to the sample profile exactly adapting power of a stove (changing the current). Assuming, the screen is regularly heated over all circular area.
At intrinsic measurement with the use of shielding one inserts between the sample base and the screen a suitable insulating layer. Under optimal conditions average gradient of temperature in orthogonal direction to the isolation layer will be zero. In this way the thermal losses are eliminated to a great extent.

It is possible to prove mathematically that trough power adjusting of the stove on the circular screen makes it possible to adjust temperature profile of the screen to that one of the cylindrical stove. Such screen possesses varieties of shielding properties. This is great advantage in comparison with two-layer screen.
It can be imagine quasi-adiabatic shielding of the cylinder bases. In that case the thermal profile of the screen would be shifted to higher temperature compare to the sample profile Required temperature difference between temperature profile of the screen and that one of the sample will be determined by (3) – will be introduced latter – despite the other situation wit comparison to the case of a platelike sample.
We notice that difference between screen temperature at its circuit and the temperature at its center is given as

$$\Delta T_{A'C'} = \frac{1}{4a_t}\left[\frac{dT}{d\tau} - \frac{2P_t}{C_t}\right] R^2$$

where P is a power of electric stove, λ_t, a_t are thermal conductivity and diffusivity of the shielding layer respectively. C_t is heat capacity of the screen. At equality of analogical temperature differences on the sample and the screen the temperature profiles will be also identical.
The parabolic temperature profile creating in the screen by the superficial heater is represented by parabola

$$T(x,\tau) = \frac{1}{4a_t}\left(\frac{dT}{d\tau} - \frac{2P_t}{C_t}\right) x^2 + T(0,\tau)$$

The power P_t of electric screening stove is managed in such manner in order that it corresponds to the sample profile. To this aim it suffices to regulate (by a change of current on superficial stove of the screen) temperature at the screen center with that one in the middle of measured sample.

3. Shielding in a case of a spherical specimen

We denote radius of a spherical sample as *r*, and outer radius of an isolation layer as *R*.
At isothermic shielding with a regime of steady temperature increase (surfaces of the sample and that one of the screen having identical temperature) minimum of the temperature inside an isolation layer is at the spherical surface which radius is $x_{\min}$ where

$$x_{\min} = \sqrt[3]{\frac{Rr(R+r)}{2}}$$

Knowledge of this value enables to correct power of a stove heating sample. Thereby, determination of sample specific heat becomes more precise. By derivation this formula we precede the same way as it was at the case of a cylindrical insulating layer.
Thermal profile in isolation by an isotermic shielding gives the relation

$$T(x,\tau) = \frac{1}{6a}\frac{dT}{d\tau}\left[R^2 - x^2 + 2x_{\min}^3\left(\frac{1}{R} - \frac{1}{x}\right)\right] + T(R,\tau)$$

The value of maximal temperature difference in isolation - between the temperature at the border of spherical isolating layer and the minimal temperature inside isolation is

$$\Delta T_{13} = \frac{1}{6a}\frac{dT}{d\tau}\left[R^2 - x_{\min}^2 + 2x_{\min}^3\left(\frac{1}{R} - \frac{1}{x_{\min}}\right)\right]$$

Temperature profile in spherical insulator layer at an adiabatic shielding is

$$T(x) = \frac{1}{6a}\frac{dT}{d\tau}\left[x^2 - r^2 + 2r^3\left(\frac{1}{x} - \frac{1}{r}\right)\right] + T_1$$

By an adiabatic shielding difference of temperature at the inner and outer surface of the isolation has to obey following formula

$$\Delta T_{21} = \frac{1}{6a}\frac{dT}{d\tau}\left[R^2 - r^2 + 2r^3\left(\frac{1}{R} - \frac{1}{r}\right)\right]$$

In a case of an adiabatic shielding the whole stove power is heating sample and so no correction of its power is needed.

Diffusivity a_s of a spherical sample (sphere) by a method of a steady increase of temperature assuming that sphere is heated by a thermal sour at its outer spherical surface - is determined as

$$a_S = \frac{r^2}{6\Delta T_S}\frac{dT}{d\tau}$$

where ΔT_S denotes the temperature difference between temperatures at outer surface of the sphere and that one at center.

For the other thermal parameters it holds

$$c_S = \frac{P}{m_S \dfrac{dT}{d\tau}}$$

$$\lambda_S = a_S c_S \rho_S$$

where their meaning is clear. By adiabatic shielding the power *P* needs no correction; by isothermic one its correction is necessary since inner part of isolation is also heated.

4. Shielding in a case of platelike samples

By shielding a (planeparalel) plate (Fig. 5) the isolation layer ISOL is platelike**.** Let us *h* denotes its thickness. A temperature profile in isolation by isothermic shielding ($T_1 = T_2$) is parabolic and symmetric. At a constant rate of temperature increase the minimum of temperature is at the plane dividing the insulator layer into two equal parts. As we choose x-axis according to the Fig. 2 it is the (vertical) plane at $x_{\min} = h/2$.

This way, one half of insulator plate is heated by the sample, which permits to correct power of a stove at the sample.

Maximal value of temperature difference in isolation is equal to

$$\Delta T_{13} = \frac{h^2}{8a}\frac{dT}{d\tau}$$

The temperature profile in insulator layer by an isothermic isolation of the platelike sample is expressed by the formula

$$T(x) = \frac{h^2}{2a}\frac{dT}{d\tau}\left(x - \frac{h}{2}\right)^2 + T_3$$

or

$$T(x) = \frac{h^2}{2a}\frac{dT}{d\tau}\left(x^2 - hx\right)^2 + T_1$$

An adiabatic shielding of the platelike sample at regime of steady temperature increase requires keeping temperature of the screen higher of amount

$$\Delta T_{21} = \frac{h^2}{2a}\frac{dT}{d\tau} \qquad (3)$$

than is the surface temperature of the sample.

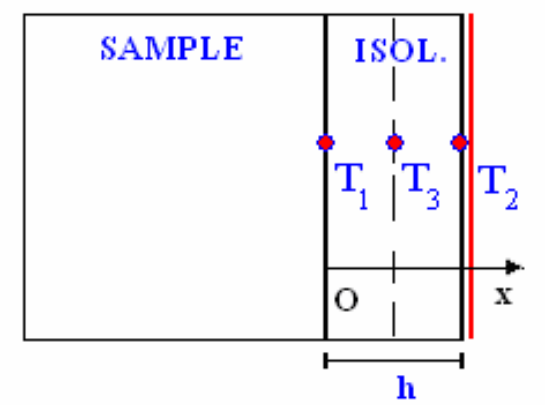

Fig. 5

The temperature profile inside insulator layer using an adiabatic isolation determines the function

$$T(x) = \frac{h^2}{2a}\frac{dT}{d\tau}x^2 + T_1$$

5. Shielding at measurement of caliducts

Thermal looses of caliducts are usually measured in a stationary regime with qualificative boundary conditions [47]. The temperature is given in the nucleus of a caliduct (temperature of the central metallic tube) and the temperature at the external caliduct surface. During a measurement stationary temperature profile is created within caliduct isolation of a radial type. That one would be disturbed (without shading) near the marginal regions of a caliduct (Fig. 6a). In order to exclude that distortion shielding of border surfaces is necessary.

A few possibilities for shielding of caliduct ends shove Fig. 6. In the case shoved in Fig. 6b a marginal part of the caliduct is employed with a separated part of central tube, which is heated to the desired temperature by a separated stove under control. Temperature field disturbances owing to heat losses throughout end areas in inner part of caliduct - where measurement is executed – will not appear.

To the shielding of the ends can be used also the other type of material (Fig. 6c), than is insulator material of caliduct. It cannot be either a thermal isolating material. It is due to fact, that a steady temperature profile at equal boundary condition will be the same in different materials. Even thought, if a material possesses better thermal conductivity the shielding will be also better and a screen may be narrower. Preferable possibility offers a multilayer screen in which metallic and insulating layers alternate (Fig.6d). Temperature profile in conduction layers of a multilayer screen improves gradually in direction to the caliduct and shielding is superior. Disturbances caused by surrounding affect significantly the external layers of the screen. Central part of the screen is heated to the desired temperature by a separated stove under control.

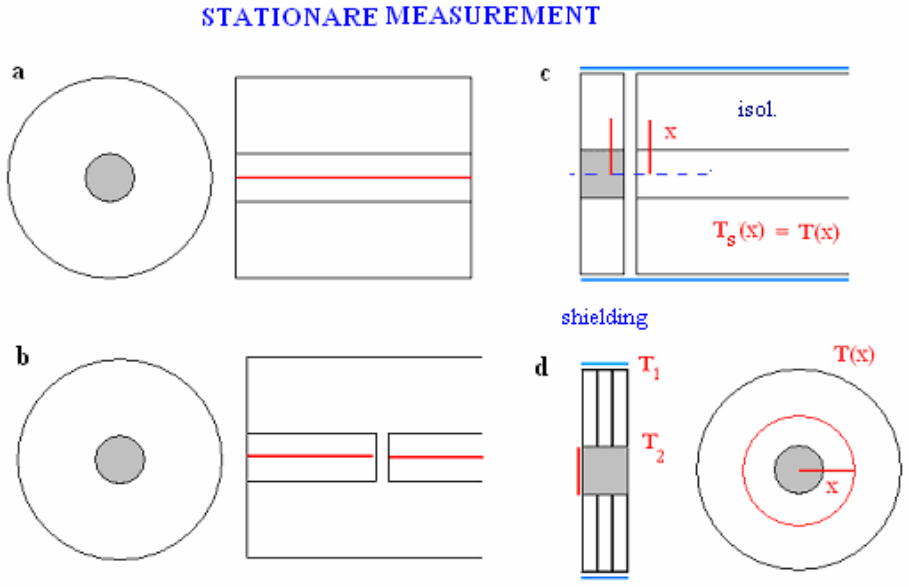

Fig. 6

The temperature field in separate screen layers one can determine using numerical methods under some reasonable simplifications.

6. Conclusion

This article suggests many methods of elimination undesirable thermal flows at thermophysical measurements using temperature shielding. It is going on some kinds of experimental setup applying a steady increase temperature method. It deals with shielding in a case of stationary regime at the laboratory measurement of caliduct losses. Temperature shielding enables to increase precision of the thermophysical measurements.

7. Acknowledgement

Financial support of the project VEGA 1/4204/07 is gratefully acknowledged.

8. References

[1] Carslaw H. S., Jaeger J. C.: Conduction of Heat in Solids, 2nd ed, Oxford University Press, reprinted 1980
[2] Carslaw H.S.,.Jaeger J.C.: Conduction of Heatin Solids, Clarendon, Oxford 1959
[3] Carlslaw H.S.: Introduction to the mathematical theoty of heat conduction, Mc. Milan, London 1921
[4] Krempaský J.: The measurements of the thermophysical Properties, SAV, Bratislava, 1969
[5] Wilkes G.B.: Heat insulation., John Willey, New York, 1950
[6] Weber R.L.: Heat and temperature Measurement, Prentice-Hill, New Jersey, 1950
[7] Kondratiev G.M.: Ispitanije na teplovodnosť po metódu reguľarnogo režima, Standartgiz, Moskva, 1936
[8] Kondratiev G.M.: Teplovyje izmerenija, Mašgiz., Moskva 1957
[9] Volkenštein V.S.: Teplo i massperenos., Izd. Akademii nauk BSSR, Minsk 1962
[10] Kiričenko J.A.: Teplo i massperenos., Izd. Akademii nauk BSSR, Minsk 1962
[11] Michejev M.A.: Osnovy teploperedači, Gosenergoizdat, Moskva 1956
[12] Lykov A.V.: Teorija teploprovodnosti, Gos.izd. tech-teor. Lit., Moskva 1952

[13] Lienhardt J. H. IV,. Lienhardt J. H V. *A heat transfer textbook. 3Edition*. Phlogiston Press, 2003
[14] Incropera F.P., DeWitt D.P. *Fundamentals of Heat and Mass transfer. 5- Edition*. John Wiley&Sons, 2002.
[15] Waddington G., Proc. 1st International Conf. Calorimetry and Thermodynamics, 25-27, PWN, Warsaw (1969)
[16] Javaitis I., Erglis K., Jakovičs A.. *Determination of Heat Conductivity of Materials by Guarded Hot Plate Method*. Proceedings of the international scientific conference Civil Engeneering '05. Jelgava, 2005.
[17] Čudnovskij A.F.: Teplofyzičeskyje charakteristiky disperznych materiálov, GIFML, Moskva 1962, p. 456
[18] Luikov A.V.: Heat and Mass Transfer in capillary-Porous Bodies, Pergamon Press, Oxford, 1966
[19] Hemminger W. Hohne G.: Calorimetry – Fundamentals and Practice, Verlag chemie, GmbH, Weinheim, Florida Basel 1984, p. 176 /transl.: Kalorimetria – teoria i praktika, Chimia, Moskva 1989/
[20] Blažek A.: Termická analýza, SNTL, Praha 1974, p. 296
[21] Kubičár Ľ: Trends in the methods of measurement of thermophysical properties in solid state, Thermochimica Acta 110 (1987) 109
[22] Kubičár Ľ.: Pulse Method of Measuring Basic Thermophysical Parameters, ELSEVIER Amsterdam1991
[23] Jarny Y., Ozisik M.N., Bardon J.P.: A general method using adjoing equation for solving ultidimensional inverse heat conduction, Int. J. Heat Mass Transfer 34, 1991,
[24] Alifanov O.M.: Solution of an inverse problem of heat conductyion by iteration method, J. Engineering Physics 26, 1972, p. 471
[25] Vretenár V.: Extended version of Pulse transient method, Proceedings of Thermophysics, 2005, Contents, pp. 92-103, October 2005, Meeting of the hermophysical Society , SAS Bratislava 2005. http://www.tpl.ukf.sk/engl_vers/thermophys/
[26] Kubičár Ľ., Krempasky J.: On the accuracy of the heat pulse method for measuring hermophysical quantities, phys.stat. sol. (a) 2 (1970) 739
[27] Vozár L., Groboth G.: *High Temp. - High Press.* 29 (1997) 191
[28] Kubičár Ľ., Boháč V.: Development of Methods for Measuring Thermophysical Parameters of Materials.Proc. of Engineering Aspect in Physics Education. SEFI – European Society for Engineering Education, WGP Seminar AZPE'99 by for Slovak University and Technology, Bratislava June 21-23, 1999 . Pub SEFI Brussels, Belgium, Doc. No 27, ISBN 2-87352-027-2, pp 80-84
[29] Kubičár Ľ., Boháč V.: A step-wise method for measuring thermophysical parameters of materials, Meas. Sci. Technol., Vol. 11, 2000, p. 252-258
[30] Kubičár Ľ., Boháč V., Review of several dynamic methods of measuring thermophysical parameters, in „Proc. of 24th Int. Conf. on Thermal Conductivity /12th Int. Thermal Expansion Symposium", ed. P.S. Gaal, D.E. Apostolescu, Lancaster: Technomic Publishing Company (1999), pp. 135-149
[31] Čulík F., Baník I., Determination of temperature field created by planar heat source in a solid body consisting of three parts in mutual thermal contact, In press.
[32] Kubičár L'., Boháč V.: Proc. 24 th Int. Conf. on Thermal Conductivity /12 th Int. Thermal Expansion Symp./, Pittsburg, October1997, p.135
[33 Hammerschmidt] U., Sabuga W.: Int. J. Thermophys. 21 (2000) 1255
[34] Hammerschmidt U., Sabuga W.: Int. J. Thermophys. 21 (2000) 217
[35 Kubičár] L'.,.Boháč V: Proc.Thermophysics 2000, Constantine the Philosopher

University, Nitra 2000, p.39
[36] .Karawacki E, Suleiman B.M.: *Meas. Sci. Technol.* 2 (1991) 744
[37] Karawacki E., Suleiman B.M., I.ul-Hag, B.Nhi: *Rev. Sci. Instrum.* 63 (1992) 4390
[38] Vozár L., Groboth G., Hohenauer W., Hübner E.: An Application of the Laser Flash Method with Repeated Pulses for the Thermal Diffusivity Measurement, in Proceedings of the 10th Int. Conf. On Photoacoustic and Phototherm. Phen., New York AIP Woodbury, 1999, pp. 351-353
[39] Perrier A., Roux H., Memoires de la Societe Vandoise ders sciences naturelles, 1923 V. 1. P. 109.
[40] Hemminger W. Hohne G.: Calorimetry – Fundamentals and Practice, Verlag chemie, GmbH, Weinheim, Deerfield Beach, Florida Basel 1984, p. 176 (transl.: Kalorimetria – teoria i praktika, Chimia, Moskva 1989)
[41] Sykes C.: Proc. Roy. Soc. London 1935, V. A 148. P. 422
[42] Moser H.: Phys. Z. 1936. Bd. 37. S. 737
[43] Baník I., Maľa P., Veselský J., Zámečník J.: Soil freezing technology, In: New requirements for structures and their reliability, Prague 1994, Czech. Tech. Univ Prague, p. 75
[44] Guide to the Expression of the Uncertainty in Measurement, ISO, Geneva, 1993
[45] Barta Š., Cesnak L., Krempasky J., Kubičár Ľ.**:** Complex analysis of disturbing factors influence upon the measurement of thermal parameters by measn of a pulse method, Czech. J. Phys. (1973) 703 B23
[46] Kubičár Ľ., Boháč V.: Accuracy analysis of intercomparison measurements of thermophysical properties, Torino September 16 – 19, 1996, Proc. of TEMPECO 96, Ed. Piero Marcarino, Publisher Lerrotto, Co&Bella, Torino, pp.505 – 511.
[47] Baník I., Baník R, Veselský J., Zámečník J.: Meranie tepelných strát teplovodov, Pozemní stavby 1 - 1984, p. 29-32

SIMULATION OF HEAT TRANSPORT EQUATION USING ANSYS SOFTWARE

Holúbek Matúš

Fakulty of Civil Engineering , Slovak University of Technology
Radlinského 11, 81368, Bratislava, Slovakia
holubek@svf.stuba.sk

Abstract:
This paper thinks over the heat transport problem in plexi-glass environment. We applied the finite element method (FEM) for simple one dimensional example and offer exact description of FEM. Further it shows comparison of experimental data from measurement and data from numerical simulation using software ANSYS, in which the accordance with measurement is demonstrate.

Keywords:
Simulation, finite element method, heat transport

THEORY

Temperature and its spatial distribution represent the driving potential for heat transport. We consider convection and conduction as a process of heat transport. The heat flux density equivalent to conduction we express in equation

$$q = -\lambda . \frac{\partial T}{\partial x}, \tag{1}$$

where λ is thermal conductivity , T temperature and q heat flux density.
The heat flux density due to convection can be written as follows:

$$q = \alpha \left(T_s - T_p \right), \tag{2}$$

where α is heat transfer coefficient, T_p represents environment temperature and T_s surface temperature of the sample, which is in contact with surrounding environment.
The heat transport equation without source term is

$$\frac{\partial T}{\partial t} = \frac{1}{c_p \rho} \frac{\partial}{\partial x} \left(\lambda \frac{\partial T}{\partial x} \right), \tag{3}$$

where T is time and space dependent temperature field, c_p is specific heat capacity and ρ material density.

SOLVED PROBLEM

The aim of our work was the comparison of measured data and simulation, in which we take into consideration all conditions from the experiment (Fig.1). The sample, on which we realized the measurement has shape of cylinder, made of plexi-glass, with diameter 0.03m and length 0.30m (material parameters: $\lambda = 0.195\frac{W}{mK}$, $\rho = 1180\frac{kg}{m^3}$, $c_p = 1465\frac{J}{kgK}$).

Bottom of the cylinder presents a heat source, in direct contact with plexi-glass. Heat source was supplied by direct currant I=0.103A and voltage U=5.24V. Heat flux density from the source has constant value $q = 382\frac{W}{m^2}$ during all measurement (1. boundary condition). Opposite side of cylinder bottom was in contact with ambient air. Its temperature has enduring value T_p=26°C (2.boundary condition) and $\alpha = 10\frac{W}{m^2K}$. The shell of the cylinder was isolated by polystyrene of 5cm thickness, hence the flux through its surface was nought (3.boundary condition). Internal temperature of cylinder was uniform T_o=26°C at the beginning of experiment (initial condition). From previous result, that we can consider only one dimensional problem.

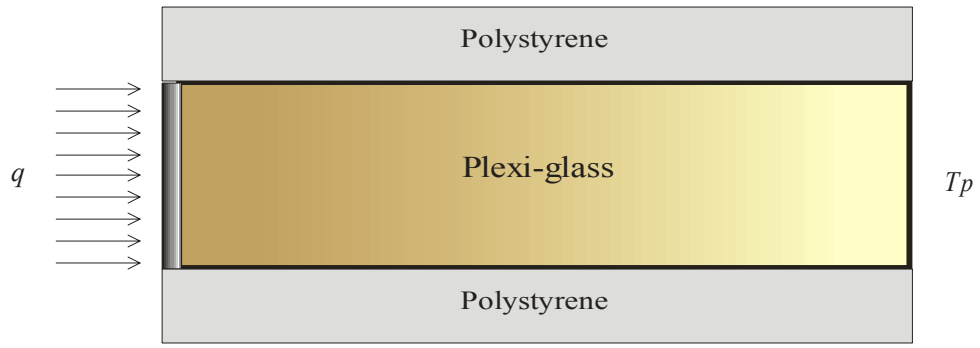

Fig.1

PROBLEM SOLUTION USING FINITE ELEMENT METHOD

We are finding solution u (note $u \equiv T$), which must satisfy mentioned initial and boundary conditions and also heat transport equation, where $c = c_p\rho$ and $a = \lambda$.

$$c\frac{\partial u}{\partial t} = \frac{\partial}{\partial x}\left(a\frac{\partial u}{\partial x}\right) \tag{4}$$

Discretization of domain

All domain, on which are we solving the problem, we divide to n elements and $n+1$ nodes (Fig.2). First node represents surface of plexi-glass next to heat source, which ensure constant heat

flux density inward the sample. Last node is surface on opposite side, which is in contact with surrounding environment. Length of chosen element is h_e.

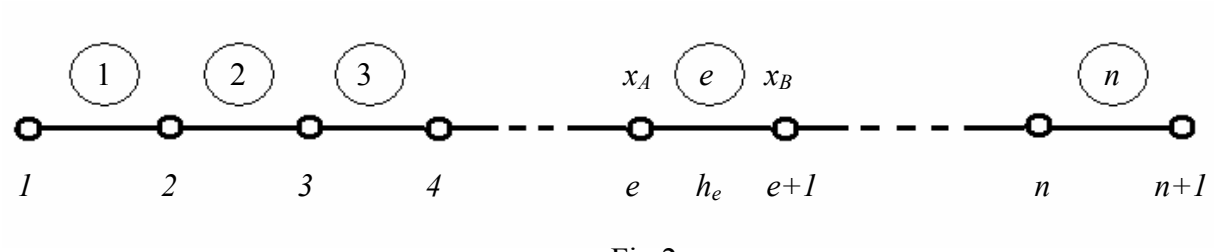

Fig.2

DERIVATION OF ELEMENT EQUATIONS

Derivation of weak form

At first, we multiply the heat transport equation by weight function w. After that we integrate all expression over an element e.

$$\int_{x_A}^{x_B} c\frac{\partial u}{\partial t} w dx - \int_{x_A}^{x_B} \frac{\partial}{\partial x}\left(a\frac{\partial u}{\partial x}\right) w dx = 0 \tag{6}$$

Using Per-partes method we obtain

$$\int_{x_A}^{x_B} c\frac{\partial u}{\partial t} w dx - \left[a\frac{\partial u}{\partial x}\right]_{x_B} w(x_B) + \left[a\frac{\partial u}{\partial x}\right]_{x_A} w(x_A) + \int_{x_A}^{x_B} a\frac{\partial u}{\partial x}\frac{\partial w}{\partial x} dx = 0\,. \tag{7}$$

Fluxes into an element e in positions x_A a x_B are defined as:

$$-a\left[\frac{\partial u}{\partial x}\right]_{x=x_A} = Q_A$$

$$a\left[\frac{\partial u}{\partial x}\right]_{x=x_B} = Q_B$$

Weak form (WF) of transient problem:

$$\int_{\mathbf{x}_A}^{x_B} c\frac{\partial u}{\partial t} dx + \int_{x_A}^{x_B} a\frac{\partial u}{\partial x}\frac{\partial w}{\partial x} dx = Q_B w(x_B) + Q_A w(x_A) \tag{8}$$

Derivation of approximate function

We are finding an approximate solution of transient problem over element e in the shape:

$$u^e(x,t) = \sum_{j=1}^{n} u_j^e(t)\varphi_j^e(x)\,, \tag{9}$$

where time development of the function u is included in time dependent value in j-th nodal point $u_j^e(t)$ and $\varphi_j^e(x)$ is spatial dependent j-th base function (n is number of nodes in element e).

Bases functions must satisfy following conditions. They have to be continuous, differentiable (up to the order, which requires the weak form) and values of approximate solution in node points are equal to real solution.

For example, the bases functions for linear approximation of solution u ($u^e = ax + b$) over element have shapes:

$$\varphi_1^e = \frac{x_B - x}{x_B - x_A}, \qquad \varphi_2^e = \frac{x - x_A}{x_B - x_A}$$

Derivation of element equations

Spatial semidiscretization

Instead of u in WF we substitute approximate solution u^e and as a weight functions w we use bases functions φ_i.

$$\int_{x_A}^{x_B} c \frac{\partial\left(\sum_{j=1}^{n} u_j^e(t)\varphi_j^e(x)\right)}{\partial t}\varphi_i^e(x)dx + \int_{x_A}^{x_B} a \frac{\partial\left(\sum_{j=1}^{n} u_j^e(t)\varphi_j^e(x)\right)}{\partial x}\frac{\partial\varphi_i^e(x)}{\partial x}dx = Q_A\varphi_i^e(x_A) + Q_B\varphi_i^e(x_B) \quad (10)$$

Now we have the system of differential equations over element e

$$\sum_{j=1}^{n}\frac{\partial u_j^e(t)}{\partial t}\int_{x_A}^{x_B} c\varphi_j^e(x)\varphi_i^e(x)dx + \sum_{j=1}^{n} u_j^e(t)\int_{x_A}^{x_B} a\frac{\partial\varphi_j^e(x)}{\partial x}\frac{\partial\varphi_i^e(x)}{\partial x}dx = Q_A\varphi_i^e(x_A) + Q_B\varphi_i^e(x_B) = F_i, \quad (11)$$

where $M_{ij} = \int_{x_A}^{x_B} c\varphi_j^e(x)\varphi_i^e(x)dx$ is mass matrix and $K_{ij} = \int_{x_A}^{x_B} a\frac{\partial\varphi_j^e(x)}{\partial x}\frac{\partial\varphi_i^e(x)}{\partial x}dx$ is stiffness matrix.

For linear approximation of solution the matrices have such shape $M = ch_e\begin{pmatrix} 1/3 & 1/6 \\ 1/6 & 1/3 \end{pmatrix}$, $K = \frac{a}{h^e}\begin{pmatrix} 1 & -1 \\ -1 & 1 \end{pmatrix}$

Further we introduce vectors: $\vec{u} = \left(u_1^e(t),\ u_2^e(t),\ ....,\ u_n^e(t)\right)$

$$\dot{\vec{u}} = \left(\dot{u}_1^e(t),\ \dot{u}_2^e(t),\ ....,\ \dot{u}_n^e(t)\right)$$

Then we get simplified matrix notation:

$$M.\dot{\vec{u}} + K.\vec{u} = \vec{F} \quad (12)$$

Time discretization

Let us consider the time evolution of $u_j^e(t)$ at j-th node of element e at time t_s with timestep Δt according to Fig. 3.

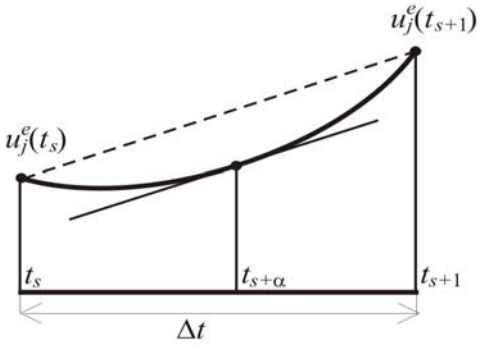

Fig.3

The value of $u_j^e(t_s)$ raises during the timestep Δt to $u_j^e(t_{s+1})$. This new value can be expressed as the sum of function value at time t_s and its increment during timestep Δt. The difficulty is in accuracy of calculating the increment. One possibility is to take the rate of temperature increase from the derivation at time t_s (we take the Taylor's expansion at time t_s and use the first two terms of it to calculate the value at time t_{s+1}). As we can see from the curve describing the development of temperature depending on time this does not fit the real dependency and the following calculations would be signate by this inaccuracy. This is because the derivative has to be consistent with the slope of line (dash line) which connecting values $u_j^e(t_s)$ and $u_j^e(t_{s+1})$. Therefore we look for another way to determine the derivative value. It is clear that there is always a point during the time step Δt where the derivative of function $u_j^e(t)$ is consistent with the tangent of the dash line. We denote it $t_{s+\alpha}$ (α can reach the value within 0 to 1). It is difficult to estimate the correct value of α. However the value of the derivative of function $u_j^e(t)$ at arbitrary chosen time during the timestep lies between of the derivative values at times t_s and t_{s+1}, therefore we achieve more accuracy. We replace the derivative at time t_s by the derivative at time $t_{s+\alpha}$ in the Taylor's expansion which results in reducing the error caused by neglecting the higher terms of the expansion. We calculate $\dot{u}_j^e(t_{s+\alpha})$ from weighted average of the derivatives at times t_s and t_{s+1}.
Then we can write:

$$u_j^e(t_{s+1}) = u_j^e(t_s) + \Delta t.\dot{u}_j^e(t_s) = u_j^e(t_s) + \Delta t.\dot{u}_j^e(t_{s+\alpha}) = u_j^e(t_s) + \Delta t.\left(\frac{(1-\alpha).\dot{u}_j^e(t_s) + \alpha.\dot{u}_j^e(t_{s+1})}{(1-\alpha)+\alpha}\right) \quad (13)$$

When we consider $\vec{u}_s = \vec{u}(t_s)$
$\vec{u}_{s+1} = \vec{u}(t_{s+1})$

then

$$\vec{u}_{s+1} = \vec{u}_s + \Delta t.\left((1-\alpha)\dot{\vec{u}}_s + \alpha.\dot{\vec{u}}_{s+1}\right). \quad (14)$$

We multiply WF in time t_s ($M.\dot{\vec{u}}_s + K.\vec{u}_s = \vec{F}_s$) by the term $\Delta t.(1-\alpha)$ and WF formulation in time t_{s+1} ($M.\dot{\vec{u}}_{s+1} + K.\vec{u}_{s+1} = \vec{F}_{s+1}$) by the term $\Delta t\alpha$. Afterward we sum both equations. Then we obtain an equation without time derivations.

$$M\left(\Delta t(1-\alpha).\dot{\vec{u}}_s + \Delta t\alpha.\dot{\vec{u}}_{s+1}\right) + \Delta t(1-\alpha)K.\vec{u}_s + \Delta t\alpha.K.\vec{u}_{s+1} = \Delta t\left((1-\alpha)\vec{F}_s + \alpha.\vec{F}_{s+1}\right) \quad (15)$$

$$M\left(\vec{u}_{s+1} - \vec{u}_s\right) + \Delta t(1-\alpha)K.\vec{u}_s + \Delta t\alpha.K.\vec{u}_{s+1} = \Delta t\left((1-\alpha)\vec{F}_s + \alpha.\vec{F}_{s+1}\right) \quad (16)$$

We put unknowns $\vec{u}_{s+1}$ on the left side and knowns $\vec{u}_s$ on the other side of equation.

$$(M + \Delta t\alpha.K).\vec{u}_{s+1} = M.\vec{u}_s + \Delta t(\alpha-1)K.\vec{u}_s + \Delta t\left((1-\alpha)\vec{F}_s + \alpha.\vec{F}_{s+1}\right) \quad (17)$$

Finally we have got system of algebraic equations over the element.

$$H.\vec{u}_{s+1} = \vec{G}_s \quad (18)$$

For value α we can choose some possibilities:

$\alpha = 0$	explicit Euler method	it can be unstable if we choose wrong time step

$\alpha = 1$	implicit Euler method	stable method
$\alpha = \frac{1}{2}$	Frank-Nicolson method	stable method

Derivation of global finite element model

Further we give some indications how to proceed to derive global system of equations over whole domain.
We consider two adjacent elements *e* and *e+1*. Their assembling is possible if we follow two conditions: 1, continuity of primary variables in connecting node points, it means $u_n^e = u_1^{e+1}$ (For the mesh of linear elements we can write: $u_1^1 = u_1$, $u_2^1 = u_1^2 = u_2$, ... $u_2^{n=1} = u_1^n = u_n$), and 2, balance of secondary variables in connecting nodes, it means $Q_B^e = -Q_A^{e+1}$
If we satisfy these simple rules, the systems of equations over each element will be arranged to one system of global equations, in which the numbering of nodes will be also global.

INCLUSION AND DISCUSSION

The flux from the heat source in experiment seems to be constant, as we can consider from constant temperature differences between source and adjacent plexi-glass surface, during experiment. We were also watching the surface temperatures on cylinder shell, that were in far regions from the source, about few tenths degree lower than on axis. In close region the differences were in order of few degrees. It shoves on fact, that dissipation fluxes over cylinder shell are not negligible, so we have to take this information into account in future simulation and instead of Neumann condition we must simulate exact structure of the equipment. Otherwise, the simulation verifies the measured data, as we can see from comparison of the simulation plots (Plot1,…, Plot4) and table of experimental data (Tab.1). We did not plot the dependence of measured data, because of wanting distances between the probes. Thus, for better monitoring of temperature field closer to heat source we have to insert much more probes into this area.

SIMULATION RESULTS AND THEIR COMPARISON WITH EXPERIMENT

Tab.1: Temperatures were measured on the cylinder axis in various distances from the source: 0, 0.1, 0.2 a 0.3m, during time period 0-200min.

	Heat source	0	0,1	0,2	0,3
0	26,075	25,940	26,100	26,200	26,425
5	35,000	32,680	26,125	26,225	26,400
10	38,600	36,350	26,125	26,225	26,400
20	43,100	40,850	26,150	26,225	26,425
30	46,275	43,875	26,225	26,250	26,425
50	50,300	48,000	26,350	26,250	26,425
100	55,460	53,550	26,800	26,300	26,475
150	57,975	56,025	27,350	26,375	26,500
200	59,075	57,450	27,800	26,450	26,525

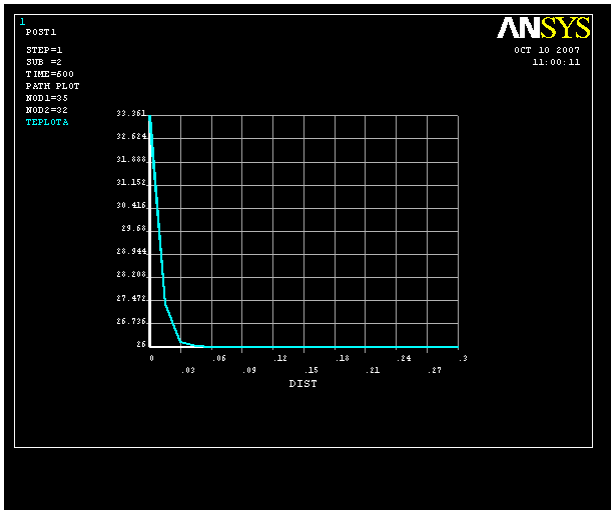

Plot1

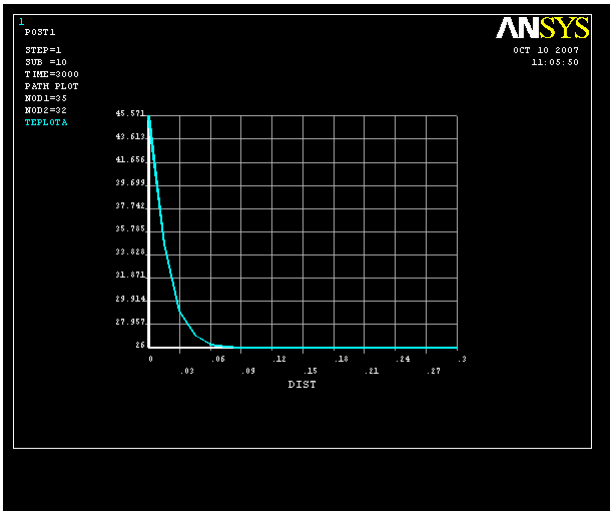

Plot2

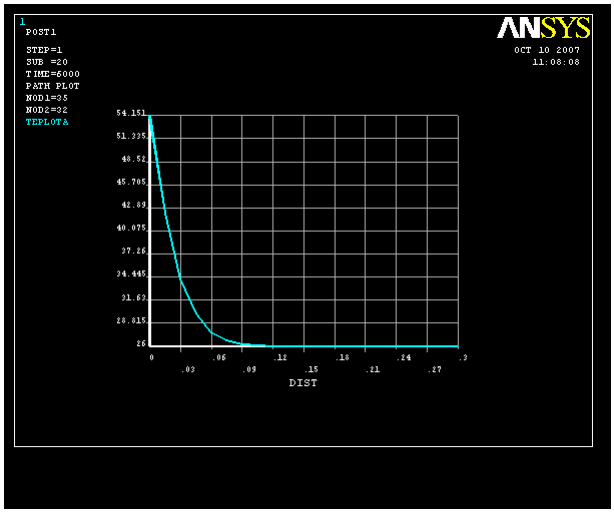

Plot3

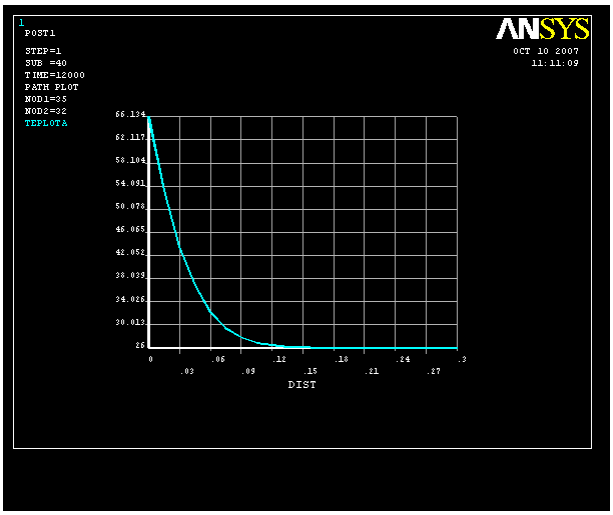

Plot4

ACKNOWLEDGEMENT

Financial support of the project VEGA 1/4204/07 is gratefully acknowledged.

REFERENCES

[1] J. N. Reddy: *An introduction to the finite element method*, Singapore, 2nd Edition, 1993

Teplotná deformácia - faktor štruktúrneho oslabenia horninového masívu

Vlčko Ján, Jezný Michal, Hvožďara* Milan, Durmeková Tatiana, Greif Vladimír

Kľúčové slová: skalný horninový masív, tepelný tok, termo-fyzikálne parametre, teplotno-mechanické procesy, svahové deformácie, Spišský hrad

Abstrakt

Povrchová časť skalných horninových masívov je ovplyvnená ako dennými, tak aj sezónnymi kolísaniami teplôt zapríčinených zmenami teploty ovzdušia, ochladzovaním vetrom a slnečným žiarením. Tieto cyklické kolísania sú čiastočne prenášané do vnútra horninových masívov v zmysle kondukcie, v súlade s Fourierovými zákonmi. Autori sa vo svojom príspevku zamerali na štúdium priebehu tepelného toku v horninovom masíve, ako aj na zistenie tých termofyzikálnych vlastností, ktoré z hľadiska teplotno-mechanického správania majú podstatný význam pri jeho rozvoľnení. Na základe výskumu bolo zistené, že povrchová vrstva do 80 cm je termicky najviac atakovaná. V nej sa generujú ***tepelne podmienené objemové zmeny*** a ***teplotné deformácie*** a snimi späté procesy dezintegrácie horninových masívov.

Úvod

Vývoj a priebeh mnohých geologických javov determinuje tepelná energia, ktorá v závislosti od slnečného žiarenia, od prenosu tepla na zemskom povrchu a jeho prieniku do horninového masívu je súčasťou tepelného režimu povrchu Zeme.

Skúmanie tepelných vlastností materiálov je vo všeobecnosti predmetom záujmu, predovšetkým fyziky, materiálového inžinierstva i viacerých technicky zameraných vedeckých disciplín. Menej výskumného priestoru, ktorý by bol zameraný na skúmanie vplyvu teploty na termo-mechanické správanie hornín, resp. horninových masívov venuje inžinierska geológia alebo geotechnika. Za kľúčové z tohto pohľadu považujeme poznatky o vplyve cyklických teplotných kolísaní (denných, sezónnych, ročných) a s týmto javom úzko spätý prenos (prienik) teploty do vnútra horninových masívov (skalných, resp. poloskalných

*Doc.RNDr. Milan Hvožďara, DrSc, Geofyzikálny ústav SAV Bratislava, Dubravská cesta 9, 845 07 Bratislava

Doc. RNDr. Vlčko, Ján, PhD; Mgr. Jezný Michal; RNDr. Durmeková Tatiana; PhD, Mgr. Greif Vladimír, PhD., Katedra inžinierskej geológie PRIF UK, 842 15 Bratislava, Mlynská dolina G

hornín), ako aj vznik teplotno-mechanických procesov, pri ktorých dochádza k teplotne podmieneným zmenám objemu hornín a vzniku trvalej (nevratnej) teplotnej deformácie. Rovnako nie je dostatočne objasnený ani vplyv trvalej teplotnej deformácie hornín na zmenu rovnováhy v svahoch tvorených skalnými horninovými masívmi.

To, že z pohľadu inžinierskej geológie a geotechniky je štúdium termofyzikálnych vlastností limitované je na jednej strane logicky odôvodniteľné i tým, že inžinierska geológia na rozdiel od geofyziky, príp. hydrogeológie nezisťuje v globálnej miere teplotné charakteristiky Zeme ako rezultáty endogénnych zdrojov tepla, resp. nezaoberá sa zisťovaním zdrojov hydrotermálnej energie a jej využitia, na strane druhej, zo strany inžinierskej geológie, príp. geotechniky sa pravdepodobne jedná o nedocenenie vplyvu teploty ako faktora s nie výrazným, v prírode pozorovateľným, deštrukčným prejavom na horninové prostredie. Nezanedbateľnú úlohu zohráva i časová a materiálová náročnosť i nákladnosť zisťovania termofyzikálnych vlastností hornín tak in situ , ako aj v laboratóriu.

Napriek vyššie uvedeným faktom aj v oblasti inžinierskej geológie, príp. geotechniky sa urobil v tomto smere istý pokrok. Vďaka laboratórnemu vybaveniu i terénnym pozorovaniam sme sa našom pracovisku zamerali na sledovanie priebehu tepelného toku v horninovom masíve i na zisťovanie jeho vplyvu na kinematiku creepových pohybov travertínového telesa Spišského hradu. S posledne menovaným úzko súvisí i optimalizácia výsledkov monitorovania svahových pohybov, keď vo väčšine prípadov síce výrobca udáva teplotné korekcie, tie sa však týkajú vlastného monitorovacieho zariadenia, nie však reálneho vplyvu teploty na teplotno-mechanické správanie sa horninového masívu a s ňou súvisiacou kinematikou monitorovaného procesu (pohybu).

Teplota – permanentný faktor vzniku svahových pohybov

Z literatúry je známy celý rad prác, ktoré synteticky hodnotia a analyzujú podmienky, príčiny a faktory, ktoré spôsobujú svahový pohyb */1 až 8/* a mnohí iní/. Na základe publikovaných poznatkov, ako i na základe pracovnej skupiny UNESCO WP/WLI a komisie IUGS WG/L */9,10/* možno v súčasnosti konštatovať, že na nestabilitu svahu, resp. na nerovnováhu vo svahu vplývajú faktory (tab. 1):

- ***permanentne*** pôsobiace, ktorých vplyv je nepatrný, zhoršujú na jednej strane podmienky rovnováhy, avšak vznik alebo aktivizáciu svahového pohybu (napr. zmena obsahu vody vo svahu, vplyvy teploty a pod.) spravidla nevyvolávajú, iba ho pripravujú (podľa niektorých autorov sa nazývajú prípravné alebo ***preparatory*** faktory). Pôsobia areálne a ich

účinkom sa nedá zabrániť (obr. 1 A); spôsobujú ***vratné zmeny,*** ktoré spočívajú v striedavom znižovaní a zvyšovaní stupňa stability svahu. Tento stav permanentného hľadania rovnováhy vo svahu vyvolávajú faktory s periodickými účinkami, pričom ***periodický faktor*** nesmie dosiahnuť ***extrémnu hodnotu, pretože v takomto prípade je už považovaný za faktor s epizodickým účinkom***

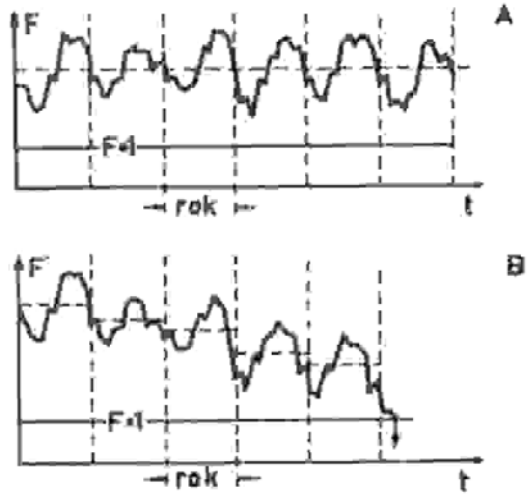

Obr.1 Vplyv permanentne pôsobiacich faktorov na stabilitu svahu /2/
A –svah v stave dynamickej rovnováhy so sezónnym kolísaním
B – postupné klesanie stability svahu až do jeho porušenia
F – stupeň stability
t - čas

- ***epizodické*** (niekedy poňaté ako neperiodické alebo spúšťacie, ***triggers)*** napr. zemetrasenie, extrémne zrážky a i. predstavujú jednorazové lokálne pôsobiace ***nevratné*** zmeny v procese vývoja svahového javu, vedú k vyvolaniu svahového pohybu; čoraz častejšie sú ovplyvňované nielen prírodnými (geologickými) faktormi ale i človekom (obr. 1 B).

Rozdiely medzi ***epizodickými*** (spúšťacími) faktormi vzniku svahových pohybov a ***permanentnými*** (prípravnými) spočíva v tom, že zatiaľ čo prvé pôsobia bezprostredne a sú impulzom vzniku svahového javu, u faktorov prípravných zohráva podstatnú úlohu ich dlhodobý kumulatívny účinok.

Tab. 1. Pôsobenie faktorov na podmienky stability podľa Pašek et al. 1995 /2/

Geodynamické faktory		**Zmeny**
Permanentné		
Erózia, akumulácia, sufózia, tektonika		- geometria svahu, napätie vo svahu
zvetrávacie procesy, pôsobenie mrazu, slnečný osvit		- mechanického stavu i chemického zloženia horninového prostredia
Epizodické		
Prírodné	*antropogénne*	
Abnormálne zrážky, odmäk, vlnobitie	zásahy do vodného režimu (úpravy tokov, vzdutie vody)	- výšky sklonu a povrchu svahov - odtokových pomerov, zvetrávania hornín
Prítoky vody do svahu (prameň), kolísanie teploty (mráz, odmäk, evaporácia)	kolísanie vody v nádržiach, kolísanie hladiny podzemnej vody spôsobenej čerpaním, zanedbané nádrže	- vlhkosti, hladiny podzemnej vody, spádu podzemnej vody
seizmické otrasy, zemetrasenia	umelé otrasy (odstrely, vibrácie, stroje, doprava)	- mechanického stavu hornín
priťaženie zrážkovou vodou a vodou z topiacich sa snehov	priťaženie násypmi, návažkami, haldami	- vonkajšieho zaťaženia, napätia vo svahu
	poľnohospodárske, lesnícke, stavebné, ťažobné práce	- geometrie svahu, odtokových pomerov

Z uvedeného prehľadu sa dá jednoznačne usúdiť, že teplota, resp. cyklické striedanie teploty patrí medzi faktory permanentne pôsobiace na svah, ktoré podľa doterajších zistení spôsobujú **zvratné zmeny.** S týmto názorom sa pravdepodobne ***nedá*** v plnom rozsahu súhlasiť. Bližšie poznanie termofyzikálnych vlastností hornín, ako aj termo-mechanické správanie hornín pri tepelnej záťaži poukazujú na trochu odlišné okolnosti. Problematika teploty a jej vplyvu na podmienky medznej rovnováhy vo svahu nebola prioritne nikdy predmetom záujmu geológov, aj napriek tomu však, viacerí autori v minulosti sa týmto problémom zaoberali. V tridsiatych rokoch minulého storočia Záruba tlmočil prvé názory, že povrchové teplotné zmeny v horninovom masíve spôsobené zmenami teploty vzduchu, môžu aktivizovať svahové pohyby v skalných horninách. Na tento jav, ako uvádza Záruba /11/, upozornil už Davidson v r.1888, ktorý zistil, že pieskovcová doska dlhá približne 1 m uložená na podklade so sklonom 17° sa v dôsledku kolísania teploty posúva približne 1 cm za 1 rok (0,0274 mm za 1 deň). Rovnako Redlich a Terzaghi (1929 in Záruba) upozornili na uvoľňovanie a posúvanie horninových blokov v dôsledku objemových zmien vyvolaných kolísaním teploty a na základe tohto poznatku vysvetľovali a opísali zosúvanie skalných sutí deponovaných na mierne sklonených svahoch a nakoniec Záruba /11/ pri štúdiu stability

svahov pri Štěchoviciach a Vranom usúdil, že príčinou aktivizácie svahového pohybu v ílovitých bridliciach algonkického veku situovaných v záreze cesty sú s najväčšou pravdepodobnosťou vplyvy kolísania teploty. Možno konštatovať, že Záruba sa ako prvý snažil svahové pohyby na základe dobrých poznatkov o termofyzikálnych vlastnostiach hornín nielen osvetliť, ale spomínaný jav aj kvantifikovať. Po zverejnení týchto poznatkov nastalo pomerne dlhé obdobie, keď vplyv teploty na vznik svahových pohybov v odbornej literatúre nebol kriticky analyzovaný. Až v poslednej dekáde sa opätovne k tejto problematike vrátili viacerí autori. Napr. Vargas /12/, ktorý študoval vznik skalných rútení v oblasti Rio de Janeira (Brazília) v období bez výraznejšieho úhrnu zrážok, počas tzv. suchej zimy, vyslovil názor, že k vzniku spomínaného javu pravdepodobne došlo v dôsledku striedania povrchovej teploty, ktoré spôsobilo v hornine vznik teplotných napätí (thermal stresses) a zničenie skalných premostení (rock-bridges) v štruktúre horniny, rozvoľnenie horniny a stratu stability skalných blokov. Podobne uvažoval i Gunzburger /6 a 7/ pri štúdiu skalného zrútenia v Rochers de Valabres (región južných francúzskych Álp). Spomínaný autor spolu so svojim kolektívom na podporu svojej idey vytvoril numerický model, ktorým potvrdil svoju hypotézu, že tepelne vzniknuté deformácie mohli byť dostatočnou príčinou zmeny krípového pohybu v pohyb translačný a z hľadiska kinematiky za pohyb rútivý. Stewart, Moore /13/ a Watson /14/ študovali veľký aktívny zosuv v oblasti priehradnej nádrže v Checkerboard Creek v Britskej Columbii (Kanada). Napriek dlhodobému komplexnému monitoringu tohto svahu (extenzometre, inklinometre, piezometre teplotné snímače a pod.) autori predpokladajú, že periodické pohyby sú z veľkej časti podmienené teplotnými zmenami, pričom ako uvádzajú, teplotné zmeny boli pozorované až do hĺbky 10 m.

V súčasnosti je možné konštatovať, že väčšina autorov zaoberajúcich sa stabilitou svahov si v plnom rozsahu uvedomuje, že teplotno-mechanické procesy reálne ovplyvňujú stabilitné správanie sa hornín vo svahu, na strane druhej, tým, že nie je naporúdzi ich kvantifikácia (napr. rýchlosť a hĺbkový dosah tepelného toku, trvalá teplotná deformácia a pod.) pri bežných podmienkach riešenia stability horninového masívu logicky termofyzikálne parametre nie sú súčasťou výpočtových riešení /15/.

Termofyzikálne vlastnosti hornín a ich vplyv na prenos tepla

Základnými údajmi potrebnými na posúdenie vplyvu teploty na mechanické správanie horninového masívu je poznanie prirodzeného teplotného poľa a termofyzikálnych parametrov hornín, ku ktorým patrí *koeficient tepelnej i teplotnej vodivosti, merné teplo*

a *koeficient dĺžkovej teplotnej rozťažnosti*. Takéto poznatky sú nevyhnutným podkladom pre štúdium priestorového i časového rozloženia teplotného poľa v horninovom masíve.

V izotropnom homogénnom prostredí je vedenie tepla určované jedinou konštantou – **koeficientom tepelnej vodivosti** (λ). Vo všeobecnosti je táto konštanta funkciou teploty, tlaku, pórovitosti, nasýtenia pórov vodou a minerálneho zloženia. Medzi najlepšie vodiče tepla z najrozšírenejších minerálov patrí kremeň (λ = *8,37* $W.m^{-1}.K^{-1}$), z hornín kvarcit, dolomit, anhydrit a kamenná soľ (λ = *4,19* až *6,28* $W.m^{-1}.K^{-1}$). Najhoršími vodičmi tepla medzi minerálmi sú sľudy (λ = *0,5* až *2,0* $W.m^{-1}.K^{-1}$), resp. horniny sedimentárneho pôvodu - ílovce (λ = *0,42* až *0,84* $W.m^{-1}.K^{-1}$). Väčšina hornín tvoriacich základnú hmotu zemskej kôry, má tepelnú vodivosť v rozmedzí *2,09* až *4,19* $W.m^{-1}.K^{-1}$ a väčšinou nevykazujú zreteľnú anizotropiu okrem hornín, na ktorých je foliácia jednoznačná - fylity, ruly, svory /16/.

Koeficient teplotnej vodivosti hornín (χ) často sa nazýva aj „súčiniteľ tepelnej vodivosti“, v anglickej literatúre „thermal diffusivity“ charakterizuje rýchlosť zmeny teploty pri pohltení alebo vydaní tepla. Táto veličina môže byť určovaná buď ako stredná hodnota, alebo ako veličina závisiaca na smere tepelného toku, resp. na smere textúrnych alebo štruktúrnych znakov (pórovitosť, kliváž, orientácia, hustota a výplň puklín a pod.) hornín.
Teplotná vodivosť priamo súvisí s tepelnou vodivosťou. Koeficient teplotnej vodivosti . závisí na koeficiente tepelnej vodivosti λ, mernej tepelnej kapacite *c* a mernej hmotnosti ρ:

$$\chi = \frac{\lambda}{\rho \, .c} \qquad [m^{-2}.s^{-1}] \qquad (1)$$

Merné teplo (*c*) je definované ako tepelná kapacita hmotnej jednotky, pričom tepelná kapacita značí množstvo tepla potrebné na ohriatie látky o 1 °C.

Relatívna dĺžková teplotná rozťažnosť - dilatancia (ε) vyjadruje relatívnu dĺžkovú zmenu vzorky **v uvažovanom teplotnom intervale**. Je definovaná rovnicou:

$$\varepsilon = \Delta l / l_0 \qquad [mm.m^{-1}] \qquad (2)$$

kde Δl je zmena dĺžky skúmanej vzorky,
l_0 – pôvodná dĺžka skúmanej vzorky.

Teplotná rozťažnosť (α) charakterizuje koeficient dĺžkovej teplotnej rozťažnosti α, ktorý je definovaný rovnicou

$$\alpha = \frac{1}{l_0}\frac{dl}{dt} \qquad (3)$$

kde l_0 je počiatočná dĺžka vzorky,

dl je zmena dĺžky spôsobená teplotnou zmenou dt.

Teplotná zmena dt je daná teplotným intervalom $\Delta t = t_2 - t_1$.

Sledovanie predĺženia vzorky v závislosti od teploty poskytuje dôležité informácie, ktoré sa dajú využiť vo výskume ako aj v praxi.

Spôsoby zisťovania priebehu teplotného toku v horninovom masíve

Z fyziky a z dennej skúsenosti je známe, že teplo sa šíri z miesta s vyššou teplotou na miesto s teplotou nižšou. V zásade sa rozlišujú tri základné spôsoby prenosu tepla, a to *vedením* (kondukciou), *prúdením* (konvekciou) a *žiarením* (radiáciou).

Prenos tepla vedením je daný tepelným pohybom na základe vzájomného energetického pôsobenia molekúl, atómov, iónov a elektrónov. Teplo sa prenáša vedením nielen v tuhých, ale i v kvapalných a plynných látkach. U pevných látok, kam patria aj horniny je jediným mechanizmom prenosu tepla. Množstvo tepelnej energie, ktoré sa prenesie cez jednotkový prierez telesa za jednotku času sa nazýva *tepelný tok* a označuje sa vektorom Q (presný názov je hustota tepelného toku).

Pokusy ukázali, že tepelný tok je priamo úmerný teplotnému gradientu (t.j. spádu teploty) a smeruje z miesta s vyššou teplotou na miesto s teplotou nižšou. Matematicky to vyjadruje *Fourierov zákon vedenia tepla*:

$$Q = -\lambda \, grad T \qquad (4)$$

kde λ je koeficient tepelnej vodivosti. Tepelný tok má rozmer $W.m^{-2}$, teplotu uvádzame v stupňoch Celzia alebo Kelvina (K). Koeficient tepelnej vodivosti λ má rozmer $W.m^{-1}.K^{-1}$ a udáva schopnosť materiálu viesť teplo. Tepelne izolujúce látky majú λ nízke, látky, ktoré dobre vedú teplo, tepelné vodiče, majú λ vysoké. Patria k nim napríklad kovy. Z Fourierovho zákona vyplýva, že tepelný tok je vektorová veličina, t. j. má veľkosť i smer.

Priebeh tepelného toku v horninovom masíve je možné stanoviť dvomi spôsobmi: priamymi meraniami in situ a analytickým výpočtom. Oba spôsoby sa vyznačujú kauzalitou a je potrebné ich vykonávať najmä preto, že výsledky in situ meraní sčasti poskytujú vstupné údaje pre analytický výpočet, na strane druhej, výpočet platí pre ideálne teleso a takto získané výsledky poskytujú akýsi etalon priebehu tepelného toku. Vzájomným porovnaním môžeme zistiť, či tepelný tok v horninovom masíve nameraný in situ má reálny priebeh alebo je zaťažený chybami (chyby v meraniach, heterogenita horninového masívu i materiálu).

Merania tepelného toku in situ sme začali realizovať v roku 2003, keď v priestore južnej časti hradu, v tzv. Perúnovej skale bolo osadených päť teplotných snímačov (obr. 2), pričom štyri sú umiestnené v rozdielnych hĺbkach travertínového masívu (6,5 cm, 25 cm, 38 cm a 80 cm) a piaty teplotný snímač zachytáva vonkajšiu teplotu. Teploty sa v pravidelných časových sekvenciách (každé štyri hodiny) zaznamenávajú a dáta sa ukladajú na pamäťové médium. Intervaly snímania teploty sú navrhnuté tak, aby boli zaznamenané najmä teplotné maximá a minimá, ktoré sú dôležité pre určenie teplotných amplitúd v skúmaných hĺbkových úrovniach skalného masívu. Z takto získaných hodnôt je možné určiť priebeh tepelného toku v čase a priestore, ako aj stanoviť fázové posuny periodických zmien teploty.

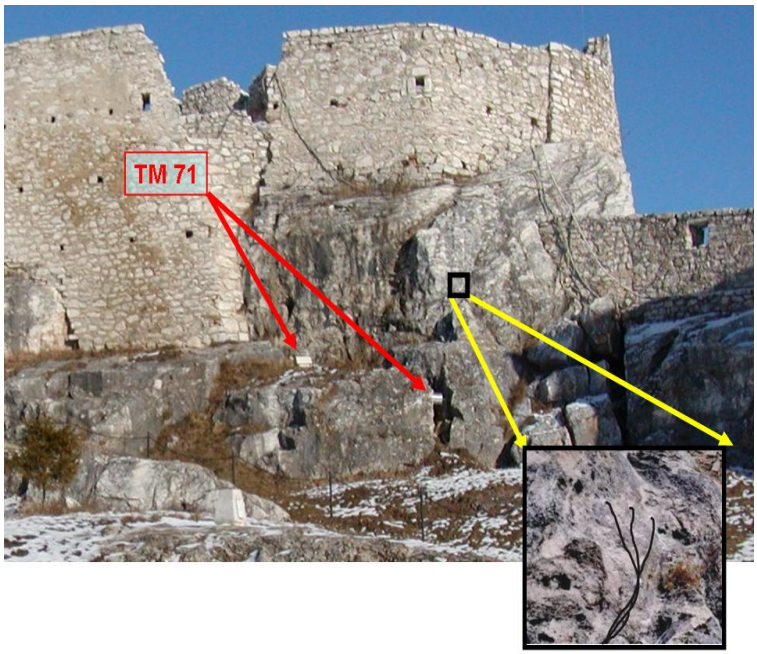

Obr.2 Perúnova skala s detailným pohľadom na umiestnenie teplotných snímačov a umiestnením opticko-mechanických meradiel TM 71

Analytický výpočet priebehu teplotného toku v horninovom masíve

Pri zjednodušenom analytickom riešení horninový masív predstavuje homogénny polopriestor s teplotnou vodivosťou χ, v ktorom nie sú zdroje tepla (uvažuje sa iba s exogénnym teplom) a rozloženie teploty potom závisí iba od hĺbky pod povrchom z a času t, a platí:

$$T(z,t) = A\,e^{-z/\delta}\cos(\omega t - z/\delta) \qquad (5)$$

ω - uhlová rýchlosť, A-amplitúda povrchovej teploty, t-čas a z-hĺbka.

kde δ je *prieniková hĺbka* vyjadrená vzťahom $\delta = \sqrt{2\chi/\omega} = \sqrt{\tau\chi/\pi}$.

Toto riešenie ukazuje, že amplitúda teplotných zmien je exponenciálne tlmená s rastúcou hĺbkou. V hĺbke $z = \delta$ je amplitúda teplotných zmien $A.e^{-1}$ približne 1/3 z amplitúdy na povrchu a súčasne dochádza aj k fázovému oneskorovaniu teplotných vĺn s hĺbkou. Kým na povrchu $z = 0$ je maximum teploty v čase $t = 0$ (na poludnie), v hĺbke z je až v čase $t_z = z/(\omega\delta) = z/\sqrt{2\chi\omega} = \sqrt[z]{\tau/4\pi\chi}$ /17/.

Najjednoduchším spôsobom zisťovania priebehu teplotných amplitúd v rozdielnych hĺbkových úrovniach (z_0 - povrch skalného masívu; z_1, z_2, z_3, z_4, z_5 – hĺbky zodpovedajúce hĺbkam v travertínovom masíve) je modelové riešenie reprezentované ideálnym telesom, ktorého povrch je vystavený vonkajším teplotným zmenám.

Pri modelovaní priebehu tepelného toku v horninovom masíve analytickým výpočtom je potrebné poznať parametre *koeficientov teplotnej* (χ) *tepelnej* (λ) *vodivosti, objemovú hmotnosť* (ρ) a *merné teplo (c).*

Pre zistenie teplotnej vodivosti *a* sme použili výpočet z in situ nameraných teplotných amplitúd, ktorý je založený na poznatku, že smerom do hĺbky horninového masívu sa teplotné amplitúdy znižujú. Potom platí nasledovný vzťah:

$$\delta = \left(Z_j - Z_i\right)/\ln\left(A_j / A_i\right), \qquad (6)$$

kde δ je hĺbka prieniku teplotných zmien (*m*),

Z_j a Z_i sú hĺbky (*m*), ktorým prislúchajú denné teplotné amplitúdy A_j a A_i (°*C*).

Pre výpočet teplotnej vodivosti χ ($m^2.s^{-1}$) platí nasledovný vzťah:

$$\chi = \left(\delta^2\pi\right)/T \ , \qquad (7)$$

kde T je perióda (s^{-1}).

Vstupné hodnoty teplotnej vodivosti a objemovej hmotnosti zodpovedajú matematicky vypočítaným, resp. laboratórne získaným hodnotám, merné teplo použité pri výpočte zodpovedá tabuľkovému údaju pre travertín (tab. 2). Pri modelovaní denných teplotných zmien sme počítali s periódou 24 hodín ($T = 24$) a amplitúdu povrchovej teploty (A) sme stanovili na 10 °C, čomu zodpovedá rozpätie teplôt 20 °C (obr. 3).

Tab. 2 Teplotné parametre použité pre výpočet tepelného toku

Parameter	Symbol	Rozmer
Teplota	T (*z, t*)	(K^{-1})
Amplitúda povrchovej teploty	*A*	(K^{-1})
Perióda teplotnej záťaže	τ	(s^{-1})
Teplotná vodivosť	χ	($m^2.s^{-1}$)
Merné teplo	*c*	$J.kg^{-1}.K^{-1}$
Objemová hmotnosť travertínu	ρ	$g.cm^{-3}$

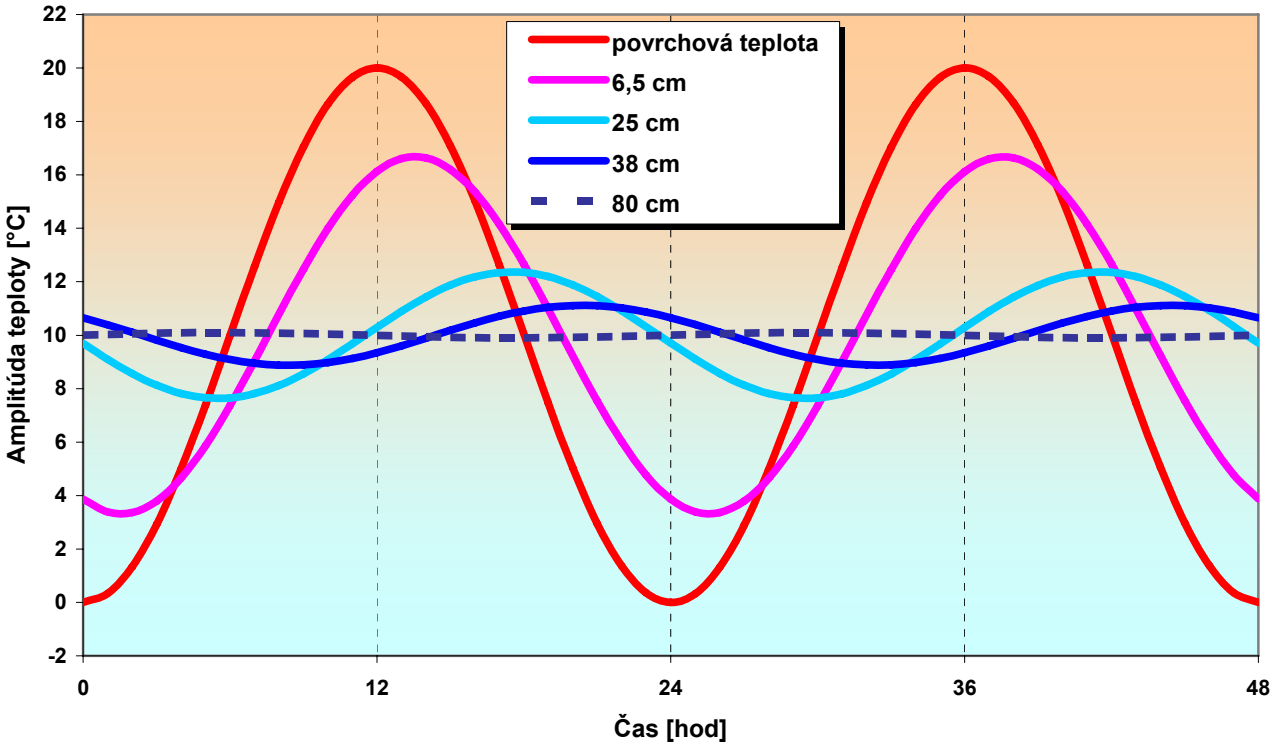

Obr.3 Priebeh teplôt v sledovaných hĺbkach skalného masívu stanovený analytickým výpočtom

Na základe výpočtového stanovenia (obr. 4) priebehu teplôt v sledovaných hĺbkach skalného masívu platí, že v čase 0 je na povrchu teplota 0 °C, v hĺbke 6,5 cm sú 4 °C, v 16 cm je 8 °C , v 25 cm je 10 °C a v 38 cm 10,6 °C . Ako ďalej vidieť, amplitúda **denných** teplotných variácií v hĺbke 6,5 cm je 6,4 °C, v 25 cm je 2,3 °C a v 38 cm je už len 1,1 °C . V hĺbke 80 cm sú teplotné zmeny prakticky nulové, čiara priebehu teplotnej vlny má charakter temer priamky (amplitúda je 0, 09 °C). Z toho vyplýva, že od **hĺbky 80 cm je v skalnom travertínovom masíve približne rovnaká teplota okolo 10 °C** (plus, mínus 0, 1°C).

Porovnanie výsledkov z meraní in situ a z analytických výpočtov

Analyticky vypočítané hodnoty priebehu denných, týždenných a mesačných teplotných zmien sa približne zhodujú s nameranými teplotami v skalnom masíve. Túto zhodnosť je možné vidieť v grafoch (obr. 4, 5, 6), v ktorých sme porovnali hodnoty teplotných amplitúd získaných z analytických výpočtov s hodnotami nameranými v travertínovom masíve podložia Spišského hradu.

Zo získaných výsledkov vyplýva, že dosah povrchových ***denných*** teplotných zmien sa prejavuje približne do hĺbky 0, 80 m travertínového masívu (obr. 4). Amplitúdy denných teplotných zmien sa v sledovaných hĺbkových úrovniach sa prakticky zhodujú, iba v hĺbke 38 cm je menší rozdiel, ktorý zodpovedá približne 1 °C.

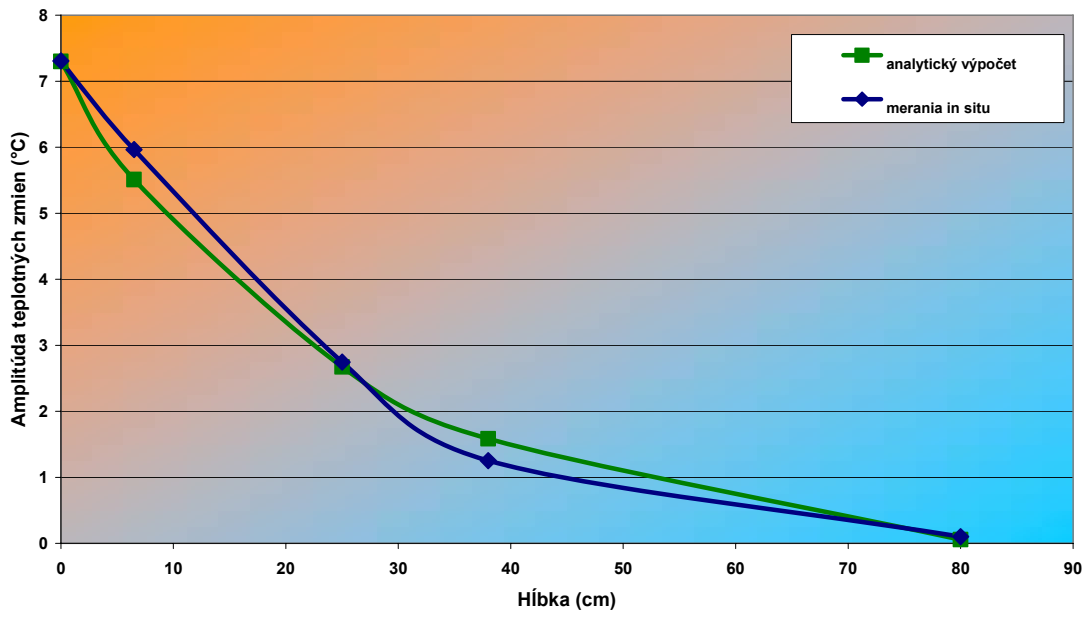

Obr.4 Porovnanie **denných** teplotných zmien získaných z analytických výpočtov a z hodnôt nameraných v skalnom masíve

Pri ***týždennej*** perióde sa amplitúdy teplotných zmien prejavujú už do hĺbky cca 2 m Na tomto grafe (obr. 5) je možné pozorovať úzku zhodu medzi meraniami in situ a hodnotami teplotných zmien stanovených výpočtom. Podobne ako v prípade denných amplitúd teplotných zmien aj tu sa v hĺbke 38 cm prejavil menší rozdiel zodpovedajúci približne 1, 1°C. V hĺbke 80 cm bola opäť zistená približná zhoda v nameraných i vypočítaných hodnotách.

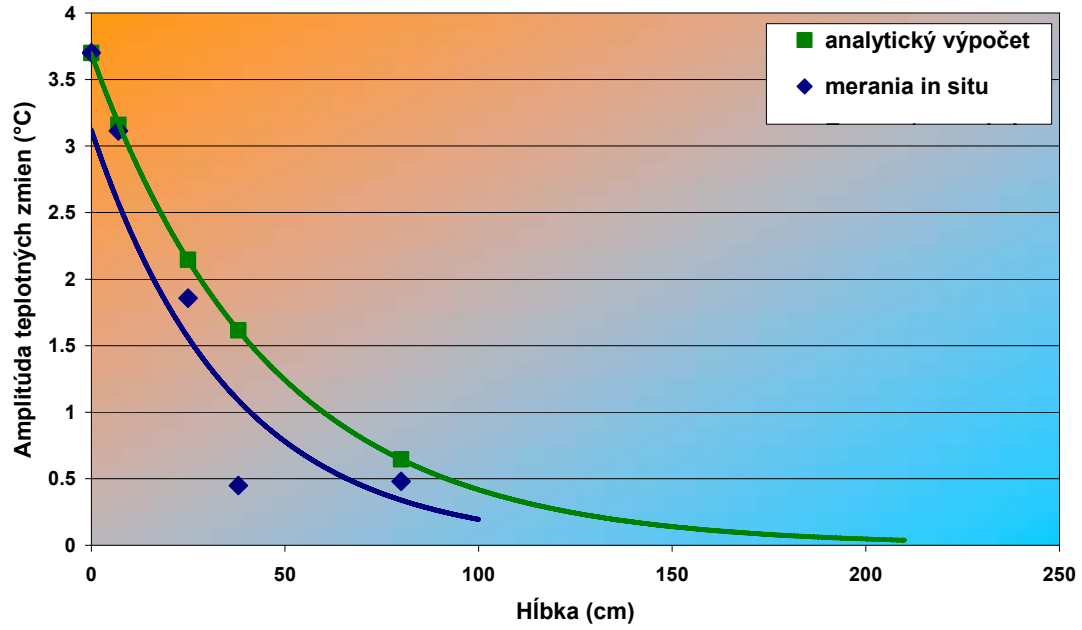

Obr.5 Porovnanie **týždenných** teplotných amplitúd získaných z analytických výpočtov a hodnôt nameraných v skalnom masíve

Pri ***mesačnej*** perióde sa amplitúdy teplotných zmien prejavujú až do hĺbky cca 3 m. V grafe na obr. 6 sa jednoznačne preukázala zhoda medzi analytickým výpočtom a in situ meraniami.

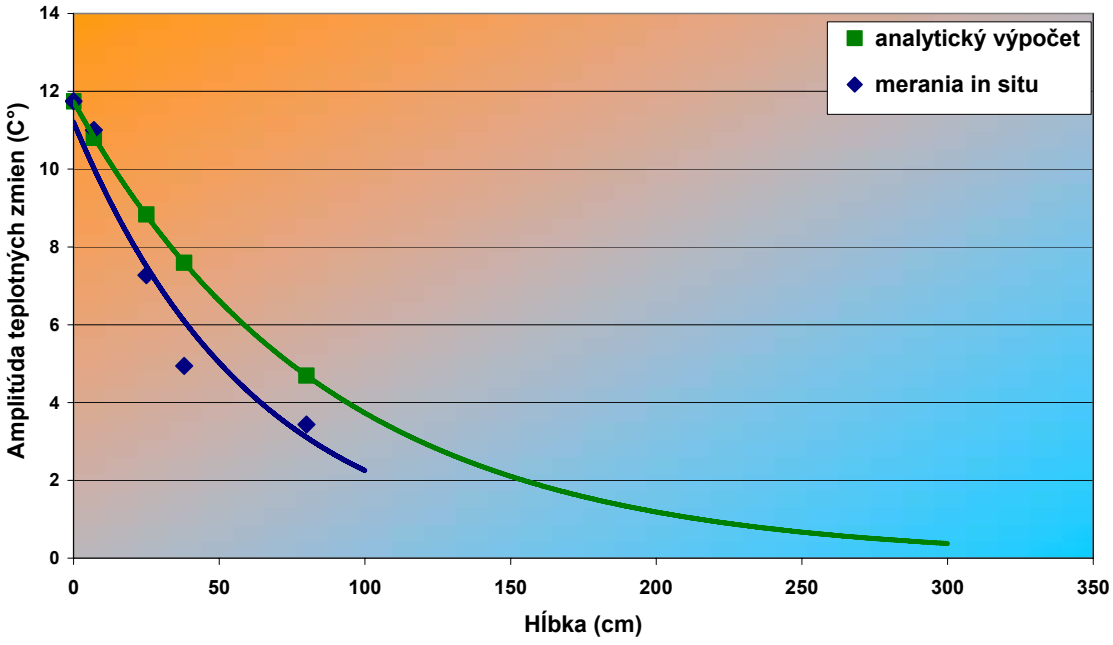

Obr.6 Porovnanie **mesačných** teplotných amplitúd získaných z analytických výpočtov a hodnôt nameraných v skalnom masíve

Interpretáciou výsledkov získaných tak z terénnych meraní, ako i z analytických výpočtov na základe rovnice vedenia tepla *(4)* vyplýva, že účinky povrchových teplotných zmien sa pri perióde jedného dňa prejavujú maximálne do hĺbky 0, 8 metra. Týždenné periódy sa prejavujú až do hĺbky približne 2,5 násobku dennej periódy, tzn. do hĺbky približne 2, 0 m a mesačné periódy sa prejavujú až do hĺbky približne 3, 5 násobku dennej periódy, tzn. do hĺbky približne 3, 0 m. Naopak, najväčšie teplotné zmeny boli zistené približne do hĺbky 0, 8 m pod povrchom, keď zistené amplitúdy teplotných zmien zodpovedali asi 75 až 80 % vonkajšej teplotnej amplitúdy. Z tohto pohľadu je možné považovať práve túto povrchovú vrstvu za termicky najviac atakovanú, následkom čoho sa v nej generujú ***tepelne podmienené objemové zmeny*** a ***teplotné deformácie.***

Teplota ako faktor štruktúrneho oslabenia hornín

Výsledkom teplotno-mechanického procesu je teplotná deformácia horniny. Kolísanie teploty vyvoláva vo vnútri skalných horninových masívov teplotné napätia (thermal stresses), ktoré sú vyvolané rozdielnou teplotnou rozťažnosťou (thermal expansion) minerálnych zŕn. Na priebeh a veľkosť teplotnej rozťažnosti vplýva najmä minerálne zloženie horniny a kryštalografické orientácie jednotlivých minerálnych zŕn /17 a 18/, pričom nemalú úlohu zohráva aj výskyt rôznych mikrotrhlín a veľkosť a distribúcia pórov /20 a 21/.Glamheden a Lindblom /22/ uvádzajú, že teplotno-mechanické procesy spôsobujú:

a) zhoršenie fyzikálno-mechanických vlastností hornín
b) vznik nových mikrotrhlín
c) otváranie existujúcich trhlín a puklín

a teda vedú k celkovému oslabeniu a degradácii horninového masívu.

Zisťovanie ***teplotnej rozťažnosti*** i ***teplotnej deformácie*** hornín nie je štandardnou skúškou laboratórií geologických pracovísk, a preto bolo pre tento účel potrebné vyvinúť špeciálny prístroj – termodilatometer, ktorý bol skonštruovaný na základe ideového návrhu jedného z autorov príspevku vo firme Applied Precision z Bratislavy. Prístrojom sa dajú testovať vzorky dĺžky 5 cm (priemer do 3,5 cm) v teplotnom intervale od –20 °C do +90 °C, s presnosťou merania teploty ± 0,5°C a rozlíšením 0,001 mm (obr. 7).

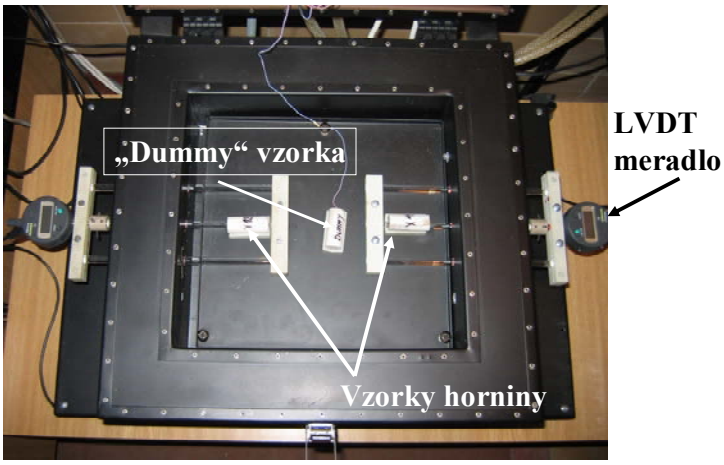

Obr. 7 Dilatometer VLAP 02.V blízkosti meraných vzoriek je uložená indentická (rovnaký petrografický typ) vzorka (tzv. dummy vzorka), slúžiaca na meranie teploty v jej jadre. Na túto teplotu je regulovaná teplota termostatu.

Na sledovanie teplotných zmien skúšobných vzoriek travertínu bol zvolený rozsah podobný priebehu kolísania teplôt v ročnom klimatickom cykle na území lokality Spišského hradu.

- Letný cyklus prebiehal v teplotnom intervale od +20°C do +55°C, čo predstavuje aproximované hodnoty teplôt v letnom období (obr. 8)
- Zimný cyklus prebiehal v teplotnom intervale od –5°C do –20°C, čo predstavuje aproximované hodnoty teplôt v zimnom období.
- Jarný / jesenný cyklus prebiehal v teplotnom intervale od + 20°C do –5°C, zohľadňuje aproximované teplotné výkyvy vypĺňajúce teplotné rozpätie medzi letom a zimou.

Na obr. 8 je záznam z letného cyklu, ktorým sme zistili relatívnu dĺžkovú zmenu vzorky $\varepsilon = 438.10^{-6}$ a trvalú teplotnú deformáciu L_r (pre skúmanú vzorku travertínu na obr. 8 $L_r = 5.10^{-6}$ m).

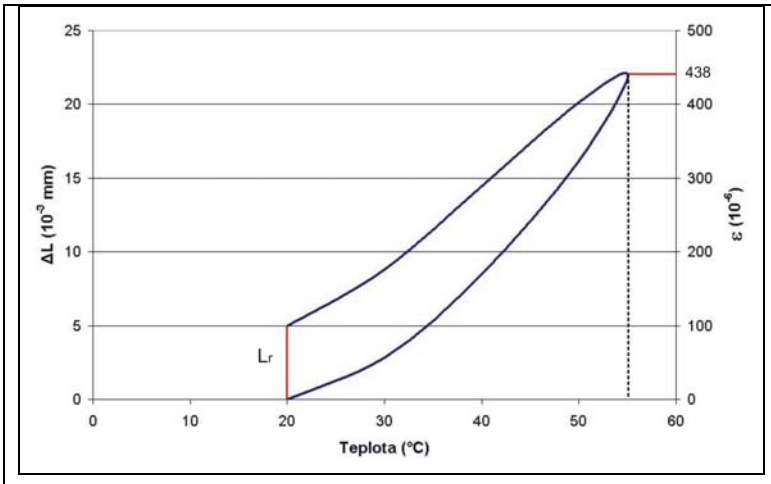

Obr. 8 Grafický záznam skúšky horniny pri teplotnej záťaži 60 °C

Na základe hodnoty ε je potom možné stanoviť dĺžkovú teplotnú rozťažnosť vzorky travertínu (α) podľa vzorca:

$$\alpha = \varepsilon / \Delta T, \qquad (8)$$

kde ΔT predstavuje interval teplôt, v ktorom sa skúmaná vzorka skúšala (20 až 55 °C). Pre skúmanú vzorku travertínu je $\boldsymbol{\alpha = 12{,}514.10^{-6}\ °C^{-1}}$.

Experimentálne získané údaje o teplotnej deformácii (priebehu tepelného toku a veľkosti teplotných deformácii) horniny (L_r) sčasti dopĺňajú predstavy Zárubu /11/, ktorý na ideálne orientovanom horninovom bloku, resp. sústave blokov uklonených pod uhlom φ dokumentoval jeho posun. Pôvodný objem bloku označený čiernou čiarou sa po zohriatí zväčši (červená čiara). Ak sú rozmery bloku relatívne malé (na základe našich výpočtov a experimentálne overených denných meraní asi hrúbky 0, 80 m) dôjde pravdepodobne k prestupu tepla v celom jeho objeme a objemové zmeny sa prejavia po celom jeho obvode. Pri väčších objemoch sa pravdepodobne preukážu len na povrchu skalného bloku (??). Ochladnutím (modrá čiara) sa horninový blok nedostane do svojej pôvodnej polohy, pretože zmenší svoj objem symetricky k ťažisku, čiže veľkosť posunu je rovná veľkosti objemovej zmeny. Termomechanické správanie horninové bloku podľa predstáv Zárubu je vo všeobecnosti akceptovateľné, až na jeden fakt, a tým je trvalá teplotná deformácia horniny, ktorá sa prejaví ak hornina je vystavená teplotnej záťaži. Keďže sa jedná rádove o hodnoty v µm, je táto pomerne obtiažne merateľná hodnota vzhľadom k uvažovanému pohybu (posunu) temer zanedbateľná.

V závislosti od hmotnosti (objemu) a sklonu a drsnosti diskontinuity bude závisieť rýchlosť posunu (kríp, zosúvanie až rútenie). Zmena ťažiska a posuny vyvolané objemovými

zmenami hornín sú tým väčšie, čím je väčší koeficient teplotnej rozťažnosti α, čím je väčší rozdiel povrchových teplôt (teplotný rozsah), čím je väčší uhol sklonu a čím je menší koeficient trenia medzi skalnými blokmi (obr. 9).

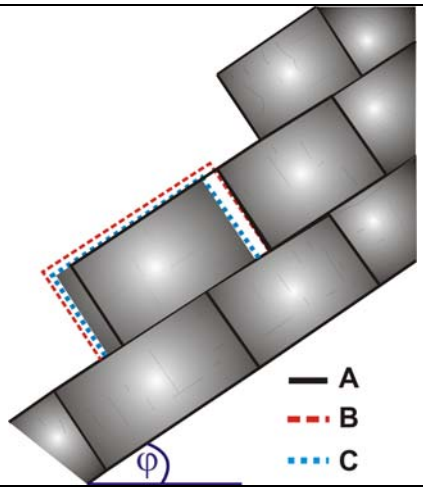

Obr. 9 Účinok teploty na stabilitu skalných stien podľa Zárubu /11/
A – pôvodný stav, B – stav po zahriatí, C – stav po opätovnom ochladení, φ – sklon svahu

Monitorovanie svahových pohybov

Monitorovanie svahových pohybov na Spišskom hrade sa započalo v roku 1980, keď boli inštalované tri meradlá typu TM – 71. Neskôr v roku 1992 pribudli ďalšie, avšak v súčasnosti sú funkčné len štyri prístroje typu TM-71, tri stanoviská (SM-1, SM-2 a SM-3), kde sa realizujú merania prenosnými meradlami SOMET (obr. 10).

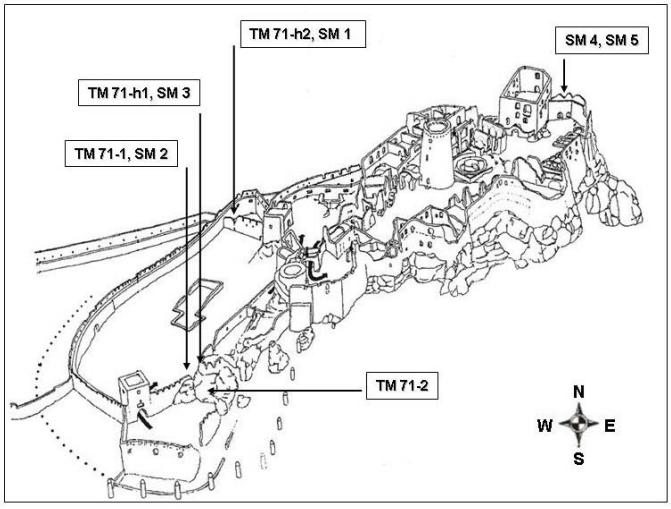

Obr. 10 Situácia monitorovacích stanovísk na Spišskom hrade

Z vyššie uvedeného počtu sa väčšina stanovísk nachádza po obvode tzv. Perúnovej skaly, ktorá na základe dlhodobých meraní vykazuje najväčšie pohyby /25/.

Meradlá zaznamenávajú periodické rozširovanie, resp. zužovanie pukliny medzi dvoma blokmi Perúnovej skaly, horizontálny posun v rovine osi x. Pri tomto jave sme chceli zistiť závislosť medzi kolísaním vonkajších teplôt a nameranými pohybmi monitorovaných skalných blokov. Snažili sme sa to vyjadriť tak, že do grafov sledovaných posunov sme zahrnuli aj priemerné denné vonkajšie teploty. Ako je z obrázkov vidieť, teplotné zmeny majú vplyv na kinematiku pohybu samotného travertínového telesa. Na monitorovacom stanovisku TM-71-h1 (obr. 11) zobrazená závislosť naznačuje, že s rastúcou teplotou sa veľkosť pukliny medzi blokmi rozširuje, naproti tomu na stanovisku TM 71-1 (obr. 12) je táto závislosť opačná (s rastúcou teplotou sa puklina zužuje). Z toho vyplýva, že periodické zmeny vonkajšej teploty vplývajú na kolísavé pohyby Perúnovej skaly, a môžu sa uplatňovať ako prípravný faktor pre pomalý plazivý pohyb.

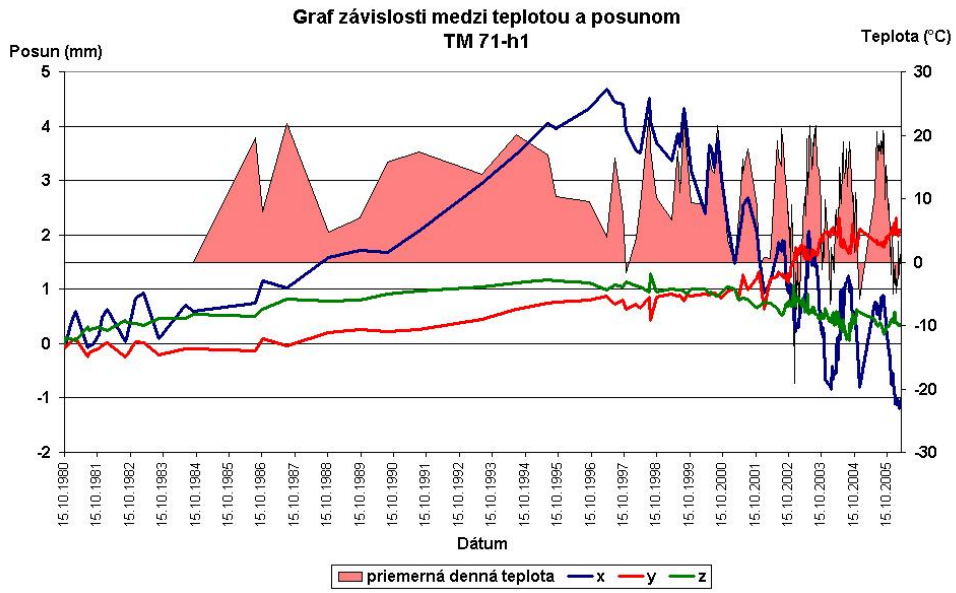

Obr.11 Výsledky monitorovania Perúnovej skaly meradlom TM 71-h1

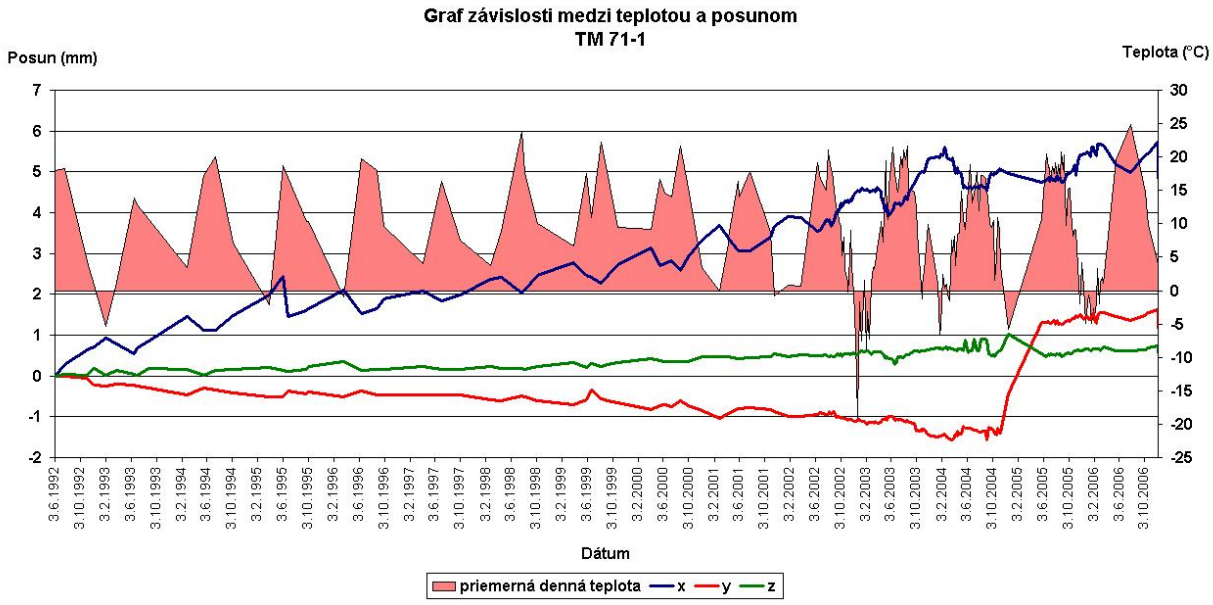

Obr. 12 Výsledky monitorovania Perúnovej skaly meradlom TM 71-1

Záver

Základnými geotermickými údajmi nevyhnutnými pre štúdium priestorového rozloženia teplotného poľa v horninovom masíve je poznanie termofyzikálnych parametrov hornín. Tepelné vlastnosti hornín závisia od množstva faktorov, predovšetkým od štruktúry horniny, jej litologického a minerálneho zloženia, pórovitosti, vlhkosti, teploty a geostatického tlaku. Modelové riešenia na základe rovnice vedenia tepla s využitím termofyzikálnych vlastností hornín nám umožňujú pomerne presne predpovedať vývoj teplotného poľa v priestore a čase. Rovnako, pri poznaní teplotnej deformácie hornín i ich termo-mechanického správania, bude možné korigovať výsledky monitorovania svahových pohybov, tak, že bude možné odlíšiť pohyb spôsobený gravitačnými silami a objemovou zmenou horninového bloku. V tomto smere je potrebné ešte vykonať viacero terénnych meraní a laboratórnych pozorovaní, pretože merania priebehu tepelného toku a stanovenia termofyzikálnych parametrov hornín môžu zaťažené rôznymi chybami, ktoré môžu vyplývať najmä z:

- doposiaľ neštandardizovanej metodiky stanovenia termofyzikálnych parametrov v pripovrchovej zóne skalných horninových masívov,
- absencia vlhkosti, ako významného fyzikálneho faktora vplývajúceho na termo-mechanické správanie sa hornín, resp. Horninových masívov
- chýb v meraniach spôsobených pri osadení teplotných snímačov,
- nereprezentatívneho stanovenia časových sekvencií zberu dát a pod.

Vyššie uvedené fakty si autori príspevku v plnom rozsahu uvedomujú, a preto ďaľšie výskumy budú orientované v smere optimalizácie získavania údajov o termo-mechanicko správaní sa hornín a horninových masívov.

Tento príspevok bol vypracovaný s finančnou podporou projektu č. APVV-0158-06 Agentúry na podporu výskumu a vývoja, ako i z prostriedkov Vedeckej grantovej agentúry MŠ SR (grant VEGA č. 1/4045/07).

Zoznam literatúry

/1/ ZÁRUBA, Q., MENCL, V.: Sesuvy a zabezpečování svahů, Academia, Československá akademie věd, Praha, 1969, 224 s.

/2/ PAŠEK, J., MATULA, M., DROZD, K., HOUSKA, J., MÜLLER, K., NOVOSAD, S., ROTH, V., VERFEL, J., ZAJÍC, J., ZEMAN, M.: Inženýrska geologie I. a II., Nakladatelství technické literatury , Praha, 1995, s. 610

/3/ CRUDEN, D. M, VARNES, D. J.: Landslide types and processes, In: Landslides investigation and mitigation, Special report 247, Transportation research board, National research council, National Academy Press, Washington, 1996, p. 36- 71

/4/ ONDRÁŠIK, R., RYBÁŘ, J.: Dynamická inžinierska geológia, Slovenské pedagogické nakladatelstvo, Bratislava, 1991, s. 267

/5/ GIANI, G. P.: Rock slope stability analysis, A. A. Balkema, Rotterdam, Brookfield, 1992, p. 361

/6/ GUNZBURGER, Y., MERRIEN-SOUKATCHOFF, V., SENFAUTE, G., PIGUET, J.P.: Influence of daily surface temperature fluctuations on rock slope stability: case study of the Rochers de Valabres slope (France), International Journal of Rock Mechanics and Mining Sciences, Volume 42, Issue 3, 2005, p. 331-349

/7/ GUNZBURGER, Y., MERRIEN-SOUKATCHOFF, V., SENFAUTE, G., PIGUET, J.P.: Field investigations, monitoring and modeling in the identification of rock fall causes, Proceedings of the Ninth International Symphosium on Landslides (ISL), Rio de Janeiro (Brasil), 2004, June 28- July 2

/8/ POPESCU, M.: Landslide Causal Factors and Landslide Remediatal Options. http://geoengineer.org/Lanslides-Popescu.pdf.

/9/ WP/WLI: International Geotechnical Societies' UNESCO Working Party on World Landslide Inventory - Cruden, D.M., Chairman. (1990). A suggested method for reporting landslide. *Bulletin IAEG*, 41:5-12.

/10/ WP/WLI: International Geotechnical Societies' UNESCO Working Party on World Landslide Inventory - Cruden, D.M., Chairman. (1991). A suggested method for a landslide summary. *Bulletin IAEG*, 43: 101-110.

/11/ ZÁRUBA, Q.: O stabilite svahů nad povltavskou silnicí u Štěchovic a Vraného, Časopis československých inženýrů, Technický obzor, 1932, číslo 16

/12/ VARGAS JR., E., CASTRO, J. T., AMARAL, C., FIGUEIREDO, R. P.: On mechanisms for failure of some rock slopes in Rio de Janeiro, Brasil: thermal fatigue? In: Lacerda et al., editors. Landslides evaluation and stabilization, Proceedings of the Ninth International Symposium on Landslides, London, 2004, Tailor and Francis Group

/13/ STEWART, T. W., MOORE, D. P.: Displacement behaviour of the Checkerboard creek rock slope, Terrain stability in the interior of British Columbia, Workshop Proceedings, 2002 May 23-25, BC Ministry of Forests, Technical Report 003

/14/ WATSON, A. D, MOORE, D. P., STEWART, T. W.: Temperature influence on rock slope movements at Checkerboard Creek. In: Lacerda et al., editors. Landslides: evaluation and stabilization, Proceedings of Ninth International Symposium on Landslides, London, 2004, Taylor and Francis Group

/15/ JING, L.: A review of techniques advances and outstanding issues in numerical modelling for rock mechanics and rock engineering. International Journal of Rock Mechanics & Mining Science, 2003, Vol. 40. p. 283-353

/16/ RYBÁR, P., KUZEVIČ, Š., RYBÁROVÁ, M., MARAS, M., ĎUROVE, J.: Modelovanie tepelného toku v zemskej kôre, Acta Montanistica Slovaca, 1999, Ročník 4, s. 238 – 244

/17/ Hvožďara, M., Prigancová, A.: Zem – naša planéta, Veda, Vydavateľstvo SAV, Bratislava, 1989, s. 85 -102

/18/ ARNDT, J., BARTEL, T., SCHEUBER, E., SCHILLING, F.: Thermal and rheological properties of granodioritic rocks from the Central Andes, North Chile, 1997, Tectonophysics Vol. 271, p. 75-88

/19/ LEISS, B., MOLLI, G.: „High – temperature" texture in naturally deformed Carrara marble from the Alpi Apuane, Italy, Journal of Structural Geology, 2003, Vol. 25, p. 649-658

/20/ COOPER, H. W., SIMMONS, G.: The effect of cracks on the thermal expansion of rocks, Earth an Planetary Science Letters, 1977, Vol. 36, p. 404-412

/21/ RAMANA, Y. V., SARMA, L. P.: Thermal expansion of a few indian granitic rocks, Physics of the Earth and Planetary Interiors, 1980, Vol. 22, p. 36-41

/22/ GLAMHEDEN, R., LINDBLOM, U.: Thermal and mechanical behaviour of refrigerated caverns in hard rock, Tunnelling and Underground space Technology, 2002, Vol. 17, p. 341-353

/23/ SIEGESMUND, S., RASOLOFOSAON, P. N. J., WEISS, T.: Thermal microcracking in Carrara marble. In Z. dt. Geol. Ges., Stuttgart, 2001, p. 621-636

/24/ BATTAGLIA, S., FRANZINI, M., MANGO, F.: High – sensitivity apparatus for measuring linear thermal expansion: Preliminary results on the response of marbles to thermal cycles. In: I1 nuovo cimento, 1993, Vol. 16 C, Pisa, N.4

/25/ Vlčko, J., Petro, Ľ., Košťák, B.: Monitorovanie skalných blokov na Spišskom hrade, Zb. Geológia a životné prostredie, Bratislava, 1998, s.102-104

UNCERTAINTY ASSESSMENT IN EXTENDED DYNAMIC PLANE SOURCE METHOD

Svetozár Malinarič

Department of Physics, Faculty of Natural Sciences, Constantine the Philosopher University, Nitra, Slovakia, smalinaric@ukf.sk

Abstract:
Extended Dynamic Plane Source (EDPS) method can be used to measure simultaneously the thermal conductivity λ and diffusivity a of low thermally conducting materials within a few minutes. However, although the method is relatively simple, the assessment of its uncertainty is a complicated task and *ISO Guide to the Expression of Uncertainty in Measurement* cannot by applied directly. The sources of errors can be divided into three groups. The first group could be defined as the deviation of the experiment from the theoretical model. The second group is caused by random errors. The third group is caused by errors of input parameters measurement. The aim of this contribution is to define the chain of operations required to determine the results and its uncertainty.

Keywords:
standard uncertainty, thermal conductivity, thermal diffusivity, extended dynamic plane source method

INTRODUCTION

The Extended Dynamic Plane Source (EDPS) method [1] is arranged for one-dimensional heat flow into a finite sample. The principle of the method is outlined in Figure 1. The plane source (PS), which simultaneously serves as the heat source and thermometer, is placed between two identical specimens. Heat sink, made of very good heat conducting material, provides isothermal boundary conditions of the experiment. Figure 2 shows the electrical circuit design. Heat is produced by the passage of electrical current through a planar electrical resistance. Turning the switch S on generates the heat flow into both specimens in the form of a step-wise function. Using the constant power resistor, the electrical current and the voltage across PS can be measured. Thus the power, the instantaneous value of PS resistance and temperature can easily be computed.

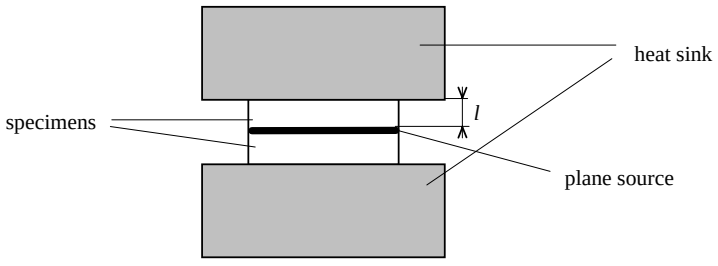

Figure 1. The setup of the experiment.

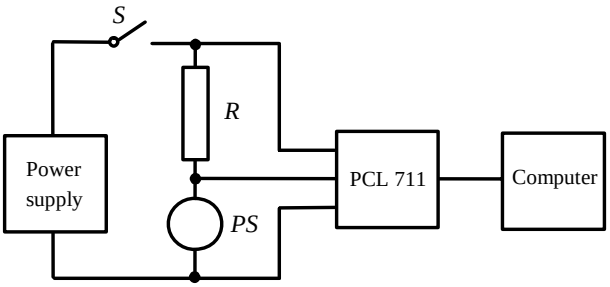

Figure 2. Experimental circuit design. *R* - constant resistor, *S* - switch.

The theoretical model of the experiment is described by the partial differential equation for the heat transport. The temperature function is a solution to this equation with boundary and initial conditions corresponding with the experimental arrangement. The theoretical temperature function is given by

$$T(t,\lambda,a,\tau)=\frac{q}{\lambda}\sqrt{\frac{at}{\pi}}\cdot\left(1+2\sqrt{\pi}\sum_{n=1}^{\infty}\beta^{n}\,\mathrm{ierfc}\left(\frac{nl}{\sqrt{at}}\right)\right)+\tau \qquad (1)$$

q is the heat current density and *l* is the thickness of the specimen. τ is an additional (nuisance) parameter which represents the offset of PS temperature due to its imperfections. β describes the heat sink imperfection and ierfc is the error function integral [2].

UNCERTAINTY ASSESSMENT

The reliability of every measurement result is confirmed by a quantitative assessment of its uncertainty. General rules for uncertainty assessment have been established in GUM [3]. The sources of error can be divided into three groups. The first could be defined as the deviation of the experiment from the theoretical model.

The model assumes that PS is a homogeneous heat source, has negligible heat capacity and perfect contact with the specimen. These conditions are not exactly fulfilled which causes so called source effect. This is solved by introducing a new parameter τ and removing the beginning of the measured temperature response using difference analysis [4].

It is supposed that there are no heat losses from the lateral sides of the specimen. This can be solved by three methods. The first is removing the end part of the measuring temperature response using difference analysis. The second is measuring with various specimen diameters and extrapolating to infinity diameter. The third is to make the experiment in vacuum.

The model also assumes the constant heat current density i.e. constant electrical power. This is not exactly fulfilled because of the change of PS resistance during the experiment. This can be solved using PC control constant power supply or by measuring with various values of power and extrapolating to zero.

The second group is caused by unknown random errors. These effects can be considered as repeatability of measurement results. Repeatability can be estimated by 10 or more successive measurements carried out under the same conditions and with the same specimen. The apparatus and specimens should be disassembled and reassembled before each measurement. The effect of apparatus assembly is probably one of the most important factors for the results dispersion.

The third group is caused by uncertainties in input parameters measurements. The main sources of uncertainty are connected with the measurement of voltage, resistance of constant resistor, temperature coefficient of resistivity (TCR) of the PS and specimen dimensions.

CONSTANT RESISTOR MEASUREMENT

Measurement of the constant resistor $R \approx 1\ \Omega$ is performed using multimeter M1T 380. Because of low accuracy it could not be done directly but using the following scheme

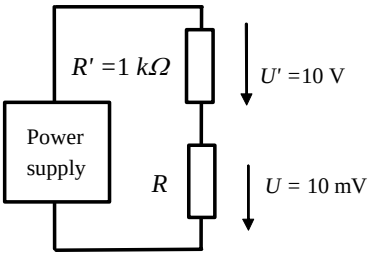

Figure 3. The measurement of the constant resistor R

The value of the resistance of the resistor R is given by the formula

$$R = R'\frac{U}{U'} \tag{2}$$

So three quantities should be measured with errors given by the multimeter producer. Error of $R' \approx 1$ kΩ measurement is 200ppm.MH + 50ppm.MHMR = 275 mΩ. Where MH is the measured value and MHMR is the maximum value of the measuring range. So the standard and relative uncertainties are given by

$$u(R') = \frac{275\ \text{m}\Omega}{1.73} = 160\ \text{m}\Omega \qquad \frac{u(R')}{R'} = 160 \cdot 10^{-6} \tag{3}$$

Error of $U' \approx 10$ V measurement is 100ppm.MH + 20ppm.MHMR = 1.3 mV and the relative standard uncertainty is

$$\frac{u(U')}{U'} = 75 \cdot 10^{-6} \tag{4}$$

Error of $U \approx 10$ mV measurement is 100ppm.MH + 20ppm.MHMR = 4.0 uV and the relative standard uncertainty is

$$\frac{u(U)}{U} = 230 \cdot 10^{-6} \tag{5}$$

Assuming no correlation between input quantities the standard uncertainty of resistance R determination can be computed by root sum square addition as follows

$$\left(\frac{u(R)}{R}\right)^2 = \left(\frac{u(R')}{R'}\right)^2 + \left(\frac{u(U')}{U'}\right)^2 + \left(\frac{u(U)}{U}\right)^2 \tag{6}$$

The standard uncertainty of resistance *R* determination becomes $u(R) = 290\mu\Omega$.

TEMPERATURE COEFFICIENT OF RESISTIVITY TCR MEASUREMENT

The PS was placed into silicon oil bath where the temperature was measured by thermometer with declared expanded uncertainty $U(T) = 0.1\,\mathrm{K}$. The standard uncertainty is given by

$$u(T) = \frac{0.1\,\mathrm{K}}{1.73} = 0.058\,\mathrm{K} \tag{7}$$

The resistance of PS was measured using following schema

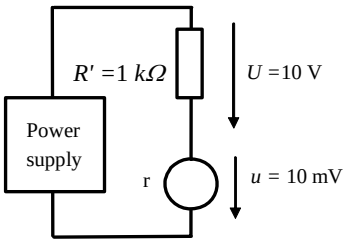

Figure 4. The measurement of PS resistance *r*

and the standard uncertainty of PS resistance $r \approx 1\Omega$ determination is as in previous section $u(r) = 290\mu\Omega$.

TCR of PS is defined by the relation

$$r = r_0(1 + \alpha(T - T_0)) \tag{8}$$

where r_0 is the resistance at the temperature T_0. TCR of nickel is $\alpha \approx 0.0047$ / K. The simplest way of determining TCR is to measure temperature and resistance at two points as seen in Figure 5.

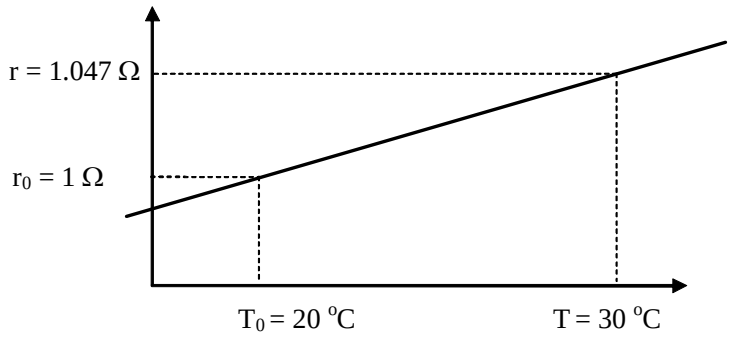

Figure 5. TCR measurement of PS

Then the TCR can be computed using following formula

$$\alpha = \frac{r - r_0}{r_0 \cdot (T - T_0)} \tag{9}$$

The first stage in evaluating uncertainty is to determine the uncertainty of the differences,

$$u(T - T_0) = \sqrt{2} \cdot u(T) = 0.082\ \mathrm{K} \qquad u(r - r_0) = \sqrt{2} \cdot u(r) = 0.41\ \mathrm{m\Omega} \tag{10}$$

then we use the root sum square addition rule

$$\left(\frac{u(\alpha)}{\alpha}\right)^2 = \left(\frac{u(r - r_0)}{r - r_0}\right)^2 + \left(\frac{u(T - T_0)}{T - T_0}\right)^2 + \left(\frac{u(r_0)}{r_0}\right)^2 \tag{11}$$

The standard uncertainty of TCR determination was stated to $u(\alpha) = 56 \cdot 10^{-6}\ \mathrm{K}^{-1}$.

PS RESISTANCE MEASUREMENT

The EDPS experiment consists in measurement of PS temperature response. This is performed by measurement of PS resistance.

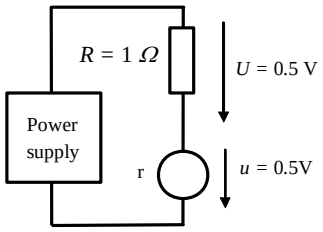

Figure 6. Measurement of time dependence of PS resistance

Now we used current I ≈ 500mA, so the PS is warmed and emitting heat flux. Both voltages *u* and *U* were simultaneously measured using multichannel Advantech PC plug-in card PCL 711. This arrangement removed power supply instability. The declared accuracy by the producer is 0.015 % of reading ± 1 LSB. The quantization noise is suppressed using averaging. The relative standard uncertainty of voltage measurement becomes

$$\frac{u(u)}{u} = \frac{u(U)}{U} = \frac{150 \cdot 10^{-6}}{1.73} = 87 \cdot 10^{-6} \tag{12}$$

The resistance of the PS and its uncertainty are given by the forms

$$r = R\frac{u}{U} \qquad \left(\frac{u(r)}{r}\right)^2 = 2 \cdot \left(\frac{u(u)}{u}\right)^2 + \left(\frac{u(R)}{R}\right)^2 \tag{13}$$

The standard uncertainty of PS resistance determination was stated to $u(r) = 320 \mu\Omega$.

HEAT CURRENT DENSITY MEASUREMENT

The heat current density is given by the following forms

$$q = \frac{P}{S} = \frac{U \cdot u}{R \cdot S} \qquad S = \frac{\pi \cdot d^2}{4} \tag{14}$$

uncertainty of PS area *S* determination is given by

$$u(S) = \frac{\partial S}{\partial d} u(d) = \frac{\pi}{2} d \cdot u(d) \tag{15}$$

The specimen diameter was measured using a caliper with a resolution 0.1 mm. The uncertainty becomes $u(d) = 0.1\,\text{mm} / \sqrt{12} = 0.03\,\text{mm}$. Then the relative standard uncertainty of heat current density determination was stated to

$$\frac{u(q)}{q} = \frac{u(S)}{S} = 2\frac{u(d)}{d} = 0.003 \tag{16}$$

THERMOPHYSICAL PARAMETERS ESTIMATION

Inverse problem consists in determining the thermophysical parameters by fitting theoretical temperature function (1) to measured points $[t_i, T_i]$. Since the output of the measurement is the resistance of the PS, the temperature function should be rewritten as

$$r(t) = \frac{\alpha \cdot r_0 \cdot q \cdot l}{\lambda \cdot \sqrt{\pi}} F(t,a) + \rho \qquad F(t,a) = \frac{\sqrt{a \cdot t}}{l}\left(1 + 2 \cdot \sqrt{\pi} \cdot \sum_{n=1}^{\infty} \beta^n \cdot \text{ierfc}\left(\frac{n \cdot l}{\sqrt{a \cdot t}}\right)\right) \tag{17}$$

where α, q ,l are scalar input quantities and $\vec{r}$ is a vector input quantity. ρ is a perturbation parameter stemming from parameter τ. Each input quantity has been determined with its specific uncertainty which contributes to the uncertainty of the thermophysical parameters estimation.

SCALAR INPUT QUANTITIES CONTRIBUTION TO THE COMBINED UNCERTAINTY

The thermophysical parameters are computed using least squares (LS) fitting which can be symbolically expressed as follows

$$y_j = \Phi_j(\vec{r}, \alpha, q, l) \tag{18}$$

where $\vec{y} = (\lambda, a, \rho)$ is a vector of unknown parameters and Φ is an inverse function defined numerically by LS algorithm. According to GUM [3], uncertainty of input quantity *x* contribution to the uncertainty of parameter y_j determination is given

$$u_x(y_j) = \frac{\partial y_j}{\partial x} \cdot u(x) = \frac{\Phi_j(1.01\,x) - \Phi_j(x)}{0.01\,x} \cdot u(x) \tag{19}$$

where the partial derivative is determined numerically.

VECTOR $\vec{r}$ CONTRIBUTION TO THE COMBINED UNCERTAINTY

The result of the measurement is represented by equi-spaced time series of PS resistance r_i $(i = 1...n)$ denoted as vector $\vec{r}$. Then the sensitivity matrix [5] is given by

$$\{\mathbf{X}\}_{ij} = \beta_j(t_i, \vec{y}) \tag{20}$$

where β_j is the sensitivity coefficient for parameter y_j defined by

$$\beta_j(t, \vec{y}) = \frac{\partial r(t, \vec{y})}{\partial y_j} \tag{21}$$

The standard uncertainty of the LS estimate of the parameter y_j is given by

$$u^2(y_j) = \left\{\left(\mathbf{X}^T \cdot \mathbf{X}\right)^{-1}\right\}_{jj} \cdot u^2(r) \tag{22}$$

where $u(r)$ is the standard uncertainty of PS resistance estimate.

SUMMARY OF EDPS METHOD

The goal of this work consist in analysing the possible sources of uncertainty in EDPS method. The analysis showed the complexity of uncertainty assessment, though most of operations were simplified or carried out schematically.

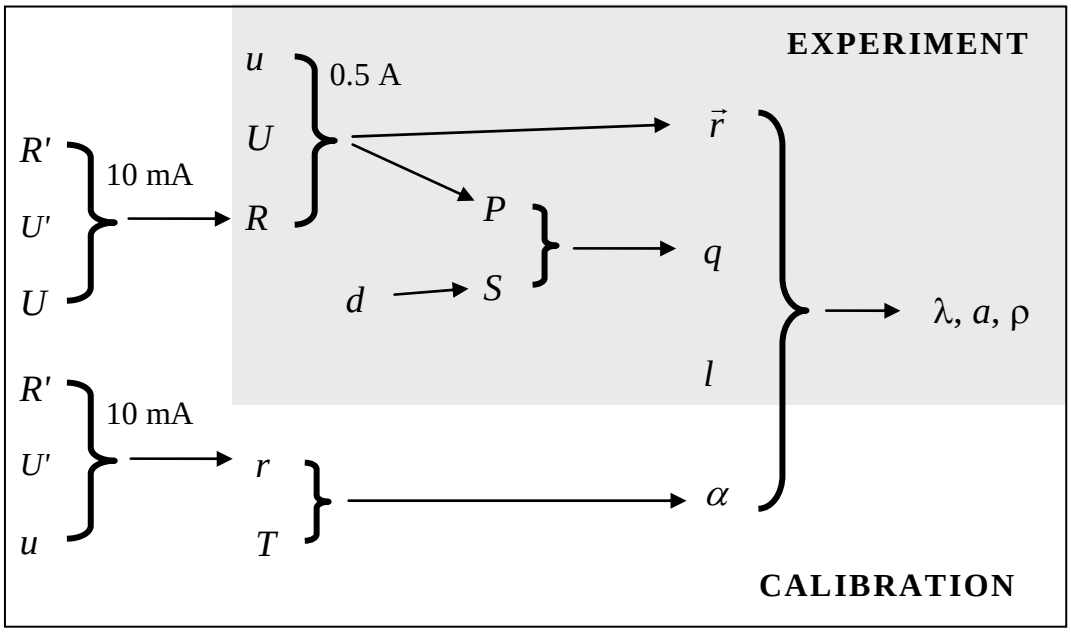

Figure 7. The chain of operations in thermophysical parameters estimation

ACKNOWLEDGEMENTS

This work was supported by the Scientific Grant Agency of the Ministry of Education of Slovak Republic and The Slovak Academy of Sciences, No 1/3178/06.

REFERENCES

[1] Karawacki, E., Suleiman, B. M., ul-Hag, I., Nhi, B.(1992): *Rev. Sci. Instrum.,* 63, 4390.

[2] Carslaw, H. S., Jaeger, J. C. (1959): Conduction of Heat in Solids, Clarendon, Oxford.

[3] *Guide to the Expression of the Uncertainty in Measurement* (1993): ISO, Geneva.

[4] Malinarič S. (2004): *Meas. Sci. Technol*. 14, 807.

[5] Malinarič S. (2007): *Int. J. Thermophys*., 28, 20.